

BRUNEL UNIVERSITY LONDON



# Design and Fabrication of GaPO<sub>4</sub> Ultrasonic Transducer for NDT at High Temperatures

by Mario Kostan

A thesis submitted to Brunel University London for the degree of  
Doctor of Philosophy

in the

College of Engineering, Design and Physical Sciences,  
Department of Mechanical and Aerospace Engineering

September 2018

# Declaration of Authorship

I, Mario Kostan, declare that this thesis submitted to Brunel University London for the degree of Doctor of Philosophy titled “Design and Fabrication of GaPO<sub>4</sub> Ultrasonic Transducer for NDT at High Temperatures” and the work presented in it are my own. Further, I confirm that:

- This research work was done wholly while in candidature for a research degree of Doctor of Philosophy at this University;
- Where I have consulted the published work of others, this is always clearly attributed;
- Where I have quoted from the work of others, the source is always given. With the exception of such quotations, this thesis is entirely my own work;
- I have acknowledged all main sources of help;
- Where the thesis is based on work done by myself jointly with others, I have made clear exactly what was done by others and what I have contributed myself.

**Mario Kostan,**

In Cambridge, September 2018

# Abstract

There is a critical need for inspection and condition monitoring of high temperature critical components such as pipelines and welds in electrical power generation and other plants operating at temperatures as high as 580°C. The high temperatures and pressures experienced in these pipelines, particularly for ageing plants lead to creep, fatigue and corrosion type defects. Safety of these plants is of paramount importance, and regular maintenance is carried out during planned outages at ambient temperatures. Ultrasonic non-destructive testing can be used to detect defects in the weld at ambient temperatures. However, at high operational temperatures, this technique cannot be applied due to the lack of high temperature transducers. This research has achieved significant advances towards enabling ultrasonic inspection and condition monitoring of high temperature critical points, by developing an ultrasonic transducer around an advanced piezoelectric single crystal material, called Gallium Orthophosphate ( $\text{GaPO}_4$ ), which can operate at the required temperature of 580°C. Based on its reported piezoelectric and other properties, and its commercial availability,  $\text{GaPO}_4$  was chosen as a candidate active material for application in a prototype high temperature transducer. In a series of confidence building tests with the selected piezoelectric material (electrical characterisation via the impedance method), it has been demonstrated that the  $\text{GaPO}_4$  piezoelectric elements are stable when subjected to 580°C for more than 600 hours. Ultrasonic thickness gauging has shown that  $\text{GaPO}_4$  works as a functional transducer generating and receiving ultrasound waves at 580°C for at least 360 hours. Furthermore, the sensitivity of the  $\text{GaPO}_4$  transducer to detect defects with simple geometry was successfully tested through measurements on steel blocks containing artificial defects (side-drilled holes) up to the same high temperatures. Based on the characterisation results from the impedance and ultrasonic measurements, a prototype ultrasonic transducer for operation at high temperatures has been designed and manufactured. The new ultrasonic transducer was tested in a laboratory environment using a steel calibration block, high temperature couplant, SONO 1100, and an electric furnace. In the range from ambient temperatures up to the target of 580°C, the ultrasonic transducer kept a signal-to-noise (SNR) level sufficiently high, above the threshold of 6 dB, which is high enough for practical non-destructive testing and condition monitoring.

# Acknowledgements

The past four and a half years have been the happiest of my life! The opportunity to do a PhD at world-class facilities of BIC and TWI has been a life changing experience. At the same time, the chance to live and work in an ancient university city like Cambridge, and to spend my days with some of the brightest minds in today's times (and to consider some of them my close friends), have made me feel incredibly happy and indebted. It is not possible to list all of their names (plus there is a chance I will miss some in the excitement of the submission), so I will name only a few, whom I feel have shared many good (and of course some bad) moments with me on this bumpy journey called a PhD.

I would like to thank my supervisors Prof Tat-Hean Gan and Prof Luiz Wrobel (with Prof Balachandran) for all of their support throughout my PhD. They have given me great freedom with my work, enabling me to conduct it at my own speed, but making sure that I produce a nice piece of academic work.

I owe special thanks to Dr Abbas Mohimi and Dr Channa Nageswaran. They have been my industrial supervisors and their day-to-day advice and discussions have contributed significantly to the outcomes of my research. Abbas (together with Dr Marko Budimir) is the main 'culprit' for giving me a chance and pushing me to pursue a doctorate at the Brunel Innovation Centre.

In the very beginning of my academic path (bachelor and master theses), Dr Marko Budimir and Eng Nikola Pavlovic offered me the opportunity to undertake research in the field of ultrasonic NDT (within the INETEC institute). Ever since, they have been and remained my great supporters in tough periods and were always on call for extensive technical questions and discussions. Guys, thank you!

My English teacher Branka Meic Salie (with her husband Moosa Salie always assisting behind the scenes), and my mountaineering guru Mico Grbac have become my family, and they have always been there when I needed them. I am especially grateful to Branka who helped me to prepare for my English exam, prior to the application for the PhD, and since then has remained my chief editor.

My closest friends have been Muntasir, Sasa, Shahrokh, Sergio and Santo. Thank you guys for lending me a hand when I needed it, or drinking with me when only a drink helped. I love our walks, our drives to London and beyond (Cornwall!), and our gym sessions. Thanks to everyone else, such as my dear *BIG BIC* people, colleagues from TWI, CUYUS committee members and all the others I have not named here (just to mention Marino, Shengrun, Ebba, Anurag, Ioanna, Cem, Simon from U. Shed...).

Finally, I would like to express my deepest gratitude to my mum Ana, brother Tomislav, father Stjepan and the rest of my lovely family (Marina and Spiro, etc.) and of course to my lovely girlfriend Theresa.

# Contents

Declaration of Authorship.....	II
Abstract.....	III
Acknowledgements.....	IV
List of Figures.....	IX
List of Tables.....	XIV
Symbols and Chemical Formulas.....	XV
Abbreviations.....	XVII
1 Introduction.....	1
1.1 The industrial problem.....	1
1.1.1 Creep behaviour of P91.....	2
1.2 Aim and objectives.....	6
1.3 Organisation of thesis.....	6
1.4 Summary of contributions to knowledge.....	7
1.5 List of publications.....	8
1.5.1 Publications.....	8
1.5.2 Conference presentations.....	9
2 Literature Review.....	10
2.1 Chapter overview.....	10
2.2 Non-destructive testing methods.....	10
2.3 Definition of ultrasound.....	11
2.4 Ultrasonic system for non-destructive testing.....	11
2.5 Display presentation for ultrasonic flaw detection equipment.....	13
2.5.1 A-scan.....	13
2.5.2 B-scan.....	14
2.5.3 C-scan.....	14
2.6 Ultrasonic transducers.....	15

## Contents

2.7	Analysis of design of high temperature transducers .....	19
2.7.1	Approach with ultrasonic waveguide .....	20
2.7.2	High temperature ultrasonic transducers with direct contact .....	21
2.8	Selection of high temperature substitutes .....	22
2.8.1	Piezoelectric element.....	22
2.8.2	Configuration of electrodes.....	25
2.8.3	Damping mass .....	26
2.8.4	Protective front plate and/or wedge .....	28
2.8.5	Acoustic insulator.....	30
2.8.6	Housing .....	31
2.8.7	Wiring and co-axial connector .....	31
2.8.8	Electrical impedance matching circuiting .....	31
2.8.9	Bonding of materials .....	32
2.8.10	Contact coupling medium .....	33
3	High Temperature Impedance Analysis of GaPO <sub>4</sub> Elements .....	34
3.1	Chapter overview .....	34
3.2	Introduction.....	34
3.2.1	Definition of electrical impedance .....	34
3.2.2	Measuring electrical impedance .....	37
3.2.3	Measuring impedance of piezoelectric elements.....	37
3.3	Effect of temperature .....	38
3.4	Determination of the key electromechanical properties.....	39
3.4.1	Electromechanical coupling factor – $k_{ij}$ .....	40
3.4.2	Piezoelectric charge constant – $d_{ij}$ .....	40
3.4.3	Compliance and stiffness constant – $s_{11}^E$ and $c_{11}^E$ .....	40
3.4.4	Calculation of complete set of electromechanical properties.....	41
3.5	Development of GaPO <sub>4</sub> elements.....	42
3.6	Impedance analysis at HT .....	42

## Contents

3.6.1	Test-rig for performing impedance measurements up to 580°C .....	43
3.7	Experimental setup and procedure.....	46
3.8	Results and discussion .....	47
3.8.1	Impedance response from 25°C up to 580°C.....	47
3.8.2	Long-term impedance response at 580°C .....	49
3.8.3	Electromechanical properties from 25°C up to 580°C.....	51
3.8.4	Long-term electromechanical properties at 580°C.....	53
4	High Temperature Ultrasonic Analysis of GaPO <sub>4</sub> Elements.....	56
4.1	Chapter overview .....	56
4.2	Introduction.....	56
4.3	High temperature ultrasonic analysis.....	57
4.3.1	Experimental setup for analysis of the initial pulse .....	57
4.3.2	Results of the initial pulse analysis .....	58
4.4	Thickness gauging at high temperatures using GaPO <sub>4</sub> .....	60
4.4.1	Base-line thickness gauging at ambient temperature .....	61
4.4.2	Results of the base-line thickness gauging at ambient temperature .....	62
4.4.3	Thickness gauging at high temperatures .....	66
4.4.4	Results and discussion of the thickness gauging up to 580°C .....	68
4.4.5	Long-term thickness gauging using GaPO <sub>4</sub> element at 580°C.....	74
4.5	Defect detection in the pulse-echo mode at up to 580°C.....	78
4.5.1	Experimental validation of high temperature damping body.....	78
4.5.2	Selection of the suitable test-frequency.....	80
4.5.3	Experimental setup for defect detection up to 580°C.....	81
4.5.4	Results and discussion on defect detection up to 580°C.....	82
5	Design, Manufacture and Testing of the Ultrasonic Transducer up to 580°C .....	86
5.1	Chapter overview .....	86
5.2	Design of the ultrasonic transducer for operation at 580°C.....	86
5.2.1	First bond layer – application of the electrode.....	87

## Contents

5.2.2	Second bond layer – application of the protective front plate.....	87
5.2.3	HT housing.....	88
5.3	Manufacture of the transducer for operation at 580°C .....	89
5.4	Electrical impedance analysis of the manufactured transducer .....	92
5.4.1	Electrical impedance matching of the transducer.....	93
5.5	Ultrasonic analysis of the manufactured transducer .....	96
5.5.1	Thickness gauging at ambient temperature .....	96
5.5.2	Defect detection at ambient temperature.....	102
5.6	Testing of SONO high temperature ultrasonic couplants .....	109
5.6.1	Testing of SONO couplants with a commercial transducer .....	109
5.6.2	Testing of SONO couplants with the manufactured transducer .....	111
5.7	Testing of the ultrasonic transducer at high temperatures .....	114
5.7.1	Ultrasonic signals received at transducer from ambient up to 580°C .....	115
5.8	Manufacture of a prototype ultrasonic transducer .....	117
5.8.1	Testing of the transducer in a high temperature environment .....	118
6	Conclusions and Future Work.....	121
6.1	Conclusions.....	121
6.2	Recommendations for future work .....	122
7	Bibliography .....	125

# List of Figures

Figure 1-1: Type IV cracking in the electron beam welded 9% Cr-1% Mo steel; a) macro and b) micro image (mm scale shown).....	3
Figure 1-2: Creep damage classification and creep curve correlation .....	4
Figure 1-3: HT NDT system developed within “HotPhasedArray” Project. ....	5
Figure 2-1: Sound waves division by frequency.....	11
Figure 2-2: The schematic of an ultrasonic test system .....	12
Figure 2-3: A real-world ultrasonic test system that detects defects in the structure.....	12
Figure 2-4: a) Example of a test-structure with three indications A, B, and C and b) illustration of the A-scan presentation for the example structure.....	13
Figure 2-5: a) Example of a test-structure with three indications A, B, and C and b) illustration of the B-scan presentation for the example structure .....	14
Figure 2-6: Example of a test-structure with an indication and illustration of the C-scan presentation .....	15
Figure 2-7: Ultrasonic transducer with vertical or flat beam .....	16
Figure 2-8: a) Schematic of an angular ultrasonic transducer, b) diagram showing the incident, reflected and refracted angles .....	17
Figure 2-9: Schematic of an angular ultrasonic transducer.....	17
Figure 2-10: An ultrasonic transducer with a delay line .....	18
Figure 2-11: A “theoretical” beam spread profile with “near field” and “far field” .....	18
Figure 2-12: Ultrasonic transducers for application in non-destructive testing .....	19
Figure 2-13: Schematic representation of a dual ultrasonic waveguide.....	20
Figure 2-14: a) Crystal structure of GaPO <sub>4</sub> and b) raw GaPO <sub>4</sub> plate, as acquired from the manufacturer Piezocryst Advanced Sensorics GmbH.....	25
Figure 2-15: Ceramic adhesives acquired for the ultrasonic transducer manufacture. ....	28
Figure 2-16: Schematic of the interface between the piezoelectric element, one of the metal electrodes and the protective front plate. The thickness of the bonding medium (adhesive) between the metal electrode and the protective front plate is taken to be negligible. ....	29
Figure 3-1: Impedance (Z) consists of a real part (R) and an imaginary part (X) .....	35
Figure 3-2: Typical impedance response over a frequency range for a piezoelectric element. ....	37
Figure 3-3: Frequency dependent impedance of ceramic bismuth titanate, from 0 to 4 MHz, and from 25 to 525°C, showing the vanishing of $f_r$ and $f_a$ peaks once Curie temperature is reached. ....	39
Figure 3-4: a) A raw GaPO <sub>4</sub> element, as purchased from “Piezocryst Ltd” and b) the raw GaPO <sub>4</sub> element is coated in platinum and shaped into slender rectangular elements. ....	42

## List of Figures

Figure 3-5: (a) Agilent 4294A impedance analyser using (b) an Agilent 16048A test-fixture and (c) BNC leads that were connected to a piezoelectric element under impedance measurement. ....	43
Figure 3-6: The schematic of the test-rig developed for performing of impedance analysis at HT. ....	45
Figure 3-7: Experimental setup used for impedance analysis of GaPO <sub>4</sub> elements at HT. ....	46
Figure 3-8: Impedance characteristics of a GaPO <sub>4</sub> element, in the temperature range from 25°C up to 580°C and in the frequency range from 1.7 MHz up to 2.5 MHz, showing the effect of increasing temperature on the $f_r$ and $f_a$ peaks.....	47
Figure 3-9: Measured values of a) resonant $f_r$ and b) anti-resonant $f_a$ frequency pair, as a function of temperature from 25°C up to the target of 580°C, averaged for five GaPO <sub>4</sub> elements.....	48
Figure 3-10: Measured values of a) resonant $Z_r$ and b) anti-resonant $Z_a$ el. impedance pair, as a function of temperature from 25°C up to the target of 580°C, averaged for five GaPO <sub>4</sub> elements. ....	49
Figure 3-11: Impedance response of a GaPO <sub>4</sub> element at constant temperature of 580°C for 600 h, showing a good thermal stability of $f_r$ and $f_a$ frequency peaks over the tested period.....	49
Figure 3-12: Measured values of a) resonant $f_r$ and b) anti-resonant $f_a$ frequency pair, at the constant temperature of 580°C, as a function of time over 600 hours. ....	50
Figure 3-13: Measured values of a) resonant $Z_r$ and b) anti-resonant $Z_a$ electrical impedance pair, at the constant temperature of 580°C, as a function of time over 600 hours. ....	51
Figure 3-14: a) Derived piezoelectric charge constant $d_{11}$ and b) electromechanical thickness coupling factor $k_t$ , in the temperature range from 25°C up to 580°C, averaged for five GaPO <sub>4</sub> elements. The constant $d_{11}$ was also compared to the provided datasheet value. ....	52
Figure 3-15: a) Derived elastic compliance $s_{11}^E$ and b) elastic stiffness constant $c_{11}^E$ , in the range from 25°C to 580°C, averaged for five GaPO <sub>4</sub> elements and compared to the datasheet values. ....	52
Figure 3-16: a) Derived charge constant $d_{11}$ and b) thickness coupling factor $k_t$ of a GaPO <sub>4</sub> element, at the constant temperature of 580°C as a function of time over 600 hours (25 days). ....	53
Figure 3-17: a) Derived elastic compliance $s_{11}^E$ and b) elastic stiffness constant $c_{11}^E$ of a GaPO <sub>4</sub> element, at the constant temperature of 580°C as a function of time over 600 hours (25 days)...	54
Figure 3-18: Impedance traces of GaPO <sub>4</sub> element at 25°C, before (blue trace) and after (red trace) the 25-day exposure to 580°C, showing an excellent stability of the piezoelectric response.....	55
Figure 4-1: Experimental setup used for analysis of the initial electrical pulse coming out from the pulser of the commercial pulser-receiver instrument TOPAZ. ....	58
Figure 4-2: a) Two consecutive pulses generated from the pulser of TOPAZ. b) An illustration of the overshoot effect followed by a “ringing” and settle time for an initial pulse of -50 V.....	59
Figure 4-3: The initial pulses coming out from the pulser of the ultrasonic machine TOPAZ, for amplitude ranging from a min of -50 V to a max of -200 V, averaged for 5 measurements. ....	60
Figure 4-4: a) A GaPO <sub>4</sub> element is coupled to steel test-block using silver adhesive with attached nickel wiring; b) The schematic of setup used for base-line experiment at ambient temperature.	62

## List of Figures

- Figure 4-5: The waveforms of the fastest arriving echo reflected from the backwall of carbon steel block at 30 mm and received by GaPO<sub>4</sub> element, for the initial pulse from -50 V to -200 V..... 62
- Figure 4-6: a) Reflected echoes received back by the GaPO<sub>4</sub> element as a function of the initial pulse ranging from -50 V to -200 V. b) SNR level (in dB) as a function of the same initial pulse. .... 64
- Figure 4-7: Bandwidth of a commercial 5 MHz transducer ..... 65
- Figure 4-8: Normalised frequency domain of the fastest arriving ultrasonic waveform that was received at the GaPO<sub>4</sub> element, for the initial pulse ranging from -50 V (min) to -200 V (max). 66
- Figure 4-9: Two GaPO<sub>4</sub> elements were mounted onto a steel block (25 mm thickness) using silver adhesive. The same adhesive was used to wire the two elements to the nickel conductors. .... 67
- Figure 4-10: a) The experimental setup for ultrasonic thickness gauging up to 580°C. b) The GaPO<sub>4</sub> samples coupled to the steel block using silver adhesive were placed inside a furnace. .... 68
- Figure 4-11: Two consecutive reflections from the backwall of the steel block that were received at a) GaPO<sub>4</sub> element No 1 up to 450°C and b) GaPO<sub>4</sub> element No 2 up to temperature of 580°C. .... 69
- Figure 4-12: The fastest arriving reflections received at the GaPO<sub>4</sub> element No 2, at 25°C (blue trace) and 580°C (red trace), showing the influence of temperature on measured time-of-flight..... 71
- Figure 4-13: SNR (in dB) for the reflections received at GaPO<sub>4</sub> element No 1 and No 2. .... 71
- Figure 4-14: Normalised frequency domain of the signals received at a) GaPO<sub>4</sub> element No 1 up to 450°C and b) GaPO<sub>4</sub> element No 2 up to the target temperature of 580°C. .... 72
- Figure 4-15: Comparison of the frequency values derived from impedance tests on five GaPO<sub>4</sub> elements up to 580°C (black markers) and the values derived from ultrasonic tests for GaPO<sub>4</sub> element No 1 up to 450°C (blue markers) and GaPO<sub>4</sub> element No 2 up to 580°C (red markers). 73
- Figure 4-16: Two consecutive ultrasonic reflections from the backwall that were received at GaPO<sub>4</sub> element No 2. The echoes were recorded on the 1<sup>st</sup>, 13<sup>th</sup>, 14<sup>th</sup> and 15<sup>th</sup> days at 580°C..... 75
- Figure 4-17: a) Generated signal amplitude and b) calculated SNR for the fastest arriving reflection from the backwall received back at the GaPO<sub>4</sub> element No 2, at 580°C for 14 days..... 76
- Figure 4-18: a) The two GaPO<sub>4</sub> elements together with the corroded steel block showing the effect of exposure to 580°C for 14 days. b) The GaPO<sub>4</sub> element No 2, with seriously damaged platinum electroding, showing the complexity of ultrasonic measurements at high temperatures. .... 77
- Figure 4-19: A detailed view of the Ceramabond 503 adhesive applied to the GaPO<sub>4</sub> element..... 79
- Figure 4-20: The adhesive Ceramabond 503 applied to the backside of the GaPO<sub>4</sub> element to serve as a backing body. a) The first layer was ~2 mm thick and b) the second one was ~4 mm..... 79
- Figure 4-21: Three consecutive echoes recorded for three cases: (i) no backing (the black trace), (ii) ceramic backing thick 2 mm (the blue trace) and (iii) backing thick 4 mm (the red trace). .... 80
- Figure 4-22: The impedance analysis of GaPO<sub>4</sub> element confirmed it to resonate at 3.5 MHz..... 81
- Figure 4-23: a) A GaPO<sub>4</sub> element was coupled to a steel test-block directly above the SDH using silver adhesive. b) Everything was placed inside a furnace for defect detection up to 580°C..... 82

## List of Figures

Figure 4-24: A-scans containing reflections from defect (SDH) and backwall of the carbon steel block that were received back to the GaPO <sub>4</sub> element at 25°C, 200°C, 400°C and 580°C.....	83
Figure 4-25: Compared reflections from defect (SDH) and backwall of the steel block received at the GaPO <sub>4</sub> element at 25°C (black trace) and at 580°C (red trace) showing the influence of temperature on the time-of-flight.....	83
Figure 4-26: Calculated SNR values for reflections from SDH and backwall, from 25 to 580°C. ....	84
Figure 4-27: Compared reflections from SDH – (a) and backwall – (b) received at GaPO <sub>4</sub> element at 25°C, before (the black trace) and after (the blue trace) the exposure to 580°C. ....	84
Figure 5-1: The GaPO <sub>4</sub> element is coated in the standard parallel electrode configuration with a 200 nm thick platinum layer. ....	87
Figure 5-2: A front plate is applied between the piezoelectric element and the test-structure that allows for both scanning and monitoring. In a) the transducer will measure thickness of the test-structure. Once moved to b), it will allow for both thickness gauging and defect (SDH) detection .....	88
Figure 5-3: Simplified design of the prototype ultrasonic transducer for application up to 580°C. ....	89
Figure 5-4: a) Steel protective plate, b) front plate is coupled to GaPO <sub>4</sub> element using adhesive, c) nickel wiring is affixed to GaPO <sub>4</sub> and front plate, d) new transducer is enclosed within steel housing, e) nickel wiring is affixed to housing to prevent possible abruption of wires during measurement and f) ultrasonic transducer is manufactured and ready for testing up to 580°C....	91
Figure 5-5: a) The experimental setup used for impedance analysis of the new transducer. b) The impedance response over the test-frequency range shows the new resonance at 1.496 MHz. ....	92
Figure 5-6: Five different equivalent circuits offered by the impedance analyser.....	93
Figure 5-7: The measured impedance response of the transducer (the black trace), and the simulated response using the equivalent circuit and the values from Table 5-3 (the red trace).....	94
Figure 5-8: Schematic of a matching circuit (network) installed between the high impedance GaPO <sub>4</sub> transducer, and the low impedance pulser-receiver instrument and the BNC cable.....	95
Figure 5-9: The setup for testing of the new transducer at ambient temperature.....	96
Figure 5-10: The A-scan containing (a) waveforms of the initial pulse applied to the transducer at different amplitudes from -50 to -200 V and (b) waveforms of the fastest arriving echo reflected from the backwall of the calibration block that were received back at the transducer. ....	97
Figure 5-11: The returned waveform of the fastest arriving echo received back at the ultrasonic transducer, for the initial pulse ranging from -50 V to -200 V. ....	98
Figure 5-12: The backwall reflection at 30 mm received back to the single GaPO <sub>4</sub> piezoelectric element, for the initial electrical pulse ranging from -50 V (min) to -200 V (max). ....	99
Figure 5-13: The backwall reflection at 50 mm received back to the ultrasonic transducer, for the initial electrical pulse ranging from -50 V (min) to -200 V (max). ....	99

## List of Figures

Figure 5-14: SNR values (in dB) for the waveforms received at the GaPO <sub>4</sub> element (blue part of the chart) and the transducer (red part of the chart); all SNR values were suitably high (>6 dB). ...	100
Figure 5-15: The frequency domain of the backwall reflection waveforms received at the manufactured transducer, for an initial pulse ranging from -50 V to -200 V.....	100
Figure 5-16: The transducer was coupled to “V1” block to determine the location of the exit-point. As a coupling medium, Ultrigel II was used. Finally, a max voltage of -200 V was applied. ....	103
Figure 5-17: Backwall at 91 mm, targeted surface at 85 mm and a backwall at 100 mm depth. ....	103
Figure 5-18: a) A-scan with three signals, one from the reflective surface at 85 mm and second and third from the backwalls at 91 and 100 mm, respectively. b) The transducer’s exit-point.....	104
Figure 5-19: The transducer coupled to “V1” block to measure the beam spread angle. As a coupling medium, couplant Ultrigel II was used. Finally, pulser voltage of -200 V was applied. ....	105
Figure 5-20: a) A-scan with two reflections from SDH & Perspex circular insert. The amplitude of the reflection from SDH is at its max value. b) A-scan with the same two reflections; however the amplitude of the reflection from SDH is here 50% (-6 dB) of its max value. ....	106
Figure 5-21: The transducer coupled to the block in the far left position with no SDH beneath. ....	107
Figure 5-22: The transducer coupled to the block above the SDH ( $d=2$ mm) at depth of 42 mm. ....	107
Figure 5-23: The transducer coupled to the block above the SDH ( $d=2$ mm) at depth of 30 mm. ....	107
Figure 5-24: The transducer coupled to the block above the SDH ( $d=2$ mm) at depth of 17 mm. ....	108
Figure 5-25: The transducer coupled to the block above the SDH ( $d=2$ mm) at depth of 4 mm. ....	108
Figure 5-26: The transducer coupled to the block in the far right position with no SDH beneath. ....	108
Figure 5-27: The setup used to test the couplant effect on the amplitude of the echo signals consisted of a normal beam transducer, a steel test-block and a digital flaw detector. ....	110
Figure 5-28: Four consecutive backwall echoes received at the commercial transducer where a different couplant was used for each of the cases: a) Ultrigel II, b) SONO 950 and c) 1100. ...	111
Figure 5-29: Ultrasonic gauging using couplant Ultrigel II (block thick. 50 mm, vel. 5920 m/s)....	112
Figure 5-30: Thickness gauging using Ultrigel II: a) time domain and b) frequency domain of the first reflection from backwall of the steel block, for the initial pulse from -50 V to -200 V. ....	112
Figure 5-31: Ultrasonic gauging using couplant SONO 1100 (block thick. 50 mm, vel. 5920 m/s)..	113
Figure 5-32: Thickness gauging using SONO 1100: a) time domain and b) frequency domain of the first reflection from backwall of the steel block, for the initial pulse from -50 V to -200 V. ....	113
Figure 5-33: Time domain comparison of the ultrasonic response when two couplants were used to facilitate the transmission of ultrasonic energy, with an initial pulse: a) -50 V and b) -200 V. .	114
Figure 5-34: Frequency domain comparison of the ultrasonic response when two couplants were used to facilitate the transmission of energy, with an initial pulse: a) -50 V and b) -200 V. ....	114
Figure 5-35: a) The transducer was coupled to block using test rig and SONO 1100. Everything was placed inside an oven. b) Detailed view of the transducer and the two thermocouples.....	115

## List of Figures

- Figure 5-36: The ultrasonic waveforms reflected from the backwall of calibration block received back at the transducer at temperatures: a) 25, b) 100, c) 200, d) 300, e) 400, f) 500 and g) 580°C. ... 116
- Figure 5-37: a) Generated voltage (mV) of the received signals at the transducer from 25°C up to 580°C. b) Calculated SNR level (dB) of the received signals in the same temperature range. ... 117
- Figure 5-38: A prototype of the commercial high temperature ultrasonic transducer. .... 118
- Figure 5-39: Ultrasonic couplant SONO 1100 for application at high temperatures..... 118
- Figure 5-40: The transducer is coupled to a P91 pipe section and ready for HT test to take place. ... 119
- Figure 5-41: The ultrasonic echoes received at the high temperature transducer at ambient temperature of 25°C (the blue trace) and at the target temperature of 580°C (the red trace). .... 119

# List of Tables

Table 2-1: Reported HT piezoelectric materials.....	23
Table 2-2: Al <sub>2</sub> O <sub>3</sub> based ceramic adhesives acquired for damping of the ultrasonic transducer .....	28
Table 2-3: Acquired electrically conductive adhesives for application at HT .....	33
Table 4-1: CETs of the materials that were used for ultrasonic thickness gauging at HT.....	70
Table 4-2: $\lambda/2$ value for the peak frequency $f_p$ derived from ultrasonic measurement on GaPO <sub>4</sub> element No 2, calculated at 25°C and at the target temperature of 580°C. ....	74
Table 5-1: Specifications of the prototype transducer for NDT at 580°C. ....	90
Table 5-2: The electrical impedance parameters of the new transducer at ambient temperature. ....	93
Table 5-3: Generated values of electrical components. ....	94
Table 5-4: The ambient temperature parameters of the transducer for operation at 580°C.....	101
Table 5-5: The highest temperature ultrasonic couplant commercially available .....	110

## Symbols and Chemical Formulas

$A$	Area (m <sup>2</sup> )
$A_0$	Voltage amplitude (V)
$AlN$	Aluminium nitride
$A_{p-p}$	Voltage amplitude peak-to-peak
$B$	Bandwidth (dB; %) or Susceptance (Siemens)
$Bi_4Ti_3O_{12}$	Bismuth titanate
$C$	Capacitance (F)
$c$	Elastic stiffness constant (Pa)
$D$	Electric displacement (C/m <sup>2</sup> )
$d$	Piezoelectric charge constant (C/N)
$E$	Young's modulus of elasticity (N/m <sup>2</sup> ); Electric field strength (V/m)
$f_a$	Anti-resonance frequency (MHz)
$f_c$	Centre frequency (MHz)
$f_l$	Lower limit frequency (MHz)
$f_p$	Peak frequency (MHz)
$f_r$	Resonant frequency (MHz)
$f_u$	Upper limit frequency (MHz)
$G$	Conductance (S)
$GaPO_4$	Gallium orthophosphate
$g$	Piezoelectric voltage constant (V·m/N)
$k$	Electromechanical coupling factor (- ; %)
$l$	Length (m)
$L$	Inductance (H)
$La_3Ga_5SiO_{14}$ (LGS)	Langasite
$La_2Ti_2O_7$	Lanthanum titanate
$Li_2B_4O_7$	Lithium tetraborate
$LiNbO_3$	Lithium niobate
$Q$	Charge (C)
$R$	Electrical resistance ( $\Omega$ )
$Re^1Ca_4O(BO_2)_2$	Oxyborate
$s$	Elastic compliance constant (pm <sup>2</sup> /N)

---

<sup>1</sup> Re = Rare earth element.

## Symbols and Chemical Formulas

$t$	Thickness (m)
$T_C$	Curie temperature ( $^{\circ}\text{C}$ )
$T_{max}$	Maximum (recommended, operating) temperature ( $^{\circ}\text{C}$ )
$T_{PT}$	Phase transition temperature ( $^{\circ}\text{C}$ )
$V$	Voltage (V)
$v$	Velocity (m/s)
$X$	Electrical reactance ( $\Omega$ )
$Y$	Admittance (S)
$Z$	Acoustic impedance ( $\text{Pa}\cdot\text{s}/\text{m}^3$ or $\text{Rayl}/\text{m}^2$ )
$Z_r$	Electric impedance at the resonant frequency ( $\Omega$ )
$Z_a$	Electric impedance at the anti-resonant frequency ( $\Omega$ )
$\alpha$	Ultrasonic beam spread angle ( $^{\circ}$ ); Coefficient of thermal expansion ( $\text{K}^{-1}$ )
$\alpha\text{-SiO}_2$	Alpha quartz
$\epsilon_0$	Permittivity of free space (F/m)
$\epsilon_{rel}$	Relative dielectric constant (dimensionless)
$\rho$	Density ( $\text{kg}/\text{m}^3$ )
$\nu$	Poisson's ratio (dimensionless)
$\lambda$	Wavelength (m)
$\omega$	Angular frequency (rad/sec)

## Abbreviations

<i>AC</i>	Alternating current
<i>ASME</i>	American Society of Mechanical Engineers
<i>CM</i>	Condition monitoring
<i>CP</i>	Ceramic paste
<i>CS</i>	Carbon steel
<i>CS</i>	Cross-section
<i>CTE</i>	Coefficient of thermal expansion
<i>DC</i>	Direct current
<i>EMAT</i>	Electromagnetic acoustic transducer
<i>FEA</i>	Finite element analysis
<i>HAZ</i>	Heat-affected zone
<i>HT</i>	High temperature
<i>NDT</i>	Non-destructive testing
<i>PA</i>	Phased array
<i>PP</i>	Power plant
<i>PRF</i>	Pulse repetition frequency
<i>PVD</i>	Physical vapour deposition
<i>PZT</i>	Lead zirconium titanate
<i>P11, P91, P22, E911</i>	Different grades of corrosion resistant high temperature steel
<i>SAW</i>	Surface acoustic wave
<i>SDH</i>	Side-drilled-hole
<i>SNR</i>	Signal-to-noise ratio
<i>SS</i>	Stainless steel
<i>UT</i>	Ultrasonic testing

# 1 Introduction

## 1.1 The industrial problem

Electricity in Europe is currently and will continue in the near future to be generated with steam turbine plants. The most common energy sources for heating the steam include conventional fossil fuels and nuclear. Generally, the higher the pressure and the temperature of the steam entering the turbine, the greater the efficiency of the electrical generator; thus the goal of both manufacturers and operators is to carry as hot and as pressurised steam as possible from the boilers to the steam turbines. As a result, a typical electrical PP (0.5 GW) has approximately 4 km of pipes operating at temperatures up to 565°C and pressures of 40 MPa [1], [2]. Continual increase in electrical power consumption has led many to reconsider nuclear power as a viable and green solution for Europe. Specifically, nuclear power plants are the second largest electricity source in Europe amounting to about 30% of total production [3]. As of February 2016, there are 185 nuclear PP units in Europe with a mean age of 27 years, where more than 75% have entered the second half of their operational lifetime [4], [5]. Plant ageing raises serious safety issues as the risk of creep and fatigue related defects is linked to total operational lifetime.

HT pipe cracks are the root of steam power failures in Europe, typically occurring every 4 years [6], and resulting in loss of human life, serious accidents, widespread power cuts and massive financial losses for the operators. According to IAEA's Reference Technology Database, such an event on a nuclear PP has an average cost of £120 million, including outage costs, emergency repair costs, insurance and legal costs [7]. Since only a single growing crack is needed to cause a major failure, they have to be inspected and monitored thoroughly. Breakdowns under these extreme operating conditions (565°C, 40 MPa) are a result of two major weld failure modes: (i) creep cracks near pipe welds – as the high pressures produce a constant hoop stress on the full length of the pipe and HT increases creep deformation, and (ii) fatigue cracks on pipe welds – as vibrations produce cyclic stresses that lead to fatigue type damage. Additionally, the areas most prone to defects include thick section pipes and headers, which are mostly composed of ferritic steels. Particularly, all over the world the most common material for steam pipes and headers is the P91 steel alloy, primarily employed for  $T \leq 593^\circ\text{C}$ . In Europe, for steam temperatures up to 620°C, E 911 steel alloy is used as it presents increased HT strength capabilities. Beyond 620°C, 12% Cr steel alloys are employed with P91 steel being the most popular choice in European PPs [8].

### 1.1.1 Creep behaviour of P91

P91 grade steel alloy, which belongs to the grade of steel martensitic-ferritic 9-12% creep-resistant steel alloys, is usually used for HT application due to its creep damage resistance. However, in some circumstances when the operating temperature and stress load are not controlled, this steel has shown sensitivity to type IV cracking in the weld region.

The use of P91 material increased significantly in the 90s when the assessment of this advanced grade of steel led to its acceptance in the ASME standardised material. Many applications related to the replacement of headers made with P11 and P22 steel alloys in power plants were reported. The use of P91 material was based on the fact that greater strength allowed increased safety margins, significant increase of component life under given creep and fatigue load, and the possibility to reduce wall thickness for tubing and piping for the same design conditions as standard steels P11 and P22. However, concern rose after several failures of P91 components within expected service time and at lower than expected temperatures [9], [10]. It was established that the failures were related to type IV cracking in the heat-affected zone (HAZ) as occurred at the West Burton coal-fired power station [9]. From the investigation of these failures, it was pointed out that although P91 steel alloy reduces the adverse effects of fatigue cracking experienced during cyclic operation of the plant, P91 steel was more prone to type IV cracking around the weld compared to conventional low alloy steel.

Type IV cracking is creep cracking which occurs in the fine-grained region on the outside edge of the HAZ next to the parent material [11]. The cracking initiates from localised formation and growth of creep voids in the “Type IV zone”. The crack can be regarded as an “unzipping” of an already creep-damaged zone. Figure 1-1 shows an example of a type IV cracking in the electron beam welded 9% Cr-1% Mo steel which can be seen adjacent to the weld.

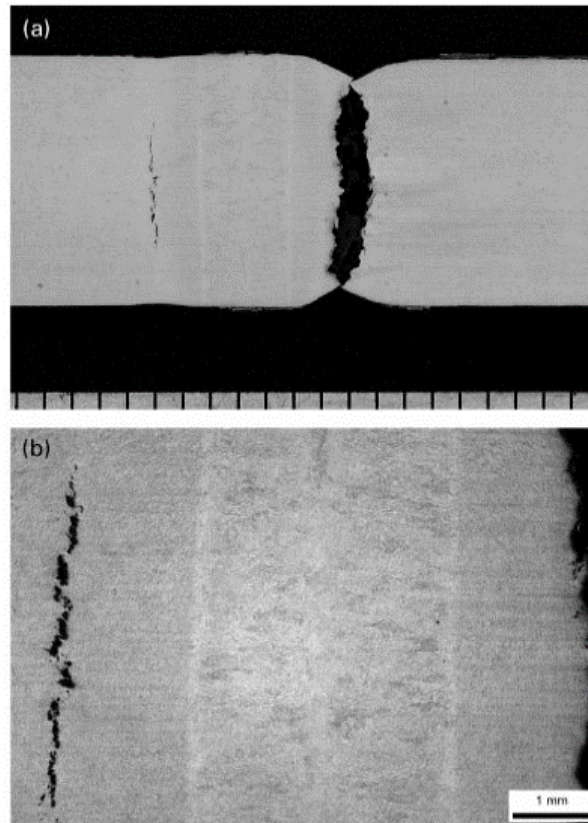


**Figure 1-1: Type IV cracking in the electron beam welded 9% Cr-1% Mo steel; a) macro and b) micro image (mm scale shown) [11].**

Even though type IV cracking is localised near a weld, this type of cracking presents the same behaviour as creep-induced damage by the mechanism of void formation and growth leading to cracking. The evolution of the creep damage is defined by the Neubauer classification [12]. This classification provides creep damage grade defined by structural assessment of the microstructure observed by metallography. Figure 1-2 shows the correlation between material behaviour under creep conditions over time (creep curve in yellow) and creep damage classification (macrograph pictures). This diagram shows the evolution of the damage and the microstructure condition over time. It can be noted that the secondary stage of isolated cavities (stage 2 a) becoming more and more dense (stage 2 b) is slow. The transition point occurs when a number of cavities take up a preferred orientation (stage 3 a) and 3 b). The evolution from advanced creep damage (stage 4 microcracks) to large creep damage (stage 5 macrocracks) progresses rapidly. Failure follows immediately after stage 5.

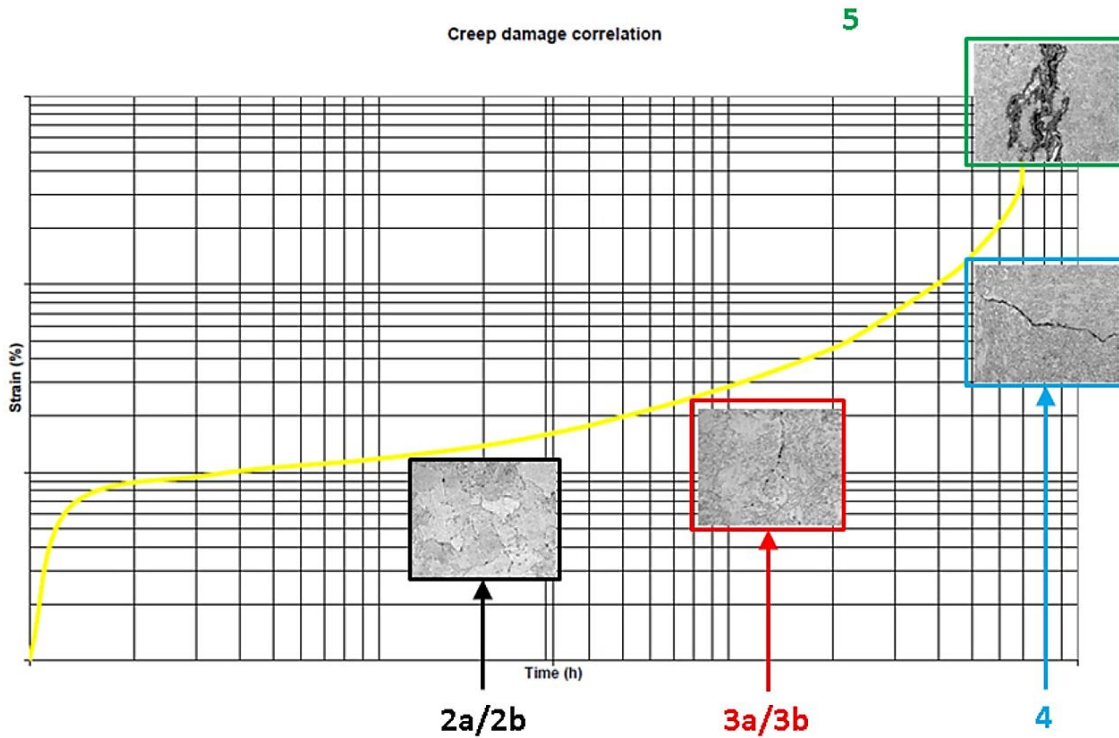


**Figure 1-2: Creep damage classification and creep curve correlation [12].**

To address the safety concerns explained above, an NDT system for operation up to the temperature of 580°C has been developed that aims to detect the creep damage at stage 4 when the cavities have joined into microcracks. The NDT system will monitor the growth of the cracks that are currently detected during regular inspections at ambient temperature, so if a crack reaches a critical size, the system will raise the alarm to the plant operator and then maintenance can take place before failure. Figure 1-3 illustrates the NDT system's concept, which consists of the following key components: i) ultrasonic transducers placed at the defective area for operation at 580°C, ii) ruggedized pulser-receiver unit, and iii) signal processing and visualisation software. The NDT system has been developed within an EC FP7 Collaborative Project under the name "HotPhasedArray" [2], where one of its key components – the ultrasonic transducer for operation at 580°C, has been entirely developed as part of this PhD work.

The reason behind the selection of 580°C as the target temperature of this work is due to thermal cycling that sometimes occurs during plant operation and that can lead to temperatures higher than the nominally rated for the pipe of interest. If the employed NDT system is not capable of withstanding higher testing temperatures than nominally rated, it is in danger of suffering a permanent damage above 565°C and thus will not be able to perform the testing anymore. As the electric furnace available for this research work allowed the maximum operation up to the temperature of 580°C, which was above the critical temperature of 565°C, this temperature was finally chosen as the target temperature of this work and thus represented a safety cushion of 15°C against the temperature overrun.

## Introduction

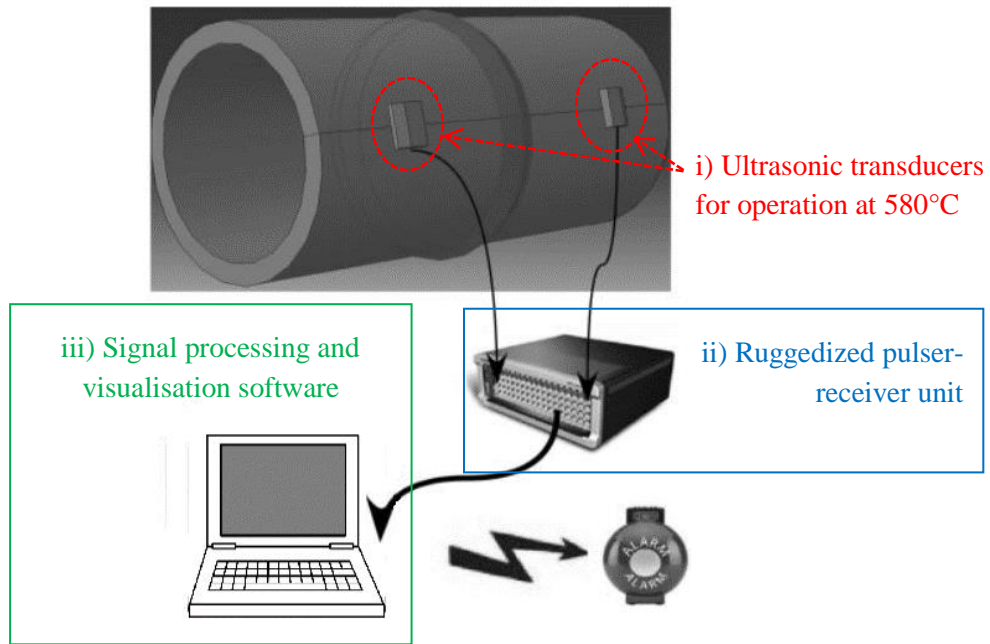


**Figure 1-3: HT NDT system developed within “HotPhasedArray” Project.**

These ultrasonic transducers use piezoelectric elements for generation and reception of ultrasound energy needed for NDT. Lead Zirconate Titanate (PZT) is the most commonly used piezoelectric for conventional ambient temperature ultrasonic transducers, but has a maximum operating temperature of around 180°C (half of the Curie temperature for PZT-5A [13]) which is not suitable for this application at 580°C. Therefore, alternative piezoelectric materials will need to be considered. A number of piezoelectric materials that can withstand operation at 580°C have been reported [14], [15].

Piezoelectric non-ferroelectric single crystals such as quartz ( $\alpha$ -SiO<sub>2</sub>), gallium orthophosphate (GaPO<sub>4</sub>), langasite (La<sub>3</sub>Ga<sub>5</sub>SiO<sub>14</sub>, LGS) and aluminium nitride (AlN) stand out because they exhibit no Curie temperature and no domain-related ageing behaviour while showing good sensitivity and ability to function over a broad temperature range, e.g. langasite crystals function up to 800°C [15].

Due to reported excellent thermal stability of most of its key material properties all the way up to 970°C (>>580°C), as well as the commercial availability of high-quality high-precision piezoelectric elements, the piezoelectric single crystal GaPO<sub>4</sub> has been selected for application in the ultrasonic transducer for long-term NDT at 580°C developed in this PhD work [16].

The three main expected benefits of this development are: (i) increase in confidence in the operational safety of nuclear and other PP; (ii) elimination of catastrophic accidents from superheated steam pipe failures; and (iii) decrease of the required shutdown time for inspection purposes.

## 1.2 Aim and objectives

The overall aim of this PhD research is to contribute to developing an early warning non-destructive testing and condition monitoring system that will utilise novel high temperature ultrasonic transducers for inspection of pipes and welds in ageing power plants to ensure their safe and reliable operation.

The specific objectives of the PhD research are as follows:

- 1) To investigate the state-of-the-art in ultrasonic transducers for non-destructive testing, and to identify their limitations for application at high temperatures up to 580°C;
- 2) To identify available and most suitable active piezoelectric and other passive materials to build an ultrasonic transducer for application at high temperatures;
- 3) To discuss and validate the key material properties of the selected piezoelectric crystal Gallium Orthophosphate up to the target temperature of 580°C;
- 4) To discuss and validate behaviour of other passive components of the transducer, such as the protective front plate, wiring and damping body, up to the same temperature level;
- 5) To integrate the selected piezoelectric crystal and other passive components within a steel housing to build a functional transducer for ultrasonic measurements at high temperatures;
- 6) To investigate performance of the novel transducer up to the target high temperature, with a series of ultrasonic thickness gauging and defect detection experiments.

## 1.3 Organisation of thesis

Chapter 2 delivers a review on ultrasonic transducers for structural integrity testing and monitoring, where limitations for their application up to 580°C are underlined. It is shown that single crystal Gallium Orthophosphate ( $\text{GaPO}_4$ ) was the most suitable piezoelectric material for application in the transducer, with a crucial contribution from its commercial availability. The crystal structure and properties of  $\text{GaPO}_4$  are also discussed. Finally, this chapter delivers a discussion of other key components of the transducer, such as metal electroding, wiring and damping body, and clearly explains the reason for their final selection in order to achieve a functional transducer for operation up to 580°C.

In Chapter 3, long-term impedance analysis of  $\text{GaPO}_4$  elements resonating at 580°C is reported. This analysis uses measured values of the resonant and anti-resonant frequencies  $f_r$  and  $f_a$ , respectively, of a piezoelectric element, together with its density and dimensions, and via known formulas derives a number of significant material properties such as thickness coupling factor  $k_t$ , piezoelectric charge constant  $d_{11}$  and elastic compliance and stiffness constants  $s_{11}^E$  and  $c_{11}^E$ , respectively. These properties are numerical measures of the efficiency, sensing capability and mechanical stability of piezoelectric

elements. The piezoelectric elements designed and manufactured from single crystal GaPO<sub>4</sub> prove to possess stable material properties when subjected to 580°C for 600 hours.

Chapter 4 delivers a long-term ultrasonic analysis of GaPO<sub>4</sub> elements coupled to steel test-blocks, performing two basic NDT tasks: (i) thickness gauging and (ii) defect detection at HT. The thickness gauging shows that piezoelectric GaPO<sub>4</sub> works as a functional transducer generating and receiving ultrasound at 580°C for 360 hours after which HT corrosion of the carbon steel test-block prevented further measurement; it is expected that the application of corrosion resistant P91 steel would allow for a much longer measurement. Further, sensitivity of GaPO<sub>4</sub> transducers to defects with simple geometry was successfully tested through measurements on a steel test-block containing an artificial defect with known geometry, at temperatures up to 580°C, keeping the defect's SNR level above 6 dB, which is high enough for practical NDT application.

Chapter 5 explains the design, manufacturing process and testing of the new ultrasonic transducer for intended operation at 580°C. Adhering to best practice, it is described how the novel transducer has been designed with the minimum number of bond-lines, which allows for a cost-effective and reliable ultrasonic transducer. The approach adopted in the development of the new transducer was to stay close to the design of a conventional transducer but to replace each of its components with appropriate HT substitutes. All HT components were integrated within stainless steel housings, together comprising a novel transducer. A critical issue, the bonding of the transducer's components, was resolved using commercial silver adhesives that were recognised as technically the best and economically the most viable bonding solution. Successful testing of the transducer showed its applicability for ultrasonic testing using a steel calibration block at ambient temperature and up to the target temperature of 580°C. Based on the results from this research work, a prototype commercial high temperature transducer was manufactured by a specialist company. The transducer was tested in a lab environment in the same setup as before, using a pipe section manufactured from high temperature grade steel P91. The transducer performed well, and enabled ultrasonic thickness gauging of the tested P91 steel pipe section up to the target temperature of 580°C.

The thesis ends with chapters "Conclusions and Future Work" and "Bibliography".

## **1.4 Summary of contributions to knowledge**

The contributions to knowledge arising from this PhD research work are described as follows:

- 1) Previously reported work indicates that the impedance measurements were successfully recorded at room temperature after a GaPO<sub>4</sub> element had been exposed to 705°C for a short period of 30 minutes. In the present research, a practical application of GaPO<sub>4</sub> elements for continuous condition

monitoring of defective parts operating at high temperatures was studied, and hence impedance measurements over a longer period were performed. The stability of a GaPO<sub>4</sub> element was tested at the intended operation at 580°C for 600 hours and found to be very stable with no deterioration in its piezoelectric performance (Figure 3-11 and Figure 3-18) observed.

- 2) In the literature it has been reported that ultrasonic measurements have been conducted up to 427°C (the heating time was not reported, but was probably short as the furnace needed to warm up). In this present research, it is shown that a GaPO<sub>4</sub> element allows ultrasonic thickness gauging to be performed at even higher temperatures, with the ultrasound waves generated, transmitted through a steel block and received back at the GaPO<sub>4</sub> element, at 580°C for 360 hours (Figure 4-16). With this, it is shown that a GaPO<sub>4</sub> element could be used for ultrasonic condition monitoring of a steel part at the operating temperature of a plant over longer periods.
- 3) The GaPO<sub>4</sub> transducers in this work are being developed to allow inspection of defective hot parts. No ultrasonic defect detection experiments using GaPO<sub>4</sub> elements have previously been reported. In the present research, a GaPO<sub>4</sub> element was used to test its defect detection capability at high temperatures. The GaPO<sub>4</sub> element was coupled to a steel block using silver adhesive, where the steel block contained a defect with simple geometry (a side-drilled hole of diameter 0.8 mm). Operated at a frequency of 3.5 MHz, the GaPO<sub>4</sub> element successfully detected the small defect at both room temperature and at 580°C (Figure 4-25). The size of the detected defect corresponds to the scale of expected damage on a reactor vessel at a nuclear plant.
- 4) Using the results of the previously characterised GaPO<sub>4</sub> elements, a novel transducer for condition monitoring at high temperatures was designed and manufactured (Figure 5-4). The transducer was tested using a pipe section manufactured from steel grade P91. The transducer performed well, and enabled thickness gauging of the tested pipe section to be performed up to 580°C (Figure 5-36). Based on the research outputs, a commercial transducer was developed by the “HotPhasedArray” consortium (Figure 5-38), together with associated signal generator and processing electronics. A consortium partner manufactured the commercial transducer, and the PhD researcher performed the initial testing up to the target temperature of 580°C (Figure 5-41).

## 1.5 List of publications

### 1.5.1 Publications

1. M. Kostan *et al.* (2016): High Temperature Gallium Orthophosphate Transducers for NDT. *Procedia Engineering* **168**, 987–990; doi: 10.1016/j.proeng.2016.11.322.

2. A. Dhutti, M. Kostan *et al.* (2016): Development of Low Frequency High Temperature Ultrasonic Transducers for In-service Monitoring of Pipework in Power Plants. *Procedia Engineering* **168**, 983–986; doi: 10.1016/j.proeng.2016.11.321.
3. M. Kostan *et al.* (2016): Assessment of material properties of gallium orthophosphate piezoelectric elements for development of phased array probes for continuous operation at 580°C. *IOP Conf. Series: Materials Science and Engineering* **108**, 1–9; doi:10.1088/1757-899X/108/1/012008.

### 1.5.2 Conference presentations

1. M. Kostan *et al.* (2017): Ultrasonic Probe using Advanced Piezoelectric Single Crystal Gallium Orthophosphate for NDT and SHM at 580°C. Talk presented at the 1<sup>st</sup> World Congress on Condition Monitoring (WCCM) in the ILEC Conference Centre, London, UK.
2. M. Kostan *et al.* (2016): Development of an early warning NDE system utilising ultrasonic arrays for continuous operation in power plants at 580°C. Talk presented at the 12<sup>th</sup> International Conference on Non Destructive Evaluation in Relation to Structural Integrity for Nuclear and Pressurized Components in Dubrovnik, Croatia.
3. M. Kostan *et al.* (2016): High temperature gallium orthophosphate transducers for NDT and monitoring purposes in nuclear power plants. Talk presented at the 55<sup>th</sup> Ann. Conf. of the British Institute of Non-Destructive Testing (BINDT) in the East Midlands Centre in Nottingham, UK.
4. M. Budimir, M. Kostan *et al.* (2016): High-temperature ultrasound NDE systems for continuous monitoring of critical points in nuclear power plants structures. Talk presented at the 11<sup>th</sup> International Conference of the Croatian Nuclear Society, former "Nuclear Option in Countries with Small and Medium Electricity Grids" in Zadar, Croatia.
5. M. Kostan *et al.* (2015): Assessment of material properties of gallium orthophosphate piezoelectric elements for development of phased array probes for continuous operation at 580°C. Talk presented at the 5<sup>th</sup> International Conference on Materials and Applications for Sensors and Transducers (IC-MAST) in Mykonos, Greece.
6. I. Vican, M. Kostan *et al.* (2015): High temperature pipe structural health monitoring system utilising phased array probes on TOFD configuration. Talk presented at the 24<sup>th</sup> International Conference Nuclear Energy for New Europe (NENE) in Portoroz, Slovenia.
7. M. Kostan *et al.* (2015): Development of phased array probes to operate in time-of-flight diffraction configuration to continuously monitor defect growth in thermal power plants. Talk presented at the 54<sup>th</sup> Annual Conference of the British Institute of Non-Destructive Testing (BINDT) in the International Centre in Telford, UK.

## 2 Literature Review

### 2.1 Chapter overview

In this chapter, a literature review is carried out on the construction of ultrasonic transducers using piezoelectric elements for generation and reception of ultrasound energy needed for NDT. First, the construction of a conventional ultrasonic transducer for application at ambient temperature conditions is discussed where the transducer is recognised as a key element of the wider ultrasonic system for NDT of critical points in PP. Then, a thorough study of its components, divided into the active piezoelectric element and other passive components, is undertaken focusing on the restrictions for its application at HT. The approach to the development of the novel ultrasonic transducer for operation at 580°C has been to stay close to the design of the conventional ultrasonic transducer, but to try to replace each of its components with appropriate HT substitutes. Advanced single crystal gallium orthophosphate is recognised as a potentially suitable piezoelectric material for the target application at up to 580°C; other substitute components such as metal electroding, protective front plate, backing body and wiring have also been selected prior to their final application in the transducer.

### 2.2 Non-destructive testing methods

Considering the wide range of applications of NDT methods, a great number of different methods and techniques have been developed, where each of the methods and techniques within a method is intended for detection of certain types of defects, for specific measurements or for inspection of the structural integrity of the material [17].

NDT methods are based on the interaction between the test-material and introduced ultrasonic energy, and on the contact between an inspection medium and the test-material, and the following classification of NDT methods is usually done: i) optical methods [18]; ii) sound and ultrasound methods [19]; iii) electro and/or magnetic methods [20]; iv) radiation methods [21]; v) penetrant methods [22]; vi) thermal methods [23]; and vii) other methods, often a combination of the others [24], [25].

Because of its great flexibility, extreme sensitivity and the reliability of the results that can be achieved, the most widely used NDT method is the ultrasonic method [17].

## 2.3 Definition of ultrasound

Ultrasound is a sound whose frequency is above the upper limit of hearing for a normal human ear, 20 kHz, whereas the frequency range for ultrasonic testing is from 100 kHz up to 50 MHz. According to the frequency, sound waves are divided into: (i) infrasound; (ii) acoustic sound; and (iii) ultrasound, as shown in Figure 2-1:

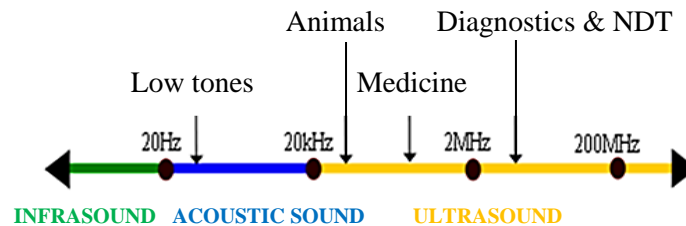


**Figure 2-1: Sound waves division by frequency [26].**

Ultrasound behaves similarly to acoustic sound, but has a much shorter wavelength. Because of this, it can be reflected from very small surfaces such as irregularities in homogeneous materials (e.g. cracks). This feature makes ultrasound useful for non-destructive testing of materials. The sources of ultrasound energy used in NDT methods of inspection are ultrasonic transducers, which, when placed on a structure for inspection or when immersed into a liquid, transmit vibration into the medium they are in contact with. Ultrasonic transducers are the essential element of the ultrasonic system for non-destructive testing.

## 2.4 Ultrasonic system for non-destructive testing

Ultrasonic waves can propagate only in the medium (they cannot propagate in a vacuum, as can electromagnetic waves). It is precisely this fact that allows detection of defects in the test structure. At the interface between two media, such as the test-structure and an irregularity/defect, ultrasonic waves will exhibit reflection and/or refraction, or other types of interactions between the medium and the transmitted ultrasonic energy. With proper interpretation of the ultrasound energy obtained after the interaction with the test-structure, one can assess the condition of the structure and the parameters of the detected defects such as defect position in the object (including the depth), orientation, size, crack surface roughness, closure and tip radius.

A schematic representation of an ultrasonic test system can be seen below in Figure 2-2. The sound waves of a given frequency distribution are sent through the examined part. If there is a flaw in the material, depending on the type of flaw, the ultrasonic waves behind it will be weakened or will not appear at all, having been reflected.

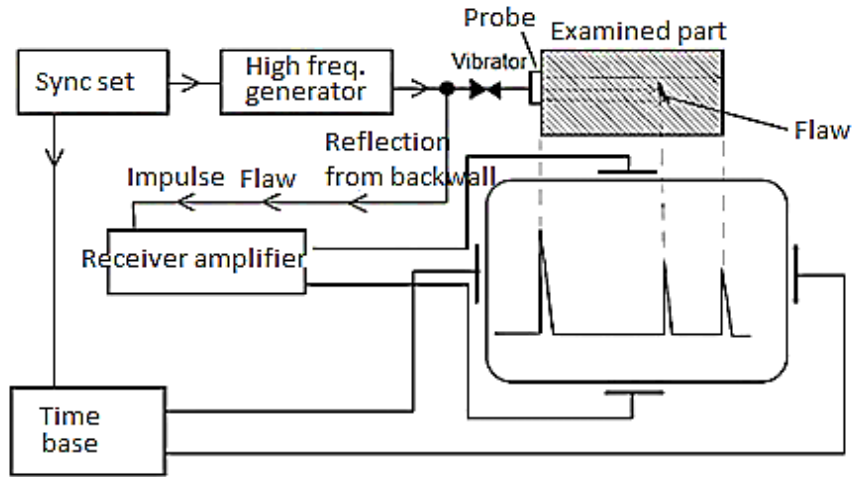


**Figure 2-2: The schematic of an ultrasonic test system [27].**

A real ultrasonic system that detects defects in the structure, records detection results and performs the analysis is shown in Figure 2-3. The system consists of: i) pulser-receiver unit; ii) ultrasonic transducer; iii) standard & reference blocks; iv) contact medium; and v) auxiliary equipment.

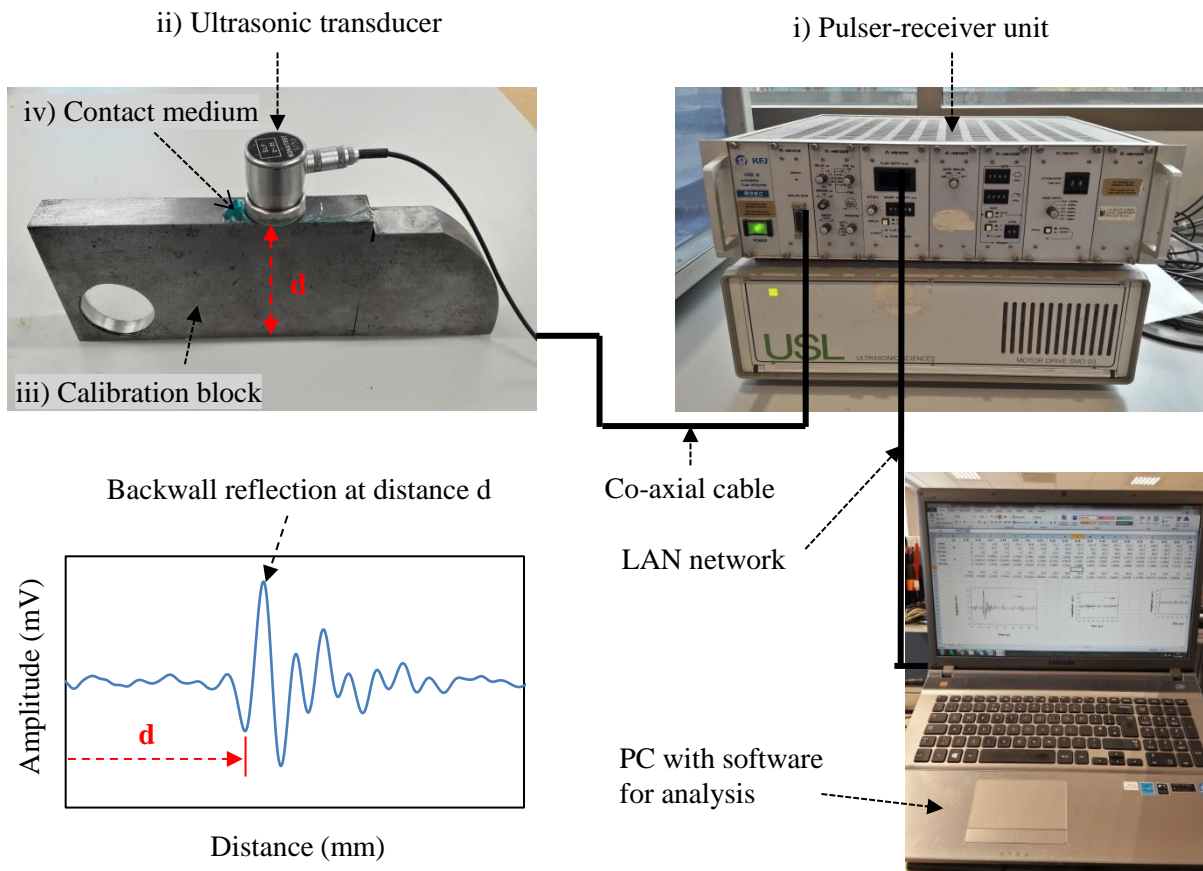


**Figure 2-3: A real-world ultrasonic test system that detects defects in the structure.**

## 2.5 Display presentation for ultrasonic flaw detection equipment

The three common ways of displaying the ultrasound test results are known as A-, B- and C-scans. Each of these provides a different way of looking at and evaluating the region of material being inspected. Today's computerised scanning systems can display data in all three scans simultaneously.

### 2.5.1 A-scan

An A-scan is a graphical representation based on the amplitude analysis of the received signal. In A-scan, the amplitude of the reflected signal is a function of the reflection depth and difference in material impedances at the reflection.

In Figure 2-4 a) one can see a test-structure with three indications. A is the reduced thickness portion of the sample, and B and C represent flaws in the structure. In Figure 2-4 b), one can see an illustration of the A-scan created by dragging a scanning transducer along the surface of the sample. In the far left position, only the initial pulse *IP* and reflection from the reduced thickness portion *A* are seen on the trace. As the transducer is moved to the right, a signal from the backwall *BW* appears later in time, showing that the sound has travelled further to reach this surface. Once the transducer is moved to a vertical position just above the flaw, signal *B* appears at time that is approximately halfway between the initial pulse *IP* and the backwall signal *BW*. Since the initial pulse signal *IP* corresponds to the front surface of the sample, this indicates that flaw *B* is about halfway between the front and back surfaces. When the transducer is vertically positioned over flaw *C*, signal *C* appears earlier since the sound travel path is shorter and signal *B* disappears since sound is no longer reflecting from it.

A-scans can be used, for example, to test welded joints of ferrite and non-ferrite materials on pressure tanks, pipelines, tanks, bridges. However, in the case where the material structure is rough, this method gives only a qualitative assessment and results can be unreliable [28].

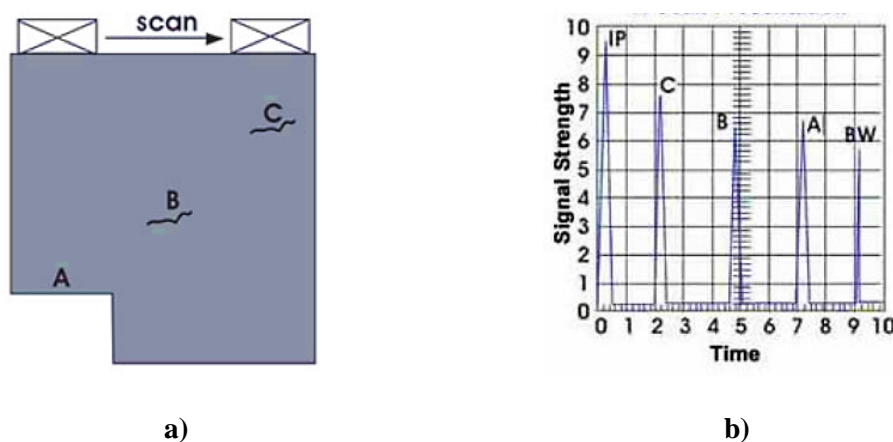


**Figure 2-4: a) Example of a test-structure with three indications A, B, and C and b) illustration of the A-scan presentation for the example structure [28].**

### 2.5.2 B-scan

B-scan is a two-dimensional graphical representation on a rectangular coordinate system, where the travel time of an ultrasound pulse is shown as a shift along the vertical axis and the movement of the transducer is shown as a shift along the horizontal axis. The B-scan shows the depth at which the reflector is located, and its approximate linear dimensions in the direction of the test. The reflected waves are presented as points of varying intensity (functions of amplitude).

In the below B-scan (Figure 2-5 b)), line A is generated while the transducer is scanned over a reduced thickness portion of the sample. When the transducer moves to the right, the backwall line *BW* is produced. Once the transducer is moved over flaws B and C, lines corresponding to the width of flaws at similar depths are produced on the B-scan. A limitation to the B-scan is that reflectors may be masked by larger reflectors nearer the surface.

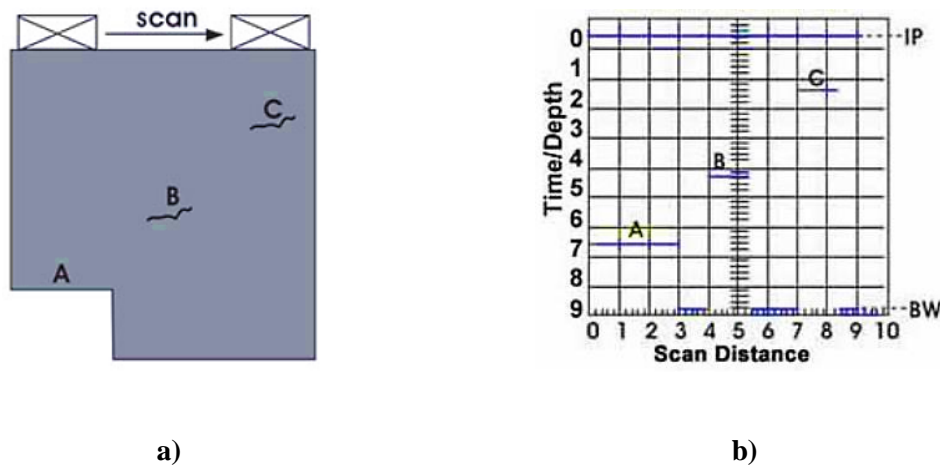


**Figure 2-5: a) Example of a test-structure with three indications A, B, and C and b) illustration of the B-scan presentation for the example structure [28].**

### 2.5.3 C-scan

The C-scan displays a plan-type view of the location and size of test specimen features. The plane of the image is parallel to the scan pattern of the transducer. A C-scan is produced with an automated data acquisition system, such as a computer controlled immersion scanner [29]. Typically, a data collection gate is established on the A-scan and either the amplitude or the time-of-flight of the signal is recorded at regular intervals as the transducer is moved over the test piece. The relative signal amplitude or the time-of-flight is displayed as a shade of grey or a colour for each of the positions where data was recorded. The C-scan presentation provides an image of the features that reflect and scatter the sound within and on the surfaces of the test piece. For an example of a test-structure with an indication and illustration of the C-scan presentation, see Figure 2-6:

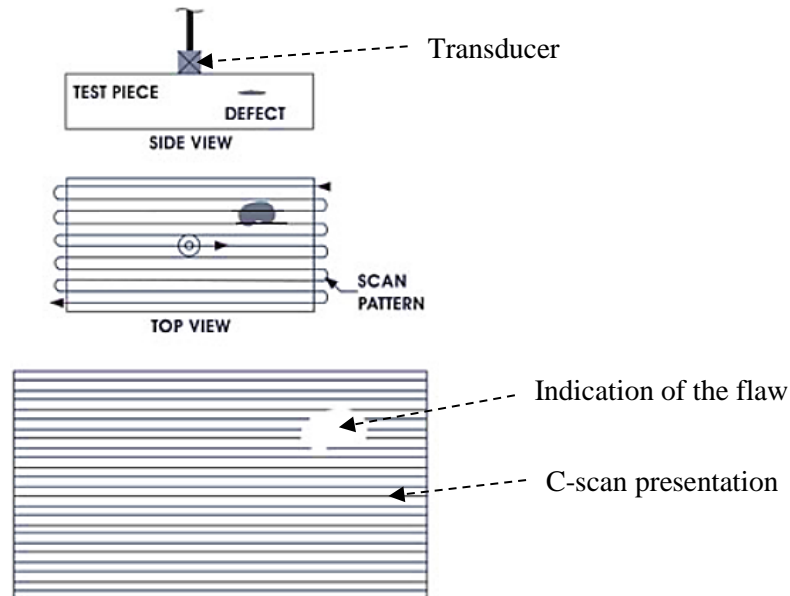


**Figure 2-6: Example of a test-structure with an indication and illustration of the C-scan presentation [28].**

To get more information about the test-piece, other more complex scans are also possible. For example, D-scan is another 2-D graphical display similar to C-scan, but provides also the information about the depth at which the indication is located. In order to get the depth of an indication, the ultrasonic system needs to measure the time between transmitting the ultrasonic waves (initial pulse) from the pulser and receiving the reflected waves (echoes) at the receiver.

## 2.6 Ultrasonic transducers

Ultrasonic transducers represent the essential element in all ultrasound non-destructive inspection procedures: whether or not some test-piece can be inspected depends mostly on them. In many cases, especially if the test-piece has a complicated geometry or an inspection is carried out under special conditions (e.g. high temperature, high pressure environment), ultrasonic inspection is possible only with a transducer having specific appropriate acoustic properties. In any case, the choice of the appropriate transducer is crucial for the quality and reliability of the ultrasonic inspection result. Today, the operation of ultrasonic transducers for non-destructive testing is based almost exclusively on the piezoelectric effect. The figures below show the structure of the four basic types of ultrasonic transducers .

In a vertical or flat beam transducer (schematics in Figure 2-7), the piezoelectric element, which converts the electrical energy into mechanical energy and vice versa, is coupled to a damping element most often referred to as "backing". The acoustic impedance of the damping element must be close to

that of the piezoelectric element, to minimise "ringing" and thereby increase the bandwidth. The second task of the damping element is to absorb the part of the ultrasonic energy from the piezoelectric element that propagates backwards [30]. The protective mask at the front of the transducer ensures that as much of the ultrasound energy as possible is transmitted into the test piece [31]. (The mask also protects the transducer against mechanical wearing, when scanning over materials that have a rough surface, or against chemical damage, when chemical aggressive fluids such "ultrasonic couplants" are used.) To ensure an efficient transmission of the ultrasound energy between the transducer and the test-piece, a means of ultrasonic coupling is normally used. There are several different methods of acoustic coupling, and three that are relevant for HT application are: dry coupling (with high pressure, high-quality finish surfaces required), liquid coupling (coupling media in a liquid state at room temperature, and solid coupling media which melt as the temperature increases) and solid coupling (soldering, diffusion bonding, ultrasonic welding, etc.) [32], [33], [34].

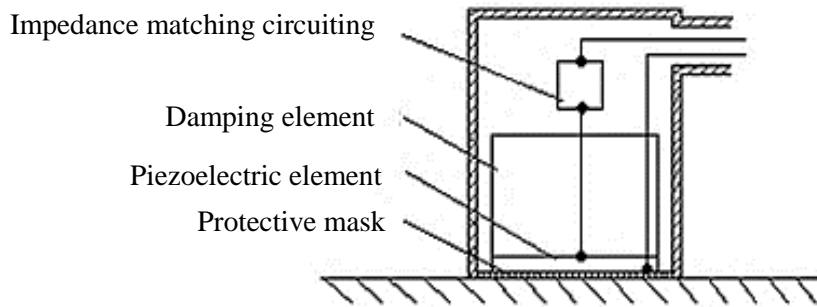


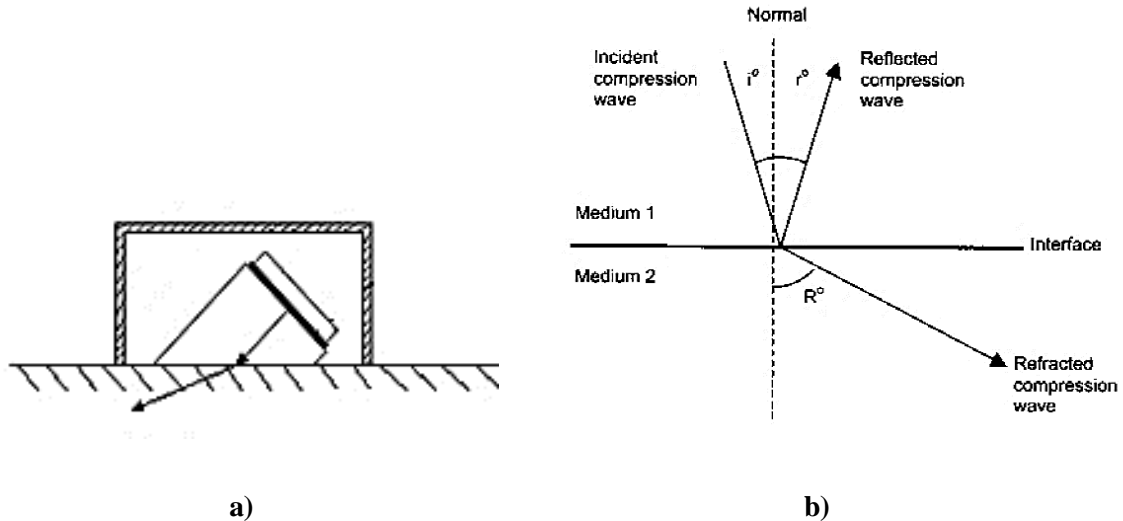
**Figure 2-7: Ultrasonic transducer with vertical or flat beam [35].**

Using vertical beam transducers, ultrasonic NDT tends to be restricted to the detection of discontinuities with surfaces parallel to the scanning surface, such as laminations and cavities. However, by angling the beam using an angular transducer [Figure 2-8 a)], it becomes possible to detect more complex weld defects such as lack of sidewall fusion and root cracks [36]. The angle of refraction  $R$ , at which the ultrasonic waves will hit the defect, can be extracted from the relationship of the angles and velocities known as Snell's Law, Eq. (2.1):

$$\frac{\sin(i)}{v_1} = \frac{\sin(r)}{v_1} = \frac{\sin(R)}{v_2} \quad (2.1)$$

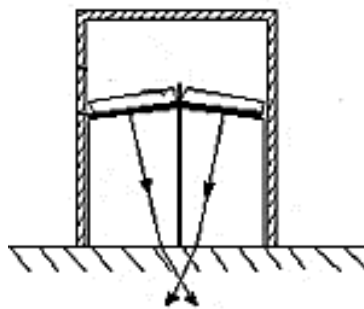
where:  $i$  = angle of incidence,  $r$  = angle of reflection,  $R$  = angle of refraction,  $v_1$  = velocity in medium 1,  $v_2$  = velocity in medium 2.

Figure 2-8 b) shows the incident, reflected and refracted angles (measured from the normal to the interface).



**Figure 2-8: a) Schematic of an angular ultrasonic transducer [35], b) diagram showing the incident, reflected and refracted angles [36].**

The dual-element transducer (Figure 2-9) consists of separate transmitter and receiver transducers with their sound fields overlapping in the examined part [37]. The piezoelectric elements are mounted onto plastic wedges, usually made of Plexiglas, Rexolite, Perspex or other plastic materials with low acoustic absorption [38]. Between the piezoelectric element and the plastic wedge, there is usually a layer of material provided for acoustic adjustment [31]. The layer provides good energy transfer between the piezoelectric element and the wedge into the test-piece. It also acts as a moderate mechanical attenuation of the piezoelectric element. All of this results in high sensitivity, very short pulses and a wide bandwidth. Therefore, such constructed angular transducers do not require a special "backing" on the back of the piezoelectric element, except when extremely short pulses are required.



**Figure 2-9: Schematic of an angular ultrasonic transducer [35].**

The construction of transducers with a delay line (Figure 2-10) generally refers to a vertical beam transducer. Here the ultrasound energy is transmitted into the test piece via an additional delay block made of low ultrasound-absorbing plastic. For such transducers, the delay line allows for an improved

resolution of flaws very near to the surface (close to the so called “dead zone” which is a part of the time-base occupied by the initial pulse) and allows thinner ranges and more accurate thickness measurements [39].

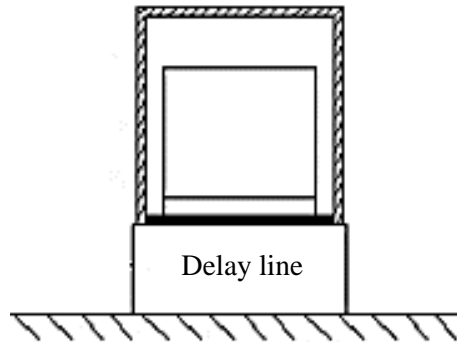


**Figure 2-10: An ultrasonic transducer with a delay line [35].**

Apart from the “dead zone”, two further important considerations are the so-called “Near Field” and “Far Field”. The near field is the distance in the material that suffers from interference and the far field is the rest of the beam beyond the near field [40]. A “theoretical” beam spread with the two areas marked can be seen in Figure 2-11 and the near field distance can be calculated from, Eq. (2.2):

$$NF = \frac{D^2}{4\lambda} \quad (2.2)$$

where  $NF$  = near field distance,  $D$  = diameter of the piezoelectric element and  $\lambda$  = wavelength.

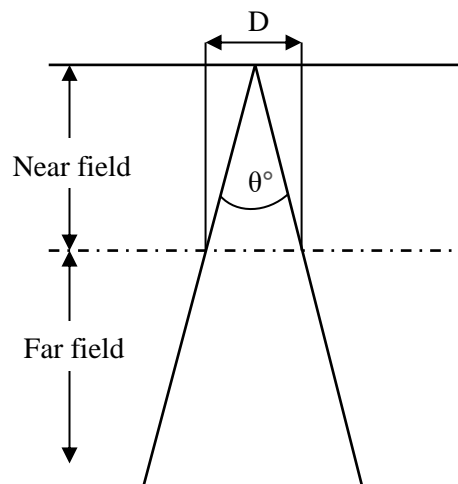


**Figure 2-11: A “theoretical” beam spread profile with “near field” and “far field” [40].**

The highest sound intensity is in the centre of the beam and gradually fades towards the edge (where there is no sound remaining). Normally, three theoretical edges of the beam are defined as: (i) the

absolute edge; (ii) the 6 dB edge (the intensity of sound has fallen to one-half); and (iii) the 20 dB edge (the intensity has fallen to one-tenth). These three edges can be expressed mathematically, where (2.3) defines the absolute edge, (2.4) defines the 6 dB edge and (2.5) defines the 20 dB edge:

$$\sin\left(\frac{\theta}{2}\right) = \frac{1.22 \lambda}{D} \quad (2.3)$$

$$\sin\left(\frac{\theta}{2}\right) = \frac{0.56 \lambda}{D} \quad (2.4)$$

$$\sin\left(\frac{\theta}{2}\right) = \frac{1.08 \lambda}{D} \quad (2.5)$$

where  $\theta$  = beam spread angle.

Depending on the specific application, the ultrasonic transducers also differ according to the size of the active piezoelectric elements, the frequency, the frequency band and the structure.

The following Figure 2-12 shows typical models of ultrasonic transducers produced in the Ultrasonic Probe Laboratory of the Institute for Nuclear Technology in Zagreb, Croatia:

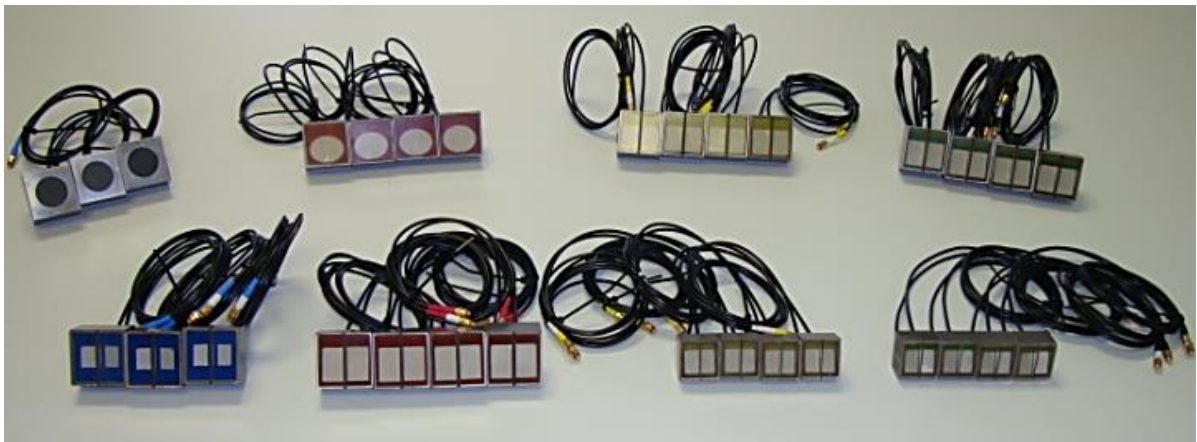


**Figure 2-12: Ultrasonic transducers for application in non-destructive testing. [Courtesy of the Ultrasonic Probe Laboratory of the Institute for Nuclear Technology in Zagreb, Croatia].**

## 2.7 Analysis of design of high temperature transducers

Conventional transducers can tolerate continuous operation up to around 50°C [41]. At higher temperatures, the transducer will ultimately suffer permanent damage due to the destruction of internal bonds in the piezoelectric element caused by thermal expansion. If the part being examined (or its environment) exhibits temperatures above 50°C, it is necessary to use high temperature transducers and

special techniques. The construction of HT ultrasound transducers depends on the selected piezoelectric element. The PZT piezo-ceramics with a high thickness coupling coefficient  $k_t$  of up to 0.5 are largely limited by their maximum operating temperatures of around 150°C (roughly half of the Curie point) [13]. In order to overcome the temperature limits of the PZT piezo-ceramics, an approach using the waveguide (protection rod for ultrasonic waves) has been developed and this approach is widely used. Various constructional solutions for waveguides are known [42]. An alternative approach is to use an ultrasonic transducer with direct contact, which must use an HT piezoelectric element (with a significantly lower coupling coefficient) and which requires a new design solution.

### 2.7.1 Approach with ultrasonic waveguide

In the construction of a waveguide, several problems need to be solved: acoustic coupling of the transducer and waveguide; transmission of the ultrasonic energy through the waveguide; etc. The material from which the waveguide is constructed must satisfy several requirements for the desired acoustic, physical (heat shock resistance, low thermal conductivity) and chemical (erosion and corrosion resistance) performance. For HT applications, e.g. molten metal flow measurement, one part of the waveguide on the transducer end is cooled sufficiently so that the transducer is not affected by the temperature of the hot end. The following Figure 2-13 shows the construction of the dual waveguide (separate transmitter and receiver of the ultrasonic signal):

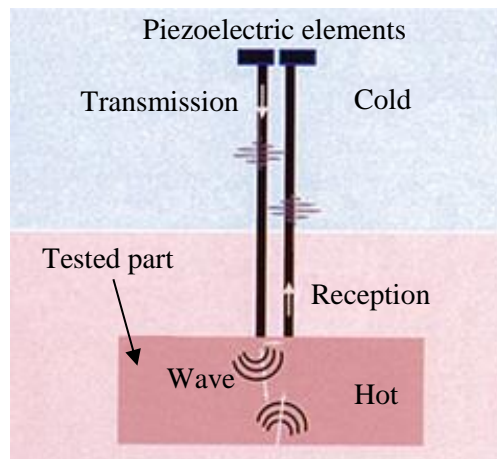


**Figure 2-13: Schematic representation of a dual ultrasonic waveguide.**

This relatively simple approach to isolating ultrasonic transducers from exposure to high temperatures has been known for over 50 years [43]. The construction of the waveguide enabled the application of ultrasonic transducers in different fields of industry and scientific research: molten metal flow measurement, monitoring of polymer extrusion and metal materials thickness at solidification, measurement of hot gas flow at high pressures, etc.

### **2.7.2 High temperature ultrasonic transducers with direct contact**

The design of ultrasonic transducers with direct contact for high temperature operation is significantly different from the design of ambient temperature working transducers. It will primarily depend on the piezoelectric element as well as on the method of coupling the element with a protective mask and a damping block. Commercial high temperature ultrasonic transducers with direct contact are offered by several companies, such as Etalon, Panametrics, Ultrasonics, SIGMA Transducers [43]. For example, all standard Panametrics high temperature ultrasonic transducers are designed to work with a duty cycle. Although the delay line isolates the inside of high temperature transducers, the recommended operating temperature range of between 90°C and 425°C should not require more than 10 seconds of hot contact (5 seconds recommended), followed by air cooling for a minimum of 1 minute [44]. Most SIGMA ultrasonic transducers can be constructed to work at higher temperatures than those initially foreseen and which are commercially available. The choice of the appropriate materials instead of epoxy and conventional soldering enables continuous operation of these transducers at temperatures up to 230°C and up to 425°C with a 15% duty cycle. Application of a delay block can slightly increase the upper temperature operational limit [45]. Some companies on the market offer special design solutions to operate at ~500°C, but only for operation in work cycles. An example is Hagisonic high temperature ultrasonic transducers with direct contact for operation at temperatures up to 500°C [46]. These transducers are used to detect defects in material at high temperatures, for high temperature thickness measurement and monitoring of the corrosion process. Specificity of these transducers is that they require special coupling medium, which must be applied very quickly for measurements with regard to the risk of drying and hardening, in which case they lose their property of high quality ultrasonic energy transmission.

The challenge in construction of transducers for operation at high temperatures is not only in finding materials that can withstand temperatures above 300°C, but also in achieving compatibility between the materials and the coupling techniques. The reason is that at high temperatures, the mutual incompatibility of different materials becomes even more pronounced. The factors such as heat conductivity, expansion coefficients, oxidation and diffusion become critical as working temperature increases and play an important role in selecting materials for the construction of HT transducers.

Finally, other methods, such as non-contact electromagnetic acoustic transducers (EMAT) and laser ultrasonic technology are also used, but in general both of these have been reported to have relatively low efficiency and detection sensitivity in comparison with the piezoelectric transducers [47], [48], [49].

## 2.8 Selection of high temperature substitutes

In the next sections, high temperature alternatives to conventional construction materials that are used to build an ultrasonic transducer are discussed and preferred solutions selected.

### 2.8.1 Piezoelectric element

The active piezoelectric element of an ultrasonic transducer is used for the generation and reception of ultrasound energy. The thickness  $t$  (m) of a piezoelectric element determines in part its fundamental resonant frequency  $f_r$  (Hz), which is directly correlated with the resolvable dimension of a defect in the structure at that frequency, Eq. (2.6), [48]:

$$f_r = \frac{v}{2t} \quad (2.6)$$

where  $v$  (m/s) is the velocity of a compression wave in the given piezoelectric material. In order to achieve maximum amplitude of the piezoelectric element vibration, the applied AC field to the piezoelectric element needs to be of the same (resonant) frequency [50].

Due to a high efficiency for electromechanical conversion (coupling factor  $k_i$ ) and sensing capability (piezo-charge constant  $d_{ij}$ ), ceramic material lead zirconate titanate (or just PZT) is the most commonly used piezoelectric today for application in conventional transducers working at ambient temperatures [15]. However, this ceramic and piezoelectric ceramics in general are usually not suitable for operation at HT. For example, PZT-5A which is considered to be an HT member of the PZT ceramics family with a Curie temperature at 365°C, is definitely not a choice for operation at 580°C. Moreover, considering a general rule of taking half of the Curie temperature as the safe upper operational temperature limit for piezoelectric materials, this further lowers the temperature limit at which this type of piezoelectric ceramics could be applied [51]. The full effect of temperature on the response of piezoelectrics is explained in section 3.3, where the main advantages of piezoelectric crystals over synthetic ceramics in the context of the HT operation will also be highlighted.

There are many piezoelectric materials, both ceramic and single crystal, that are potentially applicable up to the target temperature of 580°C, as reported below in Table 2-1. However, besides their reported material properties at HT, selection of the suitable piezoelectric material will also depend on its availability, cost and ease of manufacture. The commercial availability proved to be a limiting factor; at the time of this research. Only elements made of single crystals  $\text{LiNbO}_3$  and  $\text{GaPO}_4$  were commercially available in large quantities for application up to the temperature level stated above.

**Table 2-1: Reported HT piezoelectric materials. The materials properties are taken from: [14], [52], [53], [54], [55], [56], [57], [58], [59]. Abbreviations:  $T_C$  = Curie temperature,  $T_{PT}$  = phase transition temperature,  $T_{max}$  = maximum recommended operating temperature,  $\epsilon_{rel}$  = relative dielectric constant,  $d_{33}$  = piezoelectric charge constant,  $k_{33}$  = electromechanical coupling factor.**

Piezoelectric material	$T_C / T_{PT}$	$T_{max}$	$\epsilon_{rel}$	$d_{33}$	$k_{33}$
-	(°C)	(°C)	(-)	(pC/N)	(-)
Bismuth Titanate ( $\text{Bi}_4\text{Ti}_3\text{O}_{12}$ )	600-850	500-550	120	12-19	0.15
Lithium Niobate ( $\text{LiNbO}_3$ )	1150	650	25	6	0.23
Lanthanum Titanate ( $\text{La}_2\text{Ti}_2\text{O}_7$ )	1500	~900	46	3	0.29 ( $k_{22}$ )
Tourmaline	900	600	7.5	1.8	-
Lithium Tetraborate ( $\text{Li}_2\text{B}_4\text{O}_7$ )	917	~500	10.1	19.5	-
Aluminium Nitride (AlN)	2000	700-in air, 1100-in H and $\text{CO}_2$ atm.	-	5.6	0.2
Gallium Orthophosphate ( $\text{GaPO}_4$ )	970	700	6.1	4.5 ( $d_{11}$ )	0.16
Langasite ( $\text{La}_3\text{Ga}_3\text{SiO}_{14}$ )	>1300	700-1000	9.1	4.3-7.2 ( $d_{22}$ )	0.12-0.22 ( $k_{22}$ )
Oxyborate crystals ( $\text{Re}^*\text{Ca}_4\text{O}(\text{BO}_2)_2$ )	>1500	>1000	11-16	8-16 ( $d_{26}$ )	0.19-0.32 ( $k_{26}$ )

\*Re = Rare earth element.

### 2.8.1.1 Reported HT operation of Lithium Niobate – $\text{LiNbO}_3$

$\text{LiNbO}_3$  cement piezocomposite transducers with an area of  $10 \times 10 \text{ mm}^2$  were fabricated for ultrasonic measurements up to  $500^\circ\text{C}$  [60]. A transducer with an operating frequency of 2.6-3.3 MHz was used to demonstrate detection of artificial defects in a steel test-block using an HT couplant. Mohimi *et al.* [61] have developed a HT ultrasonic guided wave transducer for in-service monitoring of steam lines using  $\text{LiNbO}_3$  single crystals with operating frequency of 70 kHz. The transducer was shown to work up to  $600^\circ\text{C}$  where the transmitted and the received ultrasonic pulses at  $600^\circ\text{C}$  were observed to be as good as at room temperature. However, the transducer deteriorated after only 11 days and as such would not

be suitable for installation for a long-term NDT at 580°C. It is well known that LiNbO<sub>3</sub> suffers from a short lifetime at HT due to outgassing of oxygen, leading to decreased electrical resistivity and increased attenuation and intergrowth transition [14], [54]. Baba *et al.* [62] have developed two HT bulk acoustic wave transducers with frequencies of 8 MHz and 4 MHz from LiNbO<sub>3</sub> elements bonded on a stainless steel substrate using silver paste. The transducers were shown to work up to 1000°C, where stable echoes were observed from the steel substrate. However, the two transducers were heated up in a furnace at a heating rate of 1°C/min and the whole heat treatment lasted in total less than a day, which was too short for ageing of LiNbO<sub>3</sub> elements to occur.

### 2.8.1.2 Reported HT operation of Gallium Orthophosphate – GaPO<sub>4</sub>

The first industrial application of GaPO<sub>4</sub> is an uncooled miniaturised pressure transducer for internal combustion engines using the direct piezoelectric effect, in which the pressure sensitive elements are made of GaPO<sub>4</sub> single crystals. These sensors are produced since 1994 and are now well established on the market [63]. With the introduction of the new models such as GU24D or GU24DE, very high sensitivity of 45 pC/bar and maximum operating temperature of 400°C can be achieved [64]. Regarding the ultrasonic transducers application, Kazys *et al.* [65] have developed a transducer using GaPO<sub>4</sub> intended for use in imaging and measurements of nuclear reactors core which is cooled in a liquid lead-titanium (Pb/Ti) eutectic alloy with temperatures up to 250°C. Ultrasonic waveforms of the transducer with operating frequency of 5 MHz were recorded after the immersion into the alloy. Despite the achievement of a relatively low operating temperature, it was probably the first time that GaPO<sub>4</sub> was used as an ultrasonic transducer. Giurgiutiu *et al.* [66] performed a series of impedance measurement on the shear mode GaPO<sub>4</sub> samples where it was found that the samples maintained their piezoelectric activity up to 705°C. Subsequently, GaPO<sub>4</sub> samples were bonded on a steel plate in order to conduct an evaluation of their HT ultrasonic performance using the pitch-catch method. The experimental results showed that the GaPO<sub>4</sub> samples could survive exposure to temperatures up to 426°C and gave guided-wave pitch-catch signals that, in terms of their respective amplitude, differed minimally from the room temperature values. However, at 482°C the GaPO<sub>4</sub> transducers were still active but no signals were observed in the received waveform. It was believed by the authors that the reason for this was the failure of the bonding layer (aluminium oxide ceramic Cotronics 989) between the GaPO<sub>4</sub> and the steel plate. Hamidon *et al.* [67] have studied surface acoustic wave (SAW) GaPO<sub>4</sub> resonators for high frequency applications (around 434 MHz) at temperature of 600°C for 192 h and at 800°C 120 h where excellent long-term resonant frequency stability of six samples was established. The calculated relative drifts of the frequencies for the six samples were around 2 ppm/h, and the experiment was stopped after 312 hours due to oxidation of the Ti under layer of the Pt electrodes.

### 2.8.1.2.1 Crystal structure and physical properties of GaPO<sub>4</sub>

GaPO<sub>4</sub> is a transparent colourless piezoelectric single crystal belonging to the group of  $\alpha$ -quartz-type compounds that are stable at normal conditions [51]. The crystal structure of GaPO<sub>4</sub> belongs to the trigonal crystal symmetry class 32 (D<sub>3</sub>) and can be derived from the  $\alpha$ -quartz structure by replacing alternating Si-atoms by Ga and P. This leads to a doubling of the piezoelectric charge constant  $d_{11}$  from 2.3 pC/N up to 4.6 pC/N, and to the vanishing of the  $\alpha$ - $\beta$  phase transition [53], [63]. The crystal structure of GaPO<sub>4</sub> is shown in Figure 2-14 a). The number of molecules in the unit cell is 3, the same as in quartz. However, compared to quartz, the unit cell dimension into the c-direction is doubled, due to the alternating sequence of Ga and P atoms. The structure of GaPO<sub>4</sub> consists of corner-linked tetrahedra, with the oxygen atoms at the corners and gallium or phosphorus in the centre of these tetrahedra. A raw (not coated in metal electrode) GaPO<sub>4</sub> plate, as acquired from the manufacturer Piezocryst Advanced Sensorics GmbH for the purpose of this work, can be seen in Figure 2-14 b).

Other advantages over quartz are that GaPO<sub>4</sub> shows no pyroelectric effect and no outgassing, thus avoiding their retribution of the piezoelectric effect [68]. This single crystal material also possesses a high electrical resistivity with a high mechanical quality factor, which leads to decreased loss at HT and ensures sharpness of the resonance frequency [15], [66].

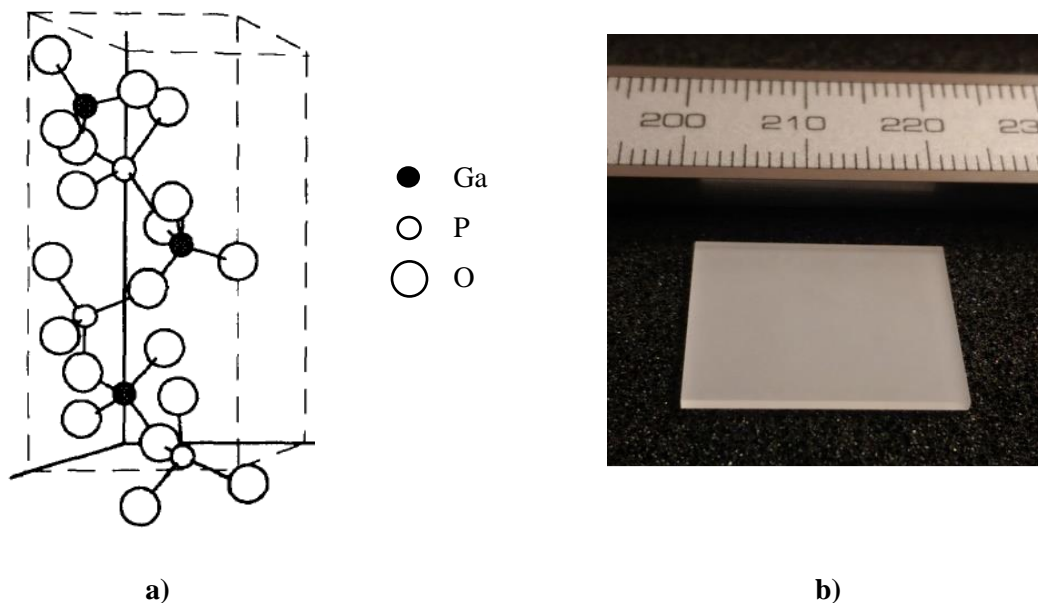


**Figure 2-14: a) Crystal structure of GaPO<sub>4</sub> [16] and b) raw GaPO<sub>4</sub> plate, as acquired from the manufacturer Piezocryst Advanced Sensorics GmbH.**

## 2.8.2 Configuration of electrodes

Thin film metal electrodes are normally deposited on the two large faces of each piezoelectric element to make them technically usable for production of transducers and other sensors. The two metal

electrodes allow wiring to be coupled and thus to deliver an AC electric field to the element or, alternatively, to obtain a generated charge signal from the.

Commonly used metals for the electrode configuration of conventional ultrasonic transducers working at ambient temperature application are silver or nickel-gold alloys. However, both of these have been reported for their severe degradation even when applied well below 500°C [69]. For this, a new non-standard solution for configuring electrodes to operate at up to 580°C will need to be established which will suit both requirements of good electrical conductivity and long-term sustainable operation at HT.

A number of electrically conductive materials have been reported as possible solutions for metal electroding of piezo-elements operating at HT, such as pure platinum, platinum-based alloys and various conductive ceramics [69]. Of these, only pure platinum coating was available from an HT electrode coating manufacturer Teer Coatings Ltd (Droitwich, UK).

According to literature, platinum electrodes show good performance in both ambient and HT operation with no surface degradation reported below 650°C [70]. Platinum is known as a metal with high melting point (1768°C), excellent conduction properties and resistance to oxidation. However, it is important to mention that some restrictions were reported for its application above 650°C due to the degradation of platinum thin films (up to 200 nm thickness) due to effects such as agglomeration and recrystallisation [71]. On the positive side, this present research does not exceed an upper temperature operational limit of 580°C. The only potential issue is the fact that the ultrasonic transducer is intended for long-term operation at 580°C, and the long-term behaviour of platinum electroding at this HT level has not been reported. Also an advantage, platinum exhibits a coefficient of thermal expansion (CTE) of  $9 \cdot 10^{-6}/^{\circ}\text{C}$  which matches well with the CET of GaPO<sub>4</sub> of  $12.78 \cdot 10^{-6}/^{\circ}\text{C}$ . For this reason, no electrode-matching layer was applied between the two materials.

The raw GaPO<sub>4</sub> plate (from Figure 2-14 b) was coated in the standard parallel electrode configuration, with an approximate thickness of the platinum layer of 200 nm, using the physical vapour deposition (PVD) magnetron sputtering technique [72].

### **2.8.3 Damping mass**

The damping mass (damping body) with its specific chemical composition and shape dampens unwanted vibrations of the piezo-element. The achieved damping will be greater, the closer are the values of the acoustic impedances of the piezoelectric element and damping mass. Maximum damping is achieved when these two are equal (no reflection) [17].

## Literature Review

The required acoustic impedance of the damping mass is achieved by adding a powder of high density to the damping mass composition e.g. for conventional application at ambient temperatures, by adding tungsten powder to an epoxy resin [73]. Further, at the ends of the damping mass, various slots and bumps are usually engraved, which further prevents the reflection of generated ultrasound energy back towards the piezo-element and the contact surface of the test-material [1]. The amount of damping applied to the back face of the piezo-element determines the ultrasonic pulse duration and consequently the resolution of the inspection that can be achieved with the given transducer [76].

Conventional ambient temperature transducers use epoxy resins for the design of the damping body, and it is possible to find some epoxy solutions performing well up to 180°C [77]. This temperature is well below the target of 580°C and thus an alternative solution must be devised.

A number of materials, such as soft ceramics, sintered metals, carbon and different cuts from austenitic welds have been studied for possible application as damping bodies and acoustic insulators for application at HT [78]. It was found that it was very hard to achieve simultaneous matched acoustic impedance and good ultrasonic attenuation. Of the tested materials, only aluminium oxide ( $\text{Al}_2\text{O}_3$ ) based ceramics, with a relatively high specific acoustic impedance of 40.6 MRayl, provided good damping to the piezoelectric elements manufactured from ceramic PZT-5A with a specific acoustic impedance of 33.7 MRayl, significantly reducing unwanted reflections. However, the ultrasonic tests were done only at ambient temperature and using conventional piezoelectric ceramic PZT-5A. The piezoelectric single crystal that is used in this work –  $\text{GaPO}_4$  – exhibits much lower specific acoustic impedance (15.6 MRayl) which imposes the question of how well these two materials will match. The explanation offered for the good damping properties of  $\text{Al}_2\text{O}_3$  based ceramics was that its porosity acts as a scatterer for the ultrasound energy, which is then further attenuated by the ceramic material itself. McNab *et al.* [1] have also speculated that  $\text{Al}_2\text{O}_3$  based ceramics are potentially good damping materials for piezoelectric transducers, but no ultrasonic experiments at HT have been reported. Finally, Mohimi [79] showed that a damping body made of  $\text{Al}_2\text{O}_3$  and vacuum brazed to a  $\text{LiNbO}_3$  piezoelectric element resulted in good ultrasonic damping of the piezoelectric element, with the transducer tested at 580°C. However, this transducer was a shear-type and intended for an ultrasonic guided wave inspection of steel pipes, while the  $\text{GaPO}_4$  elements used in this research are of compression -type and intended for bulk inspection of pipes/thick plates.

Of other materials, Parks *et al.* [80] have tested sintered porous carbon-carbon composite with low acoustic impedance. The same damping material was shown to be a limiting factor for operation at 550°C due to considerable loss of mass, which in turn reduced the coupling pressure and consequently reduced the signal amplitude. Further, they have done some tests on aluminium foil that did show better performance than the carbon-carbon composite, but more conclusive tests have been planned for future.

Since it was more feasible to obtain Al<sub>2</sub>O<sub>3</sub> ceramic than the other discussed materials, two ceramic adhesives, Ceramabond 569 [81] and Ceramabond 503 [82] have been acquired for study. Ceramabond 569 is an adhesive intended to bond and coat platinum resistance heaters to aluminium oxide cores for applications up to 1650 °C [83], and as such is potentially suitable for application to the electroding of the GaPO<sub>4</sub> transducers. The alternative was an adhesive from the same manufacturer, Ceramabond 503 that is rated for even higher temperatures, up to 1760°C [84]. The reported properties are listed in Table 2-2. Considering the adhesives will be applied directly to the platinum coating, good matching CTEs of the respective adhesives of 7.6·10<sup>-6</sup>/°C and 7.2·10<sup>-6</sup>/°C, to that of platinum (9·10<sup>-6</sup>/°C) should minimise the thermally induced stress on their bond-line.

**Table 2-2: Al<sub>2</sub>O<sub>3</sub> based ceramic adhesives acquired for damping of the ultrasonic transducer.**

Ceramic adhesive	Supplier	Base	Heat cure	Max temp.	CTE
-	-	-	(°C, h)	(°C)	(10 <sup>-6</sup> /°C) @ 20°C
Ceramabond 569	Aremco Inc.	Al <sub>2</sub> O <sub>3</sub>	93, 2	1650	7.6
Ceramabond 503			93, 2; 260, 2; 371, 2	1760	7.2



**Figure 2-15: Ceramic adhesives acquired for the ultrasonic transducer manufacture.**

### 2.8.4 Protective front plate and/or wedge

The protective front plate protects the piezoelectric element from mechanical damage, wear and corrosion that happen during contact testing. Further, the protective plate adjusts the transfer of acoustic energy from the piezoelectric element to the test-material, in which case it is also called the “matching layer” [76].

The thickness  $t$  (m) of the protective front plate is very important. It is made to be one quarter of the wavelength at the fundamental resonant frequency  $f_r$  (Hz) for the velocity of sound  $v$  (m/s) in the material of protective front plate and can be calculated from Eq. (2.7):

$$t = \frac{v}{4f_r} \quad (2.7)$$

This thickness of the protective plate ensures ultrasonic waves which are undesirably reflected back to the piezoelectric element, are out of phase in order to cancel each other through the principle of superposition [31]. Figure 2-16 shows a schematic of the interface between the piezoelectric element, one of the metal electrodes and the protective front plate.

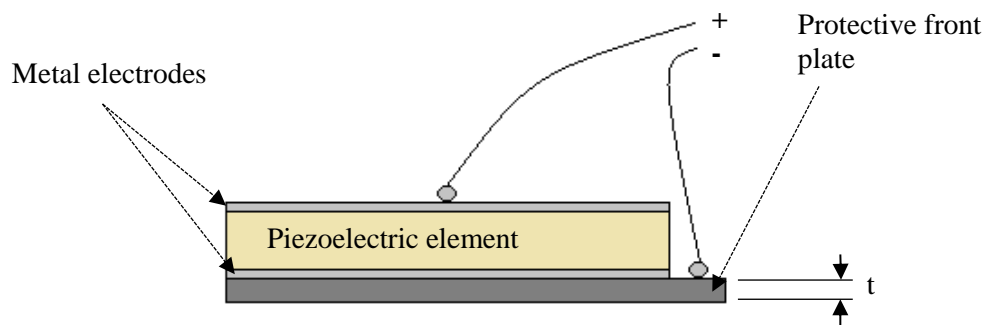


**Figure 2-16: Schematic of the interface between the piezoelectric element, one of the metal electrodes and the protective front plate. The thickness of the bonding medium (adhesive) between the metal electrode and the protective front plate is taken to be negligible.**

The protective front plate is normally made of a material with acoustic impedance between that of the piezoelectric element and that of the test-structure [85]. In conventional ultrasonic transducers, where the piezoelectric element is normally made of PZT ceramic, the specific acoustic impedance value for e.g. PZT-5A will be 33.7 MRayl. On the other hand, the specific acoustic impedance of the steel test-sample will be around 47 MRayl. In the discussed case, the material that is normally used for the design of the protective front plate is ceramic aluminium oxide (alumina) –  $\text{Al}_2\text{O}_3$  with the specific acoustic impedance value of approx. 41 MRayl, which is roughly a middle value. Besides this, alumina further exhibits an excellent resistance to mechanical damage and wear, and is not sensitive to corrosion [86]. Further, as this ceramic material comes with a very high melting point of around  $2070^\circ\text{C}$ , it also presents as a serious candidate for the intended application at  $580^\circ\text{C}$ . However, it is important to mention that application of this non-conductive ceramic for design of the protective plate also requires a very complex earthing method to be used, as a conductor wire cannot be directly soldered (or bonded with high temperature silver epoxy) to it. This does not pose a big problem when designing conventional ultrasonic transducers, but it could be an issue when designing the HT transducer.

An alternative solution is to make the protective front plate from stainless steel, which is the second most frequently encountered material used in the design of the protective front plates [76]. Similar to alumina, this steel material has a melting point that is well above the target temperature of 580°C and shows excellent mechanical wear and corrosion resistance. The advantage of steel over alumina is that it allows soldering of the conductor wire directly to the protective plate, which significantly simplifies the design of the transducer. However, the suitability of stainless steel will also depend on the choice of piezoelectric materials for operation at 580°C. As explained before, it is very important to achieve the right acoustic impedance matching between the piezoelectric element and the test-structure as this enables maximum transfer of acoustic energy into the test-material and results in a clearer picture of the structural integrity of the inspected piece. The percentage of the incident acoustic energy that is transmitted into the second material can be calculated from Eq. (2.8):

$$E=100-R \quad (2.8)$$

$R$  can be calculated from Eq. (2.9):

$$R = \left( \frac{Z_1 - Z_2}{Z_1 + Z_2} \right)^2 * 100\% \quad (2.9)$$

where  $E$  is the emitted energy,  $R$  is the reflected energy, and  $Z_1$  and  $Z_2$  are the acoustic impedances of two materials.

Finally, if one wants to transmit ultrasonic energy from the ultrasonic transducer to the test-piece at a desired angle different from normal and in accordance with Snell's Law, an ultrasonic wedge is normally used. Rexolite (up to 100°C) and Plexiglas (up to 160°C) are the most commonly encountered materials for the design of the ultrasonic wedges [35]. However, if such a wedge is required in this work, alternative HT materials will need to be considered along with the desired incident angle, method of attachment to the ultrasonic transducer, etc.

### 2.8.5 Acoustic insulator

Similar to the damping mass, the acoustic insulator is fitted between the housing and the piezoelectric element to absorb the ultrasonic energy generated from the sides of the element and thus prevent its unwanted “ringing”. Moreover, it is usually made of the same material as the damping mass, which means that all considerations in section 2.8.3 can be applied to the design of the acoustic insulator [87].

### **2.8.6 Housing**

Once all the key components of the transducer are selected, they are normally integrated within a housing to achieve a robust device for application in practice. The shape and size of the housing will depend on the given testing procedure. Consideration of different configurations of housing will be required if NDT personnel use the transducer manually, or if the transducer is integrated within a robotic arm for automated inspection. Secondly, it is good practice to design the housing to be impermeable, even if not intended for immersion testing, because penetration of a couplant medium can compromise the electrical integrity of the transducer [88]. Finally, considering the highly corrosive environment the majority of testing transducers are exposed to, corrosion resistant stainless steel proves to be a good choice for the housing construction of most commercial ultrasonic transducers in the market today. Its high stiffness and strength at temperatures well above the present target temperature level will provide a robust housing also for the HT transducer under study.

### **2.8.7 Wiring and co-axial connector**

Conductor wiring and co-axial connectors are used in transducers to effect communication between the transducer and the pulser-receiver unit. Their design should enable excellent conductor properties but also achieve lightweight, reduced size and increased flexibility of transducer handling [89].

According to literature, nickel is the material of choice for application in sensors working in harsh environments, as it shows the best balance of key properties for electrical performance at HT [43]. The conductivity of nickel is adequate and it has excellent resistance to oxidation and corrosion [90]. For this, pure nickel glass braided cable was acquired from Heatsense Cables Ltd, as it was reported to withstand continuous operation at 600°C, and can be used for work in cycles up to max 700°C [91]. Further, glass braid of the acquired cable will provide an additional protection from the heat exposure.

In terms of the wiring, it was decided that one nickel conductor will be bonded to the Pt electroding of the back face of the GaPO<sub>4</sub> element and the second conductor will be grounded to the steel protective plate. The two conductors will lead outside of the transducer to the pulser-receiver unit. Thus, co-axial connectors normally attached to the transducer's housing will not be necessary in the proposed design.

### **2.8.8 Electrical impedance matching circuiting**

Matching circuiting is used to overcome the problem of impedance mismatching between the excitation source (the pulser-receiver) and the transducer [92]. The high excitation voltage of the pulser-receiver (up to 200 V or more) allows the improvement of signal-to-noise ratio, however if no matching circuiting is used, the electric power reflected back to the high impedance transducer will reduce its

efficiency, and in a long-term can even cause permanent damage [93]. Transducers for NDT and condition monitoring normally include a tuning circuit inside the transducer housing. A common procedure is to introduce an inductance in parallel or series. The objective of this inductor is to compensate the capacitive effect of the transducer [92]. As the tuning circuit is placed inside the housing, for the high temperature application being developed in this research the electrical components need to withstand temperatures up to 580°C. As commercially available components can be used up to approx. 85°C, and some attempts of solving the electronics problem up to 300°C have been reported [94], development of internal electrical circuits was not feasible. However, electrical matching of high impedance GaPO<sub>4</sub> transducers to low impedance pulser-receiver is thoroughly discussed in section 5.4.1, where it is emphasised that for more efficient operation of the GaPO<sub>4</sub> transducer (improved SNR level), an external matching circuiting will need to be developed as part of proposed future work.

### **2.8.9 Bonding of materials**

In the transducers operating at ambient temperatures, the conductor wiring is normally soldered to two large faces of the piezo-element or one large face and the metal housing before application of the damping body. This is done using a solder that melts at low temperature, such as e.g. 96SC Tin/Silver/Copper with multicore flux (Flux type Crystal 400) [96]. For HT operation, solder alloys such as 61/24/15 Silver/Copper/Indium with melting temperatures above 600°C are available [97]. However, in practice, as with other advanced bonding methods such as brazing, diffusion bonding or cementing, these all require very expensive apparatus and complex bonding processes and procedures, as explained in [43]. On the other hand, another, much simpler and readily available bonding method has appeared as an alternative – adhesive bonding – and a number of adhesives operating up to the required temperature level were available on the market.

A number of electrically conductive adhesives for application at HT are offered, and some of these, based on their upper temperature operational limit, are listed in Table 2-3. For example, Elecolit 3653 [98] and Duralco 124 [99] are used in standard production of ultrasonic guided wave transducers for non-destructive testing up to 125°C, commercially offered by PI Ltd [100]. The silver adhesive PyroDuct 597-A was used in transducer manufacture, where it coupled the top electrode of a lithium niobate piezo-element with a mineral insulated cable, and the piezo-element to the steel substrate (front plate). The ultrasonic measurements with the lithium niobate transducer were done all the way up to 1000°C, thus outperforming this adhesive's datasheet maximum operating temperature value [62], [101]. As an alternative to these three silver-based adhesives, graphite-based Resbond 931C was also purchased for study. This graphite adhesive is characterised by its very high datasheet reported upper operational temperature limit of 1371°C [102]. Considering the target temperature level of this research of 580°C, an application of this graphite adhesive would mean a security factor of almost 2.5.

**Table 2-3: Acquired electrically conductive adhesives for application at HT [98], [99], [101], [102].**

<b>Adhesive</b>	<b>Supplier</b>	<b>Base</b>	<b>Heat cure</b>	<b>Max Temp.</b>	<b>CTE</b>
-	-	-	(°C, h)	(°C)	(10 <sup>-6</sup> /°C) @ 20°C
Elecolit 3653	Panacol GmbH	Silver	110, 0.3	<b>180</b>	18
Duralco 124	Cotronics Corp.	Silver	150, 4	<b>343</b>	18
PyroDuct 597-A	Aremco Inc.	Silver	93, 2	<b>927</b>	17.28
Resbond 931 C	Cotronics Corp.	Graphite	Air dry, 2-4	<b>1371</b>	7.38

### 2.8.10 Contact coupling medium

The conventional ultrasonic transducers are normally used in contact inspection testing where a liquid coupling medium (water, oil, or special gel, called couplant) is used to facilitate transmission of the ultrasound energy between the transducer and the test-material. The most commonly used liquid couplant today is Ultrigel II (from Magnaflux) with the operating temperature limit at 99°C [103].

There are three different concepts of acoustic coupling at HT: (i) dry coupling with high pressure; (ii) liquid (fluid) coupling; and (iii) solid coupling [78]. Unlike the shear transducers used in ultrasonic guided wave testing (such as ones already mentioned and commercially offered by PI Ltd [100]), the compression wave transducers used in standard ultrasonic testing and developed in this work are affected adversely by the load applied, where the load reduces the elongation of the vibrating piezoelectric element. This consequently reduces the amplitude of the generated electrical signals [104]. For this reason, dry coupling with a high pressure is not a desired method of coupling in ultrasonic non-destructive testing. For liquid coupling, HT couplants such as Sono 950, 1100 and 1200+ have been identified. According to the datasheets, Sono 950 can operate up to 385°C (for a few minutes), and has an auto ignition temperature at 560°C. Sono 1100 can be used for defect detection from 371°C up to 482°C and has an auto ignition temperature of 626°C, while Sono 1200+ can withstand even higher temperatures [105]. After an extensive literature review, only one report of application of Sono 1100 in a HT environment up to 500°C has been found [80]. However, the HT couplant was used only as a facilitating medium for an experimental comparison among three different HT piezoelectric materials, and not for a practical measurement with an ultrasonic transducer. Thus, if for any reason couplants Sono 950, 1100 and 1200+ fail to perform up to the temperature of 580°C, a last resort will be the aforementioned solid coupling, which assumes permanent attachment of the ultrasonic transducer to the test-structure using one of the adhesives listed in Table 2-3.

## 3 High Temperature Impedance Analysis of GaPO<sub>4</sub> Elements

### 3.1 Chapter overview

In this chapter, the piezoelectric effect of GaPO<sub>4</sub> at HT is analysed via impedance measurements. As there were no commercially available devices to allow impedance measurements up to 580°C, a special test-rig was built to enable all GaPO<sub>4</sub> elements to be tested in the same manner. Two sets of impedance measurement are reported: (i) analysis from room temperature up to the target temperature of 580°C; and (ii) at a constant temperature of 580°C over a period of 600 hours. The values of the resonant and anti-resonant frequencies  $f_r$  and  $f_a$ , respectively, taken from impedance characteristics, were used to derive a set of material properties: (i) thickness coupling factor ( $k_t$ ); (ii) piezoelectric charge constant ( $d_{11}$ ); and (iii) compliance and stiffness constants, ( $s_{11}^E$  and  $c_{11}^E$ ), respectively. These four properties represent numerical measures of the efficiency of electromechanical conversion, sensing capability and mechanical/thermal stability of piezoelectric elements. As properties from 25°C up to 580°C were available in the literature, it was possible to compare these with the measured values to validate the experimental setup and procedures used. On the other hand, it is believed that the results derived at 580°C over 600 hours are the first reported for a long-term operation of GaPO<sub>4</sub> at HT and that they confirm this piezoelectric single crystal as a good candidate material for further development of a high temperature transducer.

### 3.2 Introduction

#### 3.2.1 Definition of electrical impedance

Electrical impedance is an important parameter used to characterise electronic circuits, components, and the materials used to make components (such as piezoelectric resonators). Electrical impedance ( $Z$ ) is defined as the total opposition a device or electrical circuit offers to the flow of an alternating current (AC) at a given frequency, and is represented as a complex quantity, which is graphically shown on a vector plane. An impedance vector consists of a real part (resistance,  $R$ ) and an imaginary part (reactance,  $X$ ) as shown in Figure 3-1.

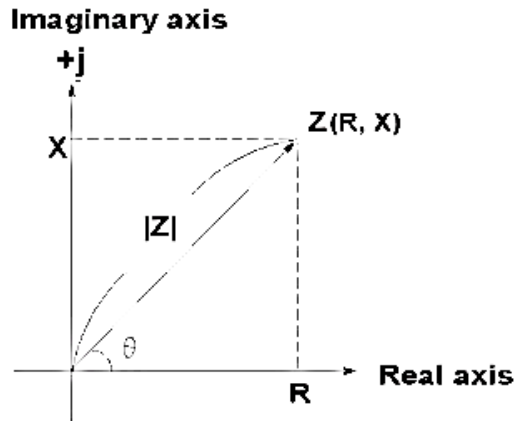


**Figure 3-1: Impedance ( $Z$ ) consists of a real part ( $R$ ) and an imaginary part ( $X$ ) [106].**

The electrical impedance can be expressed using the rectangular-coordinate form where:

$$Z = R + jX \quad (3.1)$$

or in the polar form as a magnitude and phase angle:

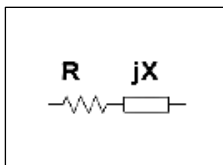
$$Z = |Z| \angle \theta \quad (3.2)$$

Further, it is possible to show the mathematical relationship between  $R$ ,  $X$ ,  $|Z|$ , and  $\theta$ :

$$\begin{cases} R = |Z| \cos\theta \\ X = |Z| \sin\theta \end{cases} \quad (3.3)$$

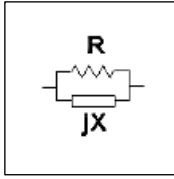
$$\begin{cases} |Z| = \sqrt{R^2 + X^2} \\ \theta = \tan^{-1} \left( \frac{X}{R} \right) \end{cases} \quad (3.4)$$

The unit of impedance is the ohm ( $\Omega$ ). Electrical impedance is a commonly used parameter and is useful for representing a series connection of the real component (resistance  $R$ ) and imaginary component (reactance  $X$ ), because it can be expressed simply as a sum:



$$Z = R + jX$$

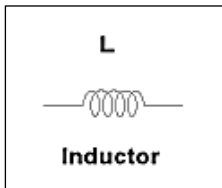
For a parallel connection:



$$Z = \frac{jRX}{R+jX} = \frac{RX^2}{R^2+X^2} + j \frac{R^2X}{R^2+X^2} \quad (3.5)$$

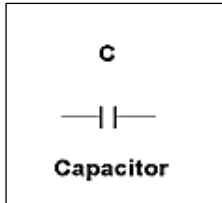
In this case, using the reciprocal of impedance or admittance  $Y$  is mathematically simpler. The unit of admittance is the Siemen ( $S$ ), and mathematical expressions and explanations of admittance and to it associated physical quantities such as conductance  $G$  and susceptance  $B$ , can be found e.g. in [106].

The imaginary component, reactance  $X$ , takes two forms: inductive ( $X_L$ ) and capacitive ( $X_C$ ). By definition,



$$X_L = 2\pi fL \quad (3.6)$$

and



$$X_C = \frac{1}{2\pi fC} \quad (3.7)$$

where  $f$  is the frequency of interest,  $L$  is inductance, and  $C$  is capacitance.  $2\pi f$  can be substituted for by the angular frequency  $\omega$  (omega) to represent:

$$X_L = \omega L \quad (3.8)$$

and

$$X_C = \frac{1}{\omega C} \quad (3.9)$$

Expressions (3.1) to (3.9) are used in calculating the  $L$ ,  $R$  and  $C$  parameters required to electrically match high impedance transducers such as the GaPO<sub>4</sub> to low impedance pulser-receiver instruments and BNC cabling (see section 5.4.1).

### 3.2.2 Measuring electrical impedance

Because electrical impedance is a complex quantity, to find it, at least two values must be measured. Modern impedance measuring instruments, such as the impedance analyser used in this research, measure the real and the imaginary parts of an impedance vector and then convert them into the desired parameters such as  $|Z|$ ,  $\theta$ ,  $R$ ,  $X$ ,  $C$ , and  $L$ . The automated impedance analyser that will be used allows a measurement to be performed by merely connecting the component such as the GaPO<sub>4</sub> piezoelectric elements to the analyser. The measured values, together with their visual representation (the impedance curves) then can easily be transferred to a PC.

### 3.2.3 Measuring impedance of piezoelectric elements

Impedance measurement of a piezoelectric element is an important contribution to the element's performance. The impedance mismatch between the small piezoelectric element, and (BNC) cable and pulser/receiver instrument is an important consideration, especially for applications with centre frequency below 4 MHz [107]. Furthermore, by extracting the values of resonant and anti-resonant frequencies from the recorded impedance response of a piezoelectric element, it is possible to derive a set of piezoelectric and electro-mechanical properties, which are useful parameters for discussing the element's sensing capability and thermo-mechanical stability when, for example, the element is operated within a high temperature environment [108]. The typical impedance response of a piezoelectric element over a frequency range is shown in Figure 3-2. At the resonance frequency  $f_r$ , when the impedance is at its minimum, the piezoelectric element vibrates most readily, and most efficiently converts the electrical energy input into mechanical energy – it is most efficient as a transmitter. On the other hand, at the anti-resonance frequency  $f_a$ , when the impedance is at its maximum, the piezoelectric element most efficiently converts the mechanical energy back into electrical energy – it is most efficient as a receiver. In order to get the best piezoelectric response from a piezoelectric element, it has to be used between these two characteristic frequencies [109].

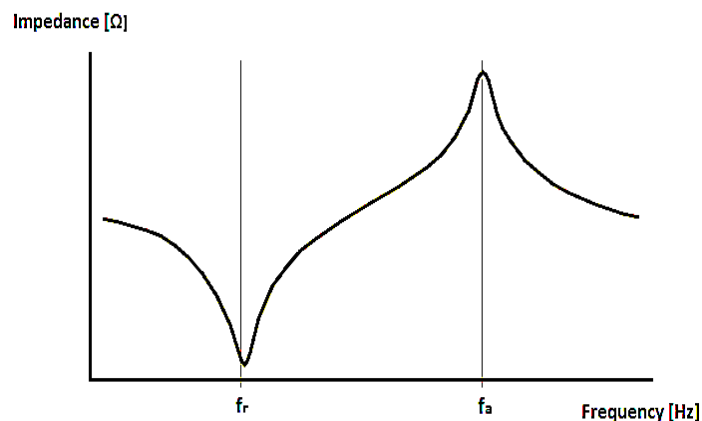


**Figure 3-2: Typical impedance response over a frequency range for a piezoelectric element.**

### 3.3 Effect of temperature

HT application of conventional piezoelectric materials such as piezoelectric ceramics is limited due to phase transitions, which in general lead to instability of the electromechanical properties with temperature and/or with regard to their respective Curie temperature above which they depolarise and lose their piezoelectric effect [13]. For example, the discussed piezoelectric ceramic PZT-5A exhibits a Curie temperature of around 365°C, and its applicability at HT is further reduced by the rule of taking half of the Curie temperature as a safe upper operational temperature limit [13], [51]. Additional issues that conventional piezoelectrics face at HT include decreased resistivity leading to increased conductivity, which contributes to charge drift interfering with piezoelectrically induced charges, increased attenuation of acoustic waves and dielectric losses with temperature and chemical decomposition, which accounts for excessive conductive ions and viscous damping [14], [52]. Finally, as the macroscopic piezoelectric effect in piezoelectric ceramics is achieved through the process known as “poling”, where their randomly oriented piezoelectric domains are aligned in only one direction, their high sensing capability and efficiency of electromechanical conversion tends to change over time [110]. This degradation of electromechanical properties is closely related with increased temperature, in which case it is known as “thermally activated ageing” [13].

To show the temperature limitation of a conventional piezoelectric ceramic, it was decided to proceed with impedance measurements on a piezoelectric with Curie temperature close to the target temperature of 580°C. Modified bismuth titanate, under the commercial name HPZ510, was purchased from “Ionix Advanced Technologies” to be tested as part of this research work. According to its datasheet, the Curie temperature of this piezoelectric ceramic is at 514°C [111]. The measured frequency dependent electric impedance response of the HPZ510 piezoelectric element, in the frequency range from 0 Hz up to 4 MHz, and in the temperature range from 25°C up to 525°C, can be seen in Figure 3-3.

From Figure 3-3 one can see that as the temperature increases, the location and amplitude of the  $f_r$  and  $f_a$  peaks change, which accounts for changes in electromechanical properties of the piezoelectric element HPZ510. At the temperature of 525°C, which is slightly above the expected value of Curie temperature reported in the datasheet, the  $f_r$  and  $f_a$  peaks virtually vanished which implied that this piezoelectric element lost its piezoelectric effect and could not be used any more for ultrasound generation and reception [112].

In contrast to ceramics, the less sensitive piezoelectric single crystals, such as quartz (SiO<sub>2</sub>) and gallium orthophosphate (GaPO<sub>4</sub>), offer advantages over piezoelectric ceramics, with non-ageing behaviour and much higher long-term stability of their key electromechanical properties at HT due to the absence of piezoelectric domains [15]. In addition, these piezoelectric single crystals possess an extended upper

operational temperature limit, owing to the absence of a Curie point transition. However, piezoelectric single crystals may possess phase transitions below their melting points [113]. For example, SiO<sub>2</sub> shows a phase transition from  $\alpha$ -SiO<sub>2</sub> to  $\beta$ -SiO<sub>2</sub> at 573°C, leading to instability of its electromechanical properties close to this temperature [114]. Compared to SiO<sub>2</sub>, GaPO<sub>4</sub> exhibits this phase transition at a much higher temperature of 970°C, which means that any possible instability of the electromechanical properties should occur far above the target temperature of 580°C.

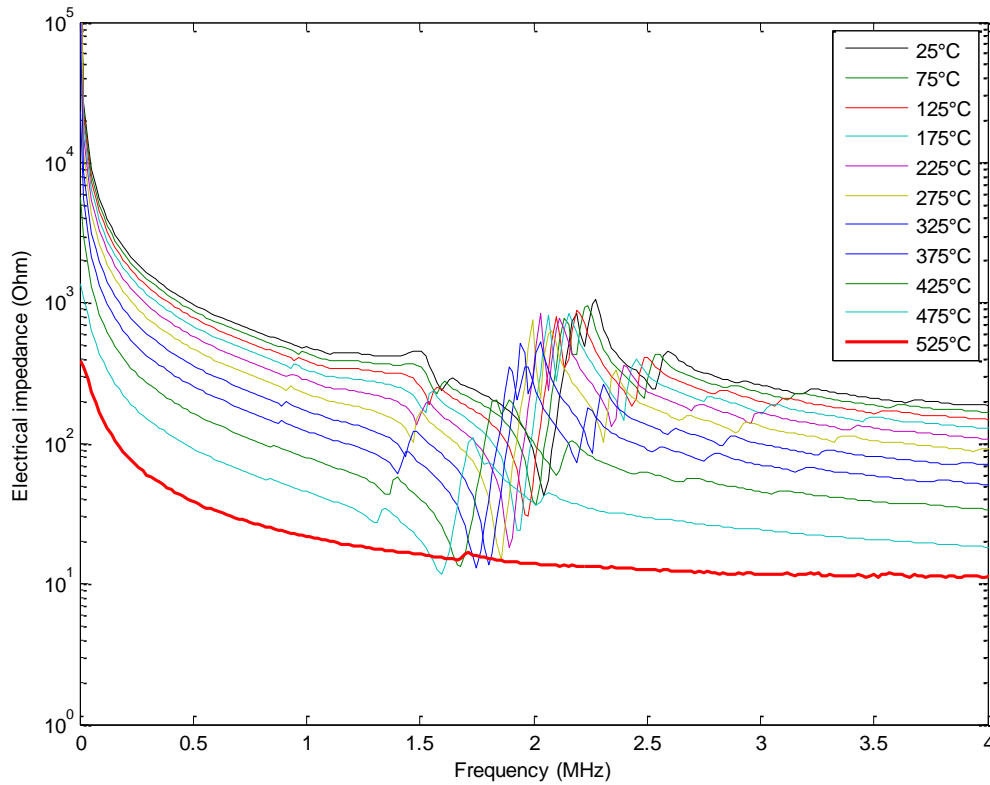


**Figure 3-3: Frequency dependent impedance of ceramic bismuth titanate, from 0 to 4 MHz, and from 25 to 525°C, showing the vanishing of  $f_r$  and  $f_a$  peaks once Curie temperature is reached.**

### 3.4 Determination of the key electromechanical properties

The electromechanical properties of piezoelectric materials are anisotropic, which means that they exhibit different values in different directions, depending on the cut in terms of piezoelectric single crystals such as GaPO<sub>4</sub> [115]. According to the Active European Standard on Piezoelectricity [108], for the X-cut single crystal GaPO<sub>4</sub> elements vibrating in the thickness compression mode, there are four relevant electromechanical properties that need to be derived: (i) thickness coupling factor  $k_t$ ; (ii) piezoelectric charge constant  $d_{11}$ ; and (iii) compliance and stiffness constants,  $s_{11}^E$  and  $c_{11}^E$ , respectively. These four electromechanical properties represent numerical measures of the efficiency for electromechanical conversion, sensing capability and mechanical/thermal stability of a piezoelectric element, respectively, as explained below.

### 3.4.1 Electromechanical coupling factor – $k_{ij}$

The electromechanical coupling factor  $k_{ij}$  is the key property when describing the vibration behaviour of piezoelectrics, expressing a numerical measure of efficiency for the electromechanical conversion [17]. The first subscript to  $k$  denotes the direction along which the electrodes are applied and the second denotes the direction along which the mechanical energy is applied / developed. The dimensions of the piezo-element dictate a unique expression of  $k$  factor [108]. For a piezoelectric transducer, such as an X-cut GaPO<sub>4</sub>, whose surface dimension is large relative to the thickness, the matching electromechanical factor is the thickness coupling factor  $k_t$  and it expresses the coupling between an electric field in direction  $I$  (thickness, compressional direction) and mechanical vibration in the same direction. A higher coupling factor is wanted for any piezoelectric transducer, as any energy not converted from one form to another will be stored in the form of heat, thereby adding to the total thermal energy content of the transducer and thus further affecting its piezoelectric response [95].

### 3.4.2 Piezoelectric charge constant – $d_{ij}$

The piezoelectric charge constant –  $d_{ij}$  gives the ratio of the electrical charge generated per unit of mechanical stress applied to a piezoelectric element, and conversely is the ratio of the mechanical strain developed by a piezoelectric element per unit of the electric field applied [108]. The first subscript to  $d$  indicates the direction of polarisation generated in the piezoelectric element and the second subscript is the direction of the applied stress or the induced strain, respectively. The matching constant for an X-cut GaPO<sub>4</sub> element vibrating in the thickness compression mode is the constant  $d_{11}$ , where the subscript  $11$  denotes that both the excitation of the piezoelectric element and the response of the element are in the same direction. The sensitivity needs to be sufficiently high so that the generated electrical signal can be detected above the background noise [95]. In practice, the generated signal is small and has to be enhanced by an appropriate charge or voltage amplifier [116].

### 3.4.3 Compliance and stiffness constant – $s^E_{11}$ and $c^E_{11}$

The elastic compliance constant  $s^k_{ij}$  relates the applied stress with the relative deformation of the material – the strain. A different way of relating the stress and strain of a material is to use the elastic stiffness constant  $c^k_{ij}$ . This constant is defined as being inversely proportional to the elastic compliance constant [108]. The matching compliance and stiffness constants of an X-cut GaPO<sub>4</sub> piezoelectric element, vibrating in the thickness compression mode, are the constants  $s^E_{11}$  and  $c^E_{11}$ , respectively, where the superscript  $E$  denotes a constant electric field applied, and the subscript  $11$  indicates that the direction of strain and the direction of stress are the same. For the  $11$  direction of a piezoelectric element, the  $c$  constant is the Young's modulus of elasticity. These two constants are a numerical measure for

the mechanical stability of piezoelectric elements vibrating at the resonance and as such are useful parameters to discuss piezoelectrics' behaviour when operated at HT.

### 3.4.4 Calculation of complete set of electromechanical properties

The mathematical relations presented in the Active European Standard on Piezoelectricity [108] were used to calculate the set of electromechanical properties, useful for understanding the behaviour of piezoelectric transducers when operated at their resonant frequency.

The thickness coupling factor  $k_t$  can be derived based on the measured  $f_r$  and  $f_a$  values, Eq. (3.10):

$$k_t^2 = \frac{\pi}{2} \frac{f_r}{f_a} \cot\left(\frac{\pi}{2} \frac{f_r}{f_a}\right) \quad (3.10)$$

The piezoelectric charge constant  $d_{11}$  can be derived from the relation of the thickness coupling factor  $k_t$ , the dielectric constant  $\varepsilon_{11}^T$  and the compliance constant  $s_{11}^E$ , Eq. (3.11):

$$d_{11} = k_t (\varepsilon_{11}^T s_{11}^E)^{1/2} \quad (3.11)$$

The dielectric constant  $\varepsilon_{11}^T$  can be calculated from the “free” capacitance  $C^T$  measured well below the lowest resonant frequency, e.g. at 1 kHz ( $T$  denotes the constant mechanical stress in the element), the thickness  $t$  of the piezoelectric element and the electrode area  $A$ , Eq. (3.12):

$$\varepsilon_{11}^T = C^T \frac{t}{A} \quad (3.12)$$

The compliance constant  $s_{11}^E$  can be derived from the thickness coupling factor  $k_t$  and the compliance constant  $s_{11}^D$ , where  $D$  denotes the constant displacement in the element, Eq. (3.13):

$$s_{11}^E = \frac{s_{11}^D}{1 - k_t^2} \quad (3.13)$$

The compliance constant  $s_{11}^D$  can be calculated directly from the measured anti-resonance value  $f_a$ , the density  $\rho$  (from datasheet) and the length  $l$  (CTE taken into account) of a piezoelectric, Eq. (3.14):

$$s_{11}^D = \frac{1}{4\rho f_a^2 l^2} \quad (3.14)$$

Finally, the compliance constant  $c_{11}^E$  can be derived from the  $k_t$  and the constant  $c_{11}^D$ , Eq. (3.15):

$$c_{11}^E = c_{11}^D (1 - k_t^2) \quad (3.15)$$

To calculate  $c_{11}^D$  one has to measure the anti-resonance  $f_a$ , density  $\rho$  and thickness  $t$ , Eq. (3.16):

$$c_{11}^D = 4\rho f_a^2 t^2 \quad (3.16)$$

### 3.5 Development of GaPO<sub>4</sub> elements

GaPO<sub>4</sub> elements (X-cut) were purchased from “Piezocryst GmbH”, to be appropriately shaped and coated with platinum, as shown in Figure 3-4 a) and b). GaPO<sub>4</sub> elements with dimensions of 3 mm x 12 mm x 1 mm (width, length and thickness, respectively) were manufactured to provide piezoelectric elements robust enough to manipulate when performing impedance measurements at HT.

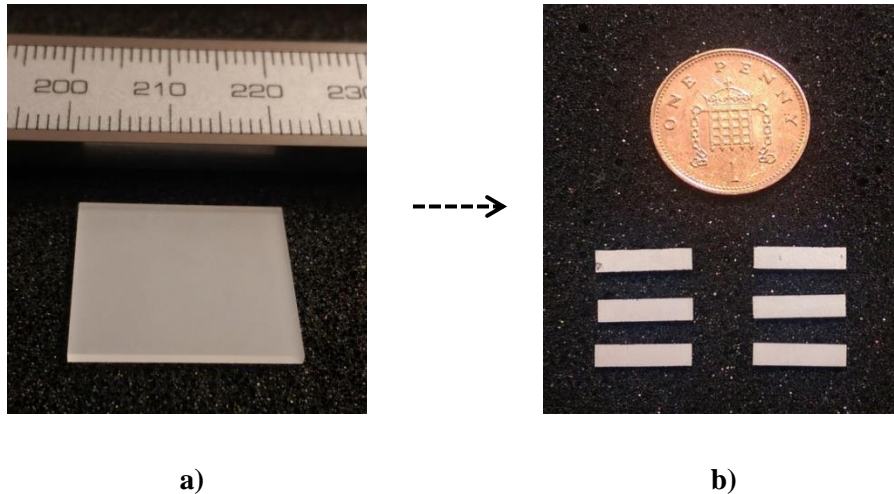


**Figure 3-4:** a) A raw GaPO<sub>4</sub> element, as purchased from “Piezocryst Ltd” and b) the raw GaPO<sub>4</sub> element is coated in platinum and shaped into slender rectangular elements.

### 3.6 Impedance analysis at HT

Material properties of piezoelectric materials provided in their respective datasheets are normally measured on simple test-pieces (discs, rods, etc.) using specific geometric and electrical boundary conditions [108]. For this reason, they should be used only as a guide to the actual properties of piezo-elements that are manufactured for a specific application such as the one developed in this work. Further, material properties of piezoelectric elements normally vary with temperature and thus their room temperature values cannot be used for application at HT [13]. A number of methods, such as the impedance method, the quasi-static method and the laser interferometry method are used to measure the electro-acoustic properties of piezoelectric elements [117]. However, all of these require specialised and accurate measuring devices [118]. Additionally, the quasi-static and laser interferometry methods are time-consuming and more demanding with respect to preparation of the measurement [119]. In view of the above and considering that an impedance analyser was already available, it was decided to proceed with the impedance method.

In the literature, electrical impedance is defined as the complete opposition an electrical component, device or circuit offers to the flow of AC at a given frequency [106]. When an AC is applied to a piezoelectric element, this results in cyclic change of its dimensions. The values of the measured frequencies at the minimum and maximum electrical impedance can then be used to derive a number of key electro-acoustic properties of the piezoelectric element under measurement [108]. An Agilent 4294A impedance analyser was used to perform impedance measurements on the GaPO<sub>4</sub> elements; see Figure 3-5. The used impedance analyser is able to cover a broad test-frequency range from 40 Hz up to 110 MHz, with an impedance accuracy of  $\pm 0.08\%$  [120].

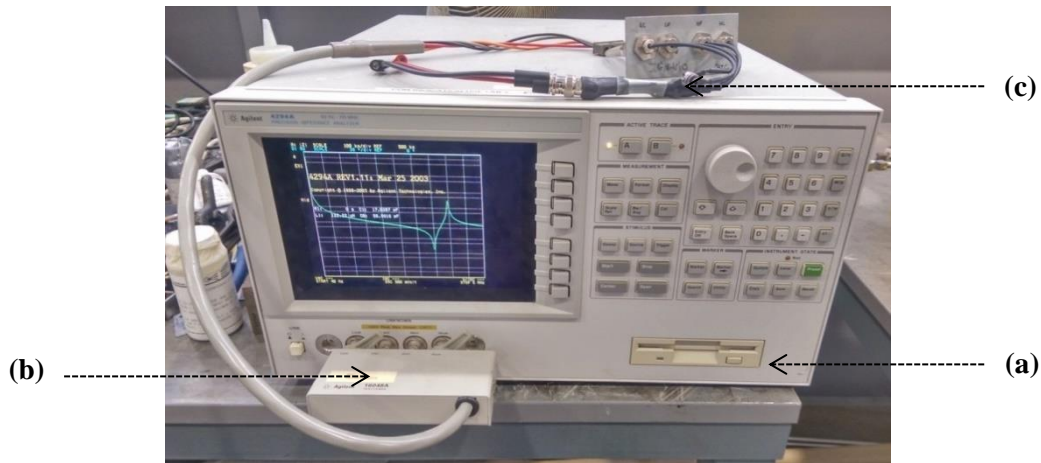


**Figure 3-5: (a) Agilent 4294A impedance analyser using (b) an Agilent 16048A text-fixture and (c) BNC leads that were connected to a piezoelectric element under impedance measurement.**

At room temperature, devices such as “smart tweezers” are normally used to connect the piezoelectric element to an impedance analyser [121]. However, these commercially available devices are not suitable for measurements at up to 580°C. Hence, a special test-rig for the GaPO<sub>4</sub> elements was designed to ensure that all the piezoelectric elements were tested in the same manner.

### 3.6.1 Test-rig for performing impedance measurements up to 580°C

In the literature, it is possible to find different approaches to the experimental setup for impedance measurements on piezoelectric elements at HT. For example, Sherrit *et al.* [122] used alumina heat insulation tubing and chrome wires to electrically connect piezoelectric elements inside a furnace to an impedance analyser for measurements at HT. The wires were affixed to piezoelectric elements using electrically conductive HT silver paste. A similar approach was adopted by Giurgiutiu *et al.* [66]. However, even though claimed to be performed in the above referenced work, the compensation technique that was used to remove the effect of parasitic impedance of metal wiring that can affect impedance measurement of piezoelectric elements was not explained – this particular problem was

given a special attention when designing this new test-rig. A purposely built piezo-element holder for the HT impedance measurements, that allowed compensation to be done to cancel the effect of the mentioned parasitic impedance, was reported by Mohimi [79]. The holder was designed to operate at HT inside an electric furnace with a maximum operating temperature at 600°C. Main components of the holder were two horizontal brass plates separated by an electrically insulating material, and two steel rods. The function of the top plate was to hold the moving rod in place, and of the base plate to hold the fixed one. The fixed rod allowed connection between the base plate and wiring leading to the Agilent 16048A test-fixture. The moving rod was manually adjustable to enable compensation to be carried out at HT. Once compensation was performed, the moving rod was gently positioned on the piezoelectric element and the impedance measurements were carried out. This HT holder was designed for impedance measurement to be performed on the shear mode piezoelectric elements that, if the voltage is applied over their faces, distort in the shear direction that is perpendicular to the position of the moving rod. However, the GaPO<sub>4</sub> elements used in this work are of compression mode. It is known that electro-acoustic properties of compression mode piezoelectric elements are significantly influenced by the load applied, e.g. the weight of the steel rod, and for example, the difference between the “free” and “clamped” electro-acoustic properties of a piezoelectric element can be as much as 80% [104]. For this reason, it was decided to design a new test-rig which would enable “free” (no load) impedance measurements with an easily feasible compensation procedure.

Figure 3-6 shows a cross-section view of the new test-rig and it can be seen that the rig was designed to partially operate outside the furnace at ambient temperature – an exchangeable pair of banana plugs with appropriate sockets, plastic panel and steel frame, and partially inside the furnace at up to 580°C – the three twin bore alumina tubes with HT nickel wiring. The plastic panel for sockets – (a) with dimensions of 70 mm x 60 mm x 40 mm, width, length and height, respectively was made of polylactide (PLA) thermoplastic polyester. The function of the panel was to hold the banana plug sockets – (b). The panel was mounted on the steel frame with four screws – (c). The function of the steel frame was double: to hold the alumina tubes – (d) and to represent a heat barrier to protect the plastic panel and banana plug sockets from the heat coming out of the furnace. Also, it was important that the selected material had a high density so that the frame would be heavy enough to remain in the default position. The melting temperature of the polylactide (PLA) thermoplastic polyester is around 200°C, and the maximum temperature for the sockets is 85°C. Thus, the criterion for the high-density frame material selection was that it should have a low thermal conductivity. Stainless steel with low thermal conductivity of 16 W/m·K and high melting point at 1350°C -1450°C, as opposed to e.g. brass with 150 W/m·K and 900°C, seemed as an ideal choice. Further, the steel frame was designed in the form of a symmetrical L-profile, so that it was possible to use a fan to accelerate convection between the heat coming out of the furnace and ambient air. The steel frame was designed with three holes ( $\phi$  9 mm) through which the alumina tubes were fed. The three twin-bore alumina tubes were used to feed three

pairs of pure nickel glass braided conductors – (e) with the maximum temperature of continuous operation at 600°C inside the furnace.

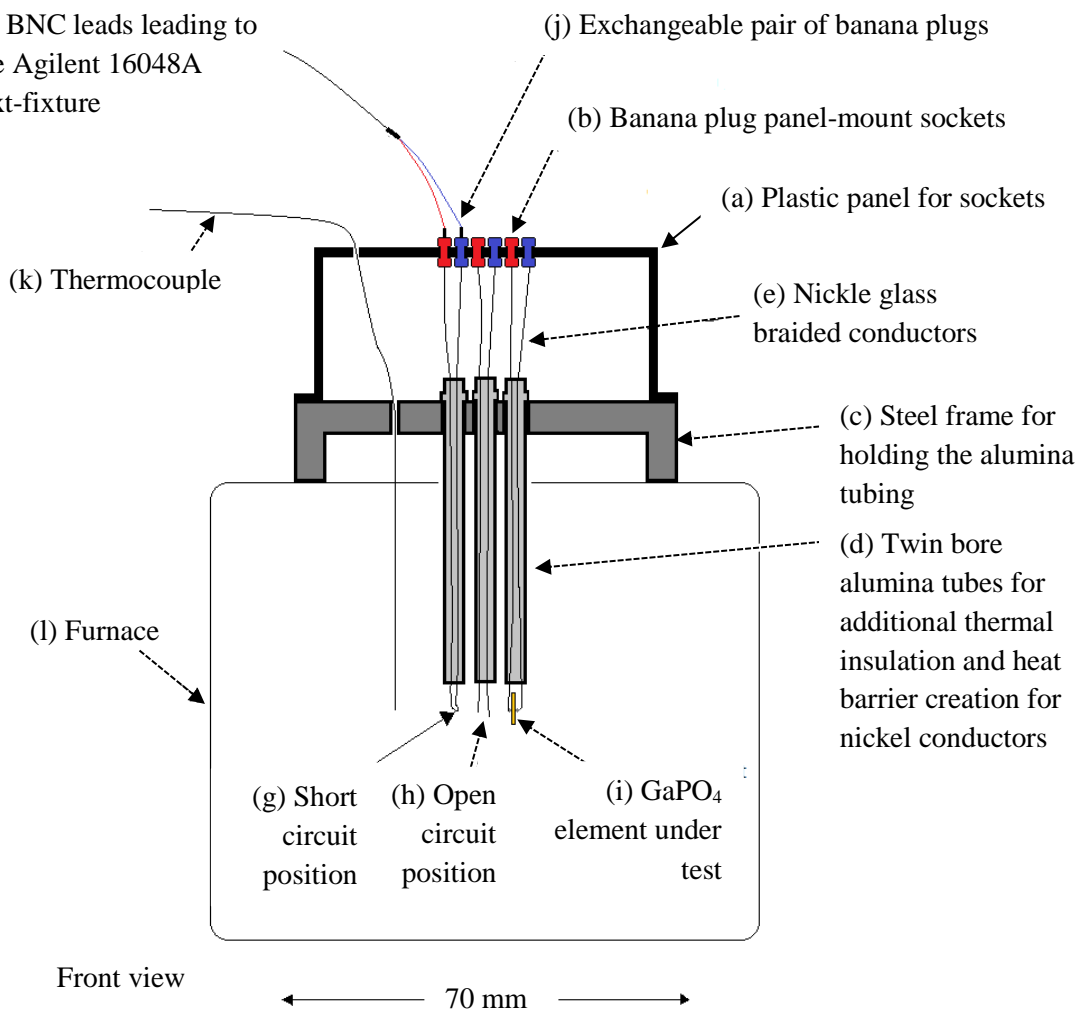


**Figure 3-6: The schematic of the test-rig developed for performing of impedance analysis at HT.**

The test-rig was designed to allow connection between BNC test-leads – (f) leading to the Agilent 16048A test-fixture and Agilent 4294A impedance analyser, and each pair of nickel conductors. Inside the oven, each pair of the nickel conductors had different function while performing impedance measurements at HT. The first pair was in the short circuit position – (g), the second pair in the open circuit position – (h) and the third pair of conductors was coupled using the silver adhesive PyroDuct 597-A to the platinum electrodes of the piezoelectric element made of GaPO<sub>4</sub>, which was under the impedance measurement – (i). Outside the oven, each of the nickel conductors was connected to a banana plug panel mount socket. Then, an exchangeable pair of banana plugs – (j) was used to carry out compensation at HT by changing between the three positions and thus cancelling the parasitic effects. Finally, a thermocouple – (k) was used in the proximity of the GaPO<sub>4</sub> element to ensure that the desired temperature was achieved inside the furnace – (l) before any measurement took place.

### 3.7 Experimental setup and procedure

Five GaPO<sub>4</sub> elements were used for impedance measurements. According to datasheet [68], the elements have velocity of 4356 m/s, and when using this value as an input to Eq. (2.6), together with the thickness of 1 mm, it is possible to calculate that the resonant frequency is 2.178 MHz. This will be further tested. The dimensions of GaPO<sub>4</sub> elements at 25°C were determined using a digital calliper to an accuracy of 0.01 mm, and for HT the dimensions were calculated using CTEs provided in datasheet.

The experimental setup can be seen in Figure 3-7. It consisted of the elements: a) GaPO<sub>4</sub> element affixed to nickel conductors using adhesive PyroDuct 597-A; b) alumina tubing; c) Carbolite furnace; d) panel with banana plugs for circuit compensations; e) BNC leads with Agilent fixture; f) fan used for cooling of the outer part of the holder; g) Agilent impedance analyser; h) logger with K-type thermocouple; and i) PC to collect data. All measurements were taken up to 2.5 MHz, corresponding to the resonant frequency of 2.178 MHz. The temperature inside the oven was measured with a thermocouple type K data logger with a resolution of 0.025°C, positioned near the GaPO<sub>4</sub> element. Prior to measurement at each temperature, short and open circuit connections were measured to determine the required corrections for the effect of parasitic capacitance that exists between the test-setup (BNC test-leads with Agilent fixture and developed test-rig) and the GaPO<sub>4</sub> element under test. The parasitic capacitance is a consequence of the mismatch that exists between different internal capacitance values of the test-setup and the piezo-element, which can cause their behaviour to depart from that of “ideal” circuit elements [122]. The “open”, “short” and “GaPO<sub>4</sub> element under test” positions can be seen in Figure 3-7.

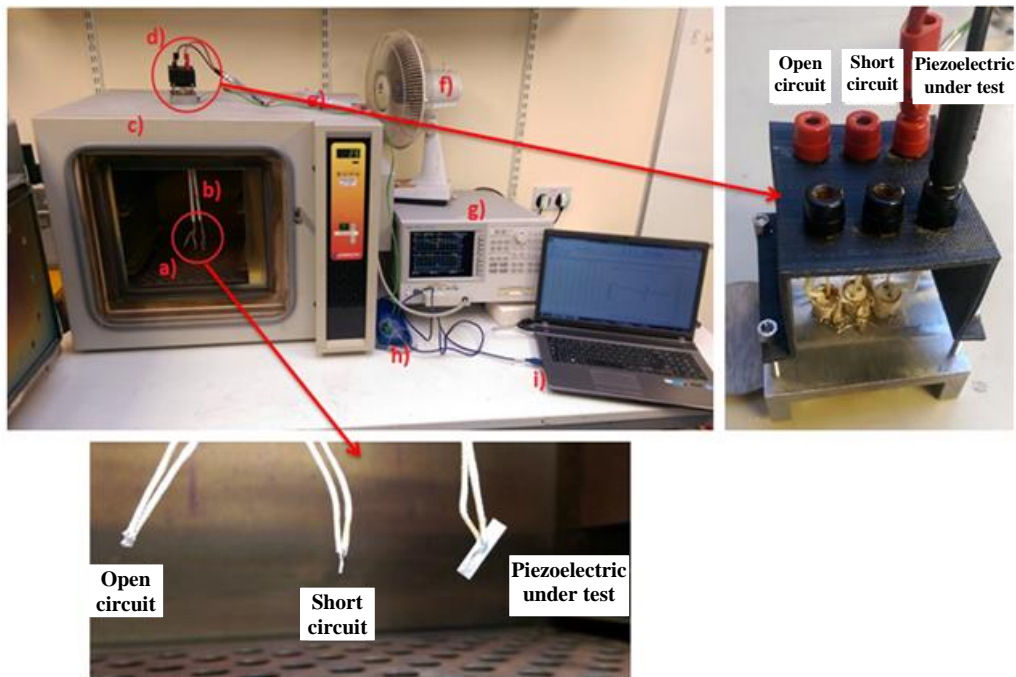


**Figure 3-7: Experimental setup used for impedance analysis of GaPO<sub>4</sub> elements at HT.**

### 3.8 Results and discussion

#### 3.8.1 Impedance response from 25°C up to 580°C

To establish a baseline, impedance characteristics of five GaPO<sub>4</sub> elements were recorded first from 25°C up to the target temperature of 580°C with an increment of 50°C, where a hold time of 15 min at each temperature was applied in order to ensure an isothermal temperature measurement. Recorded impedance characteristics of a GaPO<sub>4</sub> element from 25°C up to 580°C, plotted to show the effect of increasing temperature on the  $f_r$  and  $f_a$  peaks, can be seen in Figure 3-8.

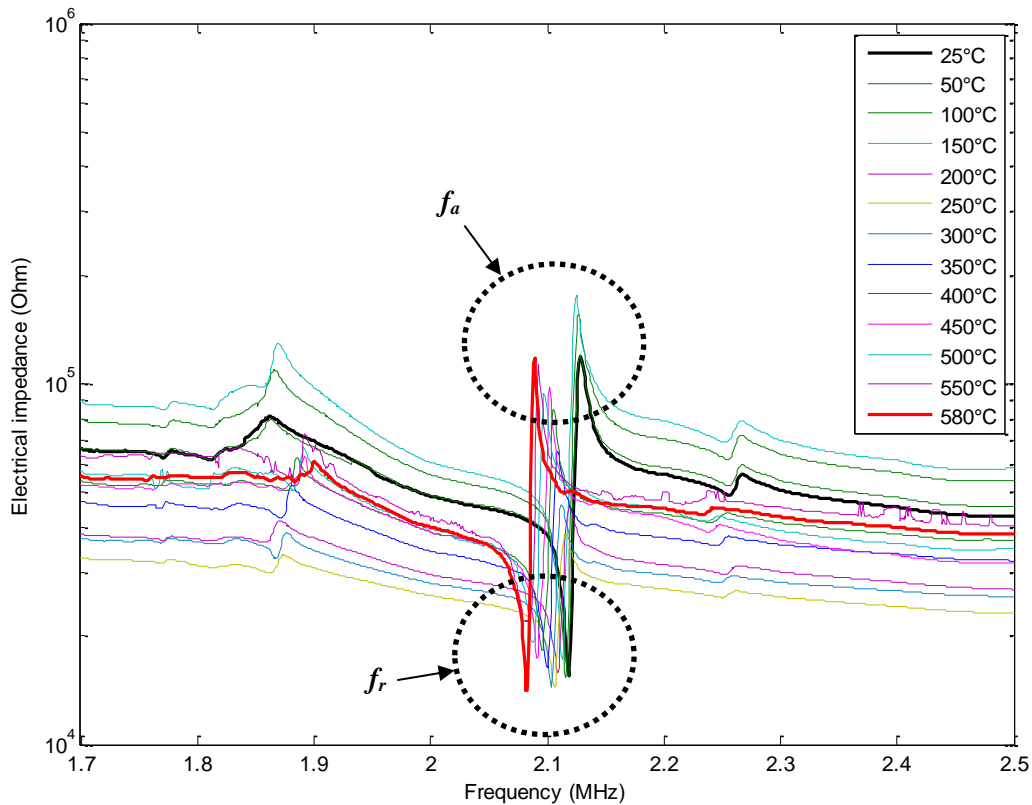


**Figure 3-8: Impedance characteristics of a GaPO<sub>4</sub> element, in the temperature range from 25°C up to 580°C and in the frequency range from 1.7 MHz up to 2.5 MHz, showing the effect of increasing temperature on the  $f_r$  and  $f_a$  peaks.**

First, one can see that the resonant frequency at 25°C was measured to be 2.117 MHz, which is a drop of 2.84% from the theoretical value of 2.178 MHz. This drop in resonant frequency was probably caused by application of the silver adhesive that was used to affix the nickel wiring to the GaPO<sub>4</sub> element, and which represented an additional load to the free vibration of the piezoelectric element.

Secondly, as clearly seen from Figure 3-9 a) and b) and Figure 3-10 a) and b) below, the rise in temperature caused the frequency pair  $f_r$  and  $f_a$  to shift to the lower frequency and higher impedance values. As the temperature goes up from 25°C to 580°C, the resonant frequency  $f_r$  goes down from

2.117 MHz to 2.077 MHz, and in the same temperature range, the anti-resonant frequency  $f_a$  decreases from 2.127 MHz to 2.087 MHz. Both frequencies have decreased less than 2% over the tested temperature range, which means that the wavelength of waves travelling through e.g. a steel structure would change less than 2%. Given the rule of thumb that a defect must be larger than one-half of the wavelength to stand a reasonable chance of being detected, this frequency decrease on a millimetre scale is so small that it can be neglected, confirming the GaPO<sub>4</sub> as a potentially suitable piezoelectric material for application in ultrasonic non-destructive testing at high temperatures.

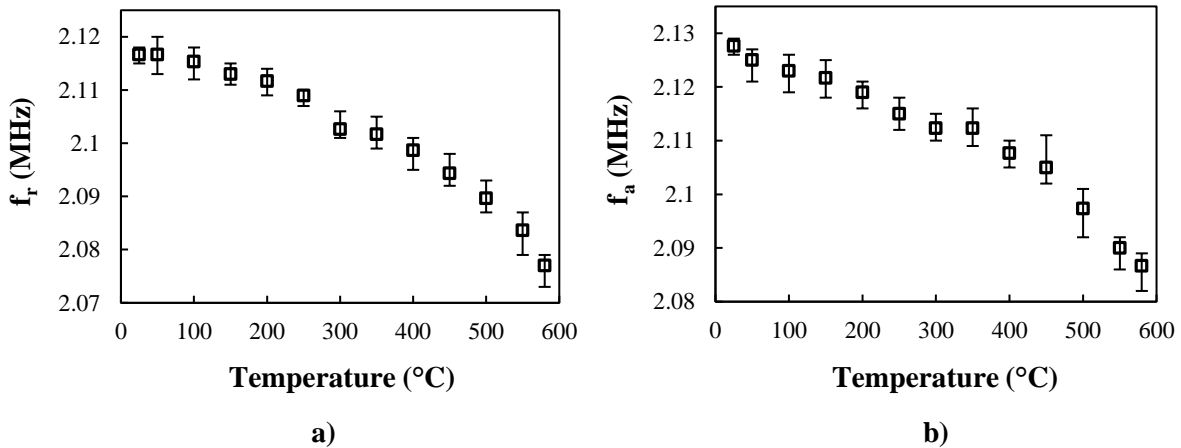


**Figure 3-9: Measured values of a) resonant  $f_r$  and b) anti-resonant  $f_a$  frequency pair, as a function of temperature from 25°C up to the target of 580°C, averaged for five GaPO<sub>4</sub> elements.**

Further, as seen from Figure 3-10 a) and b) below, as the temperature goes up to 580°C, the measured impedance at the frequencies  $f_r$  and  $f_a$  also goes up. The impedance at the resonance peak  $Z_r$  increases from 15.28 kΩ at 25°C up to 18.22 kΩ at 580°C, which is an increase of 19.24%, and the impedance at the anti-resonance peak  $Z_a$  goes up from 90.42 kΩ up to 113.89 kΩ, which is an increase of 25.96% in the same temperature range. As explained before, when the impedance is at its minimum, the piezoelectric vibrates most readily and is most efficient as a transmitter. On the contrary, when the impedance is at its maximum, the piezoelectric is most efficient as a receiver. This means that with the rise in temperature from 25°C to 580°C, the GaPO<sub>4</sub> elements will start reducing their transmission efficiency but improve their reception efficiency. Purposely designed circuiting is normally used to balance these two; however as there are no electrical components available for application at 580°C (some elements can be found for application up to max 300°C), the measurements will rely only on the in-built filters and voltage/charge pre-amplifiers of the commercial pulser-receiver instrument.

## High Temperature Impedance Analysis of GaPO<sub>4</sub> Elements

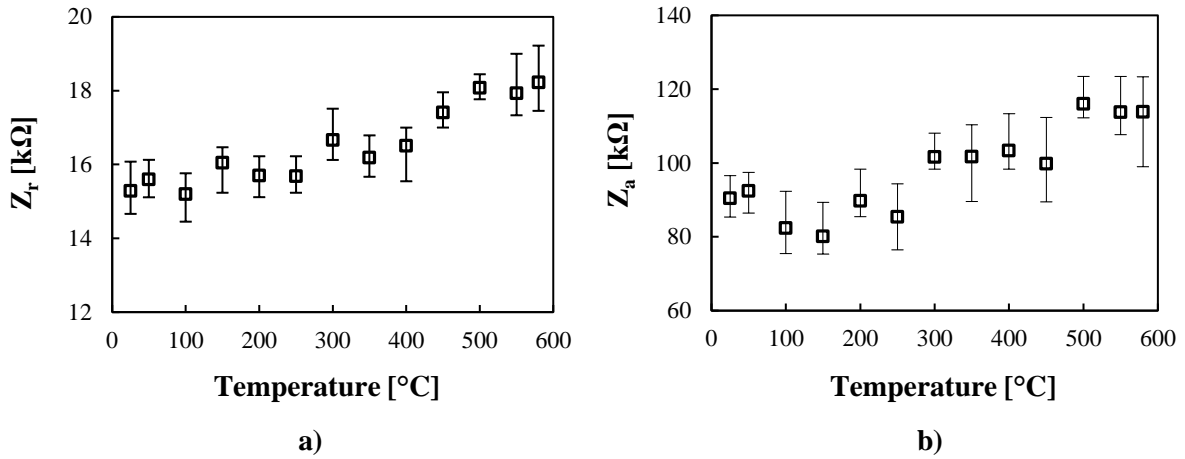


**Figure 3-10: Measured values of a) resonant  $Z_r$  and b) anti-resonant  $Z_a$  el. impedance pair, as a function of temperature from 25 $^{\circ}C$  up to the target of 580 $^{\circ}C$ , averaged for five GaPO<sub>4</sub> elements.**

### 3.8.2 Long-term impedance response at 580 $^{\circ}C$

After the five GaPO<sub>4</sub> elements were tested up to 580 $^{\circ}C$ , the impedance response of the last GaPO<sub>4</sub> element was recorded at constant temperature of 580 $^{\circ}C$  for 600 hours, as shown in Figure 3-11.

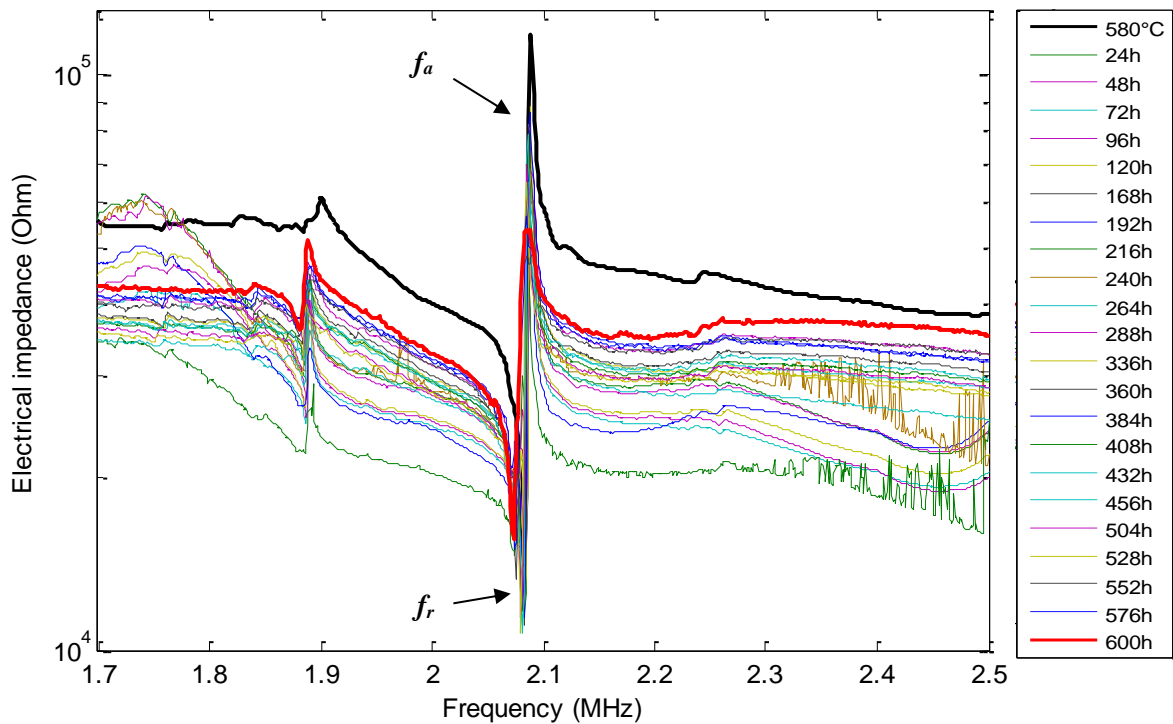


**Figure 3-11: Impedance response of a GaPO<sub>4</sub> element at constant temperature of 580 $^{\circ}C$  for 600 h, showing a good thermal stability of  $f_r$  and  $f_a$  frequency peaks over the tested period.**

After 600 hours, the impedance test was stopped because the adhesive, bonding the nickel connectors to the GaPO<sub>4</sub> element, finally failed. This experiment had a significant implication on the rest of the

research; it is believed this was the first time a piezo-resonator machined from GaPO<sub>4</sub> was tested at the given temperature level over such a long period of time. This experiment confirmed what the theory already claimed – an excellent thermal stability of the piezoelectric effect of single crystal GaPO<sub>4</sub>.

The electrical impedance characteristics recorded at 580°C over 600 hours (Figure 3-11), show the effect of a constant HT exposure of a GaPO<sub>4</sub> element and how this affects its resonant and anti-resonant peaks over time. As explained, the high temperature stability of GaPO<sub>4</sub> over time is important as the application of this piezoelectric material inside a transducer aims not only to provide individual short-term non-destructive testing of critical points in power plants but also to provide their continuous monitoring at operating conditions. According to Figure 3-12 a) and b), over the 25-day period at 580°C, the value of the resonant frequency  $f_r$  dropped less than 0.4% and the anti-resonant frequency  $f_a$  dropped less than 0.1%. This small shift to lower values of the two key frequencies when exposed to HT over time can be neglected considering the sensitivity of a transducer that would use this piezoelectric material for continuous monitoring and defect detection would stay practically the same.

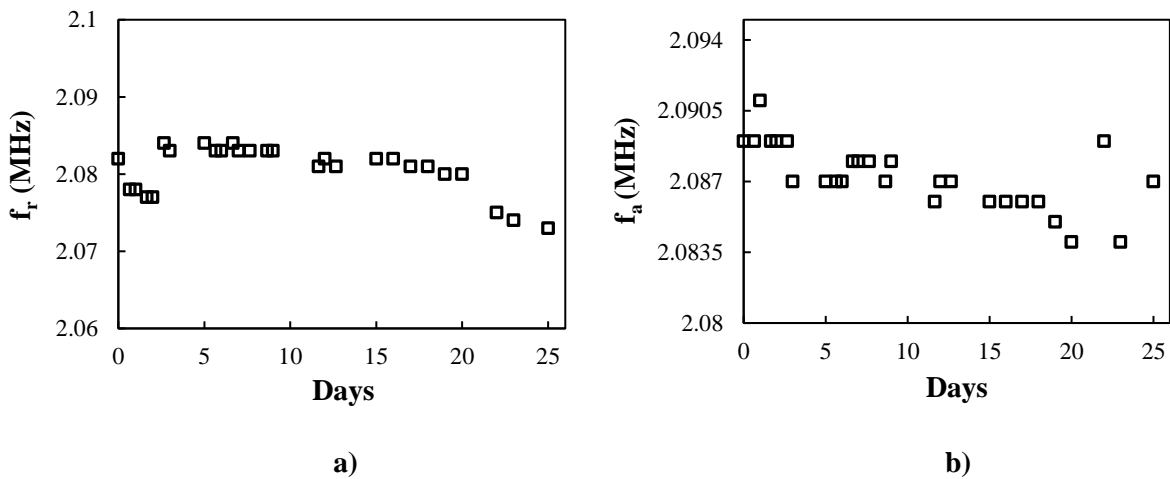


**Figure 3-12: Measured values of a) resonant  $f_r$  and b) anti-resonant  $f_a$  frequency pair, at the constant temperature of 580°C, as a function of time over 600 hours.**

In terms of the impedance,  $Z_r$  generally dropped steadily from the initial value of 14.18 k $\Omega$  at the beginning of testing to 10.71 k $\Omega$  by the 20<sup>th</sup> day, when it again increased to 15.58 k $\Omega$  on the last day; see Figure 3-13 a). The possible reason for the increment of resonant electrical impedance  $Z_r$  from 10.71 k $\Omega$  on the 20<sup>th</sup> day of testing to 15.58 k $\Omega$  on the last day lies behind the ageing of the silver adhesive applied to bond nickel wires to the GaPO<sub>4</sub> element, which in the end led the measurement to be stopped after 600 hours. On the other hand, the  $Z_a$  value dropped after only one day, from 117.64 k $\Omega$  to 73.16 k $\Omega$  and over the rest of the measurement period, the  $Z_a$  value stayed at approximately 75 k $\Omega$  and finished at 53.93 k $\Omega$  on the last day of measurement (see Figure 3-13 b). The overall change in resonant and anti-resonant impedance values at 580°C within the 25-day period was 9.87% and 56.85%, respectively.

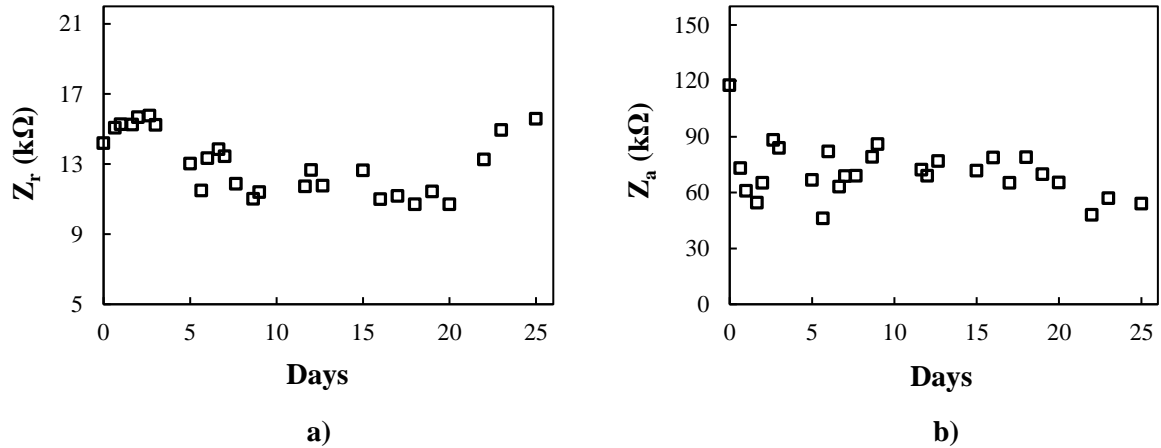


**Figure 3-13: Measured values of a) resonant  $Z_r$  and b) anti-resonant  $Z_a$  electrical impedance pair, at the constant temperature of 580°C, as a function of time over 600 hours.**

### 3.8.3 Electromechanical properties from 25°C up to 580°C

Based on the measured  $f_r$  and  $f_a$  values, the material properties  $d_{11}$ ,  $k_t$ ,  $s_{11}^E$  and  $c_{11}^E$  were derived. Looking at Figure 3-14 a), one can see that the charge constant  $d_{11}$  stayed stable from 25°C up to 580°C, with the maximum value of 4.35 pC/N at 25°C and the minimum value of 4.12 pC/N at 500°C; at 580°C the constant was 4.22 pC/N. The difference between the min and max charge constant values is thus calculated to be 5.58%. The derived  $d_{11}$  values agree well with the datasheet ones, which at 25°C is reported to be 4.5 pC/N [68].

Second, according to Figure 3-14 b), the derived thickness coupling factor  $k_t$  remained stable, with 10.5% at 25°C, a slight increase up to 11.06% at 200°C and then finished at 10.04% at 580°C. In the datasheet,  $k_t$  value of 16% was reported and according to the theory it should stay unchanged all the way up to 933°C, where an irreversible phase transition to a low quartz/cristobalite-like structure occurs [123]. However, as explained before, the reported values should only be taken as benchmarks, as the measurements were performed on piezoelectric elements with different geometries (rods, plates, etc.) and then averaged, and also with different measuring equipment from that used here (impedance analyser Agilent 4294A). Besides the differences in geometry of GaPO<sub>4</sub> elements and measurement techniques, a second reason why the  $k_t$  was lower than expected could be due to the influence of the silver adhesive used to bond the GaPO<sub>4</sub> elements to the nickel conductors and thus allow an electrical connection to the impedance analyser. The downside of using silver adhesives is that very few of their physical properties are reported, especially at HT, and it is almost impossible to really understand and quantify their influence on the overall measurement. Still, a good bonding alternative to the application of silver adhesives was not established during this work.

## High Temperature Impedance Analysis of GaPO<sub>4</sub> Elements

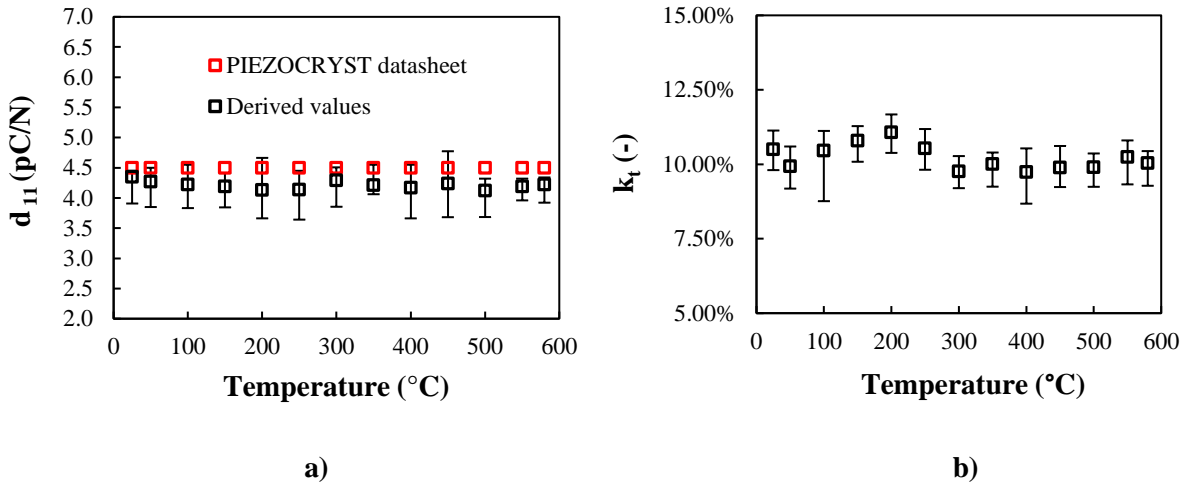


**Figure 3-14:** a) Derived piezoelectric charge constant  $d_{11}$  and b) electromechanical thickness coupling factor  $k_t$ , in the temperature range from 25°C up to 580°C, averaged for five GaPO<sub>4</sub> elements. The constant  $d_{11}$  was also compared to the provided datasheet value.

According to Figure 3-15 a) and b), the elastic compliance and stiffness constants –  $s_{11}^E$  and  $c_{11}^E$  were derived to verify the mechanical stability of GaPO<sub>4</sub> elements from 25°C up to 580°C. The  $s_{11}^E$  constant was 18.49 pm<sup>2</sup>/N at 25°C and slightly went up to 19.22 pm<sup>2</sup>/N at 580°C and in the same temperature range, the derived  $c_{11}^E$  constant dropped from the initial value of 63.84 GPa to 61.42 GPa at the higher temperature. Both changes of the elastic constants were approx. 4%. The maximum deviation of these measured (derived) values from the datasheet values can be observed at the highest achieved temperature – difference of 6.88% for  $s_{11}^E$  and difference of 7.92% for  $c_{11}^E$  at 580°C.

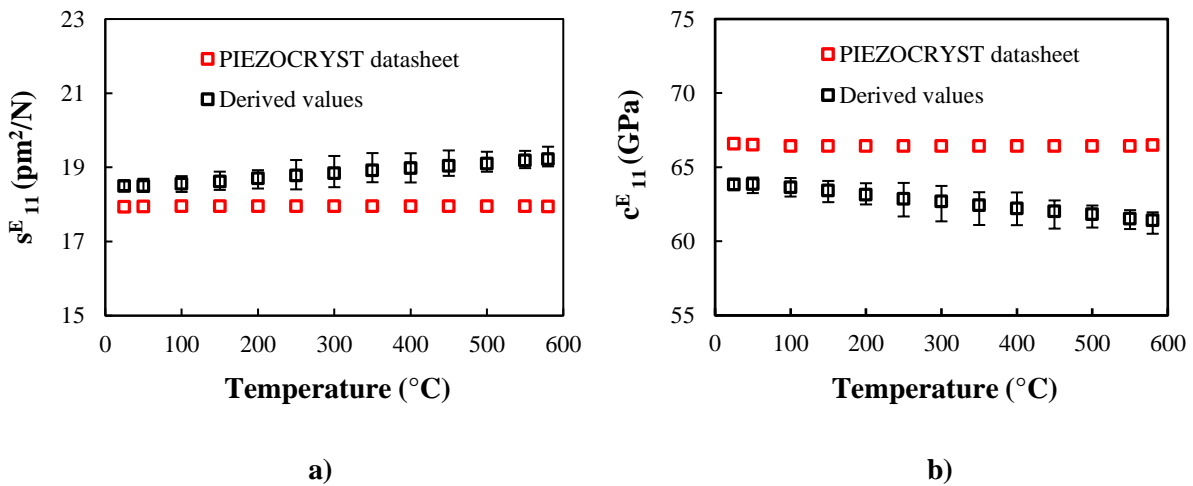


**Figure 3-15:** a) Derived elastic compliance  $s_{11}^E$  and b) elastic stiffness constant  $c_{11}^E$ , in the range from 25°C to 580°C, averaged for five GaPO<sub>4</sub> elements and compared to the datasheet values.

When comparing piezoelectric resonators machined from single crystals such as GaPO<sub>4</sub> with resonators machined from conventional ceramics such as PZT-5A, the GaPO<sub>4</sub>'s room temperature sensitivity of 4.35 pC/N, compared to PZT-5A's sensitivity of 370 pC/N, and GaPO<sub>4</sub>'s (room temperature) electromechanical conversion of 10.5%, compared to PZT-5A's conversion of 70%, seem to be very low. However, it is important to keep in mind that PZT-5A resonators are recommended for operation up to 200°C maximum, while GaPO<sub>4</sub> will perform well even at temperatures up to 580°C. Regarding the elastic constants  $s_{11}^E$  and  $c_{11}^E$  for GaPO<sub>4</sub> and PZT-5A resonators, the elastic constants of PZT-5A experience a very large drop in their respective values when exposed to temperatures up to 200°C (~ half of the Curie point). For PZT-5A, from room temperature up to 200°C, the  $s_{11}^E$  and  $c_{11}^E$  can decrease nearly 25% [124]. For GaPO<sub>4</sub> resonators, the change in value of  $s_{11}^E$  and  $c_{11}^E$  from 25°C to 580°C was measured to be only ~ 4%, where the value of  $s_{11}^E$  went up, and the value of  $c_{11}^E$  went down.

### 3.8.4 Long-term electromechanical properties at 580°C

If one looks at Figure 3-16 a), one can see that the charge constant  $d_{11}$  remains stable with around 10% deviation throughout the experiment (25 days), with a minimum of 3.7 pC/N was achieved at the 15<sup>th</sup> day and a maximum of 4.12 pC/N achieved at day 19. According to Figure 3-16 b), the electromechanical coupling factor  $k_t$  also remained stable at 10.5%, with a minimum of 10.1% achieved on the 2<sup>nd</sup>, 5<sup>th</sup> and 19<sup>th</sup> days, and a maximum of 11.1% measured in the 2<sup>nd</sup>, 8<sup>th</sup> and 11<sup>th</sup> days of the experiment. All variations were calculated to be below 10%.

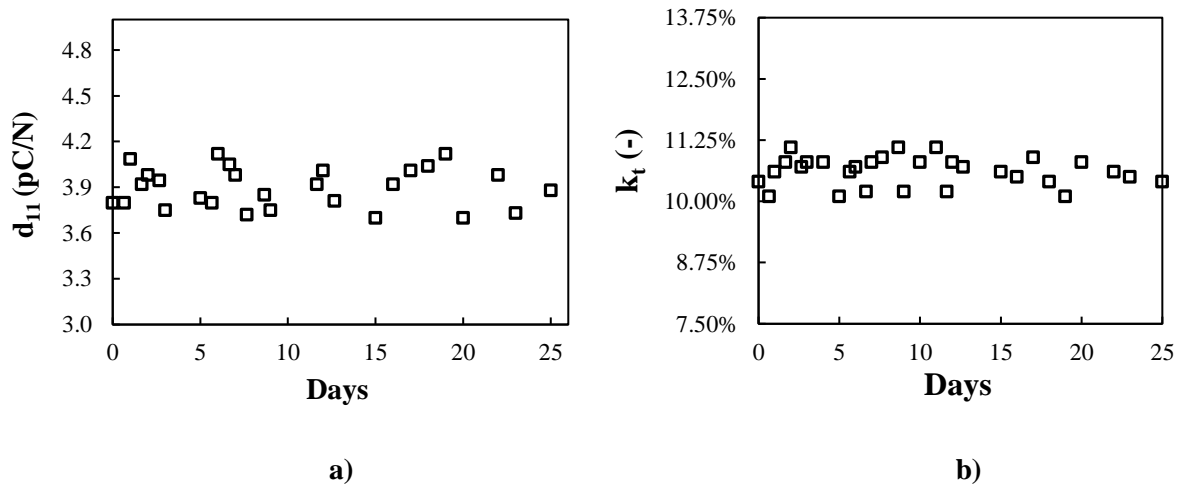


**Figure 3-16: a) Derived charge constant  $d_{11}$  and b) thickness coupling factor  $k_t$  of a GaPO<sub>4</sub> element, at the constant temperature of 580°C as a function of time over 600 hours (25 days).**

Finally, according to Figure 3-17 a) and b), both properties, the elastic compliance and stiffness,  $s_{11}^E$  and  $c_{11}^E$ , respectively, remained stable within a 1.2% variation throughout the entire 25-day period.

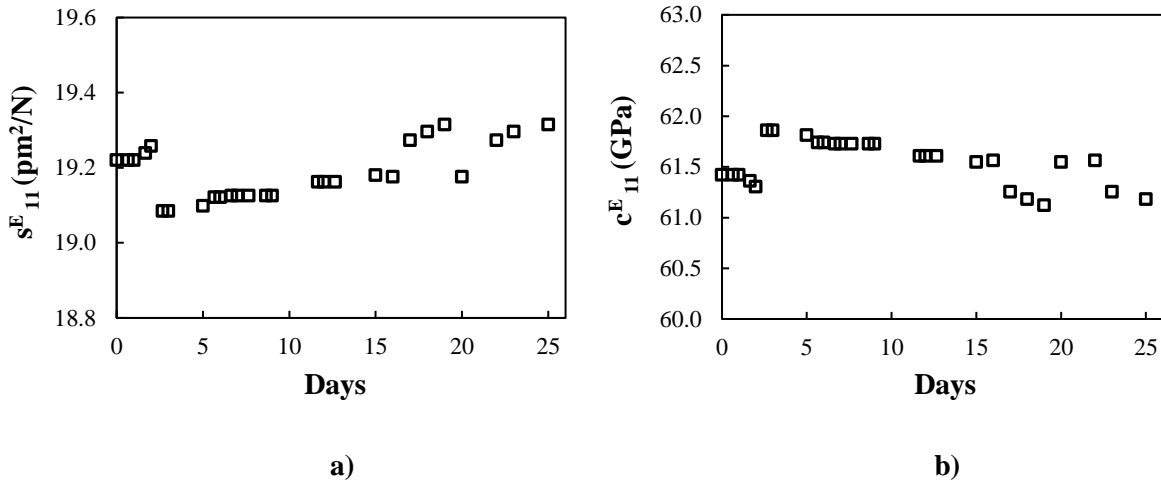


**Figure 3-17: a) Derived elastic compliance  $s^E_{11}$  and b) elastic stiffness constant  $c^E_{11}$  of a GaPO<sub>4</sub> element, at the constant temperature of 580°C as a function of time over 600 hours (25 days).**

After the GaPO<sub>4</sub> element was cooled to ambient temperature of 25°C (over 24 hours), the new silver adhesive was applied to connect the nickel wires back to the GaPO<sub>4</sub> element and the impedance measurement repeated. The compared impedance responses at ambient temperature before (blue trace) and after (red trace) the heat treatment at 580°C can be seen in Figure 3-18. This comparison confirms good thermal stability of this piezoelectric crystal even after the exposure to 580°C for a prolonged period. In both displayed traces, the  $f_r$  and  $f_a$  frequency peaks were pronounced and the resonant frequency of 2.178 MHz was virtually the same in both cases. Thus the transducer that would use the piezoelectric element machined from GaPO<sub>4</sub> for defect detection (at room temperature) would resolve the same size of defect in test-structure before and after the heat treatment at 580°C.

In this chapter, the material properties were derived for five GaPO<sub>4</sub> elements using the impedance method, as outlined in the European Standard on Piezoelectricity. To ensure that all GaPO<sub>4</sub> elements were tested in the same manner, a special holder was designed for the piezoelectric elements. The main finding in this chapter is that the GaPO<sub>4</sub> element maintains the piezoelectric effect at 580°C for at least 600 hours, which is significantly longer than previously reported work on this or other piezoelectric materials. The next step will be to examine the ultrasonic response of the GaPO<sub>4</sub> elements (their transmission and reception quality), in order to reach the final goal of this work – construction of an ultrasonic transducer to operate up to 580°C which is the temperature normally found in high temperature pipework of operational power plants.

## High Temperature Impedance Analysis of GaPO<sub>4</sub> Elements

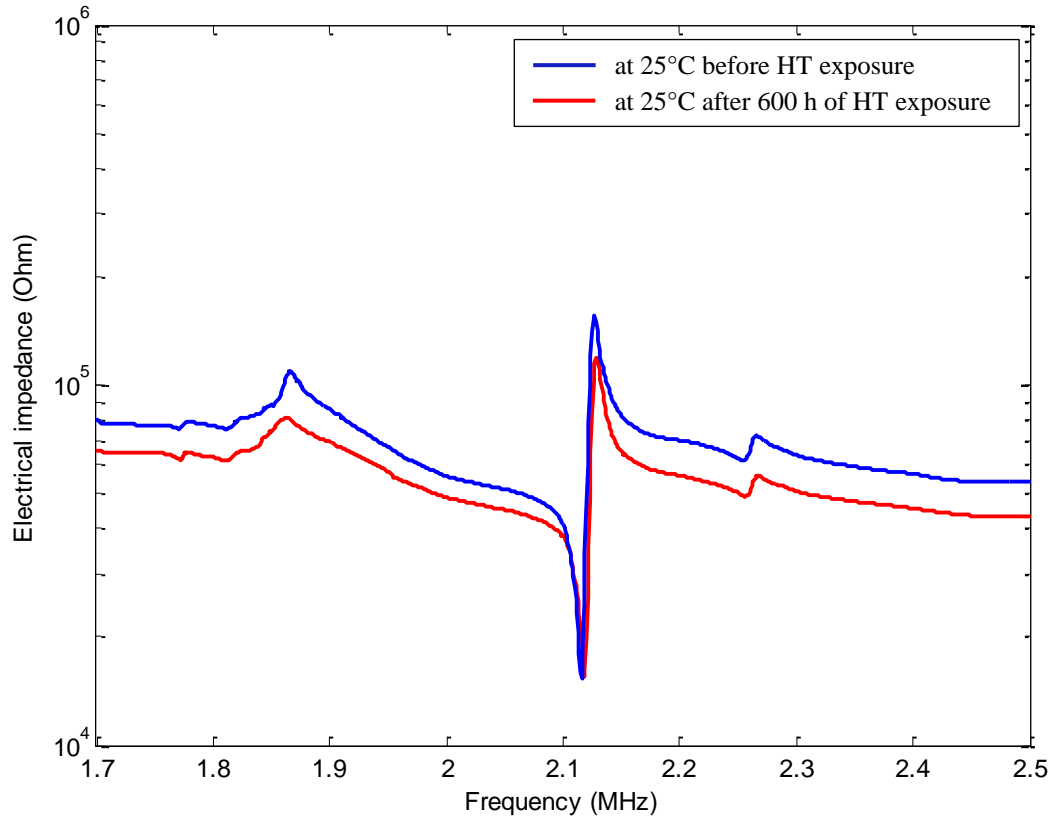


**Figure 3-18: Impedance traces of GaPO<sub>4</sub> element at 25°C, before (blue trace) and after (red trace) the 25-day exposure to 580°C, showing an excellent stability of the piezoelectric response.**

# 4 High Temperature Ultrasonic Analysis of GaPO<sub>4</sub> Elements

## 4.1 Chapter overview

Following on from the impedance analysis at 580°C, in this chapter the validation has gone a step further and has shown that GaPO<sub>4</sub> elements are capable of performing two basic non-destructive evaluation tasks, thickness gauging and defect detection, at up to the same HT level. Thickness gauging has shown that GaPO<sub>4</sub> elements work as functional piezoelectric transducers generating and receiving ultrasound at 580°C for at least 360 hours, before high temperature corrosion of the carbon steel test-block occurred leading to failure of the experiment. Considering the relevant pipework of interest for non-destructive evaluation is made of corrosion resistant stainless steel or P91 steel, changing the test-material is expected to contribute to a longer ultrasonic measurement. Finally, the GaPO<sub>4</sub> transducer's sensitivity was successfully tested through defect detection on a steel test-block containing an artificial defect with known geometry (side-drilled hole of d=0.8 mm) up to 580°C, keeping the defect's SNR level above the threshold of 6 dB, which is high enough for NDT practice.

## 4.2 Introduction

Impedance analysis reported in the previous chapter indicates that piezoelectric elements machined from single crystal GaPO<sub>4</sub> could potentially transmit and receive the ultrasound energy at HT up to 580°C. In this chapter, this will be further tested with a series of ultrasonic experiments to verify the capability of GaPO<sub>4</sub> elements when used for two basic non-destructive testing and evaluation tasks: (i) thickness gauging; and (ii) defect detection up to the same temperature level of 580°C.

As explained in the Chapter 1, pipes of interest for inspection with the HT transducer are operating at temperatures of up to 580°C and are constructed from P91 alloy steel or sometimes stainless steel. Ideally, the ultrasonic validation of GaPO<sub>4</sub> would be done using the same P91 material. However, at this stage of development, the test-samples machined from P91 were not available. For this reason, it was decided to proceed with a material that is more common – carbon steel, which was available in workshop, and later on samples machined from P91 / stainless steel would be introduced when

available. Finally, there are two basic modes of operation of each ultrasonic transducer for non-destructive testing. The first is the pulse-echo mode, where one transducer is used for both transmission and reception of ultrasound energy that was reflected from the backwall and/or a defect in the material. The second one is the through-transmission or pitch-catch mode, where one transducer is used for transmission of ultrasound energy into the test-material and the second transducer for the reception of the reflected ultrasound energy. For the reason of limited number of piezoelectric elements machined from crystal GaPO<sub>4</sub> available for this development, it was decided to proceed with the simpler and less material consuming pulse-echo mode of operation (for each measurement one element is needed and not two).

### **4.3 High temperature ultrasonic analysis**

Commercial ultrasonic pulser and receiver machine TOPAZ from ZETEC was used to deliver a short sharp electrical pulse to “pluck” the piezoelectric element machined from the crystal GaPO<sub>4</sub> and allow it to vibrate at its own fundamental resonant frequency [125]. The commonly used name of this electrical pulse is “the initial pulse” or sometimes in the literature (mainly US) “the main bang”. To increase the amplitude of ultrasonic waves generated from the vibration of the piezoelectric element, the peak voltage of the initial pulse must be increased [115]. Another possibility of achieving ultrasonic signals with increased peak-to-peak amplitude is to use the in-built amplifiers and filters that normally come with powerful ultrasonic machines such as TOPAZ. With the right combination of sufficiently strong initial pulse and application of powerful in-built amplifiers/filters, it should be possible to control the noise level during measurement with a sufficiently high SNR level.

#### **4.3.1 Experimental setup for analysis of the initial pulse**

In order to analyse the initial pulse emerging from the pulser of the pulser-receiver instrument, an experimental setup was built from the following elements: (a) TOPAZ pulser-receiver instrument; (b) passive oscilloscope transducer (Keysight Technologies, 150 MHz, 10 M $\Omega$ , <12 pF and 300 V); and (c) an oscilloscope (Keysight Technologies, MSOX3024A, 200 MHz) (see Figure 4-1). From the oscilloscope, the recorded ultrasonic waveform of the received initial pulse was transferred to a PC for further analysis simply by using a USB stick.

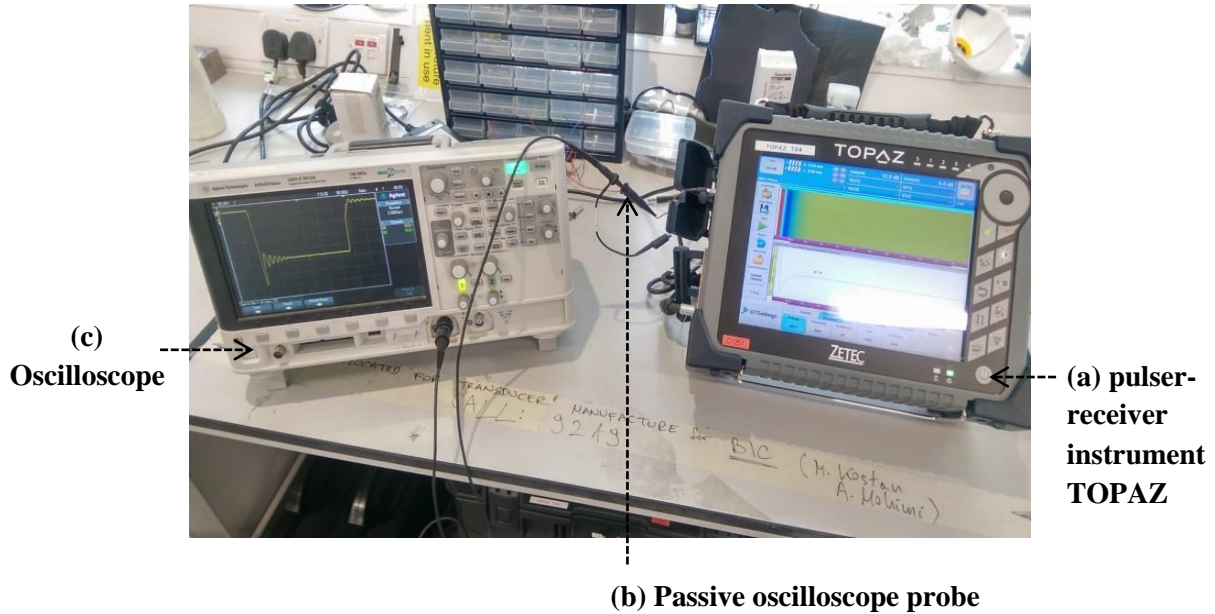


**Figure 4-1: Experimental setup used for analysis of the initial electrical pulse coming out from the pulser of the commercial pulser-receiver instrument TOPAZ.**

The working principle of a pulser-receiver instrument is that it delivers short, sharp electrical pulses at definite time intervals to the piezoelectric element of a transducer which start the element vibrating at its natural resonant frequency, producing waves of ultrasound that are then used for measurement. The pulser-receiver instrument must allow enough time for the returned ultrasound echoes from a barrier such as a backwall and/or a defect in the test-structure to be received by the piezoelectric element between two consecutive initial pulses, and thus not be masked by them. Considering that sound waves in a conventional test-material such as steel travel with a speed of  $\sim 6000$  m/s, this means that for a 50 mm thick steel plate it will take  $\sim 17 \mu\text{s}$  for a generated wave to hit the backwall and return to the piezoelectric element. A pulse repetition frequency (PRF) of 100 Hz (one pulse every 10 ms) is more than enough to acquire usable ultrasonic measurements. This is the case for pulse-echo mode of operation where the same transducer acts both as a transmitter and as a receiver. In the pitch-catch mode of operation, where one transducer is used as a transmitter and the other one as a receiver, the PRF is not that an important parameter considering the piezoelectric element of only one transducer will be triggered with the initial pulse to generate ultrasonic waves and the other transducer will be receiving the returned reflected echoes.

### 4.3.2 Results of the initial pulse analysis

An example of two consecutive initial pulses with PRF of 100 Hz and amplitude of -50 V (minimum pulser voltage) that were generated from the pulser of the TOPAZ pulser-receiver instrument and recorded using an oscilloscope can be seen in Figure 4-2 a). Although it seems at first that the two initial

pulses reach all the way to approximately -80 V, this is only because of the imperfection of the pulser-receiver unit used. TOPAZ, as any other real electrical system is characterised by an overshoot effect that is followed by a “ringing” and settle time, after which the pulse will achieve its steady-state value, in this case -50 V [126]. This can be easily checked if one of the two recorded initial pulses is stretched over a narrow period, e.g. from 310 ns up to 710 ns (Figure 4-2 b). One can now see that after the initial pulse is generated, it first sinks to approximately -80 V (overshoot), then it starts “ringing” and finally, after the settling time of approximately 50 ns, achieves the set value of -50 V.

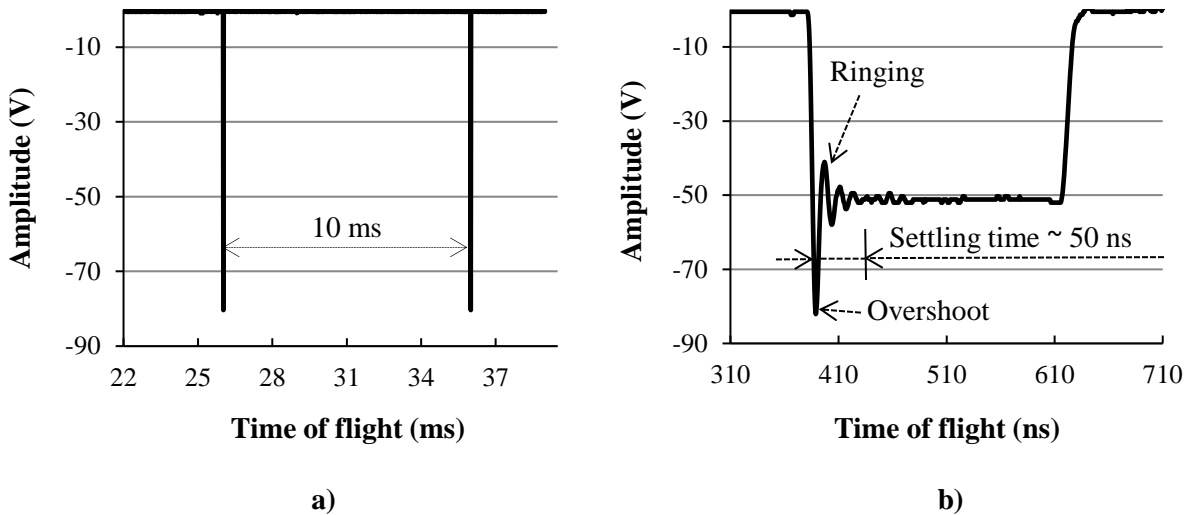


**Figure 4-2: a) Two consecutive pulses generated from the pulser of TOPAZ. b) An illustration of the overshoot effect followed by a “ringing” and settle time for an initial pulse of -50 V.**

After the initial pulse of -50 V was analysed, the same analysis was performed for a number of initial pulses with amplitudes ranging between -50 V (min) and -200 V (max), with a step of -10 V. These pulses, averaged for five measurements, can be seen in Figure 4-3. It is clear that, as the amplitude of the initial pulse increases, the electrical system becomes less stable. This is characterised through enhanced overshoot and ringing together with prolonged settling times as the amplitude goes to -200 V. At the set up value of -50 V, the overshoot will cause the pulse value to drop to approximately -80 V (difference of -30 V); however, if the setup pulser voltage value is -200 V, the pulse will drop all the way to approximately -320 V (difference of -120 V). In both cases, after the settling time of ~50 ns or ~75 ns is completed, the initial pulse will achieve the setup value of -50 V and -200 V, respectively. This is the most important result coming out from this analysis, as it shows that the initial pulse coming out from the pulser of the ultrasonic machine TOPAZ will achieve exactly the amplitude value that is setup by the user and thus can be used for planned ultrasonic measurements.

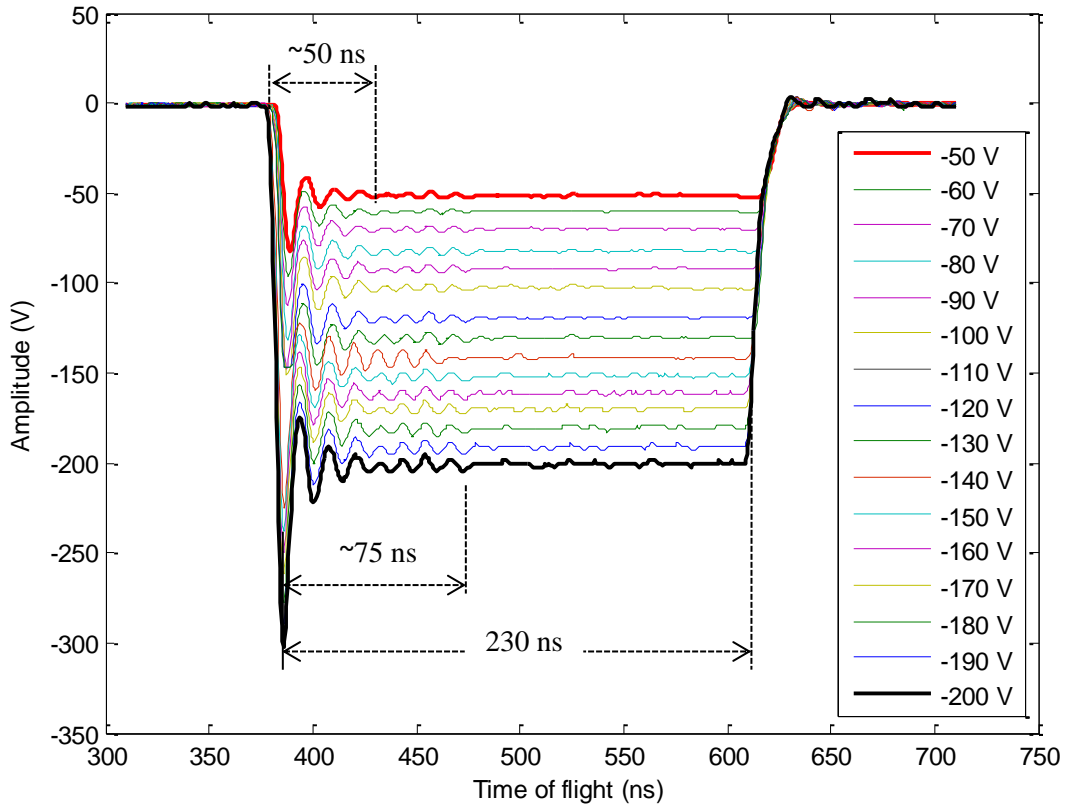


**Figure 4-3: The initial pulses coming out from the pulser of the ultrasonic machine TOPAZ, for amplitude ranging from a min of -50 V to a max of -200 V, averaged for 5 measurements.**

From Figure 4-3, it is clear that the analysed initial pulse recorded at different amplitude values has a square form of only half a cycle (in the negative phase). This is due to its main feature, to be very short and only “plucking” the piezoelectric element without driving it at a certain frequency. Taking into account Eq. (4.1):

$$N = f \cdot l \tag{4.1}$$

where  $N$  (No) is the number of cycles in a pulse,  $f$  (Hz) is the resonant frequency and  $l$  (s) is the pulse duration, it is possible to calculate that the pulse duration for the resonant frequency of 2.178 MHz (calculated for a GaPO<sub>4</sub> element 1 mm thick) and half a cycle ( $N = 0.5$ ) will be 230 ns. This value can also be directly read from Figure 4-3. Finally, for a piezoelectric element of a different thickness (and thus different resonant frequency), the pulse duration will also be different to ensure that the mentioned square-form-half-a-cycle of the initial pulse is maintained throughout measurement.

#### 4.4 Thickness gauging at high temperatures using GaPO<sub>4</sub>

Thickness gauging is the most basic measurement that can be done with a transducer. Normally it is used to assess the extent up to which mechanisms such as corrosion and erosion affect the components’

integrity by reducing their wall thickness over time [127]. As already emphasised, conventional transducers are limited to around 180 °C due to the majority of devices relying on piezoelectric ceramic material PZT to generate and detect the acoustic signal [128]. It will be shown in this thesis that by using piezoelectric single crystal GaPO<sub>4</sub>, not only it is possible to perform short-term thickness gauging at high temperatures up to 580°C (useful for non-destructive testing), but also that it is possible to do so for an extended period (useful for non-destructive monitoring).

Three thicknesses gauging experiments are reported in this chapter:

- In the first experiment, it is shown that by applying an initial pulse with an increased amplitude value (voltage) to the resonating GaPO<sub>4</sub> element, it is possible to achieve a reflected ultrasonic echo from the backwall of the steel test-block with higher peak-to-peak amplitude and that this enables a higher SNR level. Further, it is shown that the relationship between the amplitude of the initial pulse and the one of the reflected echo will be linear.
- In the second experiment, it has been shown that a GaPO<sub>4</sub> element, bonded to a steel test-sample using an adhesive, can be used for practical thickness gauging up to the target temperature of 580°C, where all the received ultrasonic echoes will stay above the noise level needed for practical NDT (>6 dB).
- Finally, it has been demonstrated that a GaPO<sub>4</sub> element can resonate at 580°C for an extended period of time (15 consecutive days) when degradation of the platinum electroding and of the steel test-sample occurs, leading to the loss of the reflected echoes.

### **4.4.1 Base-line thickness gauging at ambient temperature**

A GaPO<sub>4</sub> element coated in the parallel electrode configuration, with a Pt layer of 200 nm, an area of 100 mm<sup>2</sup> and thickness of 0.8 mm (calculated frequency  $f_r=2.723$  MHz) was coupled to a carbon steel block (30 mm thick) using silver adhesive Elecolit 3653, Figure 4-4 a). Elecolit 3653 is the least viscous of all the acquired adhesives for intended HT application (reported in Table 2-3) and, for this, it is the easiest to apply to the surface of the GaPO<sub>4</sub> element. However, it offers reported maximum operation up to 180°C only. As this first experiment was done at ambient temperature, this was not an issue. Furthermore, pure nickel glass braided wiring was used to connect the GaPO<sub>4</sub> element to the TOPAZ pulser-receiver instrument. The schematic of the setup used for this base-line ultrasonic experiment using a GaPO<sub>4</sub> element can be seen in Figure 4-4 b). In terms of the test-conditions, a pulser voltage ranging from -50 V (min) to -200 V (max) was used with a pulse width of 184 ns and a band-pass (BP) filter of 1-5 MHz. No rectification and no smoothing of the ultrasonic waveforms were applied. The pulse width of 184 ns was calculated using Equation (4.1) for the resonating frequency of 2.723 MHz in order to achieve the square-form-half-a-cycle initial pulse, as explained in section 4.3.2.

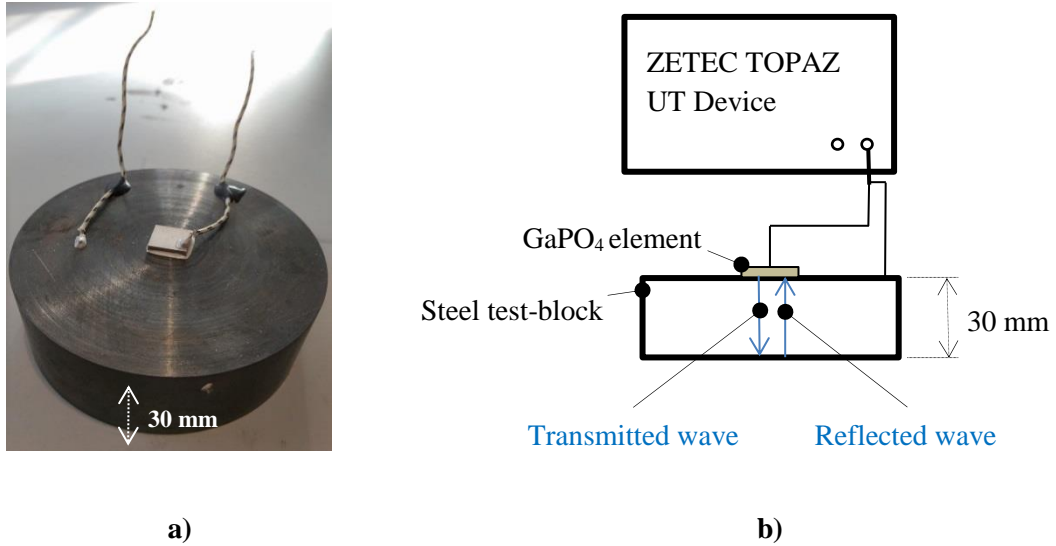


**Figure 4-4:** a) A GaPO<sub>4</sub> element is coupled to steel test-block using silver adhesive with attached nickel wiring; b) The schematic of setup used for base-line experiment at ambient temperature.

#### 4.4.2 Results of the base-line thickness gauging at ambient temperature

The A-scan containing waveforms of the fastest arriving echo reflected from the backwall of the steel test-block at 30 mm and received back by the GaPO<sub>4</sub> element can be seen in Figure 4-5.

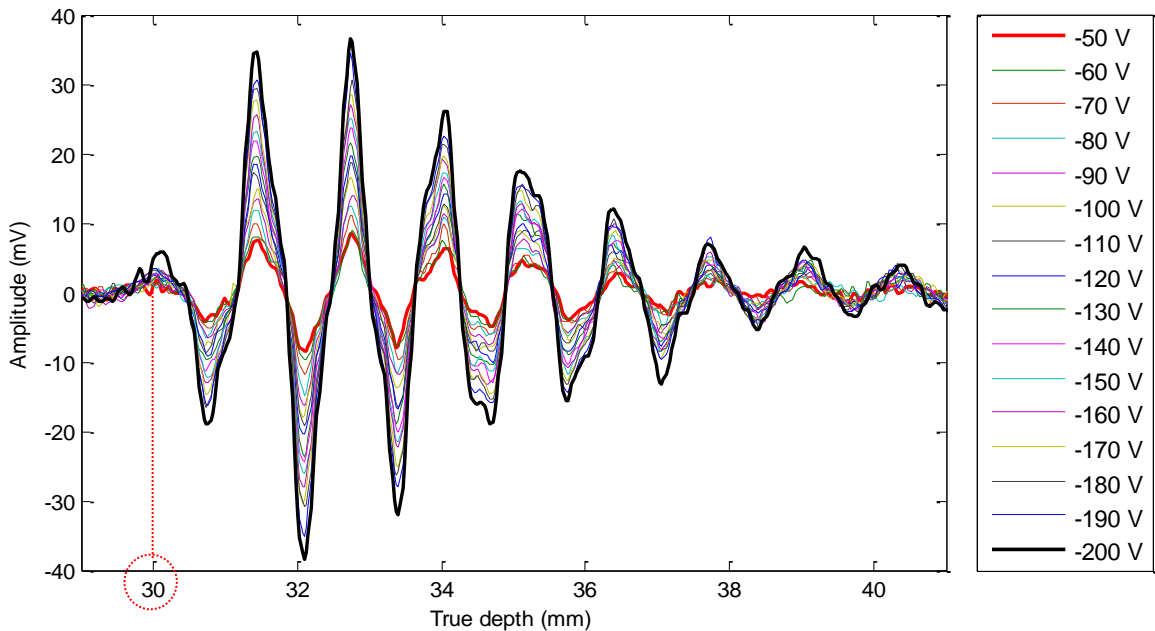


**Figure 4-5:** The waveforms of the fastest arriving echo reflected from the backwall of carbon steel block at 30 mm and received by GaPO<sub>4</sub> element, for the initial pulse from -50 V to -200 V.

First, it is clear from Figure 4-5 that as the amplitude of the initial pulse goes from the minimum value of -50 V (red trace) up to the maximum value of -200 V (black trace), the amplitude of the received echoes to the GaPO<sub>4</sub> element will also increase. For example, when an initial electrical pulse of -50 V is applied, the amplitude of the received echo will be only 16.94 mV; however, when an initial pulse of -200 V is applied, the amplitude of the received echo will go up to 74.98 mV. This means that the more electrical energy is delivered to the GaPO<sub>4</sub> element, the more electrical/ultrasonic energy will also be generated from the piezoelectric element towards the steel test material and, finally, after reflection from the backwall of the steel block, the more will be received back by the GaPO<sub>4</sub> element. Second, the amplitude of the received ultrasonic echoes to the GaPO<sub>4</sub> element, as a function of the initial pulse ranging from -50 V to -200 V can be seen below in Figure 4-6 a). From here, it is very clear that the relationship between the amplitude of the initial pulse applied to the GaPO<sub>4</sub> element and the amplitude of the ultrasonic echo / electrical signal received back by the same piezoelectric element will be practically linear. Finally, it is also interesting to see if changing the initial pulse from -50 V to -200 V will affect only the received ultrasonic echo/electrical signal, or if it will also have an impact on the level of nearby noise. In order to test the achieved SNR, the detectability of the ultrasonic reflection reported in Figure 4-5 was assessed using the SNR calculation. Calculation of the SNR level throughout this thesis is done according to Eq. (4.2):

$$SNR = 20 \log_{10} \left( \frac{|P_r|}{\sigma_{x(t)}} \right) \quad (4.2)$$

where  $P_r$  is the peak-to-peak amplitude of the reflection from the backwall and  $\sigma$  is the standard deviation of  $x(t)$ , the signal waveform under consideration [129].

The results of the SNR calculation can be seen below in Figure 4-6 b). Here one can see that by increasing the amplitude of initial pulse from minimum -50 V up to maximum -200 V, the SNR level will also go up. For example, when an initial pulse of -50 V is applied to GaPO<sub>4</sub> element, the SNR level of the received ultrasonic echo that is generated electrical signal will be 9.2 dB, and when an initial pulse of -200 V is applied to the GaPO<sub>4</sub> element, the SNR level of the echo/signal will be 19 dB.

It is important to conclude with the observation that all derived SNR values were suitably high (above 6 dB), so that ultrasonic reflections from the backwall of steel block could easily be identified above the background noise. For a practical ultrasonic measurement, the SNR level needs to be greater than 6 dB that is the signal amplitude needs to be twice as strong as the noise amplitude [130].

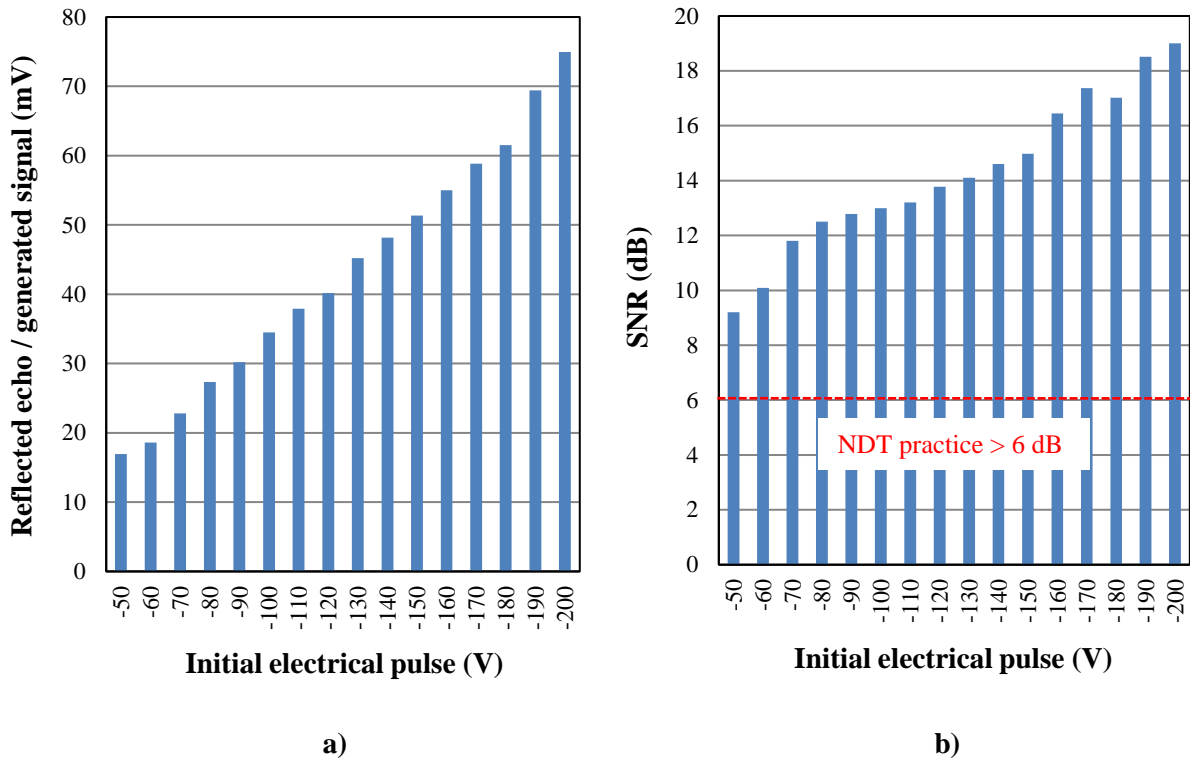


**Figure 4-6: a) Reflected echoes received back by the GaPO<sub>4</sub> element as a function of the initial pulse ranging from -50 V to -200 V. b) SNR level (in dB) as a function of the same initial pulse.**

#### 4.4.2.1 Fourier analysis and the transducer's bandwidth

Using the Fourier analysis, an ultrasonic waveform can be transformed from its original time-domain (A-scan) to a representation in the frequency-domain [131]. From here it is possible to define the bandwidth of a transducer, together with its characteristic frequencies (centre frequency  $f_c$ , lower frequency limit  $f_l$  and upper frequency limit  $f_u$ ), that are usually defined as the frequencies at which the amplitude is reduced by a given factor. This reduction factor can be taken to be 30% (-3 dB) or 50% (-6 dB) [76]. An example of a frequency-domain waveform of a commercial 5 MHz transducer, with marked bandwidth and the characteristic frequencies, can be seen in Figure 4-7.

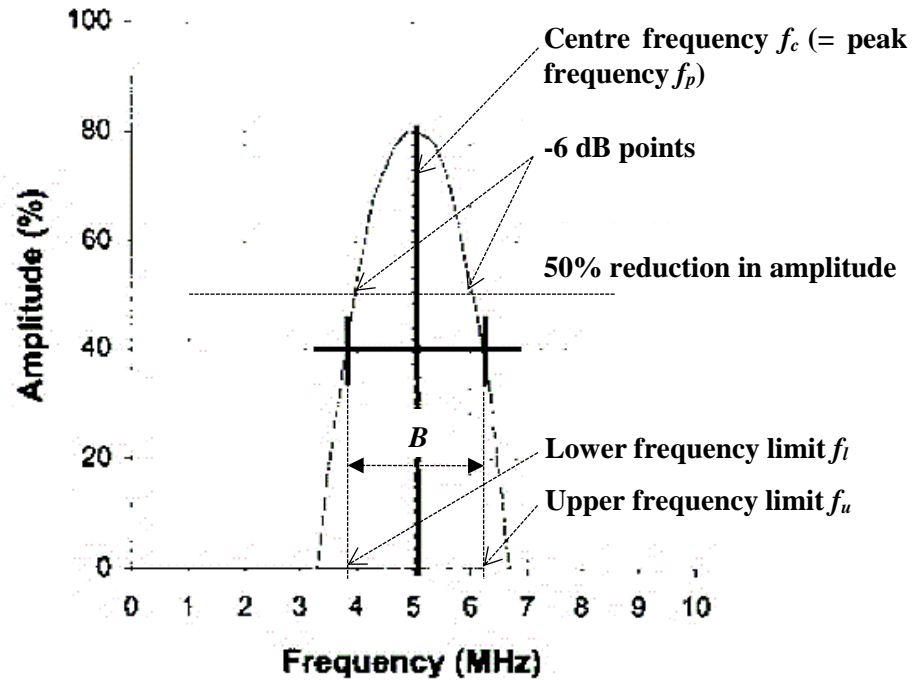
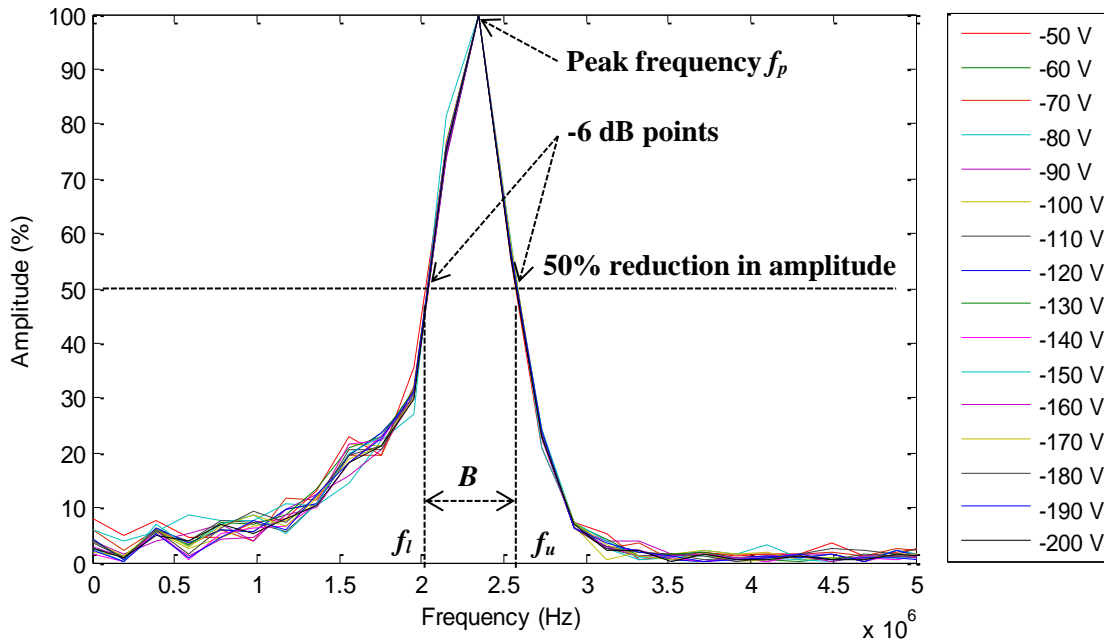


Figure 4-7: Bandwidth of a commercial 5 MHz transducer [76].

For the waveforms reported in Figure 4-5, a signal analysis in the frequency-domain was done using MATLAB R2011b software package. The normalised frequency domain of the fastest arriving waveform received at the GaPO<sub>4</sub> element (Figure 4-5) can be seen in Figure 4-8. From this figure, one can see that the centre frequency is 2.343 MHz. This is a 13.95% attenuation compared to the frequency value before the GaPO<sub>4</sub> element was attached to the steel block (2.723 MHz) and is a result of the steel block acting like a damping mass to the free vibration of piezoelectric element. The second important thing one can see here is that as the initial electrical pulse goes from -50 V to -200 V, the peak frequency will not change and it will stay constant of 2.343 MHz. This is because the frequency is not a function of the electrical energy input but rather a function of the initial pulse width, shape (square-form-half-a-cycle) and the thickness of the piezoelectric element (in this case 0.8 mm). Finally, from the same Figure 4-8 one can evaluate the frequency spectrum or the bandwidth  $B$  of the resonating GaPO<sub>4</sub> element that was coupled to the steel test-block. The lower frequency limit  $f_l$  is at 2.03 MHz and the upper frequency limit  $f_u$  is at 2.58 MHz. This means that the centre frequency  $f_c$  (at -6 dB) will be 2.17 MHz, which is close to the peak frequency  $f_p$  at 2.343 MHz (difference of 7.38%). Finally, this means that the bandwidth will be from 2.03 MHz to 2.58 MHz or  $B = 0.55$  MHz. This very narrow bandwidth is a consequence of the fact that no damping body was applied to the back face of the GaPO<sub>4</sub> element (the steel test-block was applied from the front side, and has dampened the vibration slightly as explained above), which allowed it to vibrate with around 8 cycles in each ultrasonic waveform. However, in a practical NDT measurement, too long waveforms would reduce the sensitivity that can be achieved with the given transducer. For this, the piezoelectric element of a transducer for non-destructive testing

normally comes with a damping body applied to its back face, which reduces the number of cycles in an ultrasonic waveform down to 1 or 2 only [76].



**Figure 4-8: Normalised frequency domain of the fastest arriving ultrasonic waveform that was received at the GaPO<sub>4</sub> element, for the initial pulse ranging from -50 V (min) to -200 V (max).**

### 4.4.3 Thickness gauging at high temperatures

After it has been demonstrated that a GaPO<sub>4</sub> element generates an ultrasonic waveform with an amplitude that is linearly dependent on the applied initial pulse, the next step was to examine the capability of GaPO<sub>4</sub> elements for a practical ultrasonic measurement such as thickness gauging at high temperatures. For this reason, two GaPO<sub>4</sub> elements of same configuration as before (Pt electrodes thin film of 200 nm, area of 100 mm<sup>2</sup>, thickness of 0.8 mm and resonant frequency of 2.723 MHz) were mounted onto a steel test-block with 25 mm thickness using silver adhesive Duralco 124, as shown in Figure 4-9. Finally, two nickel conductor wires were attached to the two GaPO<sub>4</sub> samples and one conductor wire was grounded to the steel block using the same silver adhesive.

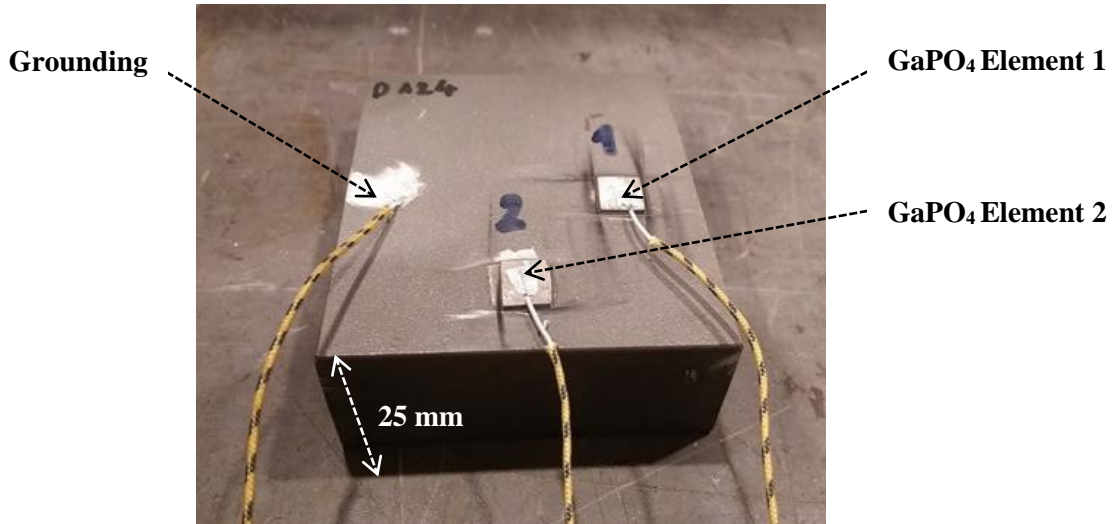


**Figure 4-9:** Two GaPO<sub>4</sub> elements were mounted onto a steel block (25 mm thickness) using silver adhesive. The same adhesive was used to wire the two elements to the nickel conductors.

#### 4.4.3.1 Experimental setup for thickness gauging up to 580°C

The experimental setup used for ultrasonic thickness gauging using two GaPO<sub>4</sub> elements can be seen in Figure 4-10 a). The two GaPO<sub>4</sub> elements coupled to the steel block were placed in furnace (1) (Carbolite LHT6-30). An opening on the top of the furnace allowed the nickel wiring to go out from GaPO<sub>4</sub> elements to TOPAZ pulser-receiver instrument (2) and also for a K-type thermocouple to USB TC-08 thermocouple data logger (3) (Pico Technology Ltd). The data collected using the pulser-receiver instrument and the thermocouple data logger were then transferred to PC (4) for further analysis. The steel block with coupled two GaPO<sub>4</sub> transducers to it, after it was placed inside the electric furnace, can be seen in Figure 4-10 b). The temperature of the steel block was measured with thermocouple type-K data logger (5) with resolution better than 0.025°C, which contacted the topside of the steel block through a heat transfer paste; see Figure 4-10 b).

The ultrasonic reflections from the backwall of the steel block were recorded at every 50°C, from 25°C up to 580°C, where the hold time of 15 minutes at each temperature interval was applied to ensure an isothermal ultrasonic measurement. Finally, the test conditions were the same as in the previous experiment, and a half-a-cycle pulse of -75 V was delivered to the two GaPO<sub>4</sub> elements.

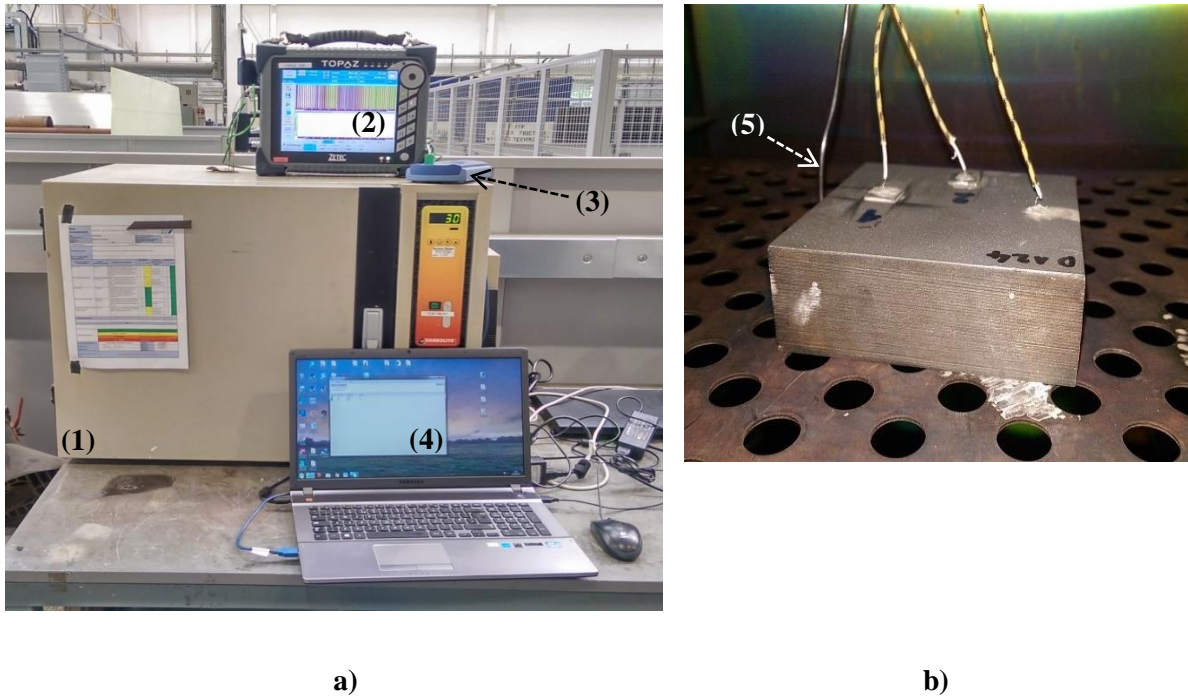
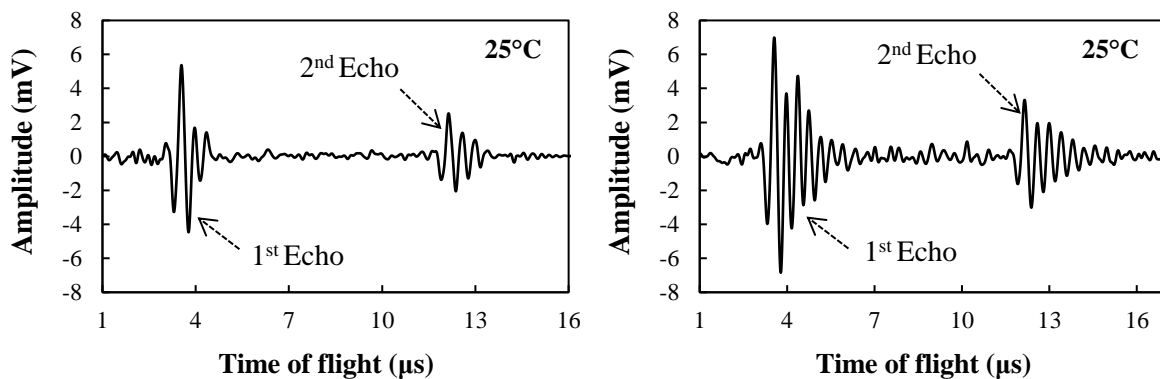


**Figure 4-10: a) The experimental setup for ultrasonic thickness gauging up to 580°C. b) The GaPO<sub>4</sub> samples coupled to the steel block using silver adhesive were placed inside a furnace.**

#### 4.4.4 Results and discussion of the thickness gauging up to 580°C

The GaPO<sub>4</sub> element No 1 failed somewhere above 450°C. It was discovered later that the silver adhesive did not achieve a good coupling between the piezoelectric element and the nickel wiring through the curing procedure and thus the wiring severed from the surface before achieving the target temperature. On the other hand, the GaPO<sub>4</sub> element No 2 performed well throughout the ultrasonic testing confirming GaPO<sub>4</sub>'s suitability for thickness gauging up to the target temperature of 580°C.

Eight A-scans containing two consecutive ultrasonic reflections from the backwall of the steel test-block that were received at the two GaPO<sub>4</sub> elements at 25°C, 200°C, 400°C and 450°C/580°C, can be seen in Figure 4-11 a) and b), respectively.



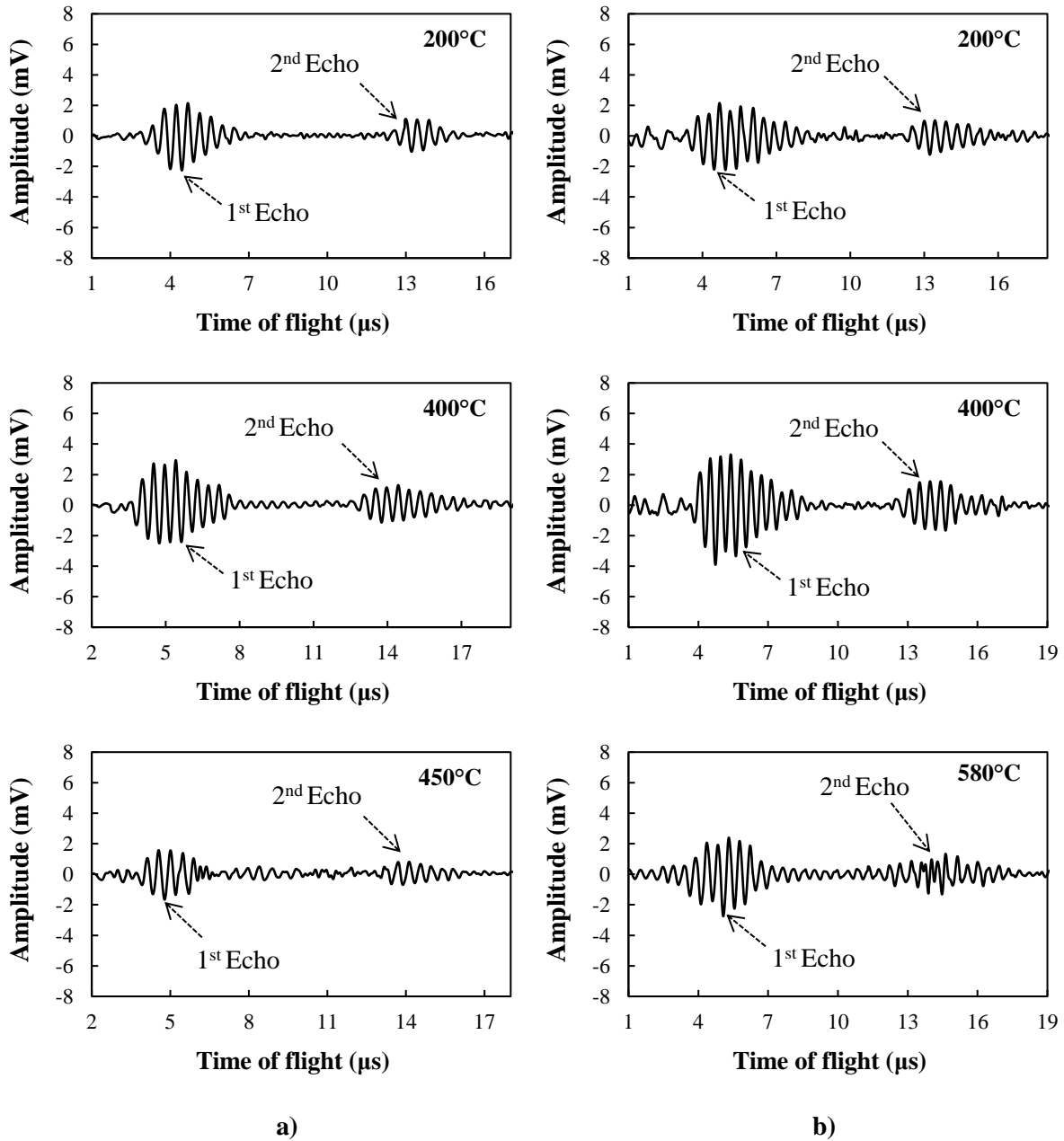


**Figure 4-11: Two consecutive reflections from the backwall of the steel block that were received at a) GaPO<sub>4</sub> element No 1 up to 450°C and b) GaPO<sub>4</sub> element No 2 up to temperature of 580°C.**

One can see that the reflected ultrasonic signals are both attenuated and lengthened with the introduction of heat. This agrees well with similar tests done on GaPO<sub>4</sub> elements coupled to steel using silver adhesives, although not up to the same temperature level [65], [66]. This reduction in sensitivity of GaPO<sub>4</sub> elements at high temperatures is suspected to be the result of an increase in attenuation of steel during heating [132]. As the temperature of the steel goes up, its modulus of elasticity  $E$  (N/m<sup>2</sup>) and density  $\rho$  (kg/m<sup>3</sup>) will decrease, and other properties such as Poisson's ratio  $\nu$  will change too [133]. For carbon steel such as AISI 12L14 that was used in thickness gauging reported here, this decrease in physical properties from 25°C up to 580°C will only be about 2% in terms of its respective density;

however, the modulus of elasticity will be reduced by more than 50% [134]. The reason is that the acoustic energy generated from the resonating GaPO<sub>4</sub> element will transfer more easily and quickly from one particle to the next in a steel material having greater elasticity, and will reflect more sharply from its backwall. As the elasticity decreases, the acoustic energy will also attenuate and once received back at the GaPO<sub>4</sub> element, this will result in a smaller generated peak-to-peak voltage on the surface of the piezoelectric element, as the sensitivity of the element has decreased. The direct consequence of the attenuation is enhanced “ringing” of the GaPO<sub>4</sub> elements that can be seen in the A-scans from Figure 4-11. As now the elasticity of steel is lower, it will take more time for the acoustic energy to travel from the GaPO<sub>4</sub> element to the backwall of the steel block and then to reflect and travel back to the GaPO<sub>4</sub> element in the same energy amount as at the lower temperature. Of course, one has to assume there was no energy loss in the process [135].

Finally, the de-bonding phenomenon caused by thermal expansion at HT is also likely to contribute to enhanced “ringing” and attenuated signals, as the rapid increase in temperature from 25°C up to 580°C in less than 8 hours could produce a thermal strain in the transducer’s components due to different CETs, as explained in [136]. Mismatching of CETs, especially regarding the silver adhesive, which exhibits a CET two times higher than the one of Pt electroding, is easily seen from Table 4-1:

**Table 4-1: CETs of the materials that were used for ultrasonic thickness gauging at HT.**

CET [ $10^{-6}/^{\circ}\text{C}$ ] @ 20°C	GaPO <sub>4</sub>	Pt electroding	Silver adhesive	Steel block
	12.78	9	18	11.7

Finally, one should pay attention to the shift of reflections to the right at the temperature of 580°C (the red waveform in Figure 4-12). This is because the velocity (that is modulus of elasticity, density and Poisson’s ratio) and thermal expansion of steel change with the rise in temperature. Ultrasonic wave velocity as a function of temperature, for different types of carbon and stainless steels, can be found in [137] and in terms of P91 alloy steel, a separate report was produced as part of this research to determine how its velocity changes with temperature [138]. The speed of sound travelling through P91 steel at 25°C will be 5940 m/s, and at temperature of 580°C will be 5127 m/s; a difference of 15%. This also means that it will take 15% more time for the waveforms to be received at the GaPO<sub>4</sub> element at 580°C, and this is why the red coloured waveform in Figure 4-12 has shifted to the right.

The working principle of commercial pulser-receiver instruments, such as TOPAZ, is to measure the time-of-flight of ultrasonic signals and then, by taking into account velocity, to calculate the thickness of the test-part and/or the depth at which a defect is located. However, as the pulser-receiver instrument normally compute using velocity values for room temperature, they will make a mistake if the

inspection is done at a higher (or lower) temperature. For this, if one wants to measure the correct thickness/location of a defect at any given temperature in a test-sample with complex geometry, this change of velocity with temperature must be taken into account by using the literature previously listed: for carbon and stainless steel [137]; and for P91 steel [138].

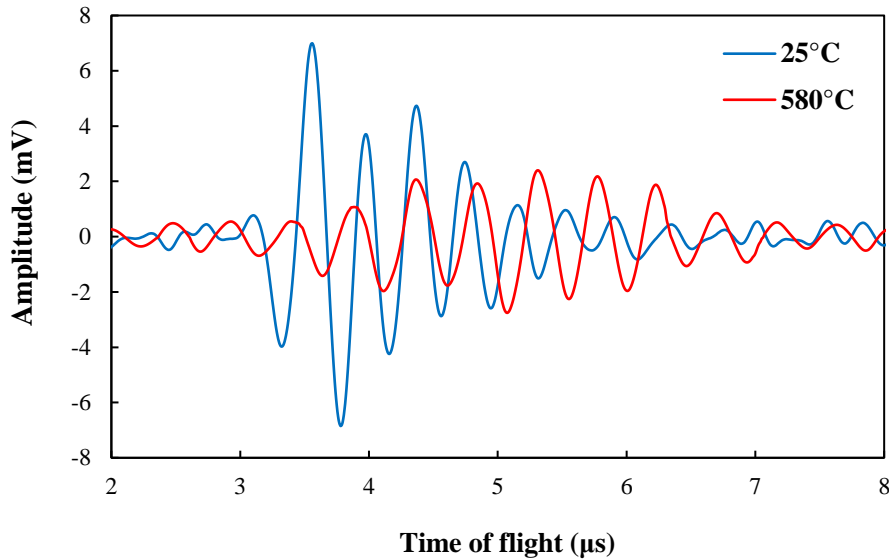


**Figure 4-12: The fastest arriving reflections received at the GaPO<sub>4</sub> element No 2, at 25°C (blue trace) and 580°C (red trace), showing the influence of temperature on measured time-of-flight.**

The calculated SNR values, for the ultrasonic waveforms received at GaPO<sub>4</sub> element No 1 (up to 450°C) and at GaPO<sub>4</sub> element No 2 (up to 580°C), are plotted together in Figure 4-13.

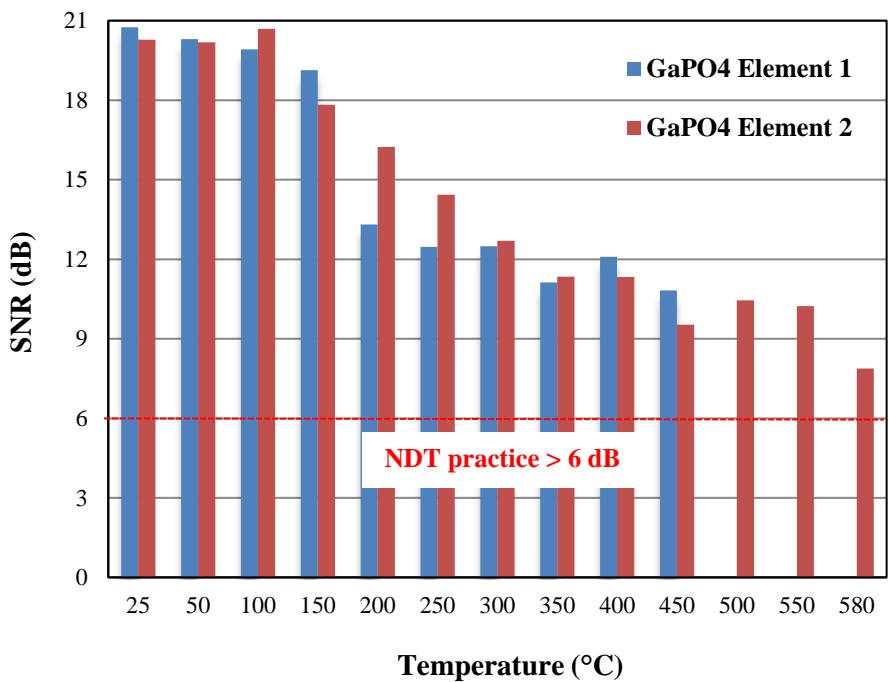


**Figure 4-13: SNR (in dB) for the reflections received at GaPO<sub>4</sub> element No 1 and No 2.**

Figure 4-13 shows good agreement between the SNR values calculated for GaPO<sub>4</sub> element No 1 (up to 450°C) and the values calculated for GaPO<sub>4</sub> element No 2 up to the same temperature level. For example, at 25°C, the SNR value was 20.75 dB (GaPO<sub>4</sub> element No 1) and 20.28 dB (GaPO<sub>4</sub> element No 2), and at 450°C was 10.83 dB (GaPO<sub>4</sub> element No 1) and 9.53 (GaPO<sub>4</sub> element No 2). A slight difference was observed between 200°C and 250°C. Second, the SNR value of GaPO<sub>4</sub> element No 2 increased between 450°C and 550°C but finally dropped down to 7.88 dB at the target temperature of 580°C. One can see from Figure 4-13 that by increasing the temperature to 580°C, the SNR level goes down due to attenuation of ultrasonic signals. However, all the calculated SNR values were still sufficiently high (above the threshold of 6 dB) that the ultrasonic reflections from the backwall of the steel test-block could easily be identified.

#### 4.4.4.1 Signal analysis in frequency-domain

Using Fourier analysis, the ultrasonic signals received at GaPO<sub>4</sub> element No 1 (up to 450°C) and at GaPO<sub>4</sub> element No 2 (up to 580°C) have been transformed from their original time-domain to a representation in the frequency-domain and these are plotted in Figure 4-14 a) and b), respectively.

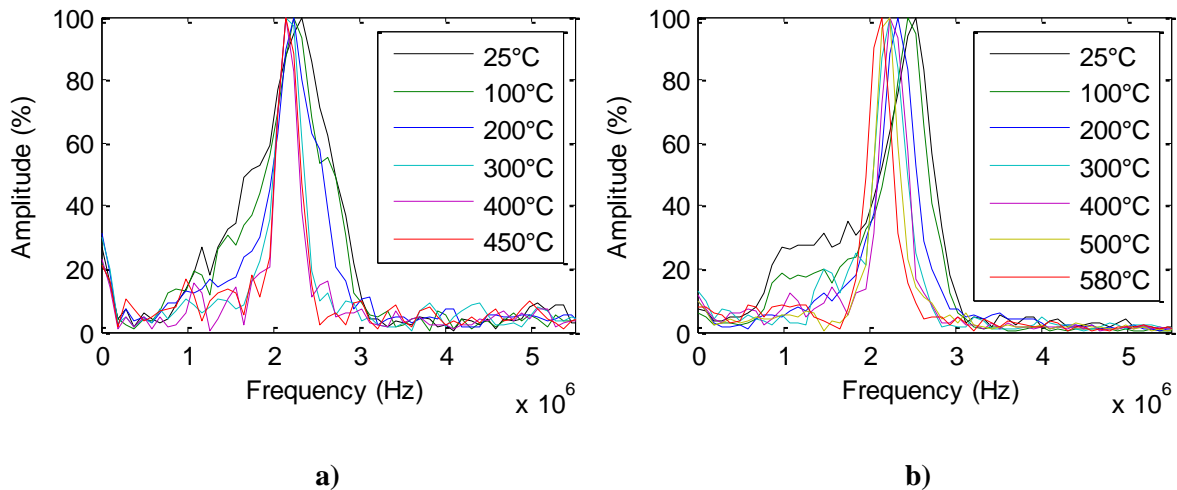


**Figure 4-14: Normalised frequency domain of the signals received at a) GaPO<sub>4</sub> element No 1 up to 450°C and b) GaPO<sub>4</sub> element No 2 up to the target temperature of 580°C.**

For easier viewing, the peak frequency values at temperatures up to 450°C (GaPO<sub>4</sub> No 1) that is 580°C (GaPO<sub>4</sub> No 2), were taken from Figure 4-14 a) (GaPO<sub>4</sub> No 1) and Figure 4-14 b) (GaPO<sub>4</sub> No 2) and then plotted together with the resonant frequency values that were measured in the earlier impedance analysis; see Figure 4-15.

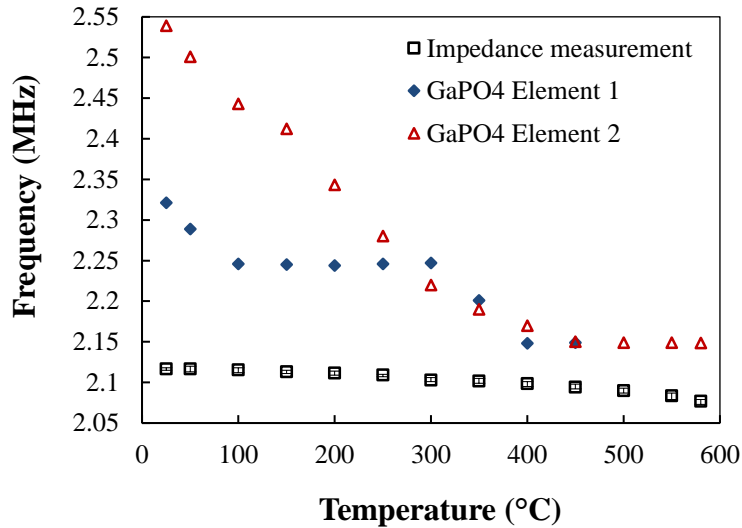


**Figure 4-15: Comparison of the frequency values derived from impedance tests on five GaPO<sub>4</sub> elements up to 580°C (black markers) and the values derived from ultrasonic tests for GaPO<sub>4</sub> element No 1 up to 450°C (blue markers) and GaPO<sub>4</sub> element No 2 up to 580°C (red markers).**

First, one can see that at 25°C, the three measurements give different frequency values. This is because the five GaPO<sub>4</sub> elements used for impedance analysis were 1 mm thick with a calculated resonant frequency of 2.178 MHz, and the two GaPO<sub>4</sub> elements used for ultrasonic analysis were 0.8 mm thick with a calculated frequency of 2.723 MHz. However, once the five GaPO<sub>4</sub> elements were affixed to nickel wiring using silver adhesive, their resonant frequency was slightly attenuated to around 2.117 MHz as explained in section 3.8.1. Similarly, once the two GaPO<sub>4</sub> elements were coupled to the steel block using the same silver adhesive, their vibration was also attenuated to 2.321 (GaPO<sub>4</sub> element No 1) and to 2.539 (GaPO<sub>4</sub> element No 2). Probably, the GaPO<sub>4</sub> element No 1 has experienced more attenuation than GaPO<sub>4</sub> element No 2 due to the deficient curing procedure of the applied adhesive, as explained in section 4.4.4.

Second, from same Figure 4-15 one can see that as the temperature in the furnace goes up, the resonant frequency value decreases in all three cases. However, the rate of this decrease was different for the impedance measurements from one of the ultrasonic measurements. The drop of the resonant frequency of five GaPO<sub>4</sub> elements derived from the impedance analysis was only 1.93% in the range from 25°C up to 580°C (black markers), which confirms good thermal stability of the piezoelectric effect of this piezoelectric single crystal. However, once the two GaPO<sub>4</sub> elements were attached to the carbon steel test-block using silver adhesive and then heated to 450°C/580°C, the occurrence of attenuation in the carbon steel test-material caused the peak frequency to decrease to a much lower value. For the GaPO<sub>4</sub> element No 1 (blue markers) from 25°C up to 450°C, this decrease was from 2.321 MHz down to 2.148 MHz, which was a drop of 7.45%. On the other hand, for the GaPO<sub>4</sub> element No 2 (red markers) from 25°C up to the target temperature of 580°C, the decrease was from 2.539 MHz down to the same value

of 2.148 MHz, and this drop was calculated to be 15.40%. This means that in the same range from 25°C to 580°C, the drop in the frequency of a GaPO<sub>4</sub> element that was coupled to the steel structure was about 8.5 times larger than the drop in the frequency of the same GaPO<sub>4</sub> element that was freely resonating in air. In practical ultrasonic measurements, where a piezoelectric elements is either permanently attached to the test-structure or it is enclosed within an ultrasonic transducer, one will need to take this frequency drop with temperature into account, and relate it to the change in size of a defect that can still be resolved with this element at any given temperature. If the already mentioned rule is applied, that a defect in the test-structure must be equal or larger than half of the wavelength to stand a reasonable chance of being detected, it is possible to calculate that for an artificial defect such as SDH of 1 mm, the  $\lambda/2$  must not to exceed 1 mm. Using the Eq. (4.3):

$$\lambda = \frac{v}{f} \tag{4.3}$$

where the velocity  $v$  of GaPO<sub>4</sub> is 4356 m/s, it is possible to calculate that even if the frequency value drops by 16.68% up to 580°C, the GaPO<sub>4</sub> element should still be able to resolve the given 1 mm hole, as the  $\lambda/2$  value at 580°C is calculated to be 1.01 mm; see Table 4-2.

**Table 4-2:  $\lambda/2$  value for the peak frequency  $f_p$  derived from ultrasonic measurement on GaPO<sub>4</sub> element No 2, calculated at 25°C and at the target temperature of 580°C.**

Temperature	$f_p$	$\lambda/2$
(°C)	(MHz)	(mm)
25	2.539	<b>0.86</b>
580	2.148	<b>1.01</b>

#### 4.4.5 Long-term thickness gauging using GaPO<sub>4</sub> element at 580°C

After reaching the temperature of 580°C, the ultrasonic reflections from the backwall of the steel block were recorded continuously at the same temperature for fifteen days. The four A-scans (in time-domain), recorded on the 1<sup>st</sup>, 13<sup>th</sup>, 14<sup>th</sup> and 15<sup>th</sup> days of testing at 580°C, can be seen in Figure 4-16.

From Figure 4-16 one can see that once GaPO<sub>4</sub> element has stabilised at the temperature of 580°C (24 hours at the temperature), less “ringing” and less attenuation was observed in the received waveforms. This is probably because previously developed stresses due to different CETs (Pt electrode, raw GaPO<sub>4</sub>, silver adhesive, carbon steel) initiated with the rapid increase in temperature from 25°C up to 580°C in less than 8 hours, was eliminated in this experiment with the constant temperature of 580°C.

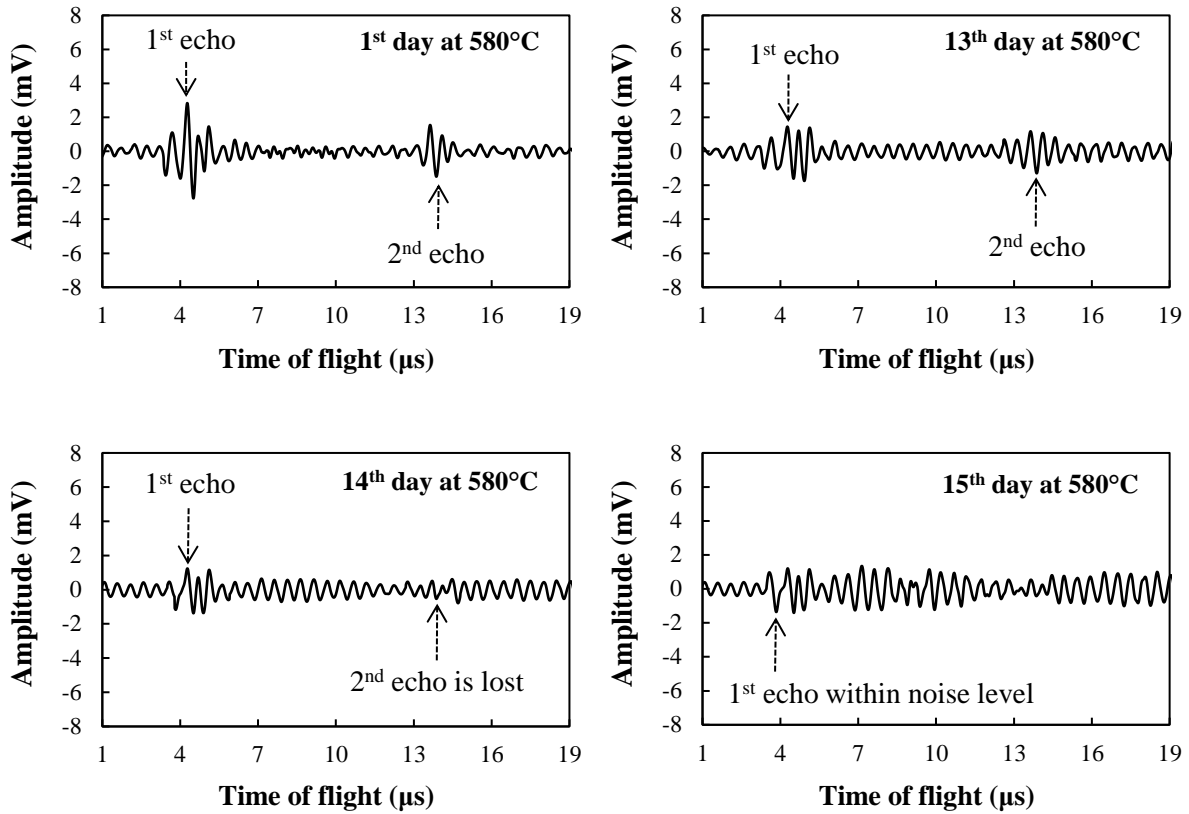


**Figure 4-16: Two consecutive ultrasonic reflections from the backwall that were received at GaPO<sub>4</sub> element No 2. The echoes were recorded on the 1<sup>st</sup>, 13<sup>th</sup>, 14<sup>th</sup> and 15<sup>th</sup> days at 580°C.**

Second, the amplitude of the received waveforms was virtually constant from the 1<sup>st</sup> day of testing until the 10<sup>th</sup> day of testing at 580°C, with a value slightly above 5 mV. The first drop in amplitude was experienced on the 11<sup>th</sup> day (4.9 mV) and then in the next 3 days the amplitude significantly reduced to 2.54 mV (14<sup>th</sup> day at 580°C). In addition, the received waveforms fell within the noise level on the 15<sup>th</sup> day, which removed the need for further measurements. All discussed amplitude values of the received ultrasonic waveforms can be seen plotted in Figure 4-17 a).

Finally, detectability of the first or fastest arriving waveform from the backwall of the steel block that was received at GaPO<sub>4</sub> element No 2 at 580°C was assessed using the same SNR calculation as before. All the calculated SNR values for each day of testing from 1<sup>st</sup> until the 14<sup>th</sup> were above the threshold of 6 dB, which was high enough for the received waveforms to be clearly resolved from the background noise, Figure 4-17 b).

## High Temperature Ultrasonic Analysis of GaPO<sub>4</sub> Elements

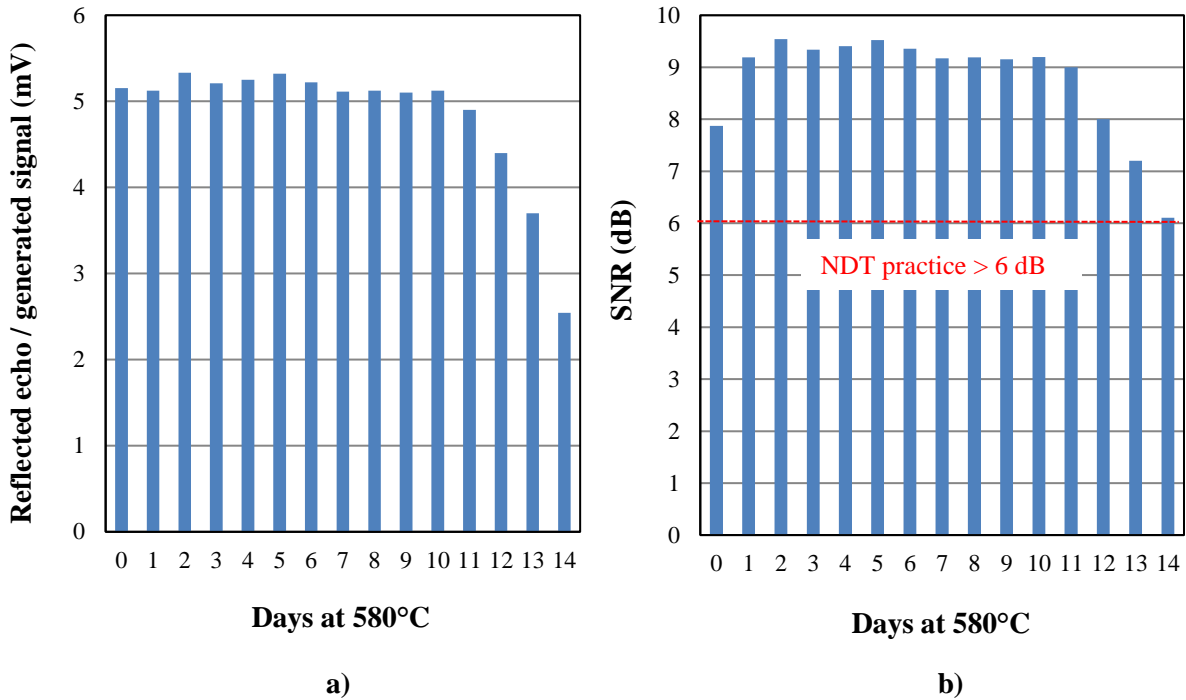


**Figure 4-17: a) Generated signal amplitude and b) calculated SNR for the fastest arriving reflection from the backwall received back at the GaPO<sub>4</sub> element No 2, at 580°C for 14 days.**

Finally, the most important result from this HT experiment is that it has been demonstrated for the first time that a piezoelectric element machined from single crystal GaPO<sub>4</sub> can be used for practical ultrasonic measurements at the operating temperature of a power plant (580°C) over an extended period (minimum 14 days). Similar ultrasonic tests that can be found in the literature have been done for a maximum period of few hours (or one day only at HT but at temperatures below 580°C) [65], [66]. It is assumed that, by replacing the carbon steel test-material with more suitable corrosion resistant such as stainless steel or P91, it is possible to allow for a much longer ultrasonic measurement using the same single crystal GaPO<sub>4</sub>. This has already been indicated through the earlier impedance analysis, where it was shown that a GaPO<sub>4</sub> element can resonate at 580°C for at least 25 days (600 hours).

After the exposure to the temperature of 580°C for 15 consecutive days, the carbon steel test-block evidenced severe oxidation/corrosion, which ruined its surface layer and accounted for a significant drop in the SNR value on the 15<sup>th</sup> day of measurement. For this reason, after the 15<sup>th</sup> day, more background noise than reflection was observed in the received waveforms. This practically prevented further measurement. The devastating effect that a long-term exposure to 580°C had on the carbon steel test-block and the coupled two GaPO<sub>4</sub> elements, can be seen in Figure 4-18 a) and b). From Figure a) one can see that the nickel wire is no longer connected to GaPO<sub>4</sub> element No 1, which answers why the reflections previously received on the element were lost somewhere above 450°C. As explained before, the nickel wire was bonded to GaPO<sub>4</sub> element using the adhesive Duralco 124. Once they were bonded

together using this silver adhesive, a curing procedure was applied in order to achieve full adhesion strength. The same was done for GaPO<sub>4</sub> element No 2 and the nickel wire bonded to it. For an unknown reason, it seems like the bond between GaPO<sub>4</sub> element No 1 and the nickel wire was not achieved in the first place, leading later to a failure of the experiment at 450°C. On the other hand, the nickel wire stayed well-bonded to GaPO<sub>4</sub> element No 2 even after the exposure to 580°C for 15 days, when the experiment was stopped because of oxidation/corrosion of the carbon steel test-block caused by heat.

The nickel wire possibly did not bond well to the GaPO<sub>4</sub> element No 1 through the curing procedure and this later on caused the measurement to fail somewhere above 450°C

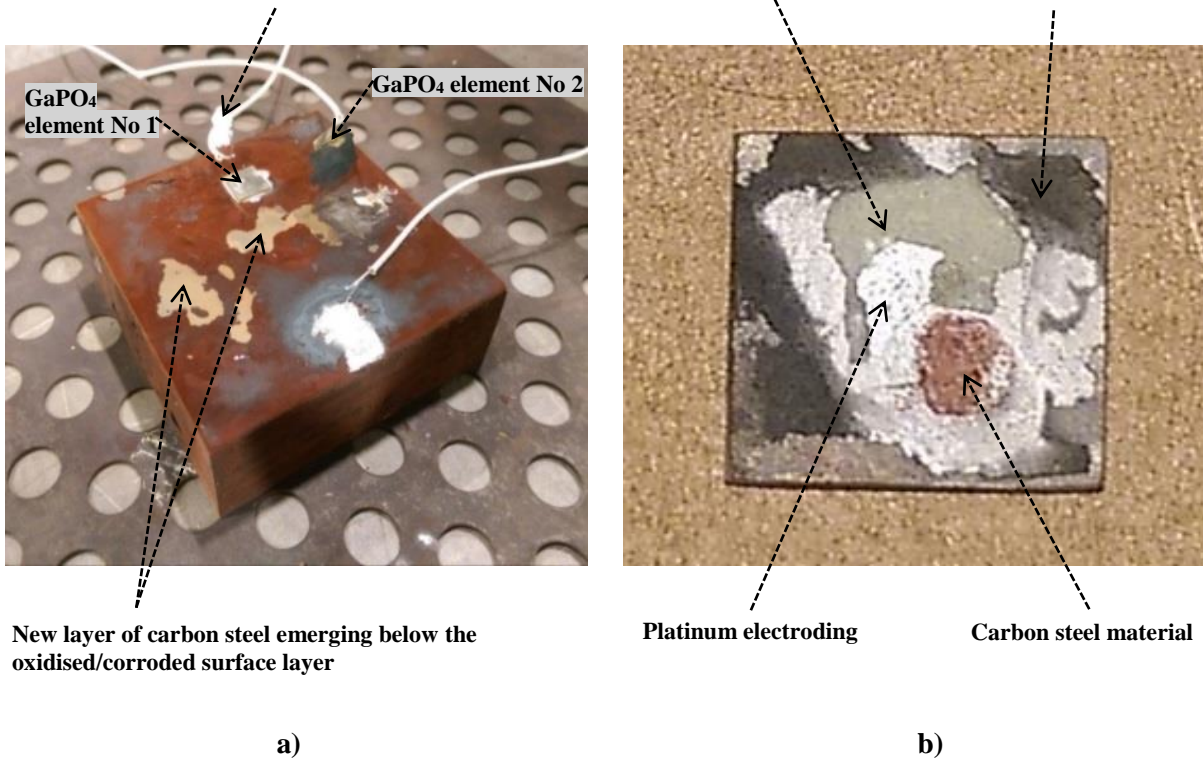


**Figure 4-18: a) The two GaPO<sub>4</sub> elements together with the corroded steel block showing the effect of exposure to 580°C for 14 days. b) The GaPO<sub>4</sub> element No 2, with seriously damaged platinum electroding, showing the complexity of ultrasonic measurements at high temperatures.**

Closer inspection of GaPO<sub>4</sub> element No 2 is displayed in Figure 4-18 b). This figure vividly shows the devastating effect the temperature of 580°C over the 15-day period had on the piezoelectric element. It has been reported in the literature that there are some limitations on the use of Pt electrode metallisation at temperatures higher than 650°C because of Pt thin film degradation phenomena as a result of agglomeration, recrystallization and dewetting effects [69]. The degradation of Pt electroding in this experiment possibly occurred as a combination of the degradation phenomena mentioned above and the degradation of the steel block surface, which probably caused an excessive stress on the bond-line between the GaPO<sub>4</sub> element, Pt electroding, silver adhesive and the steel test-block. This in the end led

to failure of the experiment after 15 days. To exclude the influence of corrosive sensitive carbon steel, all other measurements reported within this work and performed at 580°C for more than one day, were done using samples made of corrosion resistant stainless steel or P91 alloy steel. Unfortunately, all the attempts to find a better HT electroding solution failed, as the platinum electroding was only commercially available method for the required temperature level at the time this work was conducted.

Finally, the Fourier analysis of the signals recorded at 580°C showed that the peak frequency did not measurably change over 14 days and stayed at 2.148 MHz. On the other hand, the earlier impedance analysis at the same temperature showed that over 25 days the value of resonant frequency dropped for less than 0.4% and anti-resonant frequency for less than 0.1%. The main difference in these two approaches to frequency measurement is that, by using impedance analysis, the frequency is directly measured with an impedance analyser, and in the Fourier analysis the frequency is indirectly derived from the time-domain of the received ultrasonic waveforms using software such as MATLAB. It is possible that the pulser-receiver instrument TOPAZ has some limitations on its sensitivity and is not able to sense such a small change in the frequency value which even with a precise impedance analyser was measured to be less than 0.4%, that is 0.1% in an almost twice longer period of 25 days.

### **4.5 Defect detection in the pulse-echo mode at up to 580°C**

After it was demonstrated that an element machined from GaPO<sub>4</sub> can be used for thickness gauging at 580°C for a period of at least 360 h, the next step was to advance a step further towards practical non-destructive measurement by testing the GaPO<sub>4</sub>'s defect detection capability up to the same temperature.

#### **4.5.1 Experimental validation of high temperature damping body**

As discussed in section 2.8.3, the amount of damping applied to the backside of the piezoelectric will determine the pulse duration and consequently the resolution of the inspection that can be achieved with the transducer. As the next experiment with the GaPO<sub>4</sub> element was to validate its defect detection capability using a test-block with an artificial defect inside the block's volume, it was important to try to reduce the 8 cycle signal (see Figure 4-5) down to one or two cycles only. This way the GaPO<sub>4</sub> element would have the maximum chance of detecting the small defect in the volume of the test-block and the reflection from the defect would not be masked by the very long reflection from the backwall.

As discussed in section 2.8.3, two ceramic adhesives, Ceramabond 569 and 503, were acquired for application as damping materials on the back face of the GaPO<sub>4</sub> elements, and according to their respective material sheets, both of these materials could be exposed to temperatures well above the target of 580°C. In Figure 4-19 below, one can see a detailed view of the Ceramabond 503 mass applied to the back face of the GaPO<sub>4</sub> element. The final achieved thickness of the ceramic backing was 4 mm.

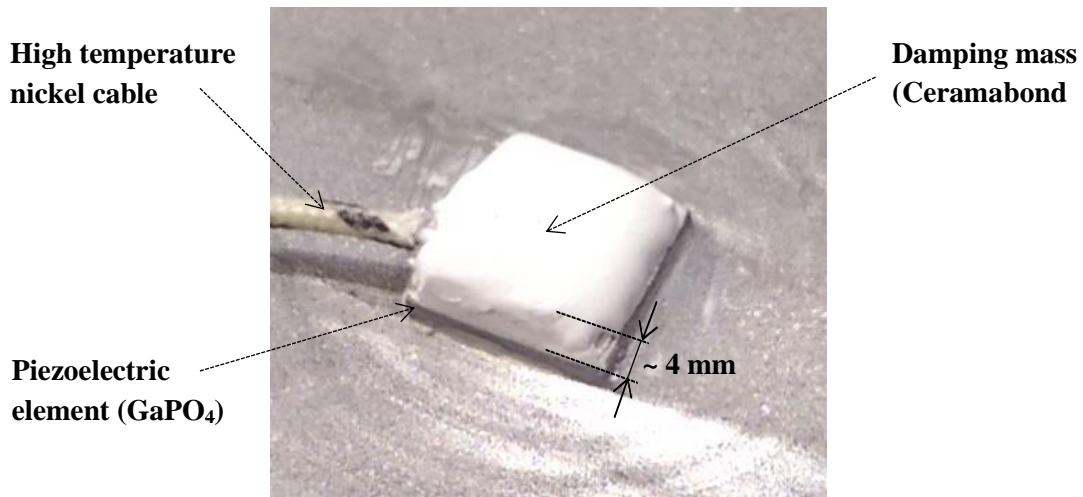


**Figure 4-19: A detailed view of the Ceramabond 503 adhesive applied to the GaPO<sub>4</sub> element.**

In Figure 4-20 and Figure 4-21 one can see how the experiment with Ceramabond 503 adhesive was executed. First, an ultrasonic reflection from the backwall of the test-block was recorded before the backing mass was applied (the black trace in Figure 4-21). Then a ceramic layer of 2 mm thickness (approx. two times  $\lambda/4$ ) was applied to the back face of the piezoelectric element [Figure 4-20 a)], and another reflection from the backwall of the block was recorded (the blue trace in Figure 4-21)). Finally, another ceramic layer of again approx. 2 mm thickness was applied to the first layer, and this meant an overall backing mass of 4 mm thickness or approx. four times  $\lambda/4$  [Figure 4-20 b)]. Then again, the ultrasonic reflection from the backwall of the block was recorded (see the red trace in Figure 4-21)).

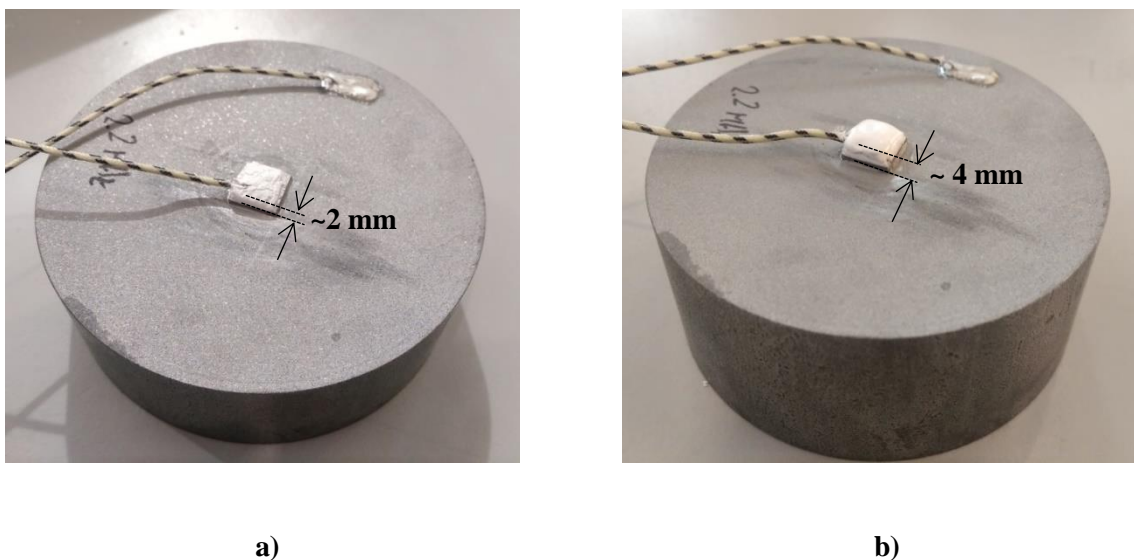


**Figure 4-20: The adhesive Ceramabond 503 applied to the backside of the GaPO<sub>4</sub> element to serve as a backing body. a) The first layer was ~2 mm thick and b) the second one was ~4 mm.**

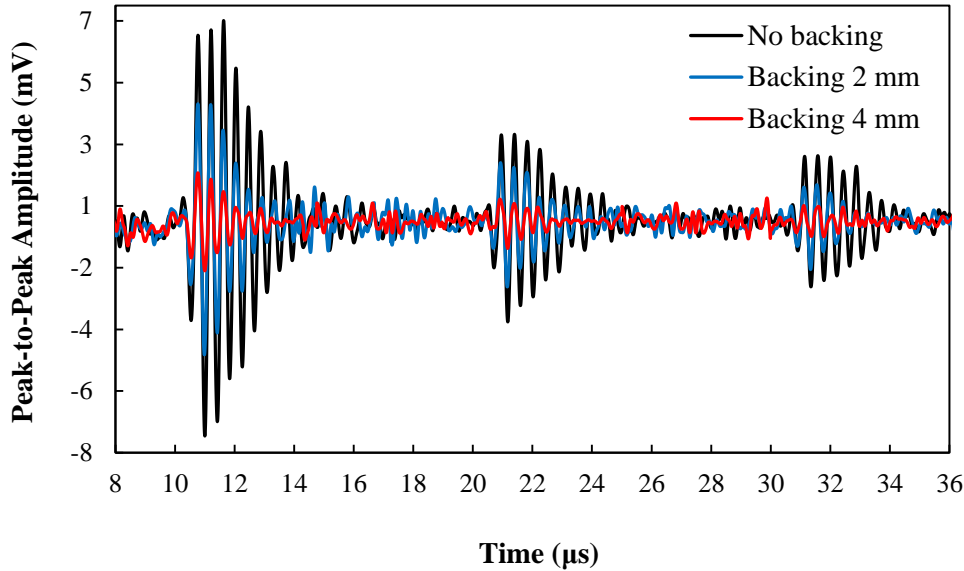


**Figure 4-21: Three consecutive echoes recorded for three cases: (i) no backing (the black trace), (ii) ceramic backing thick 2 mm (the blue trace) and (iii) backing thick 4 mm (the red trace).**

Looking at Figure 4-21, one can see that the application of a ceramic mass to the backside of GaPO<sub>4</sub> element barely reduced the number of oscillations in a pulse, from 8 cycles (no backing) to about 6 cycles (4 mm backing). At the same time, the peak-to-peak amplitude was reduced from 14.5 mV (no backing mass) down to 3.3 mV (4 mm backing). This is quite a low amplitude, and when the third layer of ceramic was applied (thus overall thickness was now 6 mm) the SNR value drop was so severe that the piezoelectric element was generating more noise than signal. Using only one or two layers of backing mass still meant losing more in terms of the generated amplitude than what was gained in terms of the pulse duration reduction. Thus, it was decided to proceed with the defect detection experiment using GaPO<sub>4</sub> element without any damping mass applied to its back face. In any case, it was already reported in literature that high temperature transducer's configuration without backing mass is possible, and that damping could be controlled by the quality of coupling between the ultrasonic transducer and the test component. Depending on the achieved quality of ultrasonic coupling between the piezoelectric element ( $\lambda/2$  thickness), the protective front plate ( $\lambda/4$  thickness) and the test-sample, the ultrasound energy loss from the front face of the piezoelectric element will affect to a greater or lesser extent the vibration of the transducer system [51].

#### 4.5.2 Selection of the suitable test-frequency

The frequency of ultrasonic waves is an extremely influential factor in ultrasonic NDT method. With the speed of sound, which is a constant for the given material, the choice of test-frequency determines the duration of ultrasonic waves in the inspected material. The wavelength is directly related to the size of defects and sensitivity of the method as explained before. By increasing the frequency, the

wavelength of waves is decreased, which has a positive effect to the sensitivity of the inspection. However, increasing the frequency causes greater attenuation of ultrasonic waves in medium, which reduces the thickness of the material that can still be examined with the selected parameters. Considering the smallest diameter of a side-drilled hole (SDH) representing an artificial defect in a steel test-structure that was achievable in the workshop was 0.8 mm, corresponding to the dimensions of the expected damage on a reactor vessel of nuclear power plant [73], and taking into account the  $\lambda/2$  rule, the required wavelength is calculated to be 1.6 mm. For carbon steel ( $v=5920$  m/s), according to Eq. (2.6), it was possible to calculate a suitable test-frequency of a GaPO<sub>4</sub> element of 3.7 MHz. The closest available match to this was a GaPO<sub>4</sub> element with  $f_r=3.5$  MHz. As can be seen from Figure 4-22, an impedance analysis of the acquired GaPO<sub>4</sub> element confirmed its resonating at 3.5 MHz. As will be demonstrated later, this frequency is high enough to successfully resolve the given defect.

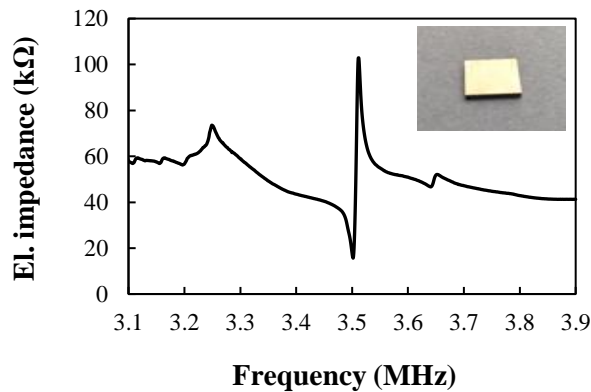


**Figure 4-22: The impedance analysis of GaPO<sub>4</sub> element confirmed it to resonate at 3.5 MHz.**

### 4.5.3 Experimental setup for defect detection up to 580°C

A GaPO<sub>4</sub> element (an area of 100 mm<sup>2</sup>, coated in a Pt layer of 200 nm and with calculated frequency of 3.5 MHz), was attached to a carbon steel block (25 mm thick) containing a side-drilled-hole (SDH, diameter of 0.8 mm) representing an artificial defect in structure, and then using nickel glass braided wiring was connected to a TOPAZ pulser-receiver instrument. The test conditions were the same as before, with a pulser voltage of -75 V. A detailed view of the steel test-block with SDH and its coupled GaPO<sub>4</sub> element is given in Figure 4-23 a). These were then placed inside a furnace for defect detection up to 580°C to take place, Figure 4-23 b). Similarly to previous experiments, the temperature of the carbon steel block was measured with a thermocouple which contacted the topside of the steel block through a heat transfer paste very close to GaPO<sub>4</sub> element. The ultrasonic reflections from the backwall and from the SDH were recorded at every 50°C up to 580°C, where the hold time of 15 min at each temperature interval was applied in order to ensure an isothermal measurement.

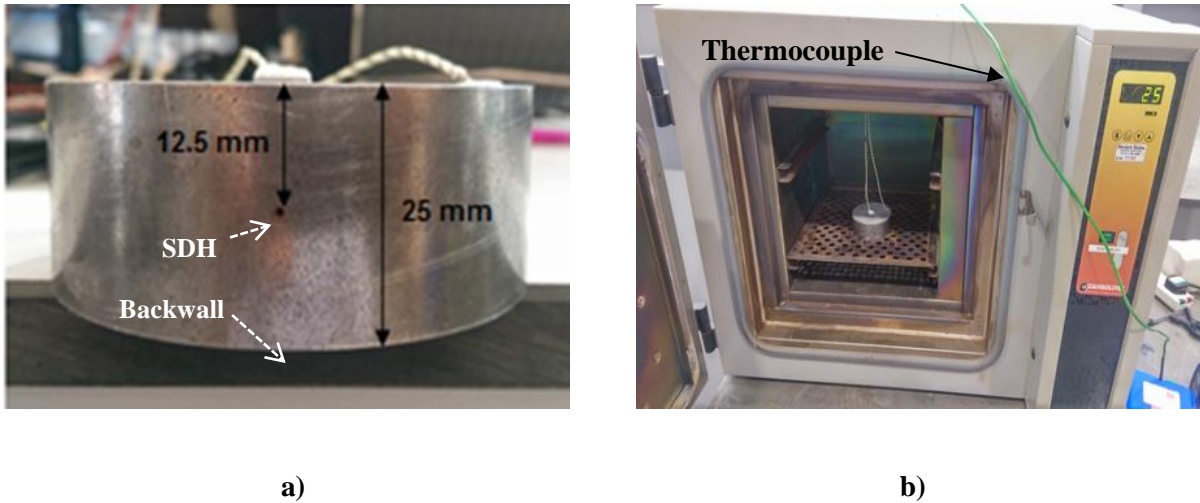


**Figure 4-23: a) A GaPO<sub>4</sub> element was coupled to a steel test-block directly above the SDH using silver adhesive. b) Everything was placed inside a furnace for defect detection up to 580°C.**

#### 4.5.4 Results and discussion on defect detection up to 580°C

Four A-scans containing ultrasonic reflections from the defect (SDH) and from backwall of the steel test-block at temperatures 25°C, 200°C, 400°C and 580°C can be seen in Figure 4-24. It is easy to confirm that the recorded signals are the right ones by multiplying the recorded time-of-flight with the respective velocity in carbon steel at the given temperature, in order to calculate that the defect is located at the depth of exactly 12.5 mm [this can also be directly read from Figure 4-23 a)]. These four A-scans confirmed that a GaPO<sub>4</sub> element with test-frequency of 3.5 MHz was sufficient to successfully resolve the given 0.8 mm defect up to the temperature of 580°C. It is believed that this was the first time that a piezoelectric element machined from a single crystal GaPO<sub>4</sub> was used for a classic NDT task such as defect detection, and particularly at the temperature level of an operational power plant.

First, it can be seen that at any given temperature the reflections from the SDH always have a lower generated peak-to-peak voltage than the respective reflections from the backwall of the steel block. This is because the cross-section (CS) of the SDH is much smaller than the CS of the GaPO<sub>4</sub> element ( $CS_{SDH} = 0.502 \text{ mm}^2 \ll CS_{GaPO_4} = 100 \text{ mm}^2$ ). For this reason, the ultrasonic energy emitted from the GaPO<sub>4</sub> element and transmitted into the steel block volume is reflected from the SDH back to the GaPO<sub>4</sub> element with a much smaller percentage than the energy from the backwall of the steel test-block.

The reflected signals from SDH and backwall are again both attenuated and lengthened with the introduction of heat. The influence of attenuation that occurs in steel at HT on the ultrasonic signals received back to the piezo-element has already been explained in section 4.4.4. Further, the de-bonding phenomenon caused by thermal expansion of the GaPO<sub>4</sub> transducer's components at HT that contributes to enhanced "ringing" and attenuated signals has also been explained in section 4.4.4.

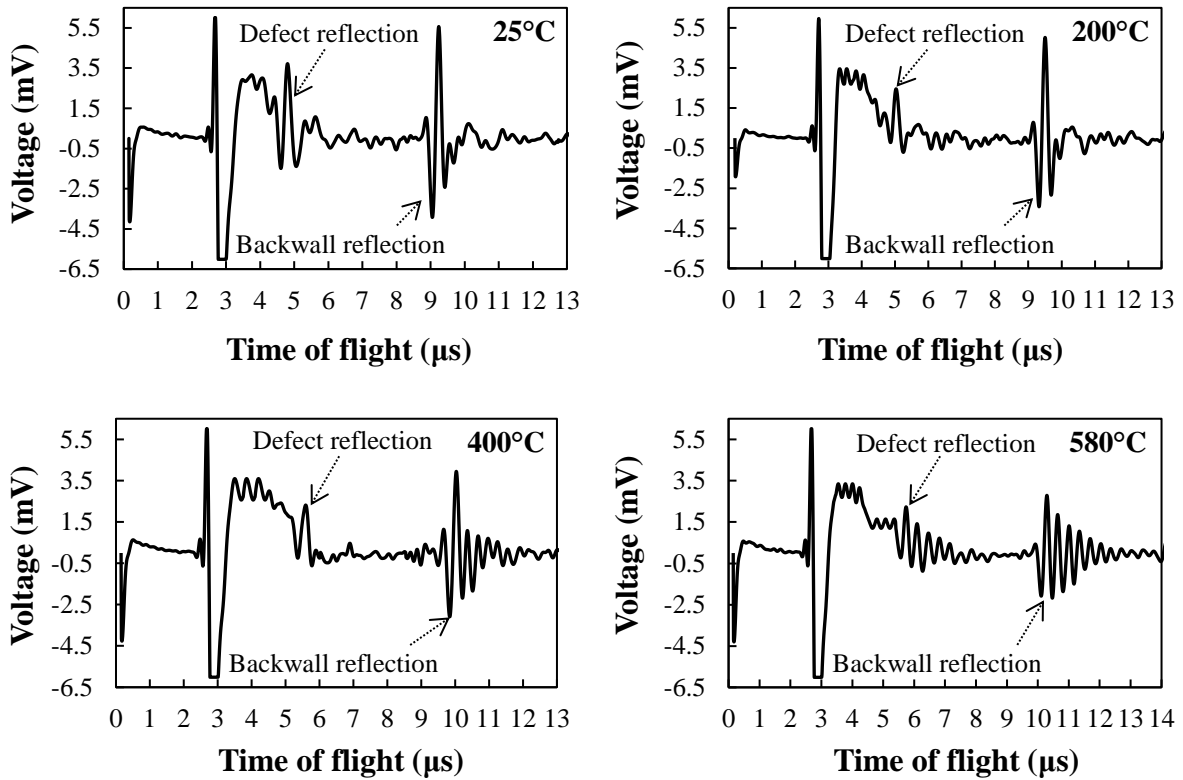


**Figure 4-24: A-scans containing reflections from defect (SDH) and backwall of the carbon steel block that were received back to the GaPO<sub>4</sub> element at 25°C, 200°C, 400°C and 580°C.**

Finally, one should notice the shift of ultrasonic reflections to the right as the temperature goes up to 580°C. As explained before, this is caused by a change in the physical properties (modulus of elasticity, density and Poisson's ratio) of the steel test-block that accompanies a rise in temperature; Figure 4-25.

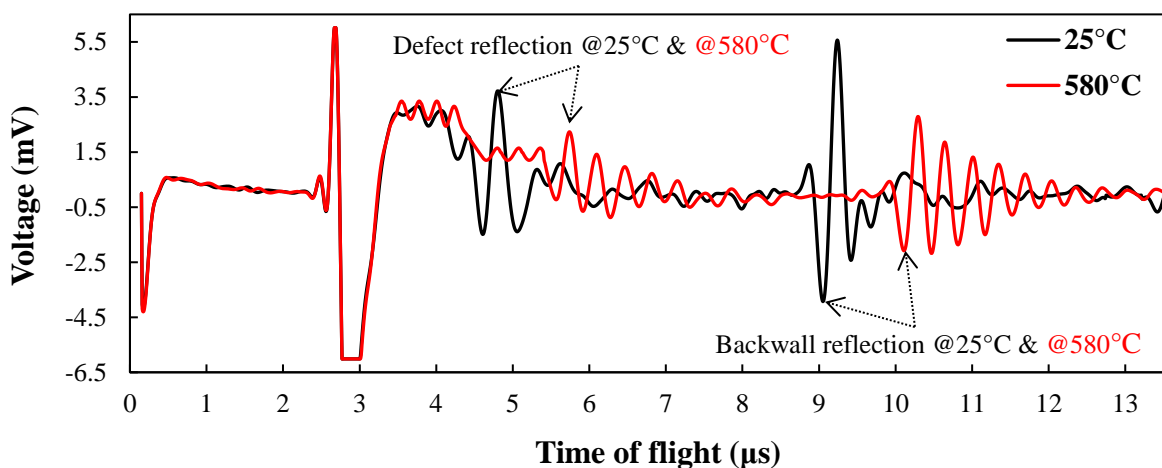


**Figure 4-25: Compared reflections from defect (SDH) and backwall of the steel block received at the GaPO<sub>4</sub> element at 25°C (black trace) and at 580°C (red trace) showing the influence of temperature on the time-of-flight.**

The detectability of reflections from SDH and backwall was assessed using SNR calculation. From Figure 4-26 it is clear that all calculated SNRs up to 580°C were sufficiently high that reflections could be identified. In addition, because an initial pulse of -100 V was used, (and not -75 V as before), the SNRs reported here come with slightly higher values than the ones reported in thickness gauging.

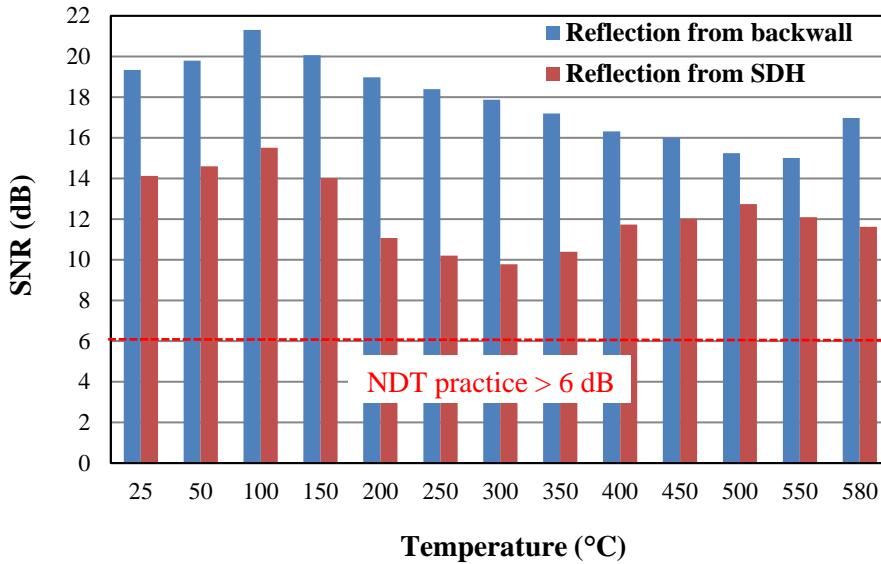


**Figure 4-26: Calculated SNR values for reflections from SDH and backwall, from 25 to 580°C.**

Finally, to check if exposure to 580°C left any trace on the performance of GaPO<sub>4</sub> element, the steel block together with the GaPO<sub>4</sub> element were left to cool to 25°C. Then, measurement took place again. From Figure 4-27, it is clear that even after the exposure to 580°C, the GaPO<sub>4</sub> element is able to detect the SDH. A small reduction in generated peak-to-peak amplitude of reflections from the SDH and backwall can be seen, but this is likely to be due to changes in physical properties in the silver adhesive as it was exposed to temperatures above the maximum recommended by its datasheet.

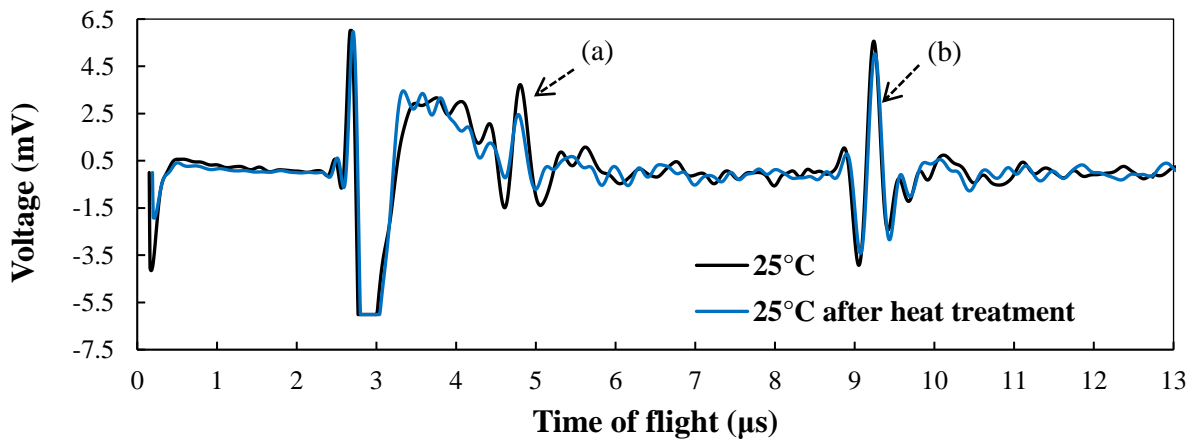


**Figure 4-27: Compared reflections from SDH – (a) and backwall – (b) received at GaPO<sub>4</sub> element at 25°C, before (the black trace) and after (the blue trace) the exposure to 580°C.**

With ultrasonic defect detection, the confidence building experiments on piezoelectric elements machined from crystal GaPO<sub>4</sub> were completed. In this chapter, it was shown that GaPO<sub>4</sub> elements could be used for practical NDT and condition monitoring, by allowing thickness gauging and defect detection to be performed up to the target temperature of this work of 580°C, where the SNR level was always high enough for a practical ultrasonic measurement. Also, it was shown that an ultrasonic transducer's sensitivity can be kept sufficiently high, even though no damping mass is applied to its back face. The next step in this work was to design and manufacture the ultrasonic transducer for practical non-destructive testing and condition monitoring, by using components machined from appropriate high temperature substitutes, as discussed in previous chapters. This should allow the new transducer to operate up to 580°C, which is the temperature normally found in high temperature pipework of operational power plants.

# 5 Design, Manufacture and Testing of the Ultrasonic Transducer up to 580°C

## 5.1 Chapter overview

Electrical impedance and ultrasonic measurements performed on GaPO<sub>4</sub> elements confirmed the potential of this piezoelectric single crystal for application in practical non-destructive testing such as thickness gauging and defect detection at high temperatures. In this chapter, it is described how a prototype high temperature transducer was designed around the GaPO<sub>4</sub> element, manufactured in five simple steps and finally tested up to the target temperature of 580°C. The approach in the development of the high temperature transducer was to stay close to the design of a conventional ambient-temperature transducer but to replace each of its components with appropriate high-temperature substitutes. All the components were integrated within a steel housing, together comprising a novel transducer for operation at high temperatures. Successful testing of the manufactured transducer in the lab environment using a steel calibration block that was placed in an oven showed its applicability for ultrasonic thickness gauging up to 580°C. Finally, to allow an efficient coupling of the transducer to the steel calibration block, the measurements up to 100°C were performed with conventional couplant Ultragel II, and for measurements at high temperatures, a special couplant SONO 1100 was used.

## 5.2 Design of the ultrasonic transducer for operation at 580°C

To get a cost-effective and reliable ultrasonic transducer for operation at HT, it is important to keep a simple design with the minimum number of bond-lines [1]. The more the bond-lines there are, especially between the piezoelectric element of the transducer and the test-material, the more ultrasound energy will be reflected back and not transmitted into the test-material. The percentage of the incident energy that is reflected back can be calculated from Eq. (5.1):

$$R = \left( \frac{Z_1 - Z_2}{Z_1 + Z_2} \right)^2 \quad (5.1)$$

where  $R$  is the reflected energy and  $Z_1$  and  $Z_2$  are the acoustic impedances of the two materials.

### 5.2.1 First bond layer – application of the electrode

For a piezoelectric element to be usable as an ultrasound transducer and integrated within a transducer, its two large faces must be coated in metal electroding. Electrical wiring which delivers the electrical signal between the piezoelectric element and the pulser-receiver instrument is then bonded to the two metal electrodes. As explained in section 2.8.2, it was decided the GaPO<sub>4</sub> elements would be coated in 200 nm thick platinum layer, which should sustain operation up to 580°C. The schematic of the GaPO<sub>4</sub> element coated in platinum thin film can be seen in Figure 5-1.

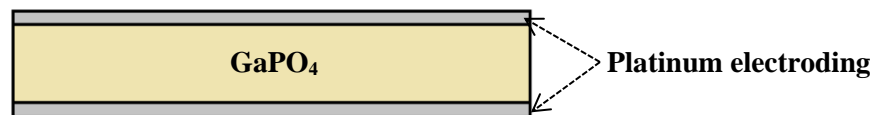


**Figure 5-1: The GaPO<sub>4</sub> element is coated in the standard parallel electrode configuration with a 200 nm thick platinum layer.**

### 5.2.2 Second bond layer – application of the protective front plate

There are two basic approaches to coupling a piezoelectric element to the test-structure. Either the piezoelectric element is permanently attached to the test-structure using one of the bonding methods listed in section 2.8.9, or a coupling medium (liquid, paste) is used between the piezoelectric element and the test-structure to facilitate transmission of the ultrasound energy as explained in section 2.8.10. In the first approach, only a single point in the test-structure can be inspected or monitored, considering the ultrasonic beam will always emerge from the piezoelectric element at the same angle. The more advanced second approach allows mechanical scanning to be done along the surface of the test-structure, which means that a larger volume can be covered with a single transducer and thus the inspection is more flexible and efficient. Further, as explained in 2.8.4, during scanning, mechanical damage, wear and corrosion of the piezoelectric element are likely to occur. For this, a protective front plate is applied to the element, even though it means an increase in the number of bond-lines.

The schematic of a piezoelectric element attached to a protective front plate can be seen in Figure 5-2 a) and b). In position a), the element will measure only the thickness of the test-structure ( $T$  = the ultrasonic energy delivered to the backwall and  $R$  = the ultrasonic energy that was reflected and received back to GaPO<sub>4</sub> element). However, once it is moved to position b), it will not only measure the thickness but also detect the SDH ( $T_1$  and  $T_2$  = ultrasonic energy delivered to the backwall and SDH, respectively, and  $R_1$  and  $R_2$  = parts of ultrasonic energy that were reflected from backwall and SDH, respectively, and then received back to GaPO<sub>4</sub> element at different time intervals).

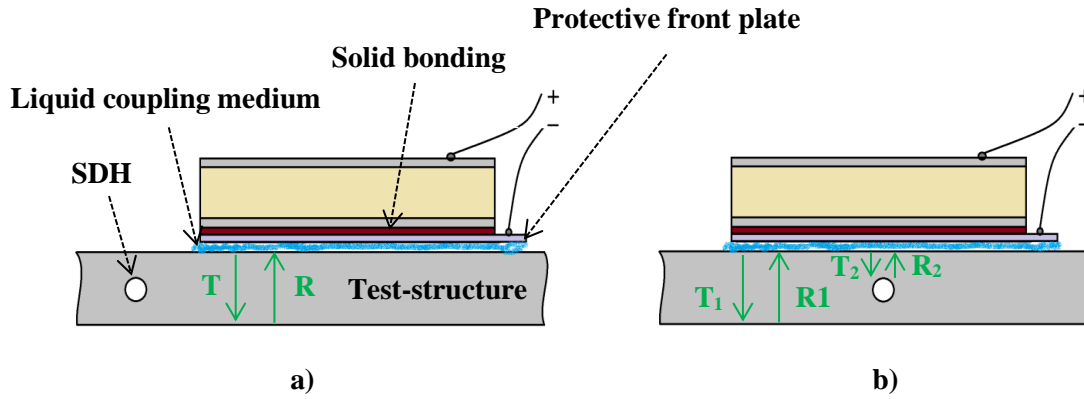


**Figure 5-2: A front plate is applied between the piezoelectric element and the test-structure that allows for both scanning and monitoring. In a) the transducer will measure thickness of the test-structure. Once moved to b), it will allow for both thickness gauging and defect (SDH) detection.**

As explained in section 2.8.4, a *lambda-quarter* protective plate/matching layer made of stainless steel will be used for construction of the new transducer. According to Eq. (2.7), for a  $\text{GaPO}_4$  element of 1 mm thickness and 2.178 MHz resonant frequency, the thickness of steel protective plate is calculated to be 0.7 mm (for *lambda-quarter*). The protective front plate will be bonded to the piezoelectric element using one of solid bonding methods discussed in section 2.8.9. The application of a bonding layer at the same time means that another interface will be added in the transducer's sound transmission path. This is why it is important that the bonding material applied does not have substantially different acoustic properties (i.e. specific acoustic impedance) from the piezoelectric element and the front plate, or otherwise the resulting mismatching will reduce the amount of ultrasound energy transmitted into the test-object [74]. Using one of electrically conductive silver-based adhesives (earlier listed in Table 2-3) is expected to minimise the problem, as they come with the specific acoustic impedance close to that of silver (36.9 MRayl), which is suitably between that of the steel plate (44.8 MRayl) and that of gallium orthophosphate (15.6 MRayl). Further, even though it has been demonstrated that the adhesive thickness is a prominent design parameter for piezoelectric transducers, its effects on the ultrasound signals have not yet been explored extensively and are normally neglected in transducer design practice [75]. The same approach was taken in this work, since to carefully examine the silver adhesives (acoustic) properties would require a separate research, and at the same time, it was not expected to significantly influence the final result – design and manufacture of an ultrasonic transducer that could withstand and operate at high temperatures in a prolonged period.

### 5.2.3 HT housing

To make the transducer technically usable and (hand) measurement with it feasible, the piezoelectric element bonded to the protective front plate was enclosed within a stainless steel housing, seen in Figure 5-3. One could argue that the proposed transducer design was still missing a damping body to be

attached to the upper face of the piezoelectric element; however, at this stage of research, no satisfactory solution for high temperature damping body was established. Some work on this can be found in section 4.5.1 “Experimental validation of high temperature damping body”. For this, it was decided to design the prototype transducer without the damping body and once it was manufactured, it would be tested to see if such a simplified transducer design could meet the requirements of a practical non-destructive testing and condition monitoring measurement, such as achieving high enough defect detection resolution and high enough SNR level.

As one can see from Figure 5-3, there are three bonding operations required to build the prototype ultrasonic transducer. First, the piezoelectric element needs to be bonded to the protective front plate. Second, nickel wiring must be added to both the piezoelectric element and the protective front plate (earthing). Finally, a third bonding operation is required to attach the stainless steel housing to the protective front plate. Even though different bonding methods exist (as explained in section 2.8.9) and potentially could be used, it was decided to proceed with the simplest and cheapest one – adhesive bonding using the commercial HT silver adhesives, as previously discussed and listed in Table 2-3.

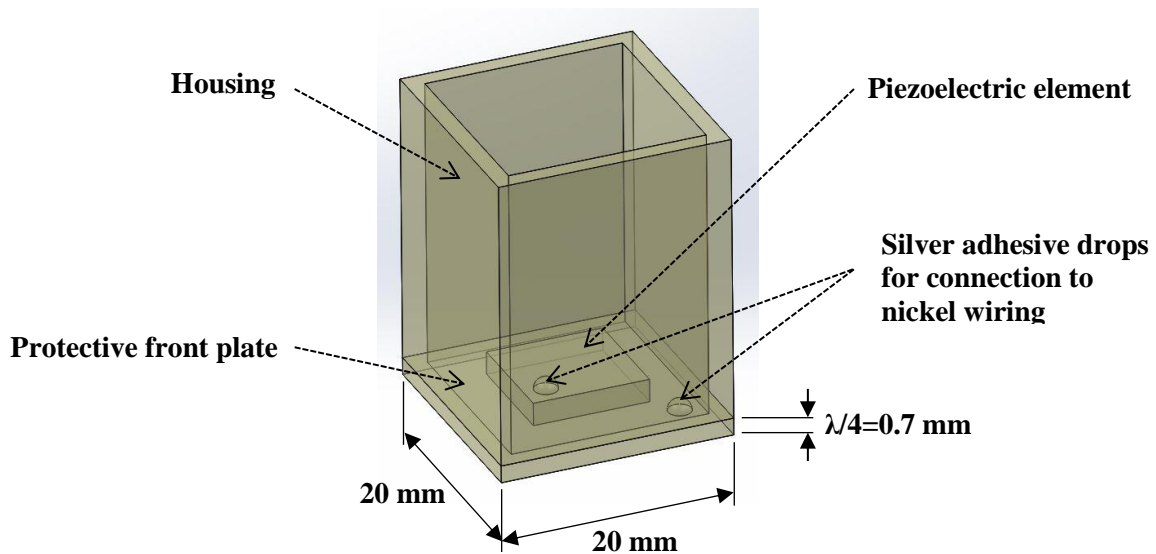


**Figure 5-3: Simplified design of the prototype ultrasonic transducer for application up to 580°C.**

### **5.3 Manufacture of the transducer for operation at 580°C**

Once design of the prototype transducer for thickness gauging/defect detection up to 580°C has been finalised, the steps in the process of manufacturing can be explained. First, it is necessary to manufacture the protective front plate. The protective plate was manufactured from a stainless steel sheet. The lambda-quarter thickness of the protective plate was calculated to be 0.7 mm and the plate has an area of 20 by 20 mm<sup>2</sup>. The manufactured protective front plate, as ready for implementation in the transducer, can be seen in Figure 5-4 a). Second, the GaPO<sub>4</sub> element needs to be coupled to the

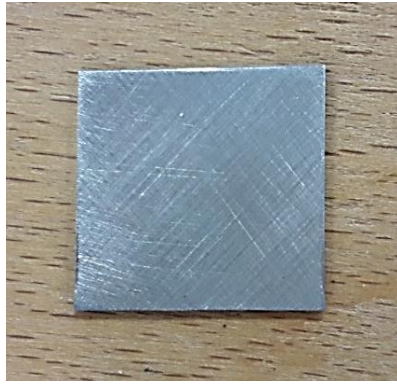
protective plate. This was done using the adhesive Duralco 124. The *lambda-half* piezoelectric element is 1 mm thick with calculated resonant frequency of 2.178 MHz. The area of the piezoelectric element is 10 mm by 9.5 mm and its two large faces are coated in a 200 nm Pt layer. The piezoelectric element coupled to the protective plate can be seen in Figure 5-4 b). Third, the HT wiring needs to be attached to the piezoelectric element and the metal protective plate (grounding). Using the same silver adhesive, one glass braided nickel conductor has been connected to one platinum electrode of the GaPO<sub>4</sub> element, and the second nickel conductor has been grounded to the steel front plate; these can be seen in Figure 5-4 c). Fourth, the piezoelectric element, the front plate and the nickel wiring must be enclosed within the transducer's housing. The housing was manufactured from corrosion resistant stainless steel with a wall-thickness of 1.5 mm. The steel housing was bonded to the protective plate using silver adhesive Duralco 124 and can be seen in Figure 5-4 d). Fifth, to prevent possible abruption of the two nickel wires from the GaPO<sub>4</sub> element and the steel front plate during transducer's operation, the nickel wiring needs additional fixing to the housing. This was done using adhesive Duralco 124 and can be seen as indicated by two red circles in Figure 5-4 e). Finally, in Figure 5-4 f), one can see the manufactured prototype of the transducer for thickness gauging/defect detection up to the temperature of 580°C. The manufactured transducer responds well to the design that was previously proposed in Figure 5-3.

Specifications of the transducer are listed in Table 5-1. One can see that besides the silver adhesive, all other HT substitutes come with operating or melting temperatures well above the required level of 580°C. However, as silver adhesive PyroDuct 597-A (with max application at 927°C) proved to be of no use, silver adhesive Duralco 124 with maximum application at 343°C had to be applied. As reported in section 4.4.5, the same adhesive was already used for long-term gauging at 580°C. From this, this adhesive was expected to be the best solution for bonding of the new HT transducer.

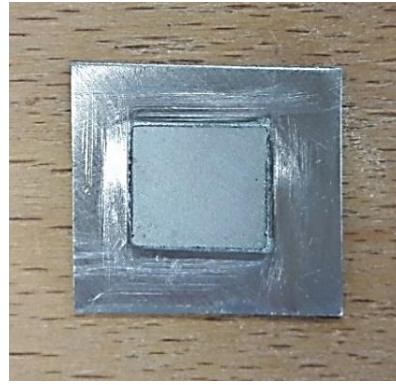
**Table 5-1: Specifications of the prototype transducer for NDT at 580°C.**

Component	Material	Thick./Diam.	Area/Cross Sec.	Acoust. Imp.	Melting Temp.
-	-	(mm)	(mm x mm)	(MRayl)	(°C)
Front plate	Stainless steel	0.7	20 x 20	44.8	1400-1450*
Adhesive	Duralco 124	NA	10 x 9.5	NA	343 <sup>#</sup>
Piezoelectric	GaPO <sub>4</sub>	1	10 x 9.5	15.6	970 <sup>^</sup>
Wiring	Nickel	0.2	NA	NA	1455
Housing	Stainless steel	1.5	20 x 20	44.8	1400-1450*

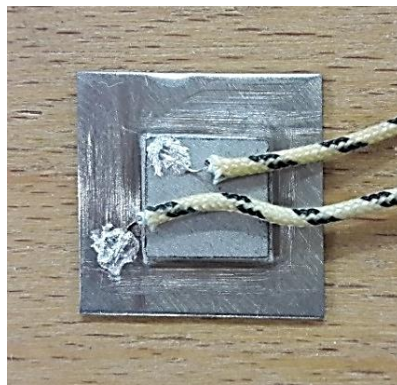
\*Stainless steel 304, NA = not applicable/available, <sup>#</sup>max recomm. temp., <sup>^</sup>loss of piezoelectric effect.



a)



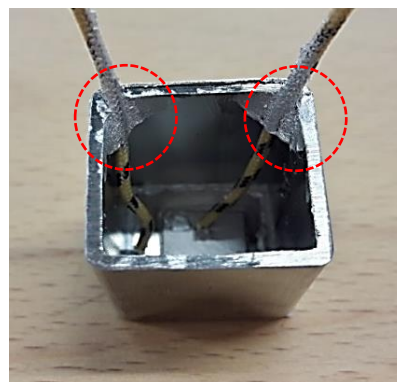
b)



c)



d)



e)

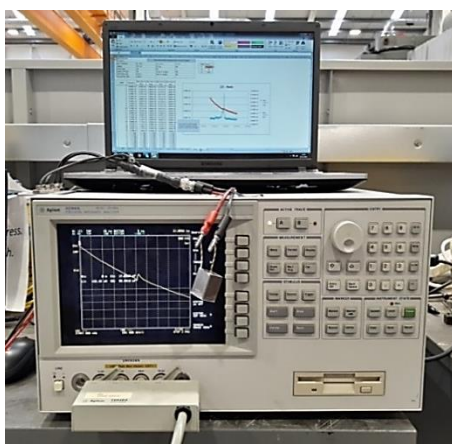


f)

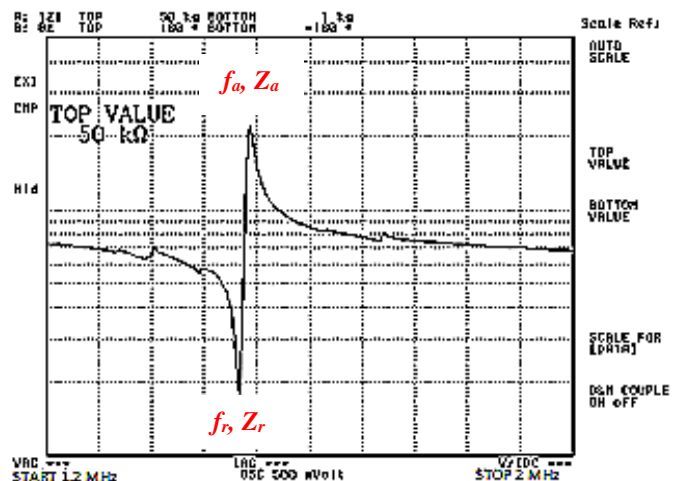
**Figure 5-4: a) Steel protective plate, b) front plate is coupled to GaPO<sub>4</sub> element using adhesive, c) nickel wiring is affixed to GaPO<sub>4</sub> and front plate, d) new transducer is enclosed within steel housing, e) nickel wiring is affixed to housing to prevent possible abruption of wires during measurement and f) ultrasonic transducer is manufactured and ready for testing up to 580°C.**

## 5.4 Electrical impedance analysis of the manufactured transducer

The manufactured transducer was tested using a GaPO<sub>4</sub> element of 1 mm thickness and the calculated resonant frequency of 2.178 MHz. However, once the protective front plate made of stainless steel sheet (0.7 mm thick) was coupled to the GaPO<sub>4</sub> element using silver adhesive, the value of the resonant frequency was changed (dampened). To measure the new resonant frequency, an experimental setup was used; see Figure 5-5 a). The transducer was directly connected to an impedance analyser (the same as in experiments reported in Chapter 3), and an electrical impedance response over the test-frequency range from 1.2 MHz up to 2 MHz was recorded; see Figure 5-5 b). One can read from Figure 5-5 b) that the protective front plate, once coupled to the piezoelectric GaPO<sub>4</sub> element, has attenuated free vibration of the piezoelectric element from 2.178 MHz down to 1.496 MHz, which is a reduction of 31.31%. All other impedance parameters ( $f_a$ ,  $Z_r$  and  $Z_a$ ) that were measured in this experiment have also changed and these have been listed in Table 5-2. As explained before, the reduction of the resonant frequency of 31.31%, means that the minimum dimension of a defect that can still be detected with this transducer will also reduce by 31.31%. One needs to consider this reduction and design such a transducer to achieve the test-frequency matching the minimum size of defects that are expected to occur in an inspected structure and that need to be detected with the transducer. The  $\lambda/2$  parameter at a frequency of 1.496 MHz is calculated to be 1.37 mm. In theory, this means that by using this manufactured transducer, one will be able to detect a minimum defect of at least the same dimension, for example a 1.37 mm in diameter for a side-drilled hole. However, as will be shown later in this work, the new transducer was sensitive enough to detect a number of standard side-drilled holes with diameter of 1 mm, thus surpassing its expected minimum ( $\lambda/2$ ) sensitivity.



a)



b)

Figure 5-5: a) The experimental setup used for impedance analysis of the new transducer. b) The impedance response over the test-frequency range shows the new resonance at 1.496 MHz.

**Table 5-2: The electrical impedance parameters of the new transducer at ambient temperature.**

Parameter	Symbol	Unit	Value @ 25°C
Resonant frequency	$f_r$	[MHz]	1.496
Anti-resonant frequency	$f_a$	[MHz]	1.512
El. impedance at resonance	$Z_r$	[kΩ]	1.766
El. impedance at anti-resonance	$Z_a$	[kΩ]	21.808

### 5.4.1 Electrical impedance matching of the transducer

To design a matching network, the first step is to approximate the transducer’s electrical behaviour around its resonant frequency by some electrical model. The Agilent 4294A analyser offers an inbuilt function of generating equivalent circuit models, and five different models can be seen in Figure 5-6:

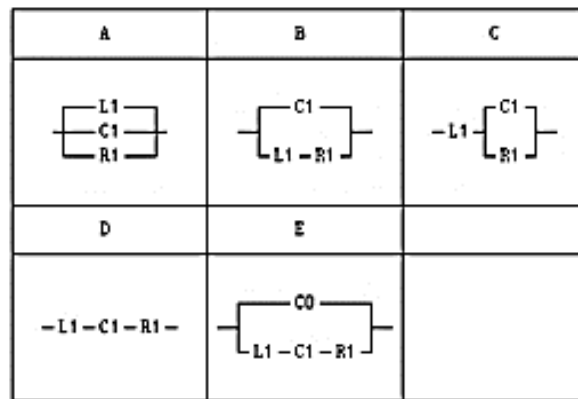


**Figure 5-6: Five different equivalent circuits offered by the impedance analyser.**

The circuit model “E” was automatically offered by the analyser, as the most appropriate circuit to describe the electrical behaviour of the GaPO<sub>4</sub> transducer around its resonance. In literature, this model is known as the Butterworth-Van-Dyke (BVD) model, and has already been used to match high impedance transducers to low impedance pulser-receiver units [92]. This BVD circuit has four electric elements: two capacitors C<sub>0</sub> and C<sub>1</sub>, one inductor L<sub>1</sub> and one resistor R<sub>1</sub>. C<sub>0</sub> represents the equivalent capacitance, R<sub>1</sub> represents the radiation and mechanical losses, and L<sub>1</sub> and C<sub>1</sub> model the resonant performance of the transducer. Assuming that mechanical losses are relatively small, the power supplied to R<sub>1</sub> can be considered as the acoustic power emitted. The values of the four quantities can be obtained by using mathematical expressions listed earlier in section 3.2.1, however here they were automatically generated by the impedance analyser and can be seen listed in Table 5-3.

**Table 5-3: Generated values of electrical components.**

Parameter	Symbol	Unit	Value @ 25°C
Resistance	$R_l$	[kΩ]	1.93404
	$C_l$	[fF]	63.1501
Capacitance	$C_0$	[pF]	9.73878
	$L_l$	[mH]	97.0114

By using the four values, it is possible to generate another impedance characteristic, which approximates the measured characteristic of the manufactured transducer previously reported in Figure 5-5 b). Figure 5-7 shows both the measured impedance characteristic (the black trace) and the simulated impedance characteristic (the red trace).

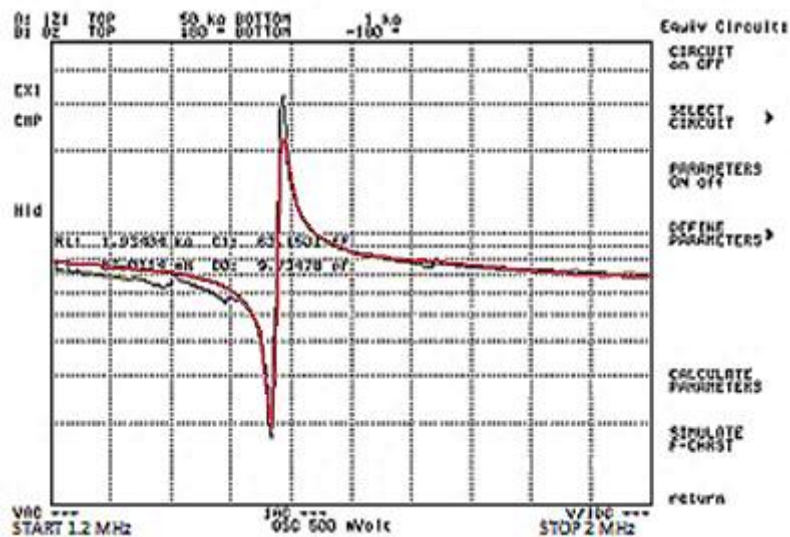


**Figure 5-7: The measured impedance response of the transducer (the black trace), and the simulated response using the equivalent circuit and the values from Table 5-3 (the red trace).**

Once the equivalent circuit simulating the behaviour of the transducer is known, a similar circuit can be used to simulate the behaviour of the pulser-receiver instrument (the equivalent circuits of commercial pulser-receiver instruments can normally be found in their technical datasheets). Once the two equivalent circuits are known, a matching network can be designed to improve the performance of the transducer. In the case of high temperature transducers, the same process needs to be repeated over the whole temperature range of interest, and then to simulate and finally build a circuit that can be fine-tuned based on the required impedance value at the given (high) temperature. A good example of a

simple matching network with only one inductor and one capacitor can be found in [92]. Here, the authors have managed to match both real and imaginary parts of the transducer's impedance, and thus deliver the power much more efficiently to the transducer. This in return has increased the level of signal-to-noise ratio and achieved better accuracy in the measurement.

Figure 5-8 shows how matching networks or impedance circuits are being applied in practice between high impedance transducers such as GaPO<sub>4</sub> (impedance at resonance 1766 Ω) and low impedance pulser-receiver instruments (commercial instrument TOPAZ: pulser output impedance 25 Ω, receiver input impedance 75 Ω) and the BNC cable (50-75 Ω). From Figure 5-8 one can see that the impedance matching circuit is placed inside the transducer's housing, just next to the piezoelectric element. Unfortunately, as explained in section 2.8.8, commercially available electrical components required to build an impedance matching network cannot be used above ~85°C, and the transducer developed here is intended for application up to 580°C. For this reason, design of a matching network for the GaPO<sub>4</sub> transducer development was not part of this research work. However, even though it was successfully demonstrated that GaPO<sub>4</sub> transducers can operate at 580°C for at least 600 h, the low measured coupling coefficient (GaPO<sub>4</sub>  $k_t = 7.5\%$  vs. conventional PZT  $k_t \approx 70\%$ ) and the piezoelectric constant (GaPO<sub>4</sub>  $d_{11}^E 4 \text{ pC/N}$  vs. conventional PZT  $d_{11}^E \approx 370 \text{ pC/N}$ ), as well as relatively low SNR level (see sections 4.4.4 and 5.7.1) suggest that a matching network will eventually need to be developed. A possible solution will be to place the matching circuit outside the transducer housing, closer to the pulser-receiver instrument and thus far enough from the hot part being inspected. As one possible direction for further development of the high temperature GaPO<sub>4</sub> transducers, development of external impedance matching circuits is listed under section 6.2 "Recommendations for future work".

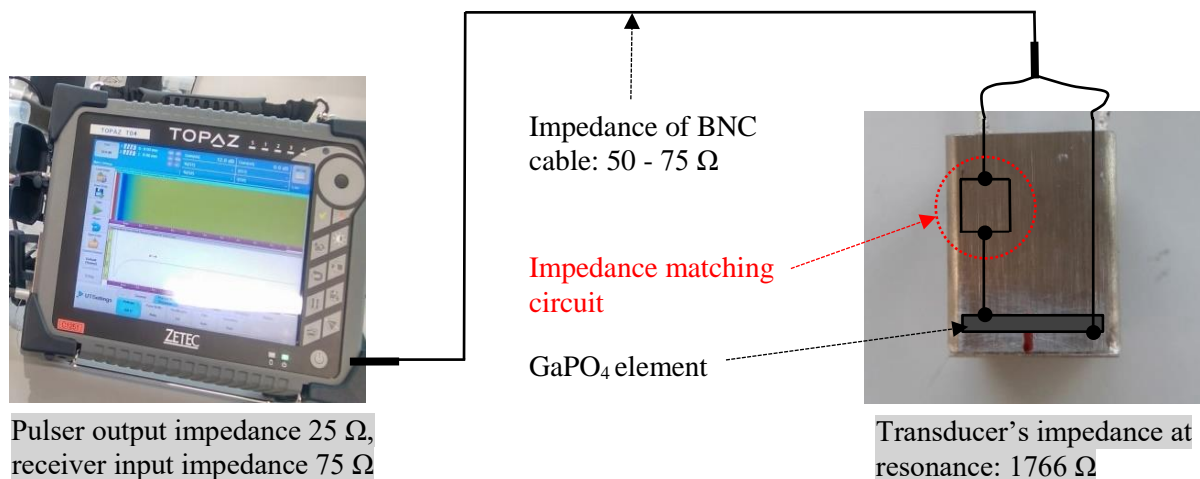


**Figure 5-8: Schematic of a matching circuit (network) installed between the high impedance GaPO<sub>4</sub> transducer, and the low impedance pulser-receiver instrument and the BNC cable.**

## 5.5 Ultrasonic analysis of the manufactured transducer

The previously reported impedance analysis was used to examine the electrical properties of the new transducer before it was connected to the pulser-receiver instrument. Once the transducer is connected to the pulser-receiver, it becomes possible to use it for thickness gauging and defect detection. Both of these capabilities of the new transducer have been tested and are reported below. The tests were initially performed at ambient temperature, and finally up to the target temperature of 580°C.

### 5.5.1 Thickness gauging at ambient temperature

The setup was the same as the one reported in Chapter 4 and can be seen in Figure 5-9. The same pulser-receiver instrument was used to trigger the GaPO<sub>4</sub> element and the test-conditions were unchanged: an initial pulse ranging from -50 V to -200 V was applied. However, after the application of the protective front plate, the resonant frequency has changed and was now measured to be 1.496MHz, so this time a low-pass (LP) filter of 2 MHz was used as this produced much better A-scans then if a band-pass (BP) filter of 1-5 MHz was used. Finally, to couple the manufactured transducer to the calibration block, an ultrasonic couplant Ultragel II was used, Figure 5-9.

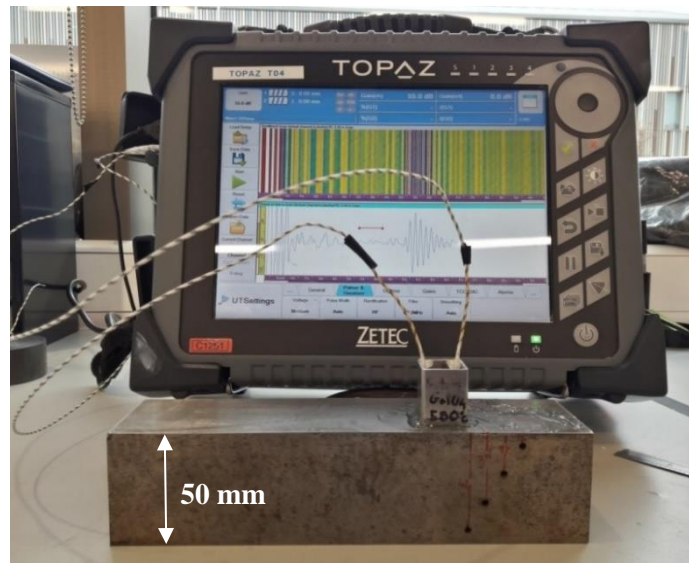


**Figure 5-9: The setup for testing of the new transducer at ambient temperature.**

In Figure 5-10 one can see the recorded A-scan containing: (a) waveforms of the initial pulse that was applied to the transducer at different amplitudes from -50 to -200 V and (b) waveforms of the fastest arriving echo that was reflected from the backwall of the block and received back at the transducer.

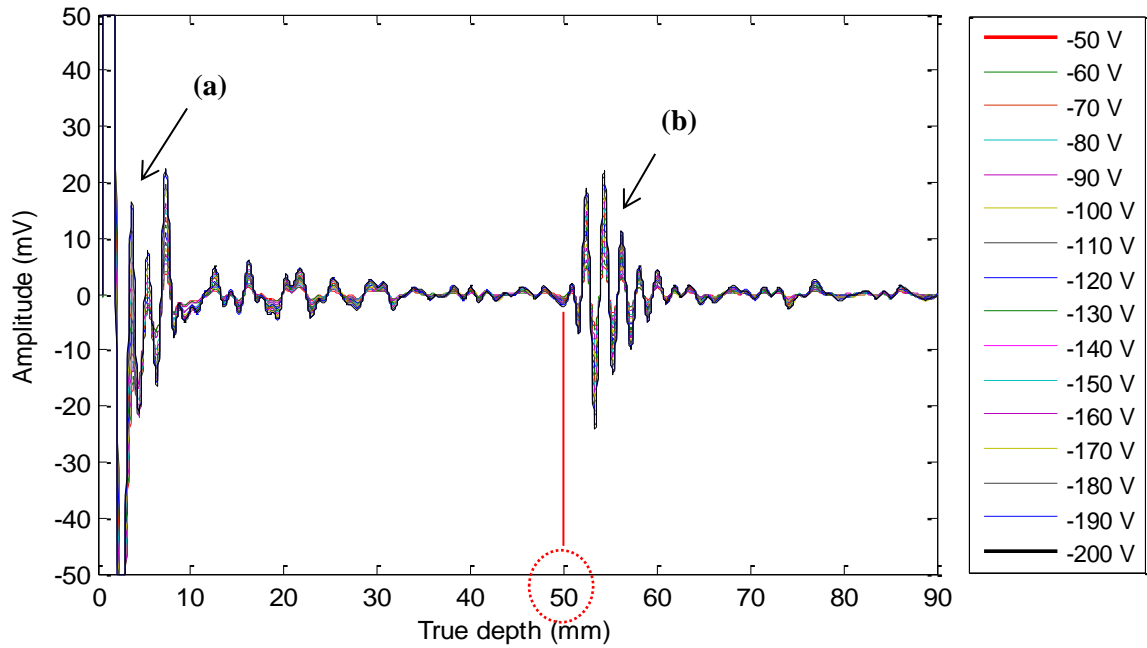


**Figure 5-10: The A-scan containing (a) waveforms of the initial pulse applied to the transducer at different amplitudes from -50 to -200 V and (b) waveforms of the fastest arriving echo reflected from the backwall of the calibration block that were received back at the transducer.**

In Figure 5-11, one can see a more detailed view of the reflected echo in Figure 5-10, plotted from 50 mm to 61 mm. Similar to the experiment reported in Figure 4-5, it is clear that as the amplitude of the initial pulse goes from -50 V to -200 V, the amplitude of the reflected (and shortly afterward received) echo will also increase. The relationship between these two amplitudes is again linear.

However, one should notice that the generated peak-to-peak amplitude of the reflected ultrasonic echo/generated electrical signal is lower than the one reflected when a single  $\text{GaPO}_4$  element is bonded directly onto the steel substrate using silver adhesive (A-scan in Figure 4-5). For example, for an initial pulse of -50 V (min), the generated peak-to-peak amplitude using the new transducer was approximately 10.5 mV while using the single  $\text{GaPO}_4$  element it was approximately 17 mV. On the other hand, for the initial pulse of -200 V (max), the generated signal using the manufactured transducer was 46 mV as opposed to generated 74 mV when a single  $\text{GaPO}_4$  element was bonded directly onto the steel substrate. In both cases, this is a drop of approx. 61%. This means that the application of the protective front plate to the front face of the  $\text{GaPO}_4$  element did not just attenuate its fundamental resonant frequency (from 2.178 down to 1.496 MHz) but also its sensitivity measured as the generated amplitude of the received ultrasonic echoes once the transducer is coupled to the steel test-structure.

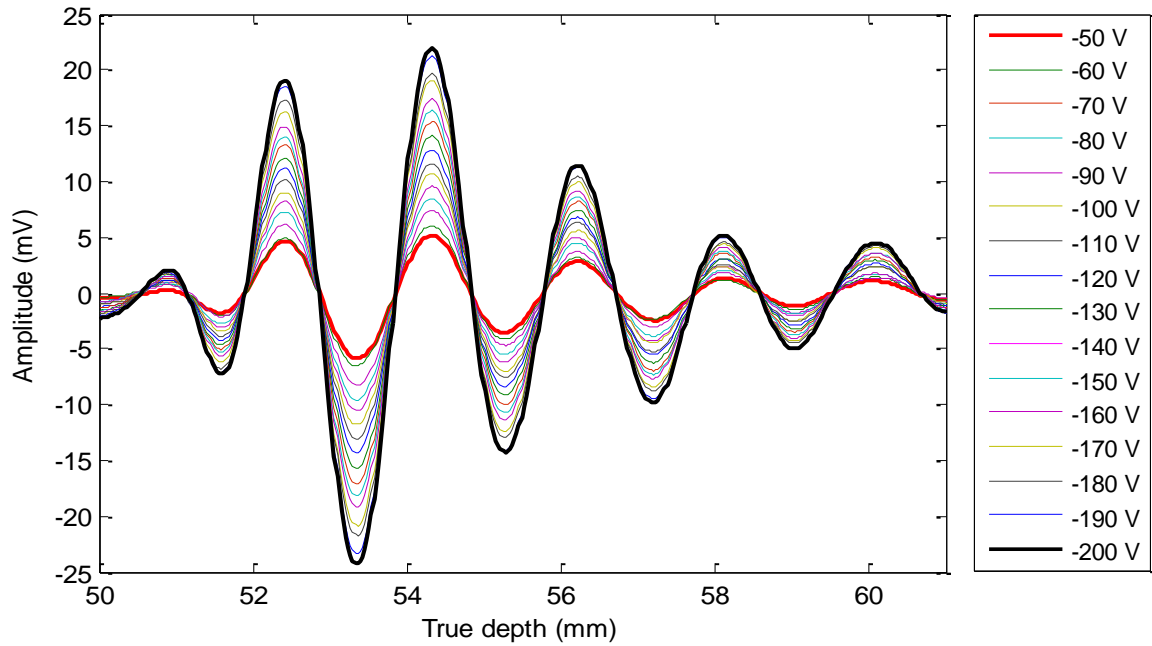


**Figure 5-11: The returned waveform of the fastest arriving echo received back at the ultrasonic transducer, for the initial pulse ranging from -50 V to -200 V.**

After it was shown that application of protective plate to the front face of GaPO<sub>4</sub> element lowered its resonant frequency as well as the amplitude of the received signals, the last test remaining was to examine whether the SNR level of the measurement using the new transducer also changed. For this, detectability of the backwall reflection that was received at the transducer (from Figure 5-11, and for an easier comparison again plotted in Figure 5-13 below) was compared with detectability of the backwall reflection that was received at the single GaPO<sub>4</sub> element (from Figure 4-5, again plotted in Figure 5-12). Calculation of the SNR level was done according to Eq. (4.2). If one looks at the two waveforms plotted next to each other (Figure 5-12 and Figure 5-13), it is easy to spot that the protective front plate machined to  $\lambda/4$  thickness has acted as a filter and cleaned the captured ultrasonic waveform from the unwanted reflections, as explained in section 2.8.4.

The single most positive result coming out from the application of the protective plate to the element has been a slight increase of the measurement's SNR level. From Figure 5-14 one can see that the derived SNR level of the signal received at the transducer is slightly higher than that received at the single GaPO<sub>4</sub> element, for the whole test range of the initial pulse from -50 V to -200 V. Although the rise in SNR level is mild and somewhat more significant at higher amplitudes of the initial pulse, it is important to say that any increase in SNR level is welcome and can only have a positive impact on the overall measurement using the ultrasonic transducer. Finally, in both cases the SNR level was above the threshold of 6 dB required for a practical NDT measurement.

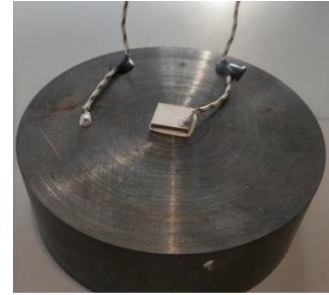
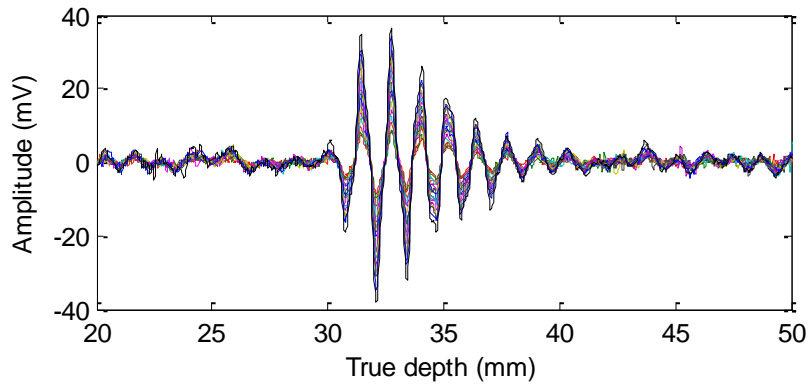


**Figure 5-12: The backwall reflection at 30 mm received back to the single GaPO<sub>4</sub> piezoelectric element, for the initial electrical pulse ranging from -50 V (min) to -200 V (max).**

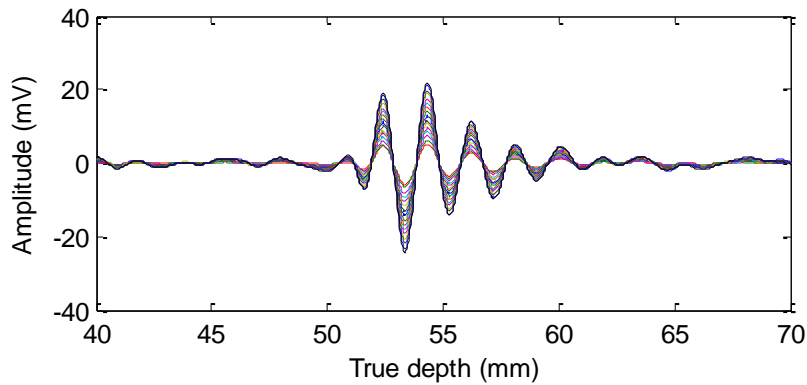


**Figure 5-13: The backwall reflection at 50 mm received back to the ultrasonic transducer, for the initial electrical pulse ranging from -50 V (min) to -200 V (max).**

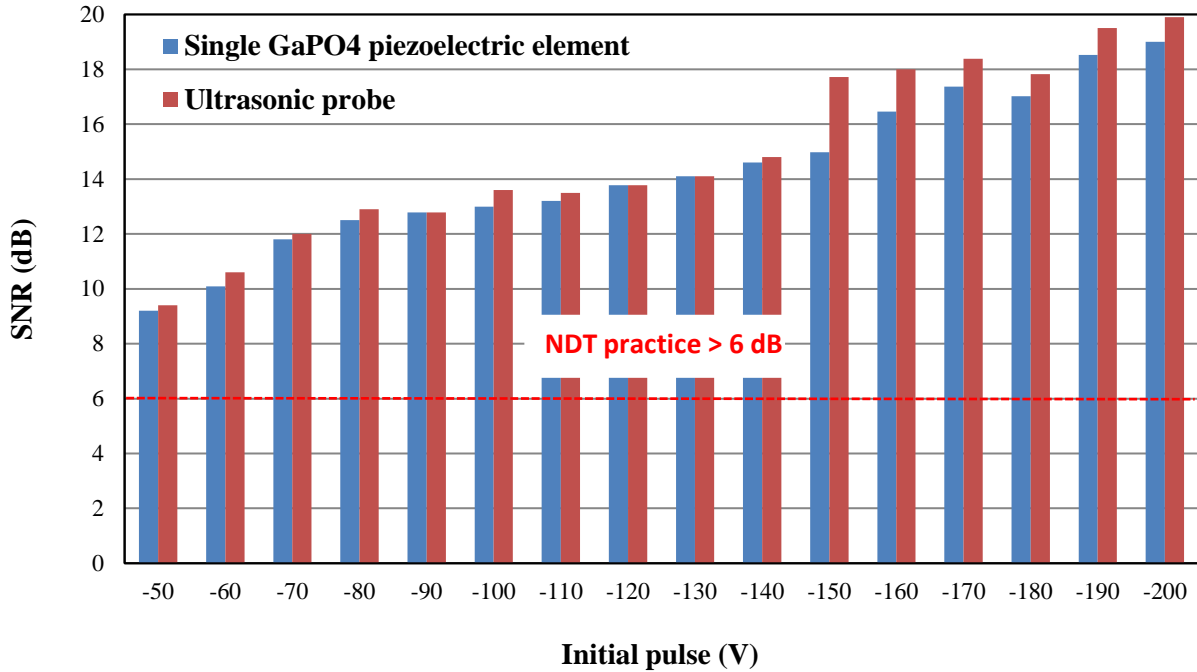


Figure 5-14: SNR values (in dB) for the waveforms received at the GaPO<sub>4</sub> element (blue part of the chart) and the transducer (red part of the chart); all SNR values were suitably high (>6 dB).

### 5.5.1.1 Fourier analysis

As can be seen in Figure 5-15, the returned waveforms at the transducer were transformed to a representation in the frequency-domain, for an initial pulse ranging from -50 V to -200 V.

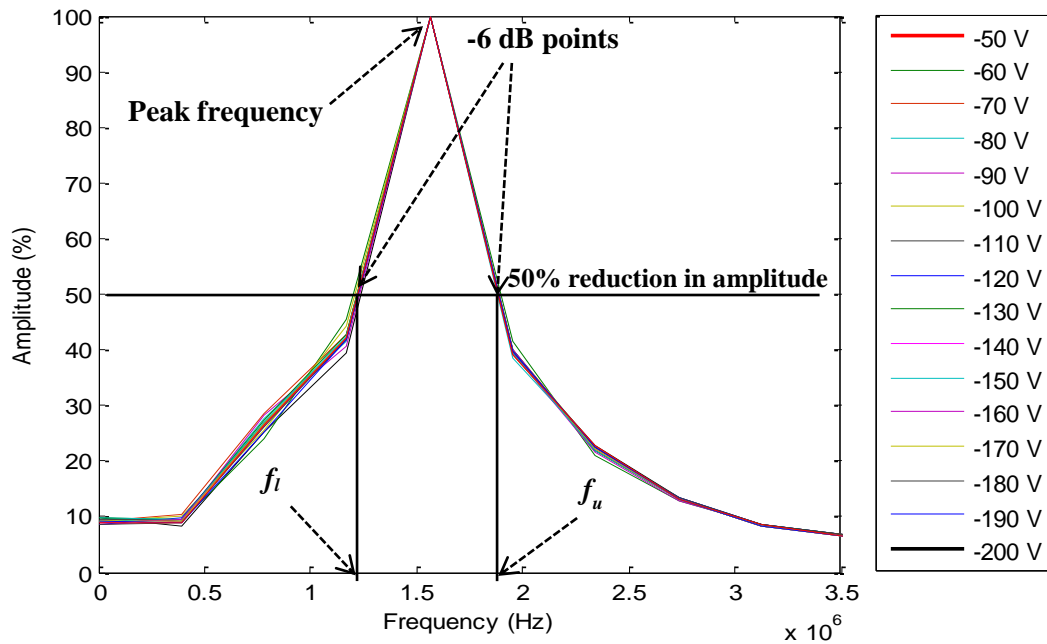


Figure 5-15: The frequency domain of the backwall reflection waveforms received at the manufactured transducer, for an initial pulse ranging from -50 V to -200 V.

From Figure 5-15 one can read the transducer's peak frequency to be 1.562 MHz and this corresponds well to its resonant frequency (1.496 MHz), previously measured using the analyser. This small frequency attenuation of 4.23%, will have no impact on the transducer's test resolution. Secondly, as with a GaPO<sub>4</sub> element permanently attached to the steel block, when operating the transducer at different initial pulses (from -50 V to -200 V), the peak frequency does not change and in this case has stayed constant at 1.562 MHz. Finally, one can calculate the bandwidth of the transducer at -6 dB to be 0.708 MHz (23.6%) with the lower frequency limit 1.319 MHz and the upper frequency limit 1.847 MHz. The centre frequency of 1.678 MHz corresponds well to the peak frequency of 1.562 MHz.

It is interesting to compare the bandwidth for the case when a GaPO<sub>4</sub> element is directly bonded to the steel substrate using silver adhesive (A-scan in Figure 5-12) with the case when the manufactured transducer is coupled to the calibration block using liquid couplant (A-scan in Figure 5-13). In the first case, the -6 dB bandwidth is derived to be 0.55 MHz and in the second case, it is 0.708 MHz. This is a broadening of approximately 29%. This means that when the protective plate is introduced between the GaPO<sub>4</sub> element and the steel structure, it acts as a damping body affecting the element's frequency and other ultrasonic parameters, as explained in [1]. For example, a direct consequence of the broader bandwidth will be the reduced number of cycles in the waveform emerging from the transducer. This is clear just by comparing the two waveforms reported in Figure 5-12 and Figure 5-13. In the first case the waveform has approx. 8 cycles in a pulse, and with the front plate coupled to the GaPO<sub>4</sub> element, the vibration is reduced to 5 cycles per pulse. As already explained, conventional transducers for non-destructive testing normally give no more than 1 or 2 cycles per pulse in order to meet the required inspection resolution [76]. However, as a damping body for the GaPO<sub>4</sub> element operating at 580°C has not been established yet, any reduction in the number of cycles is a very appreciated means of increasing the transducer's resolution. The information summary of the manufactured ultrasonic transducer is listed in Table 5-4.

**Table 5-4: The ambient temperature parameters of the transducer for operation at 580°C.**

Parameter	Unit	Symbol	Value @ 25°C
Peak frequency	(MHz)	$f_p$	1.562
Centre frequency	(MHz)	$f_c$	1.678
Lower limit frequency	(MHz)	$f_l$	1.319
Upper limit frequency	(MHz)	$f_u$	1.847
-6 dB Bandwidth	[MHz (%)]	$B$	0.708 (23.6)
Max peak-to-peak sensitivity (@ -200 V)	(mV)	$Ap-p_{max}$	46
Min peak-to-peak sensitivity (@ -50 V)	(mV)	$Ap-p_{min}$	10.5

## 5.5.2 Defect detection at ambient temperature

In defect detection, a pulser-receiver measures the time taken for each echo to arrive back at the transducer after entering the surface of the test object. If the velocity of sound in the test-material is known, it is possible to determine the distance travelled by the sound wave. If there are one or more defects in the test-structure, such as side-drilled holes (SDH) normally found in calibration blocks, depending on the position of the transducer, some of the ultrasonic energy will reflect from one or more SDHs first, and a little while later, some will reflect from the block's backwall. The arrival of the two or more reflections at the piezoelectric element will be separated by a short interval of time. If the pulse duration of any of these reflections is longer than this interval of time, then it may not be possible to distinguish the defect/SDH from the backwall. This means that at least one or more echoes will not be "resolved" and one can say that the resolution of the transducer is poor. To improve the resolution, one needs to ensure that the pulse duration is as short as possible. This is achieved with application of a damping body on the backside of the piezo-element. Considering an alternative damping body operating at 580°C has not been established, it was a question whether the "undamped" transducer with 5 cycles in its pulse was able to resolve each of the SDHs of the block. For this, the transducer's resolution (both horizontal and vertical) must be validated, but first it is important to determine the transducer's exit-point and the angular distribution of its ultrasonic beam.

### 5.5.2.1 Determination of the transducer's exit-point

The exit-point is the point where the central ray of the beam emerges from the transducer. The exit-point is a very important parameter, because the exit-point is normally taken as the starting point of each measurement with the transducer. To determine the exit-point of the transducer, the "V1" calibration block was used [139]. The "V1" block, with coupled transducer, can be seen in Figure 5-16. For the coupling, couplant Ultragel II was used and the max pulser voltage of -200 V was delivered to the GaPO<sub>4</sub> element. The transducer was placed on the block directly above the "centre mark", and directly above the reflective surface that was 2 mm wide and located at the depth of 85 mm (detailed in Figure 5-17). Then, the transducer was moved (carefully) left and right from the reflective surface, keeping the transducer's front and back surfaces parallel with the front and back surfaces of the block. At the same time, it was important to maintain a uniform pressure between the transducer and the contact surface. Finally, the transducer was stopped in the position where the max amplitude of the reflection from surface was achieved. The exit-point of the transducer was the point that coincided with the "centre mark". The same Figure 5-17, shows that left and right from the reflective surface at 85 mm, there were also two backwall surfaces: one was located at the depth of 91 mm (left from the reflective surface) and the other was at the depth of 100 mm (right from the reflective surface). These three features of the "V1" block, help to explain the A-scan from Figure 5-18 a).

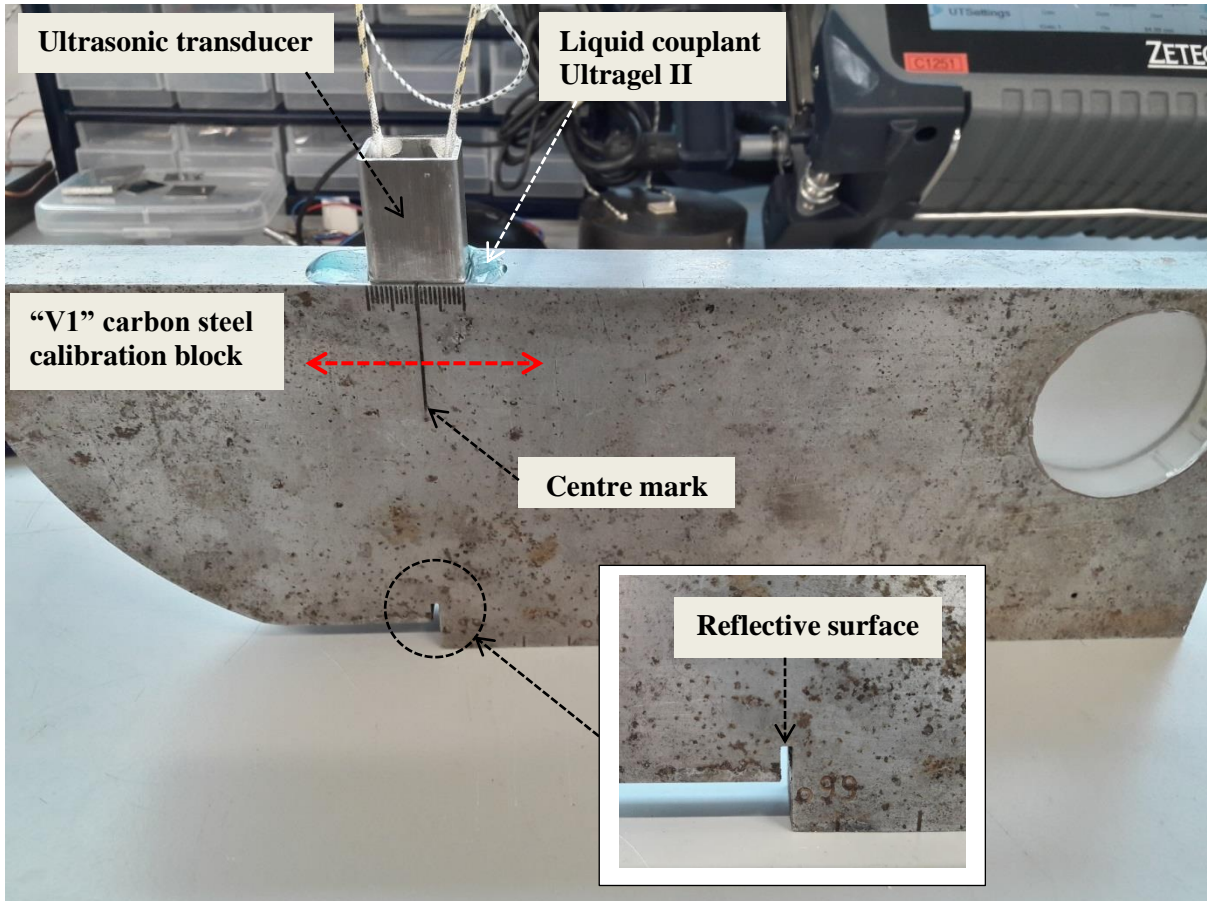


**Figure 5-16:** The transducer was coupled to “V1” block to determine the location of the exit-point. As a coupling medium, Ultragel II was used. Finally, a max voltage of -200 V was applied.

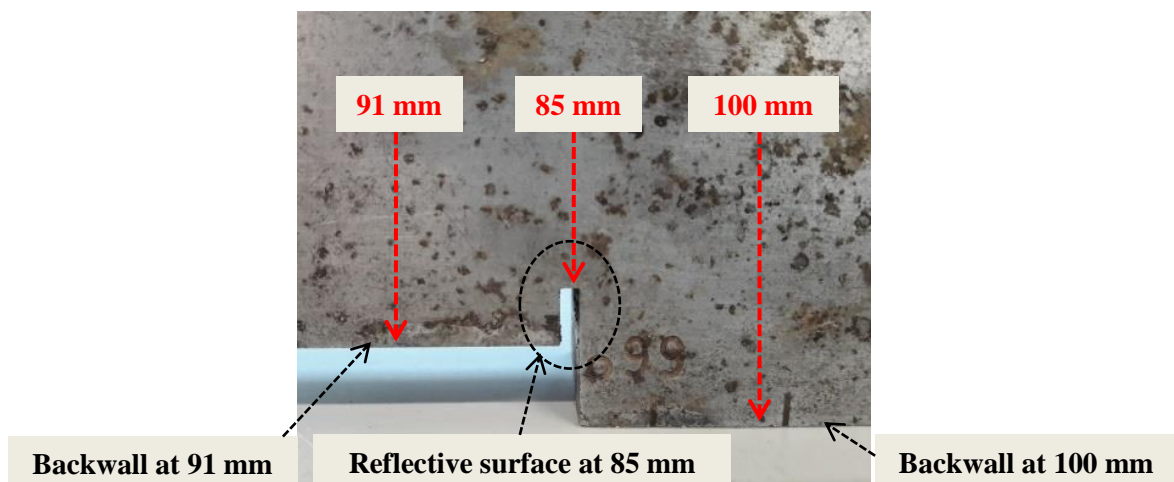


**Figure 5-17:** Backwall at 91 mm, targeted surface at 85 mm and a backwall at 100 mm depth.

In Figure 5-18 a) one can see an A-scan, with three signals. The first signal is the one from the targeted reflective surface at 85 mm, and this one is the most important for this measurement. As explained

before, the amplitude of this signal needs to be carefully observed while moving the transducer; when the amplitude comes to its maximum (in this case just below 10 mV) one knows where the exit-point of the transducer is. The second signal is the reflection from the first backwall (the one that is located left from the targeted reflective surface at the depth of 91 mm), and the third signal is another reflection from the backwall (this time the one at the right from the targeted reflective surface at the depth of 100 mm). The transducer with the marked exit-point can be seen in Figure 5-18 b).

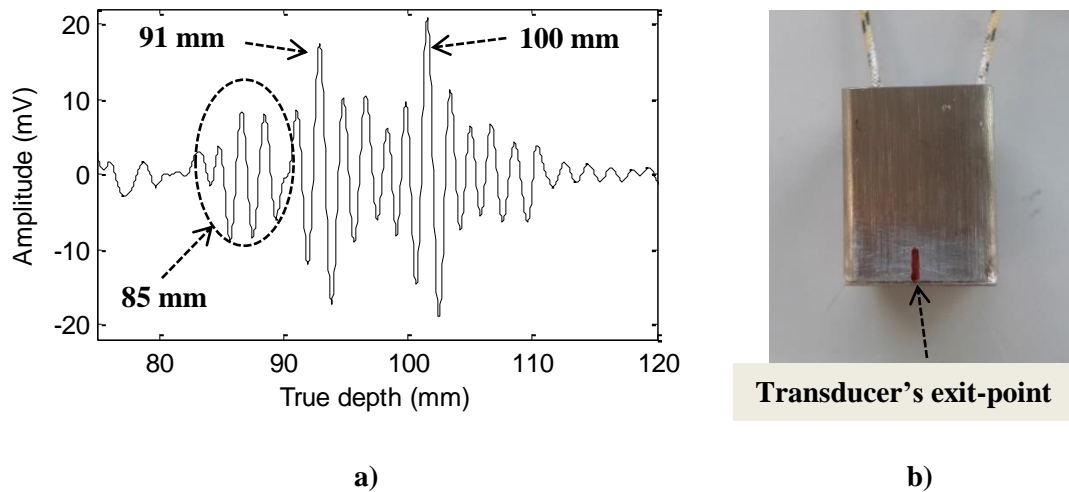


**Figure 5-18: a) A-scan with three signals, one from the reflective surface at 85 mm and second and third from the backwalls at 91 and 100 mm, respectively. b) The transducer’s exit-point.**

### 5.5.2.2 Measurement of the angular distribution of the ultrasonic beam

The ultrasonic beam emerging from the transducer normally spreads out into a conical shape, where its intensity follows the inverse square law just as it would for a beam of light or X-ray [40]. The conventional way of measuring the angular distribution of the beam is to immerse the transducer into a pool filled with water, which also contains a small spherical reflector [73]. Then, the spherical reflector is moved vertically up and down until the maximum amplitude of the reflected signal is captured. After this, the same spherical reflector is again moved up and down in a controlled way, where the unit of the vertical movement is related to an angle, in order to capture the value of the intensity of the transducer’s ultrasonic response. Since the design of the transducer was not yet finalised, and therefore the transducer was not hermetically sealed, immersion into water was not feasible. For this, an alternative way to measure the angular distribution of the ultrasonic beam was utilised. In Figure 5-19 one can see the setup used to measure the angular distribution of the beam. The transducer was coupled to the “V1” block using couplant Ultragel II. However, this time the transducer was coupled at a different location on the “V1” block, above an SDH ( $d=2$  mm) located at a depth of 15 mm. Below the SDH there was a circular insert made of Perspex ( $d=50$  mm) at the depth of 45 mm. The exit-point of the transducer coincided with the position “0”, which was positioned vertically above the SDH. At this position, the

amplitude of the reflection from SDH was the largest. The A-scan containing the maxi reflection from SDH, together with the reflection from Perspex insert, can be seen in Figure 5-20 a). The peak-to-peak amplitude of the reflection from SDH was measured to be 12.35 mV, and the amplitude of the reflection from the circular insert was 8.61 mV. After the largest reflection from the SDH was captured, the transducer was moved to the left and right from the position “0”, until a empirical edge of -6 dB was achieved. This was where the amplitude of the reflection fell to one half of its max value, at 5.94 mV. At the same time, the amplitude of the reflection from the circular insert stayed almost the same, 8.93 mV. These two reflections, at the edge of -6 dB, can be seen in Figure 5-20 b). These were previously marked positions “1” and “2” in Figure 5-19. Then two lines are drawn, one through the position “0” and the position “1” and another between position “0” and position “2”. This resulted in a measured beam spread angle of 19° (the same as Figure 5-19).

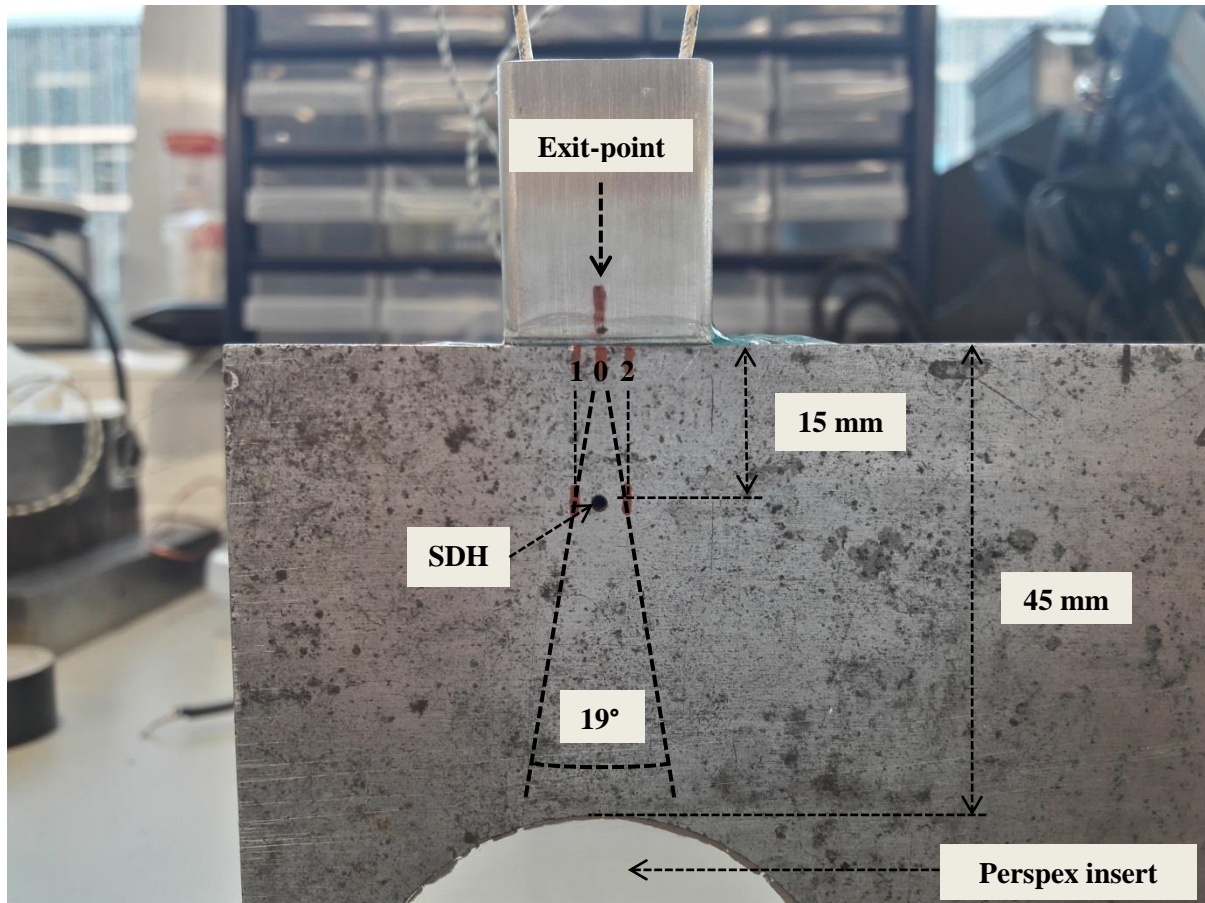


**Figure 5-19: The transducer coupled to “V1” block to measure the beam spread angle. As a coupling medium, couplant Ultragel II was used. Finally, pulser voltage of -200 V was applied.**

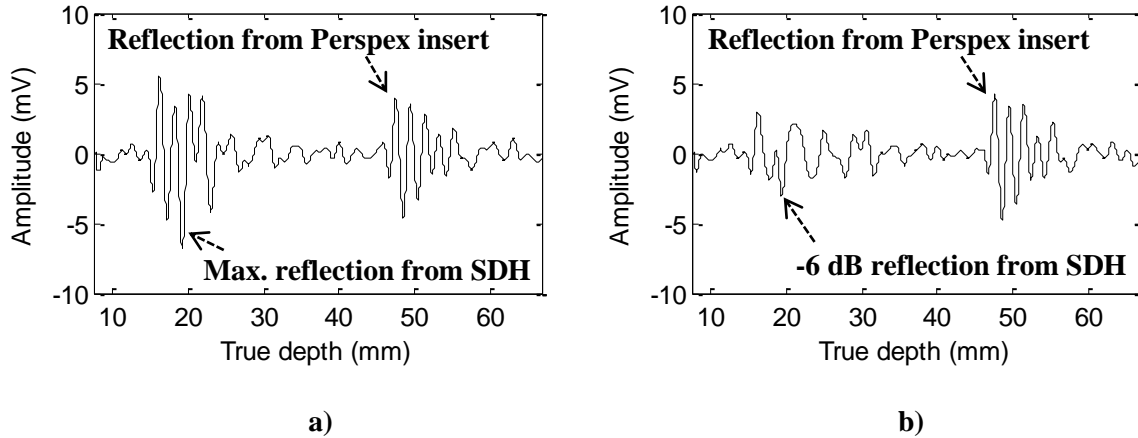


**Figure 5-20: a) A-scan with two reflections from SDH & Perspex circular insert. The amplitude of the reflection from SDH is at its max value. b) A-scan with the same two reflections; however the amplitude of the reflection from SDH is here 50% (-6 dB) of its max value.**

In the literature, it is possible to find a mathematical expression that relates the -6 dB edge (or possibly the -20 dB edge) to the beam spread angle. For a square piezoelectric element, such as GaPO<sub>4</sub> element used in this work, it is possible to calculate the ultrasonic beam spread angle by using Eq. (5.2), [140]:

$$\sin \frac{\alpha}{2} = \frac{0.44 \lambda}{a} \quad (5.2)$$

where  $\alpha$  (°) is the beam spread angle,  $\lambda$  (m) is the wavelength and  $a$  (m) is the width of the element.

For a steel calibration block ( $v=5920$  m/s) and a transducer with the peak frequency of 1.562 MHz, the wavelength  $\lambda$  is calculated to be 3.79 mm. If the width of GaPO<sub>4</sub> element is 10 mm, then the beam spread angle  $\alpha$  can be calculated to be 19.198°. This calculated beam spread angle is practically the same as the measured one (19°), confirming the chosen measurement method.

### 5.5.2.3 Defect detection with the manufactured transducer

After the exit-point was determined, and the beam spread angle was measured, the defect detection capability of the new transducer at ambient temperature was tested. The transducer was coupled to a steel calibration block using liquid couplant Ultragel II. The calibration block was the same as that depicted in Figure 5-9, containing four artificial SDHs (through thickness of the block) with diameter of 2 mm, and the backwall surface at 50 mm. The SDHs were located at four different depths: 42, 30, 17 and 4 mm, looking from left to right. The horizontal distance between two consecutive SDHs was 7 mm. Measurements with the transducer were done at six different positions on the calibration block:

- (1) the transducer was coupled to the calibration block in the far left position with no SDH below it but only the backwall at depth of 50 mm (see Figure 5-21);

- (2) the transducer was coupled directly above the SDH located at depth of 42 mm (see Figure 5-22);
- (3) the transducer was coupled to block directly above the SDH at depth of 30 mm (see Figure 5-23);
- (4) the transducer was placed above the SDH at depth of 17 mm (see Figure 5-24);
- (5) the transducer was positioned directly above the SDH located at depth of 4 mm (Figure 5-25);
- (6) and finally the new transducer was coupled to the steel block in the far right position with no SDH below it but only the backwall at 50 mm see (Figure 5-26).

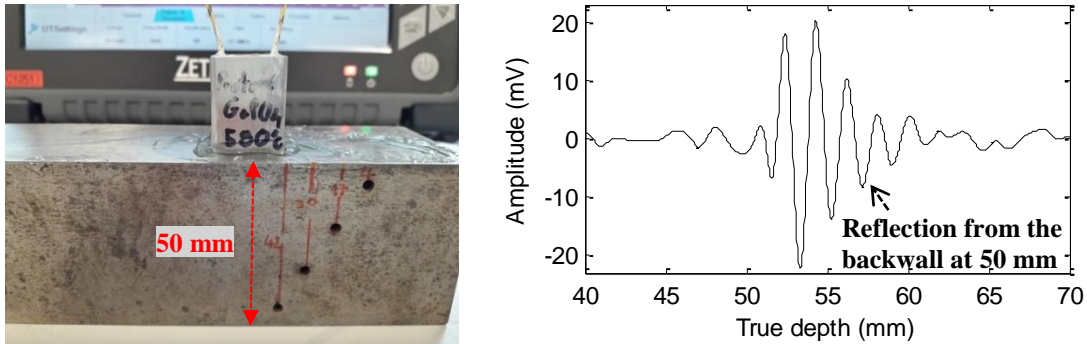


Figure 5-21: The transducer coupled to the block in the far left position with no SDH beneath.

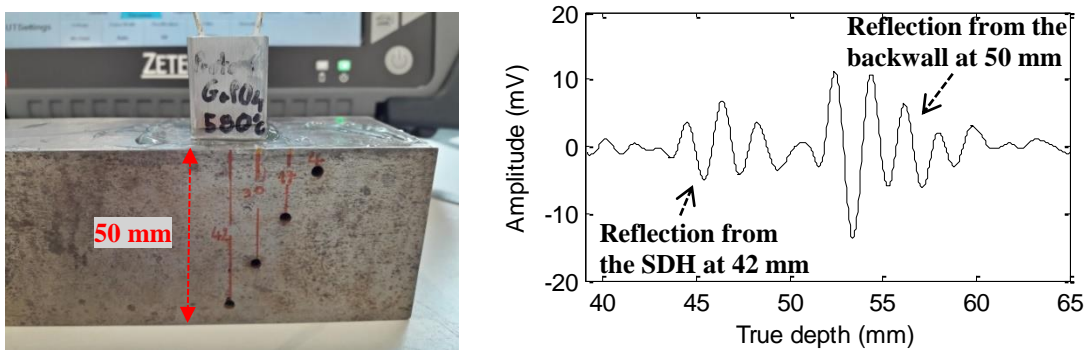


Figure 5-22: The transducer coupled to the block above the SDH ( $d=2$  mm) at depth of 42 mm.

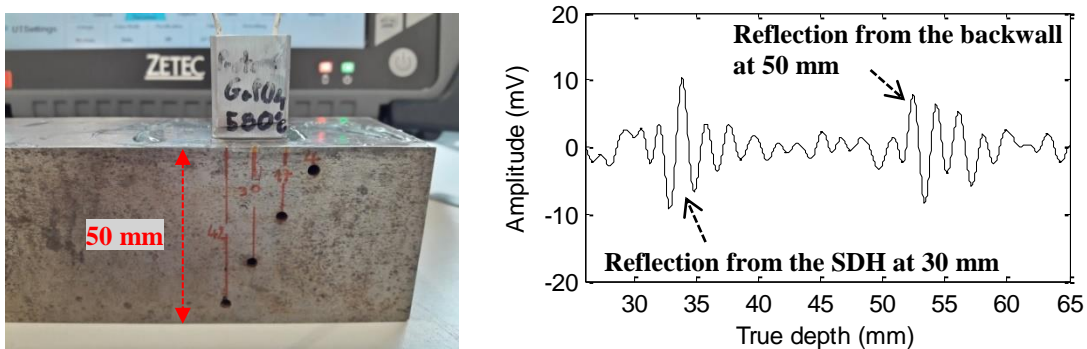


Figure 5-23: The transducer coupled to the block above the SDH ( $d=2$  mm) at depth of 30 mm.

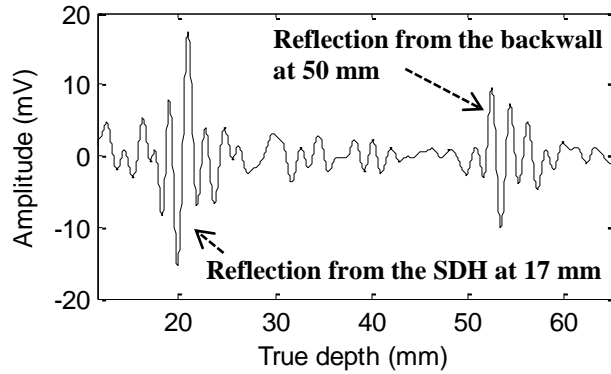
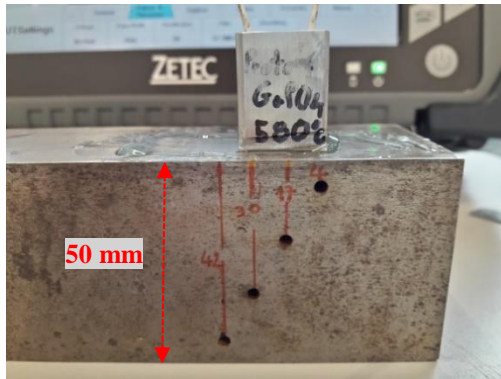


Figure 5-24: The transducer coupled to the block above the SDH ( $d=2$  mm) at depth of 17 mm.

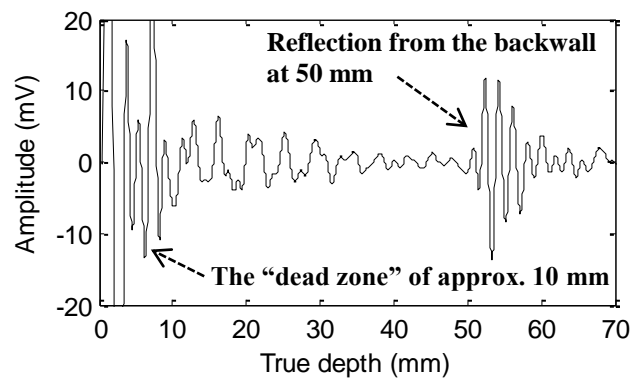


Figure 5-25: The transducer coupled to the block above the SDH ( $d=2$  mm) at depth of 4 mm.

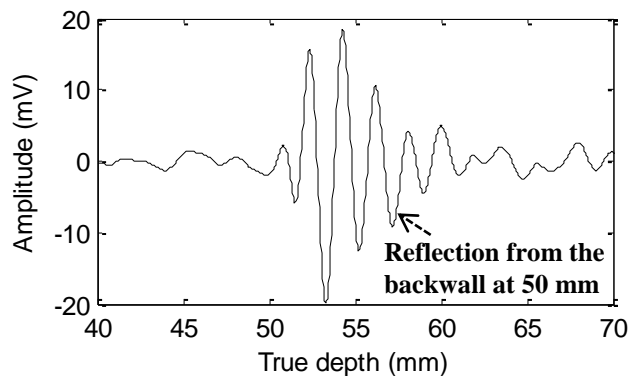
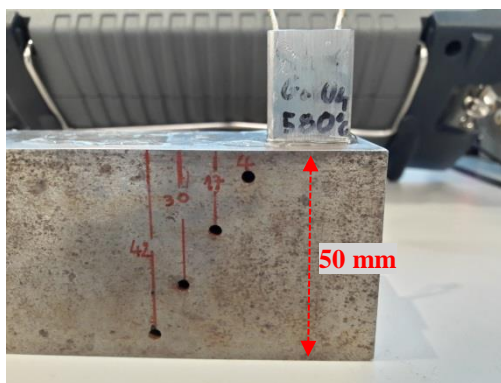


Figure 5-26: The transducer coupled to the block in the far right position with no SDH beneath.

If one looks at Figure 5-21, one can see that in the far left position, it is only possible to detect the backwall surface and measure the thickness of the calibration block at 50 mm, as there is no SDH located between the transducer and the backwall. It is interesting that in this position, the amplitude of the reflected signal is the largest (similar to that in the far right position), compared with the four cases

with an SDH inserted between the transducer and the backwall. This is because the energy is reflected from only one reflector, the backwall, and then is received back at the transducer. If there were one or more SDHs between, part of the energy would reflect from the respective SDH and another part a bit later from the backwall, as explained in section 4.5.4. However, in both cases the total amount of the energy that was reflected from the reflectors and later received at the transducer would be the same, if one assumed there was no energy loss in the process.

On the other hand, as one can see in Figure 5-22 to Figure 5-24, respectively, in the positions where the transducer was coupled above the SDHs located at 42, 30 and 17 mm, it was possible to detect both the corresponding SDH and the backwall of the block. However, once the transducer was moved to the position above the SDH that was located at depth of 4 mm (Figure 5-25), it was not possible anymore to detect the SDH but only the backwall at 50 mm. This was because the reflection from the SDH was within the “dead zone” of the transducer, which is defined as the part of the time-base occupied by the initial pulse [40]. For the transducer used in this measurement, it was possible to estimate that the “dead zone” taken by the initial pulse was approx. 10 mm (one can see this from the A-scan in Figure 5-25). This relatively large “dead zone” is a consequence of the fact that no damping body was applied to the back face of the GaPO<sub>4</sub> piezoelectric element. Finally, in the last Figure 5-26 one can see the transducer that was in the far right position. Here, similar as to the far left position, it was only possible to measure the thickness of the calibration block of 50 mm and no SDH could be detected, simply because there was no SDH located below the transducer.

## **5.6 Testing of SONO high temperature ultrasonic couplants**

After the transducer was validated with a series of confidence-building impedance and ultrasonic tests at ambient temperature, the next step was to test the behaviour of the transducer exposed to a high temperature environment. To allow an efficient ultrasonic coupling of the transducer to the steel test-block as hot as up to 580°C, a number of HT ultrasonic couplants from the SONO family (such as SONO 950, 1100 and 1200+ that were already discussed in section 2.8.10) were purchased.

### **5.6.1 Testing of SONO couplants with a commercial transducer**

Even though SONO couplants have been present on the market for some time, there is little data on their properties and ultrasonic performance. The reported properties of SONO couplants, compared to the properties of the conventional couplant Ultragel II, one can see in Table 5-5:

**Table 5-5: <sup>1</sup>The highest temperature ultrasonic couplant commercially available. <sup>2</sup>At ambient temperature. <sup>3</sup>Brookfield Helipath Spindle E @1.5 rpm. <sup>4</sup>Brookfield LV #5 @0.3 rpm.**

Couplant	Ultragel II	SONO 950	SONO 1100	SONO 1200+ <sup>1</sup>
Physical state	Slow flowing gel	Medium	viscosity	paste
Ferro. corr. inhibition rating	90	95	100	100
Viscosity <sup>2</sup> [cps]	80000 <sup>3</sup>	>3000000 <sup>4</sup>	>3000000 <sup>4</sup>	-
Relative viscosity	4	-	-	-
Density [kg/m <sup>3</sup> ]	1091	-	-	-
Velocity [m/s]	1650	-	-	-
Spec. acoustic imp. [MRayl]	1.8	-	-	-
Min. temperature [°C]	-23	315	371	371
Thickness gauging [°C]	99	315-510	371-593	371-649
Flaw inspection [°C]	93	315-385	371-482	371-482
Auto ignition [°C]	-	560	626	-

The investigation of the couplant effect on the amplitude of the signals in the test material was performed with the normal beam compressional transducer with a piezoelectric ceramic of 10 mm in diameter and with frequency of 4 MHz (GE Inspection Technologies, type K4N). The transducer was in a direct contact with the surface of the block using three different couplants: (a) Ultragel II, (b) SONO 950 and (c) SONO 1100. A digital flaw detector (Sonatest Masterscan 335) was used to excite the transducer and receive the pulse-echo signals from the backwall of the block, as well to display the recorded back-wall echoes on a LCD panel. The experimental setup can be seen in Figure 5-27:



**Figure 5-27: The setup used to test the couplant effect on the amplitude of the echo signals consisted of a normal beam transducer, a steel test-block and a digital flaw detector.**

Figure 5-28 a) to c) shows four consecutive echoes received at the commercial transducer as reflections from the backwall of the steel block, where a different couplant was used for each of the three cases: a) Ultragel II; b) SONO 950; and c) SONO 1100.

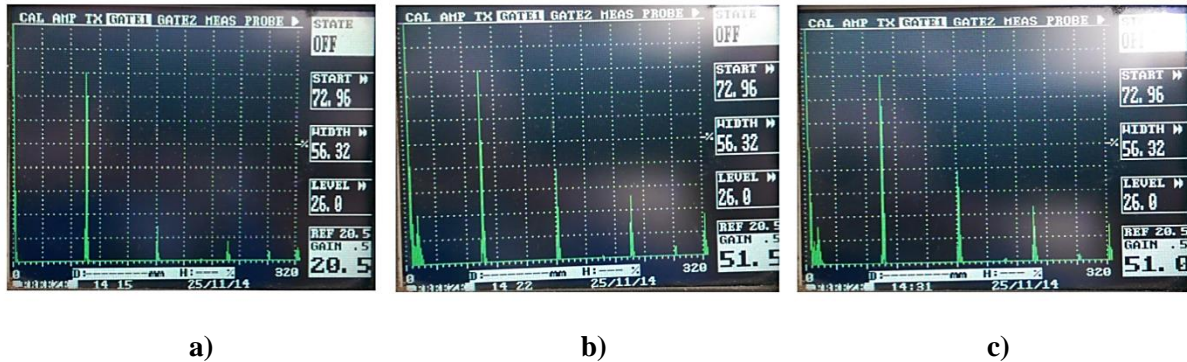


**Figure 5-28: Four consecutive backwall echoes received at the commercial transducer where a different couplant was used for each of the cases: a) Ultragel II, b) SONO 950 and c) 1100.**

To keep the first backwall echo at 80% of full screen, HT couplants SONO 950 and 1100 require 31 dB and 30.5 dB, respectively, higher gain than the conventional couplant Ultragel II. In addition, the rate of decrease of the backwall echoes are different, and the second and third back-wall echoes using Ultragel II decline several times faster than those using HT couplants. This is because the intensity of the first echo increases with the transmission coefficient, and that of the second echo and consecutive echoes decrease as the transmission coefficient increases in line with the characteristic acoustic impedance. According to the material data sheet (Sonotech NDT Ultrasonic Couplants), the minimum operating temperature for SONO 950 and SONO 1100 is 315°C and 371 °C, respectively. Thus, one can expect that the ultrasonic properties of these two HT couplants will improve above the minimum operating temperatures. With the expected increase of the characteristic acoustic impedance with temperature, the transmission coefficient, i.e. the intensity of the first echo, will increase. For better flaw detection, the amplitude of the first backwall echo should be large [141].

### 5.6.2 Testing of SONO couplants with the manufactured transducer

Again, a comparison of Ultragel II and SONO couplants was performed, however this time using the manufactured transducer. In Figure 5-29, one can see how the new transducer was used to perform ultrasonic thickness gauging on a steel calibration block (50 mm thick) using the conventional couplant Ultragel II. The recorded time domain response of the first reflection from the backwall of the block (at 50 mm) can be seen in Figure 5-30 a), and the same ultrasonic response of the transducer in the frequency domain can be seen in Figure 5-30 b). The initial pulse applied to the transducer ranged from

-50 V (min) to -200 V (max), and a clearly proportional relationship between the initial pulse applied to the transducer and its ultrasonic response can be seen in the below figures.



**Figure 5-29: Ultrasonic gauging using couplant Ultragel II (block thick. 50 mm, vel. 5920 m/s).**

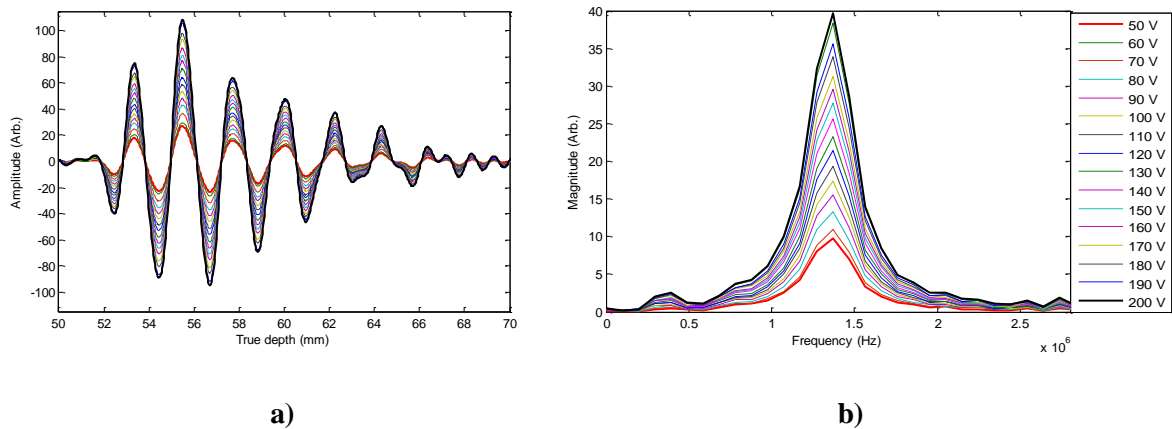


**Figure 5-30: Thickness gauging using Ultragel II: a) time domain and b) frequency domain of the first reflection from backwall of the steel block, for the initial pulse from -50 V to -200 V.**

Figure 5-31 shows, how the ultrasonic thickness gauging with the transducer was performed using the HT couplant SONO 1100. The recorded time domain response of the first reflection from the backwall of the block (at 50 mm) can be seen in Figure 5-32 a), and the same ultrasonic response of the transducer in the frequency domain can be seen in Figure 5-32 b). Again, the initial pulse applied to the transducer was from -50 V (min) to -200 V (max), and again a proportional relationship between the initial pulse applied and the transducer's response can be seen in the figures.



**Figure 5-31: Ultrasonic gauging using couplant SONO 1100 (block thick. 50 mm, vel. 5920 m/s).**

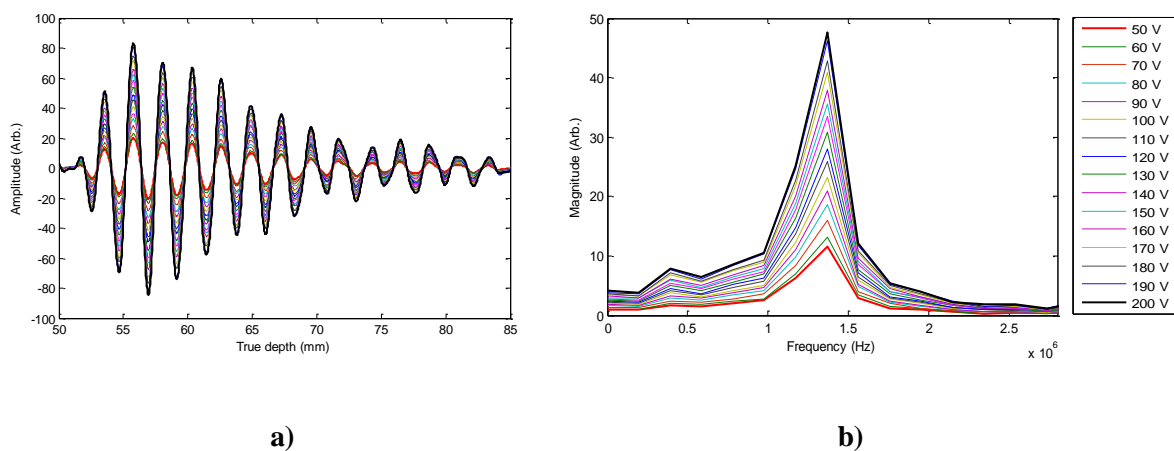


**Figure 5-32: Thickness gauging using SONO 1100: a) time domain and b) frequency domain of the first reflection from backwall of the steel block, for the initial pulse from -50 V to -200 V.**

### 5.6.2.1 Comparison of Ultrigel II and SONO 1100

The comparison of the response when conventional couplant Ultrigel II and HT couplant SONO 1100 are used, can be seen in Figure 5-33 for time domain and in Figure 5-34 for frequency domain. In Figure 5-33 a) and Figure 5-34 a), a minimum initial pulse of -50 V was applied, and in Figure 5-33 b) and Figure 5-34 b), a maximum initial pulse of -200V was applied. From the time domain response it is clear that using the conventional couplant Ultrigel II will result in a higher generated amplitude and less “ringing” of the transducer (in literature “ringing” is sometimes called the “surface noise” [142]). In general, the optimum sound transmission and lowest surface noise is achieved with application of couplants with high acoustic impedance [143]. In terms of frequency response, regardless of the couplant applied (Ultrigel II or SONO 1100) or the amplitude of the initial pulse (-50 V or -200 V), the peak frequency of the transducer did not change and stayed constant at ~ 1.4 MHz.

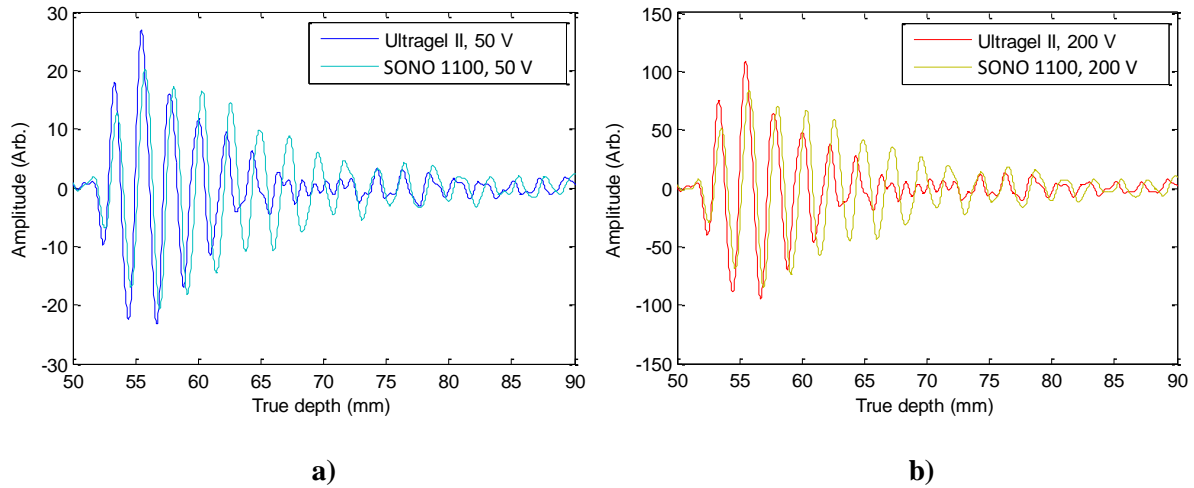


**Figure 5-33: Time domain comparison of the ultrasonic response when two couplants were used to facilitate the transmission of ultrasonic energy, with an initial pulse: a) -50 V and b) -200 V.**

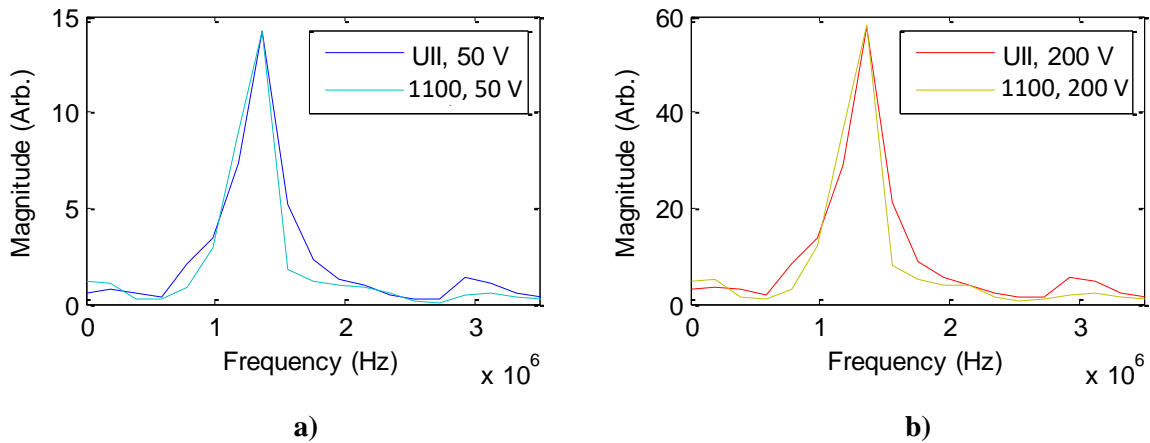
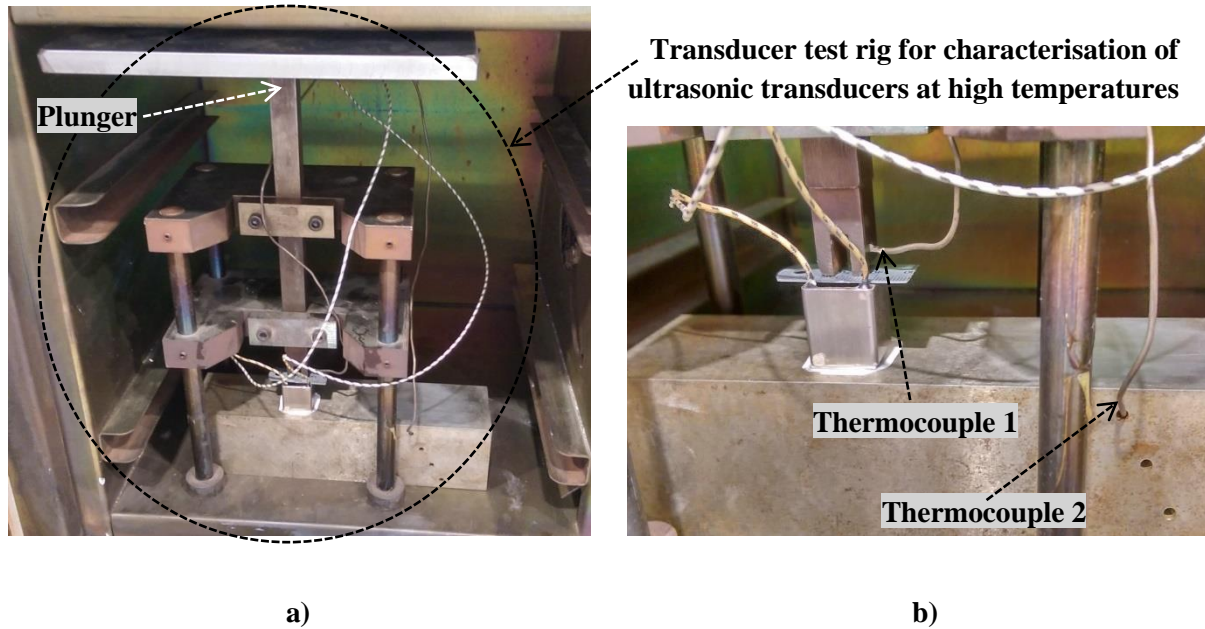


**Figure 5-34: Frequency domain comparison of the ultrasonic response when two couplants were used to facilitate the transmission of energy, with an initial pulse: a) -50 V and b) -200 V.**

## 5.7 Testing of the ultrasonic transducer at high temperatures

The experimental setup for thickness gauging using the manufactured transducer can be seen in Figure 5-35 a). The temperature of the steel block was measured with two thermocouples, where one measured the temperature of the surface very close to the place where the transducer was placed, and the second was inserted in an SDH close to the surface to measure the temperature achieved inside the block (Figure 5-35 b). After the same temperature was measured using both thermocouples, the electric furnace was open in order to remove used/apply new couplant between the transducer and the test surface and then the furnace was closed again. Once the same temperature was achieved for the second time, the thickness gauging took place. The test was performed at 25°C steps from room temperature up to the target temperature of 580°C. The transducer test rig used in this measurement was developed within an

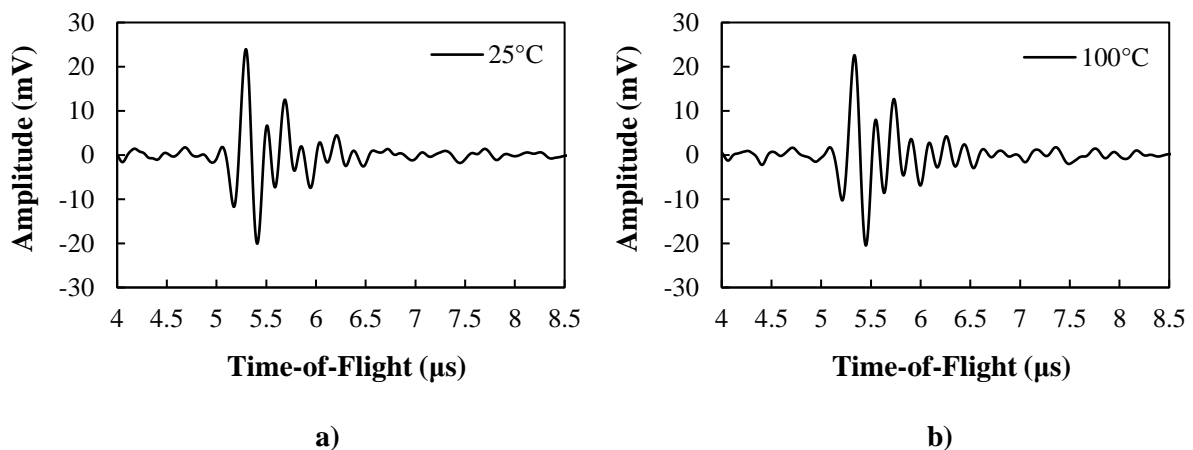
earlier development of high temperature guided wave transducers [144]. Finally, it can be mentioned that even though the test rig allowed application of an additional load, because of the adverse effects that load have on compression wave transducers (discussed in section 3.6.1), only own load of the test rig' plunger of 17 N was used for coupling.



**Figure 5-35:** a) The transducer was coupled to block using test rig and SONO 1100. Everything was placed inside an oven. b) Detailed view of the transducer and the two thermocouples.

### 5.7.1 Ultrasonic signals received at transducer from ambient up to 580°C

The A-scans containing echoes from the backwall of the block, and received back at the transducer up to 580°C can be seen in Figure 5-36 a) to g). The pulser-receiver unit was operated in the Time-of-Flight mode ( $\mu\text{s}$ ). For the first two measurements (25°C and 100°C), couplant Ultragel II was used, and between 200°C and 580°C, HT couplant SONO 1100 was used.



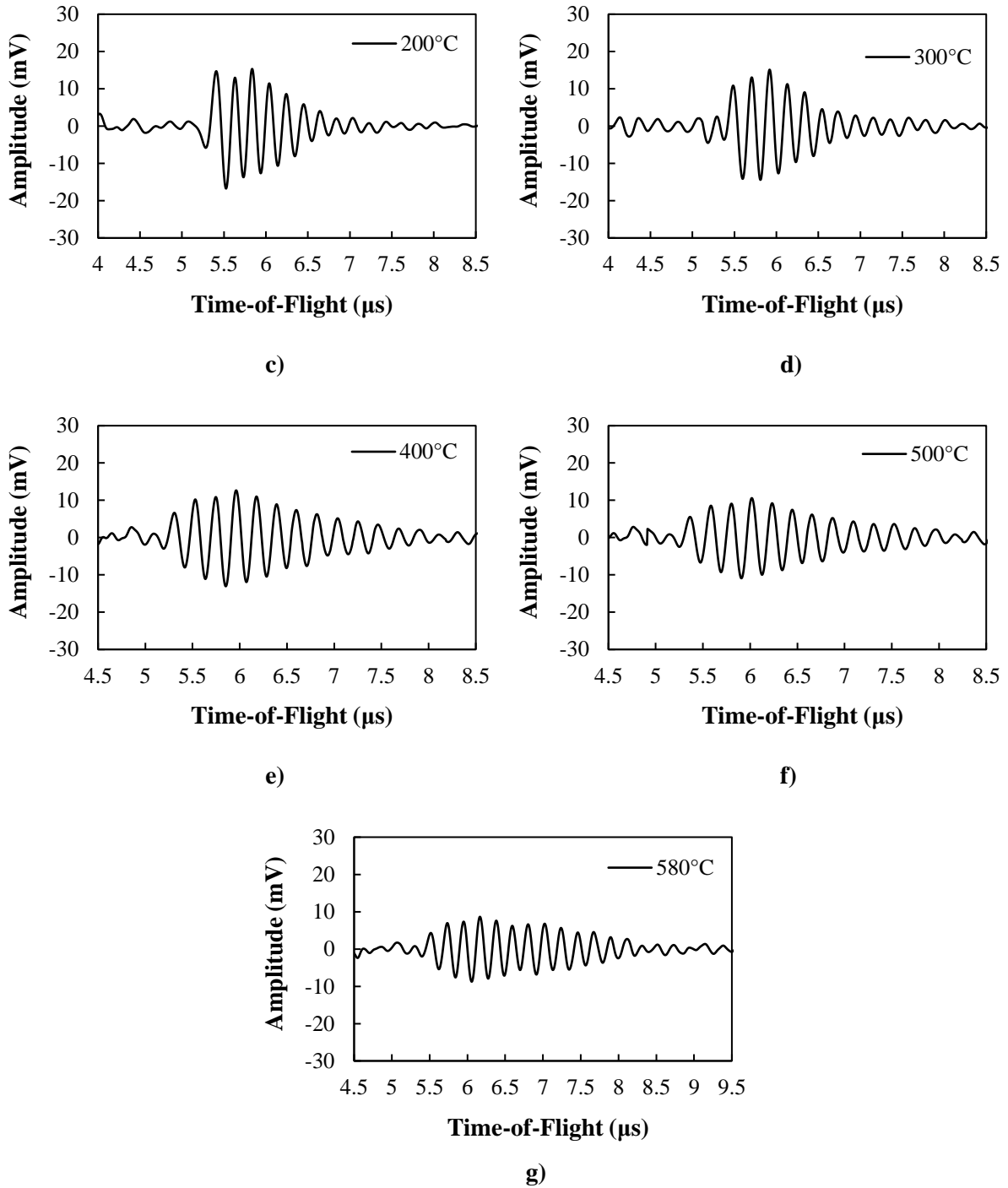


**Figure 5-36: The ultrasonic waveforms reflected from the backwall of calibration block received back at the transducer at temperatures: a) 25, b) 100, c) 200, d) 300, e) 400, f) 500 and g) 580°C.**

In Figure 5-37 a) one can see that as temperature increased from 25°C to 580°C, the generated peak-to-peak voltage of the received signals decreased. The effect of HT attenuation in steel material was already explained in section 4.4.4. At 25°C, the generated voltage was 43.75 V, and at 580°C it was 16.6 V, a decrease of 62.06%. Exactly the same trend was also noted for SNR level. In Figure 5-37 b), one can see that in the same temperature range up to 580°C, the calculated SNR level significantly

reduces and this is a direct consequence of reduction of the generated peak-to-peak voltage with increasing temperature. At 25°C, the SNR level was 21.88 dB, while at 580°C it was 13.28 dB. However, even though the SNR level went down almost 40%, it is still well above the minimum required level for a practical NDT (6 dB).

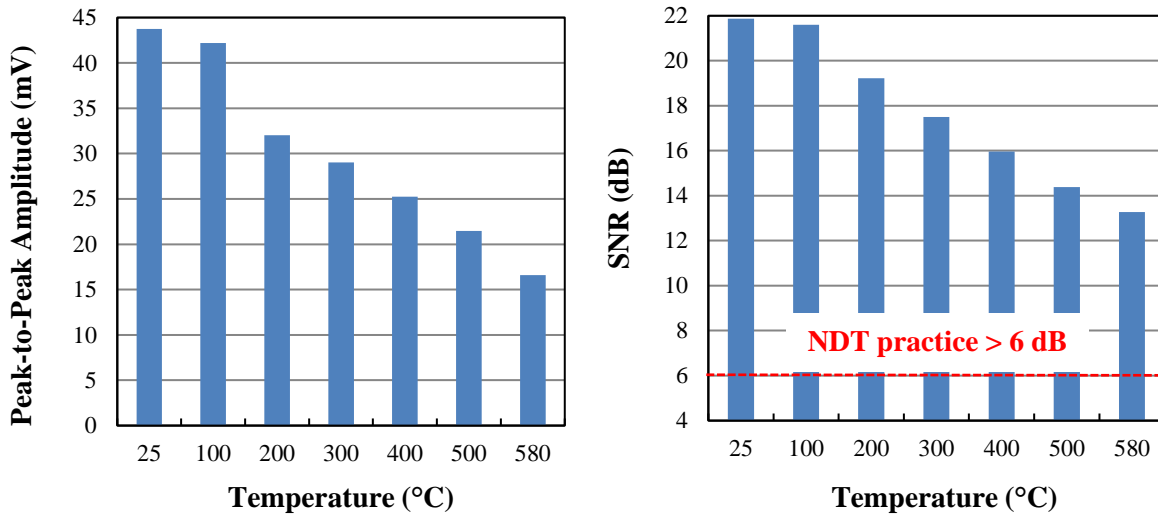


**Figure 5-37: a) Generated voltage (mV) of the received signals at the transducer from 25°C up to 580°C. b) Calculated SNR level (dB) of the received signals in the same temperature range.**

## 5.8 Manufacture of a prototype ultrasonic transducer

Based on the results from this research, a prototype high temperature transducer was manufactured by a specialist company. The transducer can be seen in Figure 5-38. The specifications of the transducer are listed below:

- As a protective front plate, a stainless steel sheet of thickness 0.7 mm was used;
- A silver adhesive was used for coupling between the steel sheet and the piezoelectric element;
- A metal spring was holding the piezoelectric elements in position and also for wiring;
- No backing/additional matching layer was used for this ultrasonic transducer.

The manufacturer carried out an initial test of the transducer. Tests in water with a steel target placed at about 50 mm using a standard Panametrics 507PR pulser/receiver were conducted. Due to the transducer configuration (e.g. no backing), the transducer's sensitivity was rated as "satisfactory", the centre frequency was measured at approximately 2 MHz and the bandwidth was very limited.

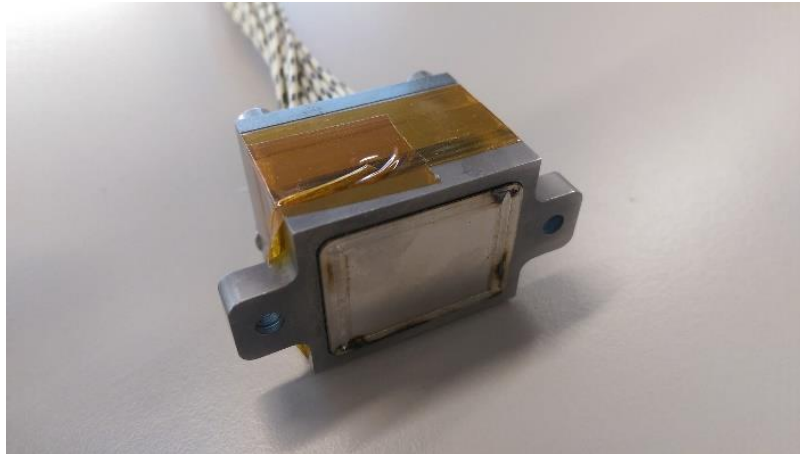


**Figure 5-38: A prototype of the commercial high temperature ultrasonic transducer.**

### 5.8.1 Testing of the transducer in a high temperature environment

As part of this research, the manufactured ultrasonic transducer was tested in a lab environment up to the target temperature of 580°C. For ultrasonic coupling, HT couplant SONO 1100 was used (Figure 5-39). Tests and discussion on this high temperature couplant can be found in section 5.6 (the suggested temperature range for its application is between 371 and 593°C).



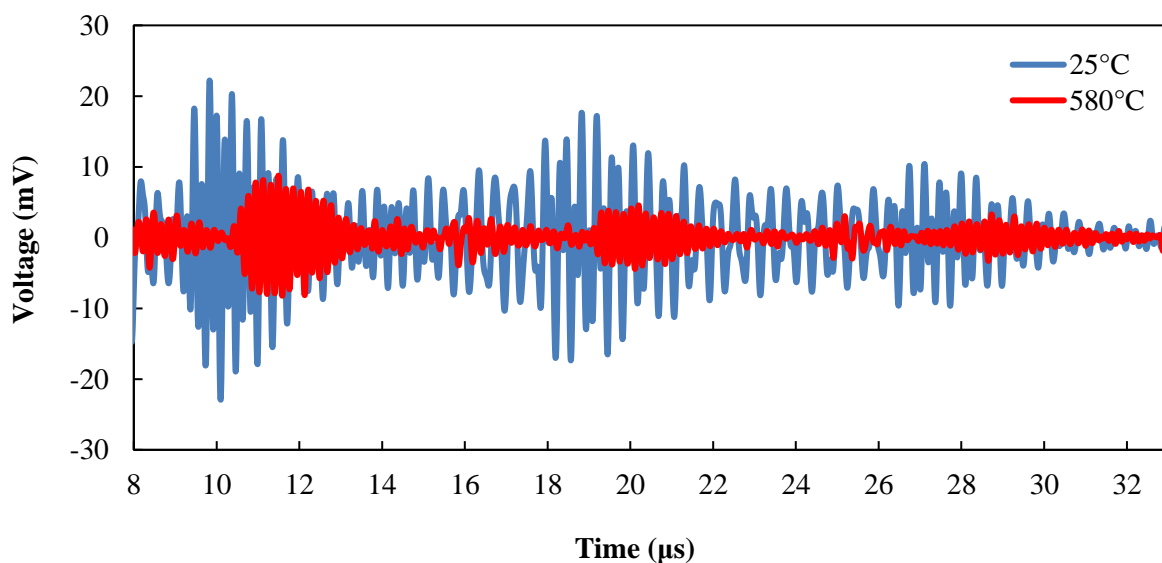
**Figure 5-39: Ultrasonic couplant SONO 1100 for application at high temperatures.**

Figure 5-40 shows the transducer coupled to a 25 mm thick P91 steel pipe section using high temperature couplant SONO 1100 and placed in an oven. Two thermocouples were used to ensure the temperature on the surface of the pipe section was correctly achieved. After the pipe section was heated to the target temperature of 580°C, ultrasonic thickness gauging was performed to validate the manufactured transducer's performance in a lab environment.



**Figure 5-40: The transducer is coupled to a P91 pipe section and ready for HT test to take place.**

Figure 5-41 shows the echoes that were reflected from the pipe section's backwall and received at the transducer. The blue trace shows the waveform received at 25°C, and the red trace shows the waveform received at 580°C. The waveform at 580°C (the red trace) is delayed compared to the waveform at 25°C due to decrease in velocity of P91 steel with rise in temperature. In addition, it is easy to see that there is more noise in the waveform at 25°C than at 580°C. This is possibly because the same SONO 1100 was used in both measurements, and according to its data sheet, the minimum operating temperature is 371°C at which the couplant changes from a powdered paste to a viscous liquid and enables much better transmission of the energy between the transducer and the test piece.



**Figure 5-41: The ultrasonic echoes received at the high temperature transducer at ambient temperature of 25°C (the blue trace) and at the target temperature of 580°C (the red trace).**

A transducer for operation at high temperatures was successfully developed, as discussed in this chapter. The transducer design is very similar to the one of a conventional transducer for application at ambient temperature; however, each of its components was manufactured using high-temperature substitute materials. The transducer was tested in a lab environment, using a calibration block, high temperature couplant SONO 1100 and an electric furnace. In the range from 25°C up to the target temperature of 580°C, the transducer kept its signal-to-noise level sufficiently above the threshold of 6 dB for practical ultrasonic non-destructive testing and condition monitoring. Based on the results from this research work, a prototype commercial high temperature transducer was manufactured by a specialised company. The transducer was tested in a lab environment in the same setup as before (pulsar-receiver instrument TOPAZ, an electric oven and SONO 1100 couplant), using a pipe section manufactured from high temperature grade steel P91. The transducer performed well, and enabled successful ultrasonic thickness gauging of the tested steel pipe section up to the target temperature of 580°C.

## 6 Conclusions and Future Work

### 6.1 Conclusions

Today, a great number of ageing power plants around the world have been receiving extension of their service life as they are approaching the end of their designed life. Even a single growing crack on a pipe or component such as a weld can cause a failure. If pipe crack(s) are identified during regular inspection at ambient temperature, there is always a question whether to replace the defective pipe/repair the weld or the crack is not severe enough and can be left for inspection at the next outage. However, uncertainties in calculation of lifetime of the defective part between two consecutive inspections can lead to very expensive consequences (plant not operating ~£1M/day, cost per major failure up to £120M) with even tragic results (injury, loss of human life). For this reason, the industry requires *in-situ* inspection and monitoring techniques to be developed; for steam pipes and headers fabricated from P91 steel for temperatures  $\leq 580^{\circ}\text{C}$ . This research work has achieved significant advances towards enabling ultrasonic inspection and monitoring of critical components at high temperatures, by developing an ultrasonic transducer based on an advanced single crystal piezoelectric Gallium Orthophosphate ( $\text{GaPO}_4$ ) material that can operate at the required temperature level. With this, the main goal of this research work was achieved.

Other objectives, set at the beginning of the PhD work, were also achieved. Conventional ultrasonic transducers can continuously operate only up to  $\sim 50^{\circ}\text{C}$  and some high temperature transducers do exist, operating still below the target temperature of this work and with a lot of limitations (e.g. Olympus: up to  $425^{\circ}\text{C}$ , max 10 sec of hot contact; Hagisonic: up to  $500^{\circ}\text{C}$ , in cycles and special coupling medium required). For this reason, the main challenge was to select the materials to continuously withstand the temperature of  $580^{\circ}\text{C}$ , and to be compatible between themselves to achieve a functional transducer. The critical parameters such as heat conductivity, oxidation and diffusion or coefficients of thermal expansion were taken into account to select the right combinations of high temperature materials. After the materials were selected, they were procured from commercial vendors so that they could be tested in the lab, namely with a series of impedance and ultrasonic tests. Five piezoelectric elements manufactured from  $\text{GaPO}_4$  kept resonating at virtually the same frequency while exposed to a hot environment with the temperature being raised from ambient up to the target of  $580^{\circ}\text{C}$ . One of the

transducers operated at 580°C for the duration of 600 h, which was considered as a significant improvement compared to the work reported by other researchers. The ultrasonic tests conducted on the same piezoelectric material demonstrated that GaPO<sub>4</sub> works as functional ultrasonic transducers, transmitting and receiving ultrasonic waves at temperatures as high as 580°C for a minimum of 360 hours. Finally, a GaPO<sub>4</sub> element (frequency 3.5 MHz) coupled to a steel test-block successfully detected an artificial defect with a simple geometry (a side-drilled hole with  $d=0.8$  mm) up to the same temperature level. The resolved defect corresponded to the scale of expected damage on a reactor vessel of a nuclear power plant. Based on these characterisation results, a prototype ultrasonic transducer for operation at high temperatures was designed and manufactured from the most optimum combination of high temperature materials. The transducer was tested in a laboratory environment, using a steel calibration block, high temperature ultrasonic couplant SONO 1100 and an electric furnace. In the range from ambient up to the target temperature of 580°C, the ultrasonic transducer kept its signal-to-noise ratio (SNR) level sufficiently above the threshold of 6 dB for practical ultrasonic NDT. Based on the results from this research, the prototype of a commercial ultrasonic transducer for operation at high temperatures was manufactured by a specialised NDT company. The transducer was tested in a lab environment, where it was shown to perform well all the way up to the target temperature of 580°C.

Although the main objectives of this research were achieved by developing the transducer to operate at high temperatures, further work is still required to optimise its performance especially on pipes and welds with defects arising from creep and fatigue. Some of these recommendations for future work are described below.

## 6.2 Recommendations for future work

### ➤ Development of low-noise signal amplifiers and impedance matching circuiting

The GaPO<sub>4</sub> elements proved to possess stable piezoelectric properties when subjected to 580°C for 600 hours. However, the very low measured values of the coupling coefficient  $k_t$  of 7.5% (PZT  $k_t \approx 70\%$ ) and the piezoelectric constant  $d_{11}^E$  of 4 pC/N (PZT  $d_{11}^E \approx 370$  pC/N) suggest caution and further study is needed. One of the proposed solutions to utilise this very low percentage of the converted energy (low efficiency) and low sensing capability of GaPO<sub>4</sub> elements, is the development of low-noise signal amplifiers to amplify very low-power signals without significantly degrading the SNR level. In addition, the measured impedance of GaPO<sub>4</sub> elements is in k $\Omega$ , which is several orders of magnitude higher than the load on standard BNC cable and pulser receiver unit (up to 75  $\Omega$ ). Appropriate matching circuits could bridge this impedance mismatch and enhance the operation of GaPO<sub>4</sub> transducers in both transmission and reception modes. As there are currently no electrical components available to operate at temperatures as high as 580°C, an alternative approach needs to be adopted. Researchers in the field of high temperature ultrasonics have started looking into the development of matching circuiting that is

placed outside of the transducer's housing and thus far enough from the heat zone, and this approach might be worth further exploration.

### ➤ **Development of high temperature damping body**

The damping body with its specific chemical composition and shape will determine the pulse duration and the resolution of the ultrasonic inspection. For transducers operating at ambient temperatures, the damping body is normally designed by mixing high-density powders such as tungsten with damping resins such as epoxies and these combinations perform well up to around 180°C. In the literature, a number of materials, such as soft ceramics, sintered metals, carbon and different cuts from austenitic welds have been studied and reported for possible application as HT damping bodies. In addition, ceramic mixtures Ceramabond 569 and 503 have been tested as part of this research. In the end, none of these materials achieved a functional damping of the tested GaPO<sub>4</sub> elements. The weight of the ceramics bodies, actually even further reduced the low sensitivity of GaPO<sub>4</sub> elements. Recently, some researchers have speculated that it is possible to use unbacked piezoelectric elements, which are damped only from the front by good coupling to the test object. In practice, this means that the specific acoustic impedance of GaPO<sub>4</sub> (15.6 MRayl) and the specific acoustic impedance of steel test-object (47 MRayl) will have to be balanced by application of a material that will have an impedance value between the two previously stated values and will also have to withstand temperatures up to 580°C.

### ➤ **Application of an automatic couplant feed/retrieval system**

The idea behind this research and the "HotPhasedArray" project is to have a smart and automated ultrasonic system for monitoring of existing defects in operating pipes and welds, which do not yet require replacement. To prevent the NDT personnel from unnecessary exposure to very hot surfaces of parts being monitored (temperatures up to 580°C), and to make the monitoring process more independent from the operator, an automatic couplant feed/retrieval system needs to be developed. The couplant feed/retrieval system could be based on available high temperature ultrasonic couplant solutions (e.g. SONO 1100) and commercially available pumps, and it would facilitate transmission and reception of the ultrasound energy from the transducer to the hot part being inspected.

### ➤ **Development of phased array using GaPO<sub>4</sub>**

Advanced ultrasonic techniques, such as Phased Array (PA) can be used to monitor defects while providing a much more immediate and easily interpreted presentation of results than it is possible with single-element transducers. By using dynamic depth focusing, it is possible to maintain the sensitivity to defects throughout the depth of a test-piece and allow for a better defect position measurement accuracy. By combining beam steering with beam focusing, it is possible to allow the ultrasonic waves

## Conclusions and Future Work

to focus anywhere within the test-piece, consistent with various limitations, which means that full area coverage can be completed much more quickly with a suitable phased array than with a single-element transducer. At the moment, the phased array transducers that can work up to 580°C do not exist (actually they do not work even at much lower temperatures), and in their future development GaPO<sub>4</sub> could prove to be a very useful high temperature piezoelectric material for application in PA.

### ➤ **Resistance to radioactive ( $\gamma$ -rays and thermal neutrons) radiation**

One application of ultrasonic transducers is to monitor critical assets inside nuclear power plants, and thus selected piezoelectric elements and other parts of the transducer (cables, front plate, etc.) have to be suitable for operation under both high temperatures and strong radioactive radiation. Some tests have been performed on GaPO<sub>4</sub> and can be found in literature, but more extensive research is required, especially into the long-term exposure of vibrating GaPO<sub>4</sub> elements to the radioactive environment.

## 7 Bibliography

- [1] A. McNab, K. J. Kirk and A. Cochran (1998): Ultrasonic transducers for high temperature applications. *IEE Proc-Sci Meas Technol* **145** (5), **229-236**.
- [2] EC FP7 Project (2013): High Temperature Pipe Structural Health Monitoring System utilising PA probes on TOFD configuration-HotPhasedArray. Grant Agree. No. 605267. Available at: <http://www.hotphasedarray.eu/project>.
- [3] Eurostat. Available at: [http://ec.europa.eu/eurostat/statistics-explained/index.php/Electricity\\_production\\_consumption\\_and\\_market\\_overview](http://ec.europa.eu/eurostat/statistics-explained/index.php/Electricity_production_consumption_and_market_overview). Accessed on: 20/09/2016.
- [4] European Nuclear Society: Nuclear Power Plants in Europe. Available at: <https://www.euronuclear.org/info/encyclopedia/n/nuclear-power-plant-europe.htm>. Accessed on: 20/09/2016.
- [5] The World Nuclear Industry Status Report 2015. Available at: <http://www.worldnuclearreport.org/The-World-Nuclear-Industry-Status-Report-2015-HTML.html>. Accessed on: 30/06/2016.
- [6] B. Shepherd, L. Gandossi and K. Simola (2009): ENIQ Technical Report- Link between Risk-Informed In-Service Inspection and Inspection Qualification. ENIQ Report No. 36, EUR 23928.
- [7] IAEA's Reference Technology Database. Available at: <http://www.iaea.org/OurWork/ST/NE/databases.html>. Accessed on: 17/04/2015.
- [8] R. Viswanathan, J. F. Henry, J. Tanzosh, G. Stanko, J. Shingledecker, B. Vitalis, and R. Purgert (2005): U.S. Program on Materials Technology for Ultra-Supercritical Coal Power Plants. *JMEP* **14** (3), **281-292**.
- [9] A. I. Shibly and K. Coleman (2006): Failures of P91 Steel at the West Burton Plant in England Raise Concerns about the Long Term Behaviour of Advanced Steel. 1. Technical report, European Technology Development Available at: <http://www.ommi.co.uk/etd/etd-epri-%20p91%20failures.pdf>. Accessed on: 23/09/2016.
- [10] S. J. Brett (2008): Early Type IV Cracking on Retrofit Grade 91 Steel Headers'. *Proc of the IIW Int Conf*, Graz, Austria.
- [11] D. J. Abson and J. S. Rothwell (2013): Review of type IV cracking of weldments in 9-12% Cr creep strength enhanced ferritic steels. *International Materials Reviews* **58** (8), **437-473**.
- [12] ECCC Recommendations (2005): Residual life assessment and microstructure. ECCC **6** (1). Available at: <http://www.ommi.co.uk/etd/eccc/advancedcreep/V6i1x.pdf>. Accessed on: 23/09/2016.

## Bibliography

- [13] M. W. Hooker (1998): Properties of PZT-Based Piezoelectric Ceramics Between -150 and 250°C. NASA / CR- 1998-208708.
- [14] D. Damjanovic: Materials for high-temperature piezoelectric transducers (1998). *Curr Opin Solid State Mater Sci* **3**, 469–473.
- [15] S. Zhang and F. Yu (2011): Piezoelectric Materials for High Temperature Sensors. *J Am Ceram Soc* **94** (10), 3153-3170.
- [16] P. Kremlj (1994): Quartz Homeotypic Gallium-Orthophosphate – A New High Tech Piezoelectric Material. *IEEE Proc UT Symp*, 949-954.
- [17] V. Krstelj (2003): Ultrazvučna kontrola – Odabrana poglavlja. Faculty of Mechanical Engineering and Naval Architecture University of Zagreb, Croatia. ISBN 953-6313-54-5.
- [18] Y.-K. Zhu, G.-Y. Tian, R.-S. Lu and H. Zhang (2011): A Review of Optical NDT Technologies. *Sensors* **11** (8), 7773–7798.
- [19] J. Blitz and G. Simpson (1996): Ultrasonic Methods of Non-destructive Testing. Book published by Chapman & Hall London, ISBN 0 412 60470 1.
- [20] S. Takahashi and H. Kikuchi (2007): Electromagnetic Nondestructive Evaluation. IOS Press, ISBN 978 1 58603 752 9.
- [21] BiNDT: Radiographic NDT. Available at: <http://www.bindt.org/What-is-NDT/Radiography/>. Accessed on: 27/11/2018.
- [22] NDT Resource Center: Penetrant-Testing Materials. Available at: <https://www.nde-ed.org/EducationResources/CommunityCollege/PenetrantTest/PTMaterials/ptmaterials.htm>. Accessed on: 27/11/2018.
- [23] NDT Resource Center: Introduction to Thermal Testing. Available at: [https://www.nde-ed.org/EducationResources/CommunityCollege/Other%20Methods/IRT/IR\\_Intro.htm](https://www.nde-ed.org/EducationResources/CommunityCollege/Other%20Methods/IRT/IR_Intro.htm). Accessed on: 27/11/2018.
- [24] A. Vakhguel't, S. D. Kapayeva, M. J. Bergander (2017): Combination Non-Destructive Test (NDT) Method for Early Damage Detection and Condition Assessment of Boiler Tubes. *Procedia Engineering* **188**, 125-132.
- [25] C. Colla *et al.* (2002): Combination of NDT techniques for site investigation of non-ballasted railway tracks. *NDT & E International* **35** (2), 95-105.
- [26] Wikipedia. Available at: <http://en.wikipedia.org/wiki/Ultrasound>. Accessed on: 30/04/2018.
- [27] Faculty of Mechanical Engineering University of Slavonski Brod. Digital book: “Analiza tehnološkičnosti zavarenih konstrukcija”. Authors: I. Samardžić, Š. Klarić. A. Kožul, B. Despotović, V. Topić. Available at: [http://www.sfsb.hr/kth/zavar/na\\_dipl4/5.pdf](http://www.sfsb.hr/kth/zavar/na_dipl4/5.pdf). Accessed on: 06/12/2012.
- [28] NDT Resource Centre: NDT Data Presentation. Available at: <https://www.nde-ed.org/EducationResources/CommunityCollege/Ultrasonics/EquipmentTrans/DataPres.htm>. Accessed on: 30/04/2018.

## Bibliography

- [29] D. Stubbs *et al.*: An automated ultrasonic system for inspection of aircraft turbine engine components. University of Dayton Research Institute, Dayton, OH USA. Available online: <https://pdfs.semanticscholar.org/3ff2/0745fe78bd0ddfd7a96e30be0f408424273a.pdf>. Accessed on: 01/05/2018.
- [30] NDT Resource Centre: Ultrasonic damping. Available online: <http://www.ndt.net/ndtaz/content.php?id=102>. Accessed on: 01/05/2018.
- [31] L. F. Brown (2000): The Effects of Material Selection for Backing and Wear Protection/Quarter-Wave Matching of Piezoelectric Polymer Ultrasound Transducers. *IEEE Ultrasonics Symposium* **1029-1032**; 0-7803-6365-5/00/\$10.
- [32] Innerspec Brochure: Dry-Coupled Ultrasonic Testing. Available online: <https://www.innerspec.com/assets/files/2016-DCUT-Brochure-.pdf>. Accessed on: 01/05/2018.
- [33] Olympus: Ultrasonic couplants. Available online: <https://www.olympus-ims.com/en/applications/ultrasonic-couplant/>. Accessed on: 01/05/2018.
- [34] B. Drinkwater and P. Cawley: The practical application of solid coupled ultrasonic transducers. *Proc 14<sup>th</sup> World Conf NDT*, N. Delhi, 8-13 Dec 1996. **4**, **2041–2044**.
- [35] M. Lach, M. Platte and A. Ries (1996): Piezoelectric materials for ultrasonic probes. *NDTnet* **1 (9)**. <http://www.ndt.net/article/platte2/platte2.htm>.
- [36] J. C. Drury (2005): Ultrasonics – Refraction and mode conversion. *Insight* **47 (1)**, **44-46**.
- [37] Olympus: Dual Element Transducers. Available online: <https://www.olympus-ims.com/sv/ultrasonic-transducers/dualelement/>. Accessed on: 01/05/2018.
- [38] Precision Acoustics: NDT Wedges. Available online: <https://www.acoustics.co.uk/product/ndt-wedges/>. Accessed on: 01/05/2018.
- [39] Olympus: Replaceable Delay Line Transducers. Available online: <https://www.olympus-ims.com/sv/ultrasonic-transducers/delay-line/>. Accessed on: 02/05/2018.
- [40] J. C. Drury (2005): Ultrasonics – The ultrasonic beam. *Insight* **47 (5)**, 297-299.
- [41] Olympus: Contact Ultrasonic Transducers. Available online: <https://www.olympus-ims.com/en/ultrasonic-transducers/contact-transducers/>. Accessed on: 02/05/2018.
- [42] F. B. Cegla, P. Cawley, J. Allin and J. Davies (2011): High-temperature (>500°C) wall thickness monitoring using dry-coupled ultrasonic waveguide transducers. *IEEE Trans. Ultrason. Ferroelectr. Freq.*, **58 (1)**, **156-167**.
- [43] R. Kazys, A. Voleisis and B. Voleisiene (2008): High temperature ultrasonic transducers: review. *Ultragarsas (Ultrasound) Journal* **63 (2)**, **7-17**.
- [44] Olympus: Panametrics – NDT high temperature transducers. Available online: <https://www.olympus-ims.com/en/applications/high-temperature-ultrasonic-testing/>. Accessed on: 03/05/2018.
- [45] SIGMA Transducers: High Temperature Applications Transducers. Available online: [http://www.sigmatx.com/high\\_temp.htm](http://www.sigmatx.com/high_temp.htm). Accessed on: 03/05/2018.

## Bibliography

- [46] Hagisonic Ultrasonic Transducers. Available online: <http://www.hagisonic.com/>. Accessed on: 03/05/2018.
- [47] M. Budimir, A. Mohimi, C. Selcuk and T.-H. Gan (2011): High Temperature NDE Ultrasound Transducers for Condition Monitoring of Superheated Steam Pipes in Nuclear Power Plants. *Proc. 20<sup>th</sup> Int. Conf. NENE*, **502.1-502.8**.
- [48] J. C. Drury (2005): Ultrasonics – Transducers for generating and detecting sound waves. *Insight* **47 (2)**, **98-100**.
- [49] S. Krishnaswamy and F. Zhang (2012): Theory and Applications of Laser Ultrasonic Techniques: Engineering & Biomedical Applications. In T. Kundu (Ed.), *Ultrasonic & Electromagnetic NDE for Structure and Material Characterization: Engineering & Biomedical Applications*, **457-492**, CRC Press.
- [50] BOSTON PIEZO-OPTICS INC.: Intro to piezoelectric transducer crystals. Available at: <http://bostonpiezooptics.com/intro-to-transducer-crystals>. Accessed on: 27/09/2016.
- [51] K. J. Kirk, A. McNab, A. Cochran, I. Hall and G. Hayward (1999): Ultrasonic Arrays for Monitoring Cracks in an Industrial Plant at High Temperatures. *IEEE Trans. Ultrason., Ferroelect., Freq. Control.* **46 (2)**, **311-319**.
- [52] S. J. Zhang, J. Luo, D. W. Snyder and T. R. Shrout (2008): High Performance, High Temperature Piezoelectric Crystals. **130–157** in *Handbook of Advanced Dielectric, Piezoelectric and Ferroelectric Materials – Synthesis, Characterization and Applications*. Edited by Z. G. Ye. Woodhead Publishing Ltd., Cambridge, England.
- [53] S. J. Zhang, X. N. Jiang, M. Lapsley, P. Moses, and T. R. Shrout (2010): Piezoelectric Accelerometers for Ultrahigh Temperature Application. *Appl. Phys. Lett.* **96**, **3**.
- [54] R. Turner, P. Fuierer, R. Newnham and T. Shrout (1994): Materials for high-temperature acoustic and vibration sensors: A review. *Appl. Acoust.* **41**, **299-324**.
- [55] S. Zhang, Y. Zheng, H. Kong, J. Xin, E. Frantz and T. R. Shrout (2009): Characterization of high-temperature piezoelectric crystals with an ordered langasite structure. *J. Appl. Phys.* **105**.
- [56] K. Jacobs, P. Hofmann, D. Klimm, J. Reichow and M. Schneider (2000): Structural phase transformations in crystalline gallium orthophosphate. *J. Solid State Chem.* **149**, **180-188**.
- [57] K. Shimamura, H. Takeda, T. Kohno and T. Fukuda (1996): Growth and characterisation of lanthanum gallium silicate  $\text{La}_3\text{Ga}_5\text{SiO}_{14}$  single crystals for piezoelectric applications. *J. Cryst. Growth* **163**, **388-392**.
- [58] K. Jacobs, P. Hofmann, J. Reichow: Hydrothermal Growth of Gallium Orthophosphate Crystals – a Comparison with Quartz Crystal Growth. Institut für Kristallzüchtung, Germany.
- [59] A. De and K. V. Rao (1988): Dielectric properties of synthetic quartz crystals. *J. Mater. Sc.* **23 (2)**, **661-664**.

## Bibliography

- [60] K. J. Kirk, R. Hou, N. Schmarje, N. M. Pragada, L. Torbay and D. Hutson (2015): Investigation of high-temperature ultrasonic transducer design using lithium niobate piezocomposite,” *Insight* **57** (4), **193-199**.
- [61] A. Mohimi, T.-H. Gan and W. Balachandran (2013): Development of high temperature ultrasonic guided wave transducer for continuous in service monitoring of steam lines using non-stoichiometric lithium niobate piezoelectric ceramic. *Sensor Actuat A-Phys* **216**, **432-442**.
- [62] A. Baba, C. T. Searfass and B. R. Tittmann (2010): High-temperature ultrasonic transducer up to 1000°C using lithium niobate single crystal. *Appl. Phys. Lett.* **97**; doi: 10.1063/1.3524192.
- [63] P. M. Worsch, P. W. Krempl and W. Wallnofer (2002): GaPO<sub>4</sub> Crystals for Sensor Applications. *Proc IEEE Sensors* **1**, **589-593**.
- [64] AVL Group: Pressure sensors for combustion analysis. Available at: <https://www.avl.com/documents/10138/885965/AVL+Pressure+Sensors+for+Combustion+Analysis/6c844a54-7a84-429d-8e57-4f34e948f95d>. Accessed on: 18/11/2015.
- [65] R. Kazys, A. Voleisis, R. Sliteris, L. Mazeika, R. V. Nieuwenhove, P. Kupschus and H. A. Abderrahim (2005): High Temperature Ultrasonic Transducers for Imaging and Measurements in a Liquid Pb/Bi Eutectic Alloy. *IEEE Trans. Ultrason., Ferroelect., Freq. Control.* **52**, **4**.
- [66] V. Giurgiutiu, B. Xu and W. Liu: Development and Testing of High-temperature Piezoelectric Wafer Active Sensors for Extreme Environments. *Struct. Health Monitoring*. Available: <http://shm.sagepub.com/content/early/2010/03/23/1475921710365389.full.pdf+html>. Accessed on: 27/11/2015.
- [67] M. N. Hamidon, V. Skarda, N. M. White, F. Krispel, P. Krempl, M. Binhack and W. Buff (2005): Fabrication of high temperature surface acoustic wave devices for sensor applications. *Sensor Actuat A-Phys* **123/124**, **403-407**.
- [68] GaPO<sub>4</sub> Material Data Sheet: GaPO<sub>4</sub> Resonators. Piezocryst Advanced Sensorics GmbH.
- [69] X. Jiang, K. Kim, S. Zhang, J. Johnson and G. Salazar (2014): High-Temperature Piezoelectric Sensing. *Sensors* **14**, **144-169**; doi: 10.3390/s140100144.
- [70] D. Richter and H. Fritze (2011): High-temperature Stable Electrodes for Langasite Based Surface Acoustic Wave Devices. *Proc Sensor+Test Conf*, in Germany on 9<sup>th</sup> June, **532–537**.
- [71] J. Puigcorbe, D. Vogel, B. Michel, A. Vila, I. Gracia, C. Cane and J. Morante (2003): High-temperature degradation of Pt/Ti electrodes in micro-hotplate gas sensors. *J. Micromech. Microeng.* **13**, **119–124**.
- [72] D. M. Mattox (2001): Physical vapour deposition (PVD) processes. *J Metal Finishing (Elsevier)* **99** (1), **409-423**.
- [73] S. Galosic (2010): Master thesis. Faculty of Mechanical Engineering and Naval Architecture, University of Zagreb, Croatia.

## Bibliography

- [74] E.K. Sittig (1969): Effects of Bonding and Electrode Layers on the Transmission Parameters of Piezoelectric Transducers Used in Ultrasonic Digital Delay Lines. *IEEE Transactions on Sonics and Ultrasonics*, **16 (1)**, 2-9.
- [75] M. M. Islam and H. Huang (2016): Effects of adhesive thickness on the Lamb wave pitch-catch signal using bonded piezoelectric wafer transducers. *Smart Mater. Struct.* **25**. Available at: <http://iopscience.iop.org/article/10.1088/0964-1726/25/8/085014/ampdf>. Accessed on: 14/08/2018.
- [76] J. C. Drury (2005): Ultrasonics – Probe construction. *Insight* **47 (3)**, 168-171.
- [77] Easy Composites Ltd.: Very High Temperature Epoxy Laminating Resin. Available at: <http://www.easycomposites.co.uk/#!/resin-gel-silicone-adhesive/epoxy-resin/very-high-temperature-epoxy-laminating-resin.html>. Accessed on: 27/09/2016.
- [78] H. Mrasek, D. Gohlke, K. Matthies and E. Neumann (1996): High Temperature Ultrasonic Transducers. *NDTnet* **1 (9)**. Available at: [http://www.ndt.net/article/mrasek/mrasek\\_e.htm](http://www.ndt.net/article/mrasek/mrasek_e.htm).
- [79] A. Mohimi (2014): High Temperature Ultrasonic Guided Wave Transducers. PhD Thesis. Brunel University London.
- [80] D. A. Parks, S. Zhang and B. R. Tittmann (2013): High-Temperature (>500°C) Ultrasonic Transducers: An Experimental Comparison among Three Candidate Piezoelectric Materials. *IEEE Trans. Ultrason., Ferroelect., Freq. Control.* **60, (5)**, 1010- 1015.
- [81] Aremco Products Inc.: Ceramabond 569. Available at: <http://www.aremco.com/news-item/new-ceramabond-569-bonds-coats-platinum-resistance-heaters/>. Accessed on: 29/09/2016.
- [82] Aremco Products Inc.: Ceramabond 503. Available at: <http://www.aremco.com/news-item/ceramabond%E2%84%A2-503-now-used-to-bond-aluminum-oxide-ceramics/>. Accessed on: 29/09/2016.
- [83] Aremco Products Inc.: <http://www.aremco.com/news-item/new-ceramabond-569-bonds-coats-platinum-resistance-heaters/>. Accessed on 30/03/2016.
- [84] Aremco Products Inc.: <http://www.aremco.com/news-item/ceramabond%E2%84%A2-503-now-used-to-bond-aluminum-oxide-ceramics/>. Accessed on 30/03/2016.
- [85] NDT Resource Centre: Characteristics of Piezoelectric Transducers. Available at: <https://www.nde-ed.org/EducationResources/CommunityCollege/Ultrasonics/EquipmentTrans/characteristicspt.htm>. Accessed on: 27/09/2016.
- [86] AZO Materials: Alumina - Aluminium Oxide - Al<sub>2</sub>O<sub>3</sub> - A Refractory Ceramic Oxide. Available at: <http://www.azom.com/properties.aspx?ArticleID=52>. Accessed on: 27/09/2016.
- [87] J. Baun (2009): Principles of General & Vascular Sonography – Chapter 8, Transducers. 93-100. Available at: [http://traktoria.org/files/sonar/transducer/simple\\_transducer\\_intro.pdf](http://traktoria.org/files/sonar/transducer/simple_transducer_intro.pdf). Accessed on: 27/09/2016.

## Bibliography

- [88] D. A. Silber, B. S. Garrison and S. Williams (1998): Ultrasound probe housing with reduced control pressure grip and method for manufacturing same. Patent No. US 5928154 A. Available at: <http://www.google.co.uk/patents/US5928154>. Accessed on: 27/09/2016.
- [89] TE Connectivity: Ultrasound cable assembly. Available at: <http://www.te.com/usa-en/industries/medical-healthcare/applications/ultrasound-cable-assembly.html?tab=pgp-story>. Accessed on: 27/09/2016.
- [90] National Electronic Alloys Inc.: High Temperature & Corrosion Resistant Alloys. Available at: <http://www.nealloys.com/high-temp-alloys.php>. Accessed on: 29/09/2016.
- [91] Heatsense Cables Ltd.: Pure Nickel Glassfibre Cable Material Data Sheet. Available at: [http://www.heatsensecables.co.uk/product/pure\\_nickel\\_glassfibre](http://www.heatsensecables.co.uk/product/pure_nickel_glassfibre). Accessed on: 12/03/2015.
- [92] M. Garcia-Rodriguez *et al.* (2010): Low cost matching network for ultrasonic transducers. *Physics Procedia* **3**, 1025-1031.
- [93] J. An, K. Song, S. Zhang, J. Yang and P. Cao (2014): Design of a Broadband Electrical Impedance Matching Network for Piezoelectric Ultrasound Transducers Based on a Genetic Algorithm. *Sensors* **14**, 6828-6843; doi: 10.3390/s140406828.
- [94] C. Hammerschmidt (2016): High-temperature electronics operates at 300°C. Available at: <http://www.electronics-eetimes.com/news/high-temperature-electronics-operates-300%C2%B0c>. Accessed on: 28/09/2016.
- [95] A. Chauhan, R. Vaish and C. Bowen (2015): Piezoelectric material selection for ultrasonic transducer and actuator applications. *Proc IMechE Part L: J Materials: Design and Applications* **229**(1), 3-12. DOI: 10.1177/1464420713493591.
- [96] Noliac Piezoelectric Actuators: Soldering Procedure. Available at: <http://www.noliac.com/tutorials/technical-support-actuators/soldering-procedure/>. Accessed on: 07/12/2016.
- [97] Indium Corporation: Solder Alloy Selector Guide. Available at: <http://www.indium.com/solder-alloy-guide/results.php>. Accessed on: 28/09/2016.
- [98] Panacol-Elosol GmbH: Elecolit 3653. Datasheet available at: <http://www.panacol.com/fileadmin/pdfs/Elecolit-3653-english-TDS-Panacol-adhesive.pdf>. Accessed on: 29/09/2016.
- [99] Cotronics Corp.: Duralco 124. Datasheet available at: <https://www.cotronics.com/vo/cotr/pdf/120.pdf>. Accessed on: 29/09/2016.
- [100] Plant Integrity Ltd.: Ultrasonic testing of high temperature lines (<125°C). Available at: <http://www.plantintegrity.com/teletest/applications/>. Accessed on: 29/09/2016.
- [101] Aremco Inc.: PyroDuct 597-A. Datasheet available at: <http://www.aremco.com/news-item/pyro-duct-597-c-high-temp-electrically-conductive-coating-now-available-2/>. Accessed on: 29/09/2016.

## Bibliography

- [102] Cotronics Corp.: Resbond 931C. Datasheet available at: <http://www.cotronics.com/catalog/32%20904-%20931.pdf>. Accessed on: 29/09/2016.
- [103] Magnaflux: High Performance Ultrasonic Couplant Ultrigel II. Available at: <http://magnaflux.com/Magnaflux/Products/Ultrasonic-Couplants/Ultrigel-II.htm>. Accessed on: 07/12/2016.
- [104] M. Budimir (2006): Piezoelectric anisotropy and free energy instability in classic perovskites. PhD Thesis; EPFL.
- [105] Magnaflux: Ultrasonic NDT Couplants for High Temperature Application. Available at: [http://www.magnaflux.com/Products/UltrasonicCouplants\(Sonotech\)/HighTemperatureCouplants/Sono/tabid/2251/Default.aspx](http://www.magnaflux.com/Products/UltrasonicCouplants(Sonotech)/HighTemperatureCouplants/Sono/tabid/2251/Default.aspx). Accessed on: 30/09/2016.
- [106] Agilent Impedance Measurement Handbook – A guide to measurement technology and techniques. 4<sup>th</sup> Edition. Agilent Technologies, Published in USA, September 10<sup>th</sup>, 2013.
- [107] S. M. Rhim *et al.* (2008): Piezoelectric single crystals for medical ultrasonic transducers. Handbook of Advanced Dielectric, Piezoelectric and Ferroelectric Materials. Woodhead Publishing Limited.
- [108] Active European Standard. Piezoelectric properties of ceramic materials and components – Part 2: Methods of measurement – Low power. EN 50324-2:2002.
- [109] APC International, Ltd.: Determining resonance frequency. Available at: <https://www.americanpiezo.com/piezo-theory/determining-resonance-frequency.html>. Accessed on: 23/06/2016.
- [110] APC International Ltd.: Physical and piezoelectric properties of APC materials. Available at: <https://www.americanpiezo.com/apc-materials/piezoelectric-properties.html>. Accessed on: 03/03/2015.
- [111] Ionix Advanced Technologies Ltd: HPZ510 Ceramics Datasheet. Available at: <http://5c024cc18d36ac025052-ddc1051a69b5635d7095b9e0f44f0f03.r99.cf3.rackcdn.com/hpzdatasheet510.pdf>. Accessed on: 04/10/2016.
- [112] C. Cavalloni, R. Sommer and M. Waser (2011): High temperature stability of new single crystal piezoelectric sensors. *SENSOR+TEST Conf Proc* **520 – 525**, DOI 10.5162/sensor11/d1.1.
- [113] P. Hofmanna, K. Jacobsa, H. Federmannb, M. Schulzb, H. Fritzeb and H.L. Tullerc (2006): Growth and high-temperature properties of gallium orthophosphate. *Solid State Ionics* **177 (35–36), 3175–3178**.
- [114] Physics of Crystalline Dielectrics: Volume 2 Electrical Properties, **Pg 567**. Edited by I. S. Zheludev; Springer Science & Business Media, 29 Jun 2013.
- [115] J. C. Drury (2005): Ultrasonics, Part 4 – Transducers for generating and detecting sound waves. *Insight* **47 (2), 98-100**.
- [116] G. Gautschi (2002): Piezoelectric Sensorics, Springer-Verlag, New York.

## Bibliography

- [117] W. P. Mason and H. Jaffe (1954): Methods for Measuring Piezoelectric, Elastic, and Dielectric Coefficients of Crystals and Ceramics. *Proc of IRE* **42 (6)**, 1731-1737.
- [118] B. Jaffe, W. R. Cook Jr. and H. Jaffe (1971): Piezoelectric Ceramics. Academic Press – London and New York, **Pg 315**; ISBN 0-12-379550-8.
- [119] J. Fialka and P. Benes (2013): Comparison of Methods for the Measurement of Piezoelectric Coefficients. *IEEE Transactions on Instrumentation and Measurement* **62 (5)**, 1047-1057.
- [120] Keysight: 4294A Precision Impedance Analyzer, 40-110 MHz. Available at: <http://www.keysight.com/en/pd-1000000858%3Aepsg%3Apro-pn-4294A/precision-impedance-analyzer-40-hz-to-110-mhz?cc=GB&lc=eng>. Accessed on: 03/10/2016.
- [121] Keysight Technologies, 16334A Test Fixture (Tweezers Contacts). Available at: <http://www.keysight.com>. Accessed on 13/04/2015.
- [122] S. Sherrit, X. Bao, Y. Bar-Cohen and Z. Chang (2004): Resonance Analysis of High Temperature Piezoelectric Materials for Actuation and Sensing. *SPIE* **5387**, San Diego, CA.
- [123] P. Davulis, J. A. Kosinski and M. Pereira da Cunha (2006): GaPO<sub>4</sub> Stiffness and Piezoelectric Constants Measurements using the Combined Thickness Excitation and Lateral Field Technique. *IEEE International Frequency Control Symposium and Exposition* **664-669**.
- [124] R. G. Sabat, B. K. Mukherjee, W. Ren and G. Yang (2007): Temperature dependence of the complete material coefficients matrix of soft and hard-doped piezoelectric lead zirconate-titanate ceramics. *J Appl Phys* **101 (6)**.
- [125] Zetec Inc., Topaz 32 Brochure. Available at: [http://www.zetec.com/wp-content/uploads/2016/04/Topaz32\\_Brochure.pdf](http://www.zetec.com/wp-content/uploads/2016/04/Topaz32_Brochure.pdf). Accessed on: 20/07/2016.
- [126] B. C. Kuo and F. Golnaraghi: Automatic control systems. 8<sup>th</sup> Edition, Published by Wiley, New York, **Pg 236–237**, 2003.
- [127] Ionix Advanced Technologies Ltd: Developing permanently installed system for ultrasonic thickness monitoring in demanding environments based on Hot Sense technology. Available at: <http://ionixadvancedtechnologies.co.uk/perch/resources/case-study-thickness-monitoring.pdf>. Accessed on: 11/10/2016.
- [128] OLYMPUS: Ultrasonic transducers. Available at: <http://www.olympus-ims.com/en/ultrasonic-transducers/contact-transducers/>. Accessed on: 11/10/2016.
- [129] M. K. Yucel, S. Fateri, M. Legg, A. Wilkinson, V. Kappatos, C. Selcuk and T.-H. Gan (2016): Coded Waveform Excitation for High-Resolution Ultrasonic Guided Wave Response. *IEEE Transactions on Industrial Informatics* **12 (1)**, 257-266.
- [130] H. Mrasek, D. Gohlke, K. Matthies and E. Neumann (1996): High Temperature Ultrasonic Transducers. *NDTnet* **1 (9)**. Available at: [http://www.ndt.net/article/mrasek/mrasek\\_e.htm](http://www.ndt.net/article/mrasek/mrasek_e.htm). Accessed on: 17/12/2016.

## Bibliography

- [131] L. Klingenberg (2005): Frequency Domain Using Excel. Technical report produced for San Francisco State University, School of Engineering.  
Available at: [http://www.stem2.org/je/Excel\\_FFT\\_Instructions.pdf](http://www.stem2.org/je/Excel_FFT_Instructions.pdf).
- [132] Ionix Advanced Technologies Ltd: Developing the Hot Sense High Temperature Crack Monitoring Probe. Available at: <http://ionixadvancedtechnologies.co.uk/perch/resources/case-study-crack-monitoring.pdf>. Accessed on: 13/07/2016.
- [133] J. Outinen and P. Makelainen (2004): Mechanical properties of structural steel at elevated temperatures and after cooling down. *Fire and materials* **28** (2-4), 237–251.
- [134] The Engineering Toolbox: Elastic properties and Young’s modulus for metals and alloys like cast iron, carbon steel and more. Available at: [http://www.engineeringtoolbox.com/young-modulus-d\\_773.html](http://www.engineeringtoolbox.com/young-modulus-d_773.html). Accessed on: 12/10/2016.
- [135] J. L. Rose (2008): Ultrasonic Waves in Solid Media. Cambridge University Press.
- [136] P. N. Bilgunde and L. J. Bond (2015): Effect of Thermal Degradation on High Temperature Ultrasonic Transducer Performance in Small Modular Reactors. *Physics Procedia* **70**, 433-436.
- [137] J. Szilard (1982): Ultrasonic Testing – Testing at high temperatures. Published by J. Wiley & Sons Ltd.
- [138] M. Kostan (2015): Temperature dependent compression wave velocity in P91 steel. Deliverable Report No 2.1, as part of EC FP7 Project Hot Phased Array.
- [139] J. C. Drury (2005): Calibration and Reference Standards. *Insight* **47** (6), 364-365.
- [140] E. Ginzler (2001): Beam Width Analysis. *NDT.net* **6** (9). Available at: <http://www.ndt.net/article/v06n09/ginzler/ginzler.htm>. Accessed on: 13/01/2017.
- [141] Y. H. Kim and S.-J. Song: A study on the couplant effects in contact ultrasonic testing. Available at NDT Net: <http://www.ndt.net/article/apcndt01/papers/1041/1041.htm>. Accessed on: 02/03/2018.
- [142] NDT Products Ltd: [http://www.ndtproducts.ca/products/files/ULTRAGEL\\_II\\_data\\_sheet.pdf](http://www.ndtproducts.ca/products/files/ULTRAGEL_II_data_sheet.pdf). Accessed on: 01/09/2016.
- [143] Diagnostic Sonar Ltd. Available at: [http://www.diagnosticsonar.com/artman/publish/printer\\_23.shtml](http://www.diagnosticsonar.com/artman/publish/printer_23.shtml). Accessed on: 01/09/2016.
- [144] A. Mohimi (2014): High Temperature Ultrasonic Guided Wave Transducers. PhD Thesis; Brunel University London.